

DISSERTATION

# Learning to Predict, Discover, and Reason in High-Dimensional Discrete Event Sequences

Transformers, Scalable Causal Discovery, and Multi-Agent System for  
Automated Error Pattern Detection in Vehicles

Hugo Math

Submitted in  
March 2026

at the  
Faculty of Applied Computer Science  
University of Augsburg

to obtain the doctoral degree  
Dr. rer. nat.



Universität  
Augsburg  
University

FACULTY OF APPLIED COMPUTER SCIENCE  
UNIVERSITY OF AUGSBURG

Advisor: Prof. Dr. rer. nat. Rainer Lienhart  
Reviewers: Prof. Dr. rer. nat. Rainer Lienhart  
Prof. Dr. rer. nat. Elisabeth Andre

Thesis defense: June, 2026

# Abstract

Electronic control units (ECUs) embedded within modern vehicles generate a large number of asynchronous events known as diagnostic trouble codes (DTCs). These discrete events form complex temporal sequences that reflect the evolving health of the vehicle’s subsystems. In the automotive industry, domain experts manually group these codes into higher-level error patterns (EPs) using Boolean rules to characterize system faults and ensure safety. However, as vehicle complexity grows, this manual process becomes increasingly costly, error-prone, and difficult to scale. Consequently, manufacturers urgently require automated solutions capable of anticipating malfunctions, reducing downtime, and lowering warranty and repair costs. Notably, the number of unique DTCs in a modern vehicle is on the same order of magnitude as the vocabulary of a natural language, often numbering in the tens of thousands. This observation motivates a paradigm shift: treating diagnostic sequences as a language that can be modeled, predicted, and ultimately explained. Traditional statistical approaches fail to capture the rich dependencies and do not scale to high-dimensional datasets characterized by thousands of nodes, large sample sizes, and long sequence lengths. Specifically, the high cardinality of categorical event spaces in industrial logs poses a significant challenge, necessitating new machine learning architectures tailored to such event-driven systems. This thesis addresses automated fault diagnostics by unifying event sequence modeling, causal discovery, and large language models (LLMs) into a coherent framework for high-dimensional event streams. It is structured in three parts, reflecting a progressive transition from prediction to causal understanding and finally to reasoning for vehicle diagnostics. Part I introduces Transformer-based architectures for predictive maintenance from DTC sequences. Part II develops a suite of three scalable causal discovery frameworks that leverage pretrained autoregressive models as neural density estimators. OSCAR and CARGO recover the direct causes of each outcome label at the sample- and population-level respectively, while TRACE addresses a complementary problem: recovering the event-to-event causal graph from a single sequence. Finally, Part III integrates these causal structures with large language models in a multi-agent system (CAREP) that automates the synthesis of Boolean EP rules. Together, these contributions establish a coherent, scalable pipeline from raw event streams to human-readable diagnostic knowledge.



# Acknowledgments

First and foremost, I would like to express my deepest gratitude to my supervisor, Prof. Rainer Lienhart, for his openness to ideas, constant investment throughout my PhD, and scientific rigor. His support and vision were essential in shaping both this thesis and my growth as a researcher. I am grateful to have been offered this opportunity. I also extend my sincere thanks to Prof. Elisabeth Andre for her time and effort in reviewing this thesis. I am also sincerely thankful to my PhD colleagues, Julian Lorenz, Daniel Kienzle, Robin Schön and Mrunmai Phatak, for their help, support, and camaraderie. They made this journey not only productive but also enjoyable. The countless discussions, collaborations, and shared moments have been a source of motivation and inspiration. I warmly thank my BMW supervisors, Stefan Oelsner for his deep expertise, creativity, and knowledge, and Stefan Mueller for his rigorous guidance, constructive feedback, and support in every phase of the Promotion program. I also thank Stefan Kirsch for his interest, support and the opportunity to connect academic research with real-world industrial challenges at BMW. I am thankful to Michael Decker and Ingo Stock for their support and time reviewing this thesis. Their insights and the collaboration between BMW and the University of Augsburg greatly enriched this work. Additionally, I would like to acknowledge all my BMW colleagues, particularly Bernd Postmaier for his orientation and advice, Stefan Benesch for operational guidance, and Lisa Jobst for her positive spirit in the office. Finally, I am deeply grateful to my family, especially my parents, Bertrand and Audrey Math, for their constant encouragement and unwavering support. They greatly helped me stay motivated and keep moving forward. I hope I can make them as proud as I am to have them as parents. I also want to thank my sister, Laura, for her presence, and my two grandfathers, Henri and Jean, whose memory continues to inspire me. And of course, my close friends, particularly Nathan Haudot, for his encouragement and companionship throughout this journey.



# Contents

<b>Abstract</b>	<b>iii</b>
<b>Acknowledgments</b>	<b>v</b>
<b>Contents</b>	<b>vii</b>
<b>1 Introduction</b>	<b>1</b>
1.1 From Industrial Challenge to Scientific Question . . . . .	2
1.2 Research Areas, Challenges and Open Problems . . . . .	2
1.3 Contributions . . . . .	4
1.3.1 Predictive Sequence Modeling of Vehicle Diagnostics . . . . .	4
1.3.2 Multi-Label Causal Discovery in High-Dimensional Event Sequences	6
1.3.3 Scalable Sample-Level Causal Discovery in Event Sequences . . . . .	8
1.3.4 Automated Causal Reasoning with Multi-Agent Systems for Error Pattern Rule Automation . . . . .	10
1.3.5 Software . . . . .	11
1.4 List of Publications . . . . .	12
1.5 Thesis Outline . . . . .	13
<b>I Predictive Sequence Modeling</b>	<b>15</b>
<b>2 Foundations of Event Sequence Modeling</b>	<b>17</b>
2.1 Hawkes Processes . . . . .	17
2.1.1 Background . . . . .	17
2.1.2 Self-exciting property . . . . .	18
2.1.3 Mutually Exciting Hawkes Processes . . . . .	19
2.1.4 Limitations . . . . .	19
2.1.5 The High-Dimensional Discrete Event Stream Regime . . . . .	20
2.2 Language Models . . . . .	20
2.2.1 Word Level . . . . .	20
2.2.2 Word Embeddings . . . . .	21
2.2.3 Transformers . . . . .	21
2.2.3.1 Attention . . . . .	22
2.2.3.2 Feed-forward Layers . . . . .	22
2.2.3.3 Normalization . . . . .	23
2.2.3.4 Positional Encoding . . . . .	23
2.2.3.5 Autoregressive Transformers . . . . .	23

2.3	Metrics . . . . .	24
2.3.1	Next-Event Prediction . . . . .	24
2.3.2	Next-Time Prediction . . . . .	24
2.4	Dataset . . . . .	25
2.4.1	Vehicular Fault Sequences . . . . .	25
2.4.1.1	Diagnostic Trouble Code: DTCs . . . . .	25
2.4.1.2	Error Patterns . . . . .	26
<b>3</b>	<b>Error Pattern Prediction from Vehicle Diagnostic Event Sequences</b>	<b>29</b>
3.1	Introduction . . . . .	29
3.2	Background . . . . .	30
3.2.1	Transformers for Event Streams . . . . .	30
3.3	Dataset Description . . . . .	31
3.3.1	Time and Mileage . . . . .	31
3.4	Methodology . . . . .	32
3.4.1	CarFormer . . . . .	32
3.4.1.1	Embeddings . . . . .	32
3.4.1.2	Multi-Task Learning . . . . .	34
3.4.2	EPredictor . . . . .	35
3.4.2.1	Limitations of Next-Event Prediction . . . . .	35
3.4.2.2	Multi-Label Event Prediction . . . . .	36
3.4.2.3	Imbalanced Labels . . . . .	37
3.4.2.4	Losses . . . . .	37
3.5	Experiments . . . . .	38
3.5.1	Ablation I: CarFormer Embeddings . . . . .	38
3.5.2	EPredictor Experiments . . . . .	38
3.5.3	Ablation II: EPredictor Architecture & CPMW . . . . .	39
3.6	Summary . . . . .	41
3.7	Outlook . . . . .	41
<b>4</b>	<b>Multimodal Sequence Modeling for Error Pattern Classification</b>	<b>43</b>
4.1	Introduction . . . . .	43
4.2	Related Work . . . . .	44
4.2.1	Failure Detection in Vehicles . . . . .	44
4.2.2	Multimodal Fusion & Learning . . . . .	44
4.3	Dataset Extension with Environmental Conditions . . . . .	46
4.3.1	Integration . . . . .	46
4.4	BiCarFormer . . . . .	48
4.4.1	DTC Embeddings . . . . .	48
4.4.2	Positional Embeddings . . . . .	48
4.4.3	Environmental Embeddings . . . . .	48
4.4.4	Co-attention for Vehicle Event Sequences . . . . .	49
4.4.5	Multimodal Learning . . . . .	51

4.5	Experiments . . . . .	51
4.5.1	Settings . . . . .	51
4.5.2	Metrics . . . . .	52
4.5.3	Multi-label Classification Performance Analysis . . . . .	52
4.5.4	Cross-Attention Scores Interpretations . . . . .	53
4.5.5	Error Pattern in Battery Electric Vehicles . . . . .	55
4.6	Applications to Downstream Tasks . . . . .	56
4.7	Summary . . . . .	57
4.8	Outlook . . . . .	57
<b>II Understanding Causal Structures in High-Dimensional Event Sequences</b>		<b>59</b>
<b>5</b>	<b>Foundations of Causal Discovery and Information Theory</b>	<b>61</b>
5.1	Information Theory . . . . .	61
5.1.1	Marginal, Conditional, and Relative Entropy . . . . .	61
5.1.1.1	Definitions . . . . .	61
5.1.1.2	Properties . . . . .	62
5.1.2	Mutual Information and its variants . . . . .	63
5.1.2.1	Definitions . . . . .	63
5.1.2.2	Properties . . . . .	64
5.2	Graphical Models . . . . .	64
5.2.1	Bayesian Networks . . . . .	64
5.2.1.1	Motivation . . . . .	64
5.2.1.2	Definitions . . . . .	64
5.3	Tasks . . . . .	65
5.3.1	Causal Discovery . . . . .	65
5.3.1.1	Assumptions . . . . .	66
5.3.1.2	Classes of Causal Discovery Algorithms . . . . .	66
5.3.2	Multi-Label Causal Discovery . . . . .	67
5.3.3	Evaluation Metrics for Multi-Label Causal Discovery . . . . .	68
5.3.3.1	Set-Based Metrics . . . . .	68
5.3.4	Evaluation Metrics for Event-to-Event Causal Discovery . . . . .	68
5.3.5	Structural Hamming Distance (SHD) . . . . .	68
<b>6</b>	<b>Sample-Level Multi-Label Causal Discovery</b>	<b>69</b>
6.1	Introduction . . . . .	69
6.2	Related Work . . . . .	70
6.2.1	Neural Autoregressive Density Estimation . . . . .	70
6.2.2	Transformers as Causal Learners . . . . .	71
6.2.3	Multi-label Causal Discovery . . . . .	71
6.3	Methodology . . . . .	71
6.3.1	Autoregressive Event Sequence Models. . . . .	71

6.3.2	Assumptions . . . . .	72
6.3.3	Lemmas . . . . .	73
6.3.4	Conditional Mutual Information Estimation via Autoregressive Models . . . . .	74
6.3.5	Sequential Markov Boundary Recovery . . . . .	76
6.3.6	Computation . . . . .	77
6.4	Causal Indicator . . . . .	79
6.5	Empirical Evaluation . . . . .	79
6.5.1	Settings . . . . .	79
6.5.2	Vehicle Event Sequences Dataset . . . . .	79
6.5.3	Comparisons . . . . .	80
6.5.4	Results . . . . .	80
6.6	Limitations . . . . .	81
6.7	Summary . . . . .	83
6.8	Outlook . . . . .	83
<b>7</b>	<b>Population-Level Multi-Label Causal Discovery</b>	<b>85</b>
7.1	Introduction . . . . .	85
7.2	Related Work . . . . .	85
7.3	Methodology . . . . .	87
7.3.1	Structural Fusion of Markov Boundaries . . . . .	87
7.3.2	Aggregation under imperfect CI-tests . . . . .	88
7.3.3	Adaptive Fusion for Structural Discovery in Long-Tail Distributions . . . . .	89
7.4	Empirical Evaluation . . . . .	90
7.4.1	Benchmark Against Multi-Label Causal Discovery Methods . . . . .	90
7.4.2	Ablation on Aggregation Criteria for Phase 2 . . . . .	91
7.5	Summary . . . . .	92
7.6	Outlook . . . . .	92
<b>8</b>	<b>Sample-Level Event-to-Event Causal Discovery</b>	<b>93</b>
8.1	Introduction . . . . .	93
8.2	Related Work . . . . .	94
8.2.1	Causal Discovery in Event Sequences . . . . .	94
8.3	Methodology . . . . .	95
8.3.1	Data-Generating Process . . . . .	95
8.3.2	Sample-Level Causality . . . . .	96
8.3.3	Summary-Level Causality . . . . .	96
8.3.4	Autoregressive Density Estimation . . . . .	97
8.3.5	Assumptions . . . . .	97
8.4	Single Stream Causal Discovery . . . . .	98
8.4.1	Conditional Mutual Information . . . . .	98
8.4.2	Estimation and Approximation Error . . . . .	99
8.4.3	Identifiability . . . . .	101
8.4.4	Lagged Effects via Simulated Interventions . . . . .	102

8.5	Algorithm: Parallel Causal Discovery . . . . .	103
8.5.1	Scalability of TRACE . . . . .	104
8.6	Experiments . . . . .	105
8.6.1	Settings . . . . .	105
8.6.2	Comparative Analysis . . . . .	106
8.6.3	Scalability and Robustness Analysis . . . . .	106
8.6.4	Application to Vehicles Diagnostics . . . . .	109
8.7	Limitations . . . . .	109
8.7.1	Causal Sufficiency . . . . .	110
8.7.2	Temporal Precedence & Instantaneous Effects . . . . .	110
8.7.3	Consistency Through Time . . . . .	111
8.7.4	Amortization . . . . .	111
8.8	Summary . . . . .	111
8.9	Outlook . . . . .	112
<b>III From Causal Discovery to Automated Reasoning</b>		<b>115</b>
<b>9</b>	<b>Multi-Agent Causal Reasoning System for Error Pattern Automation</b>	<b>117</b>
9.1	Introduction . . . . .	117
9.2	Related Work . . . . .	119
9.2.1	Multi-Agent Fault Diagnosis . . . . .	119
9.2.2	Error Pattern Rule Automation . . . . .	119
9.3	Methodology . . . . .	120
9.3.1	Causal Discovery . . . . .	120
9.3.2	Contextual Information . . . . .	122
9.4	Experiments . . . . .	122
9.4.1	Evaluation Metrics . . . . .	122
9.4.1.1	Structural Evaluation . . . . .	123
9.4.1.2	Semantic Evaluation . . . . .	123
9.4.2	Settings . . . . .	123
9.4.3	Comparison . . . . .	123
9.4.4	Results . . . . .	124
9.5	Summary . . . . .	125
9.6	Outlook . . . . .	126
<b>10</b>	<b>Conclusion and Outlook</b>	<b>131</b>
10.1	Conclusion . . . . .	131
10.2	Outlook . . . . .	133
10.2.1	Toward a Unified Causal Graph over Events and Outcomes . . . . .	133
10.2.2	Toward Multimodal and Multi-Resolution Causal Discovery . . . . .	134
10.2.3	Unseen Domain and Continuous Learning . . . . .	134
10.2.4	Industrial Foundation Models . . . . .	135

<b>List of Figures</b>	<b>137</b>
<b>List of Tables</b>	<b>143</b>
<b>Bibliography</b>	<b>145</b>
<b>A Appendix of Part I</b>	<b>167</b>
A.1 Error Pattern Prediction . . . . .	167
A.1.1 Multivariate Hawkes Process Log-likelihood Derivation . . . . .	167
A.1.2 CarFormer Pretraining Details . . . . .	167
A.1.3 Models Definition . . . . .	168
A.1.4 Random Event Injection . . . . .	168
A.2 Multimodal Error Pattern Offline Prediction . . . . .	169
<b>B Appendix of Part II</b>	<b>171</b>
B.1 Sample-Level Multi-Label Causal Discovery . . . . .	171
B.1.1 PyCausalFS . . . . .	171
B.1.2 MI-MCF . . . . .	171
B.1.3 NADEs Quality. . . . .	171
B.1.4 Sampling Procedure for CMI . . . . .	171
B.1.5 Sampling Number . . . . .	173
B.1.6 Dynamic Thresholding . . . . .	173
B.1.7 Figures . . . . .	174
B.1.7.1 Explanation Examples . . . . .	174
B.1.8 Implementation of OSCAR . . . . .	175
B.2 Population-Level Multi-Label Causal Discovery . . . . .	178
B.2.1 Definition of Scoring Criteria . . . . .	178
B.2.2 Criteria . . . . .	178
B.2.3 Frequency . . . . .	178
B.2.4 Expected FPR Adjustment . . . . .	178
B.2.5 Mutual Information . . . . .	179
B.2.6 Implementation of Phase 2 . . . . .	180
B.3 Sample-Level Event-to-Event Causal Discovery . . . . .	182
B.3.1 Flexible Assumptions . . . . .	182
B.3.2 Evaluation . . . . .	182
B.3.3 Additional Ablations . . . . .	183
B.3.3.1 Number of Particles $N$ . . . . .	183
B.3.3.2 Empirical Validation of $\epsilon$ -Strong Faithfulness. . . . .	183
B.3.3.3 Scaling Law for Causal Identifiability . . . . .	184
B.3.4 Additional Summary Causal Graph . . . . .	184
B.4 CAREP: Multi-Agent System for Automatic Rule Generation . . . . .	184
B.4.1 Input Format . . . . .	184

# Glossary

CAREP	<u>C</u> ausal <u>A</u> utomated <u>R</u> easoning for <u>E</u> rror <u>P</u> attern, a multi-agent system for automated error rule generation. iii, 10, 117, 132
CARGO	<u>C</u> ausal <u>A</u> ggregation via <u>R</u> obust <u>G</u> raph <u>O</u> perations, a scalable multi-label causal discovery framework designed to construct global causal structures from a batch of high-dimensional event sequences. 7, 85
CML	Causal Machine Learning is a field of machine learning that learns cause-and-effect relationships in data to improve robustness of machine learning models (intervention, counterfactual, causal graphs). 4, 118
DNN	Deep Neural Networks, neural network architectures comprising multiple layers of parameterized transformations, enabling the hierarchical learning of representations from raw data. 1
DTC	Diagnostic Trouble Code, standardized codes generated by a vehicle's electronic control unit to indicate a precise event within the vehicle (malfunctions, software update, ...). iii, 4, 25
ECU	Electronic Control Unit, embedded system controlling one or more electrical systems or subsystems in a vehicle. iii, 1, 25
EP	Error Pattern, a higher-level abstraction of DTC sequences defined by domain experts to characterize specific vehicle faults using Boolean rules, example shown in Fig. 9.1. 1, 25, 26
LLM	Large Language Model refers to a Transformer model with billions of parameters, typically trained via self-supervised learning objectives on a large-scale text corpora. iii, 1, 4, 113, 117
NADE	A Neural Autoregressive Density Estimator is an autoregressive model that factorizes the joint distribution over a sequence into a product of conditionals, each parameterized by a neural network. 7, 69, 70

## Contents

NLP	Natural Language Processing, the study of computational techniques for processing human language. 20
OSCAR	<u>One-Shot Causal AutoRegressive Discovery</u> is a causal discovery method described in Chapter 6 that infers a directed acyclic graph representing events-to-outcome relationships from a single sequence of events leading to outcomes. 7, 85
RAG	Retrieval-Augmented Generation is a technique that improves the accuracy of the LLM answers by allowing the model to access and cite external data sources before generating a response. 4, 118
TPP	Temporal Point Process, a stochastic process used to model sequences of discrete events over continuous time. 32, 112
TRACE	<u>Temporal Reconstruction via Autoregressive Causal Estimation</u> is a causal discovery method described in Chapter 8 that infers a summary and instance-time causal graph [6] from a single sequence of discrete events. 9

# Notations

We summarize the notation used throughout this thesis here. We followed the standard notation from *Deep Learning* [42] available at [https://github.com/goodfeli/dlbook\\_notation/](https://github.com/goodfeli/dlbook_notation/)

## Numbers and Arrays

$a$	A scalar (integer or real)
$\mathbf{a}$	A vector
$\mathbf{A}$	A matrix
$\mathcal{A}$	A tensor

## Sets and Graphs

$\mathbb{A}$	A set
$\mathcal{X}$	An alphabet
$\mathbb{R}$	The set of real numbers
$\{0, 1\}$	The set containing 0 and 1
$\{0, 1, \dots, n\}$	The set of all integers between 0 and $n$
$[a, b]$	The real interval including $a$ and $b$
$(a, b]$	The real interval excluding $a$ but including $b$
$\mathbb{A} \setminus \mathbb{B}$	Set subtraction, i.e., the set containing the elements of $\mathbb{A}$ that are not in $\mathbb{B}$
$\mathcal{G}$	A graph
$\mathcal{D}$	A dataset
$Pa_{\mathcal{G}}(X_i)$	The parents of $X_i$ in $\mathcal{G}$

## Probability and Information Theory

$X$	A discrete random variable with alphabet $\mathcal{X}$
$X_t$	A random variable referred to as an event occurring at a time step $t$ in a sequence
$x_t$	A realization of a random variable at a time step $t$
$Y$	A discrete random variable characterizing an outcome or a label (e.g., an error pattern) drawn from $\mathcal{Y}$
$\mathbf{X} = \{X_1, \dots, X_n\}$	A set of discrete random variables
$P(X)$	A probability distribution over a discrete random variable $X$
$P_\theta(X)$	A probability distribution parametrized by $\theta$ , e.g., a pre-trained model
$\hat{P}(X)$	A probability distribution over a discrete random variable $X$ estimated empirically based on a data sample
$p(x)$	The probability mass function for the random variable, $X$ i.e., $p(x) = P(X = x), x \in \mathcal{X}$ . We denote $p(x)$ instead of $p_X(x)$ for convenience
$X \sim P$	Random variable $X$ has distribution $P$
$\mathbb{E}_{p(x)}[f(X)]$ or $\mathbb{E}f(X)$	Expectation of $f(X)$ with respect to $P(X)$
$\text{Var}(f(X))$	Variance of $f(X)$ under $P(X)$
$H(X)$	Entropy of the random variable $X$
$D_{\text{KL}}(P  Q)$	Kullback-Leibler divergence of $P$ and $Q$
$\mathcal{N}(\mathbf{x}; \boldsymbol{\mu}, \boldsymbol{\Sigma})$	Gaussian distribution over $\mathbf{x}$ with mean $\boldsymbol{\mu}$ and covariance $\boldsymbol{\Sigma}$

## Functions

$f : \mathcal{A} \rightarrow \mathcal{B}$	The function $f$ with domain $\mathcal{A}$ and range $\mathcal{B}$
$\log x, \ln x$	Natural logarithm of $x$ , we follow the convention that $\ln x = \log x$
$\sigma(x)$	Logistic sigmoid, $\frac{1}{1+\exp(-x)}$

# 1 Introduction

The increasing digitization of modern vehicles has transformed automotive systems into complex, interconnected networks of electronic control units (ECUs) continuously generating streams of Diagnostic Trouble Codes (DTCs). Each vehicle now asynchronously produces thousands of discrete events that document the behavior and health of its subsystems. These data consist of vast collections of sequences, each containing hundreds of events drawn from a large vocabulary of unique codes, effectively forming high-dimensional datasets. For decades, automotive manufacturers have relied on domain experts to manually analyze these codes and define higher-level Boolean rules called Error Patterns (EPs) to characterize system faults and ensure safety. However, with the increasing complexity of vehicles and the proliferation of embedded software, this manual process has become prohibitively expensive, time-consuming, and error-prone. This challenge illustrates a broader industrial problem: how can we automatically learn, understand, and reason about event-driven systems? The answer is not merely one of prediction, but of understanding why events occur and how they interact with each other, thereby transforming data-driven systems into explainable and autonomous diagnostic agents.

Over the past decade, the rise of Deep Neural Networks (DNNs) has profoundly reshaped the landscape of artificial intelligence. From image recognition to speech understanding, their ability to model complex, nonlinear relationships has led to significant progress across multiple fields. Among these advances, Transformer architectures have become the cornerstone of modern deep learning, spanning vision, audio, and sequence modeling. They underpin the development of Large Language Models (LLMs) that excel not only at compressing vast textual corpora but also at exhibiting emergent induction mechanisms. Beyond a certain scale of parameters, training data, and with appropriate fine-tuning, LLMs appear to exhibit remarkable reasoning capabilities. Additionally, language models embody a general principle: sequences, whether words, medical signals, or machine events, encode meaning through their temporal structure. This observation opens a new research frontier, extending the power of language modeling to machine-generated data in industrial settings. In such domains, event logs, sensor readings, medical test results, or diagnostic codes constitute a machine-generated “language” through which complex systems express their internal state. By interpreting this language, deep learning models can uncover hidden patterns of operation, anticipate failures before they occur, and even infer causal relationships within large-scale systems. The same architectures that revolutionized natural language processing now hold the potential to transform how industries understand, monitor, and reason about the behavior of complex machines.

## 1.1 From Industrial Challenge to Scientific Question

The automotive industry presents one of the most demanding real-world contexts for developing such intelligent systems. Vehicles must be safe, reliable, and explainable, yet their internal states are observed indirectly through asynchronous, heterogeneous, and noisy event logs. Traditional statistical and rule-based approaches struggle to capture the rich dependencies underlying these sequences; they remain applicable only when the event vocabulary is small and sequences are short. Additionally, diagnostic data exhibits all the hallmarks of complex event-driven domains: extremely high cardinality of event types, sparse temporal observations, and a high degree of redundancy. It is essential to develop techniques that not only anticipate such events but also explain their underlying causal mechanisms. These characteristics make automotive diagnostics an ideal testbed for advancing machine learning at scale, particularly in event-sequence modeling, multimodal learning, causal discovery, and multi-agent systems. What begins as a challenge in fault detection thus becomes a general scientific endeavor: building models that not only predict, but also explain and reason over sequences of events.

## 1.2 Research Areas, Challenges and Open Problems

This thesis builds upon the convergence of three complementary research areas:

**Sequence Modeling** Modern language models have demonstrated remarkable ability to capture long-range dependencies and contextual relations in structured sequences. Beyond their success in natural language, they establish a general and practical paradigm: training a model on a large-scale, self-supervised task such as next-token prediction, and then adapting it to downstream applications where labeled data are scarce.

In contrast, machine-generated data in complex systems such as vehicles, aircraft, hospitals, or computer networks is inherently noisy, repetitive, and scattered across time. Vehicle diagnostic logs, for instance, comprise tens of thousands of distinct DTCs, each irregularly triggered by sensor anomalies, environmental fluctuations, or transient software behavior. Similar challenges arise in other domains: sequences of electrocardiogram spikes or clinical events in healthcare, network intrusions and security alerts in cybersecurity, flight logs in aeronautics, and transactional traces in finance—all of which consist of heterogeneous event streams. These data are often non-stationary, dominated by repetitive or redundant events, and corrupted by noise or incomplete information, which makes it difficult for classical methods to extract stable temporal dependencies or causal relations.

Modeling such event sequences with modern sequence models, such as Transformers [150], offers a powerful alternative. Their self-attention mechanism enables the capture of long-range dependencies, modeling of multiscale temporal dynamics, and integration of heterogeneous modalities, such as sensor readings, timestamps, and textual metadata, through fusion mechanisms. Despite these advantages, the use of autoregressive and bidirectional Transformers for machine-generated event data, particularly in

automotive diagnostics, remains underexplored. In addition, the applicability of Transformers to prognosis and long-horizon forecasting in event-driven systems remains poorly studied.

**Causal Discovery in Event Sequences** Predictive accuracy alone is insufficient in safety-critical domains. To truly anticipate failures, prevent accidents, or mitigate risks, one must understand *why* events occur and how they influence one another. This is the central goal of causal discovery: recovering, from observational data, the underlying mechanisms that generate the observed phenomena. In practice, this involves learning a compact Directed Acyclic Graph (DAG) that captures direct causes, mediating effects, and potential confounders influencing an outcome such as a vehicle defect or a disease. Once established, this DAG can be used to perform causal inference, i.e., to answer counterfactual questions such as 'what if' or to measure the average causal effect of a variable on the outcome.

In event-driven domains, causal discovery becomes particularly intricate. Unlike static cross-sectional data or regularly sampled time series, event sequences are asynchronous, irregularly spaced, and highly context-sensitive. In these settings, the causal effect of an event is not fixed; it may vary significantly depending on its precise timing, its position within a sequence, and its co-occurrence with other markers. In general, two main perspectives emerge. The first, events-to-outcome causal discovery (or multi-label causal discovery), seeks to identify which events or combinations thereof cause a higher-level outcome, such as a disease from symptoms, a security breach from system alerts, or an EP from DTCs. The second, event-to-event causal discovery, focuses on uncovering causal influences between events themselves, forming the basis for understanding asynchronous system behavior and performing root-cause analysis.

Traditional causal discovery methods, such as constraint-based algorithms (PC [139]), score-based optimization (GES [21]), and functional causal models (LiNGAM [133]), are ill-suited to this setting. They typically assume low-dimensional variables. When applied to high-dimensional sequences with thousands of discrete event types, long temporal dependencies, and intense noise, these methods quickly become intractable due to their computational complexity and statistical assumptions. Even recent approaches for time series and event sequences (THP [179], SHTP [118], CAUSE [173], CASCADE [24]) are applied to dozens or, at most, a hundred variables on short sequences which is not applicable in many scenarios. In practice, they fail to scale, restricting their applicability in industrial contexts where datasets are both massive and heterogeneous. As a result, the field of causal discovery in large-scale event sequences remains largely underexplored. Practical adoption is hindered by three central challenges: (1) the combinatorial explosion of possible event interactions, (2) the lack of scalable, GPU-compatible algorithms, and (3) the absence of production-ready methods that reuse pre-existing architectures for inference, like Transformers or other autoregressive models. As a consequence, practitioners are seeking automated solutions to identify causal relationships in high-dimensional sequence datasets in a reasonable amount of time, leveraging existing pretrained sequence models. In the automotive domain, EPs are defined as deterministic

## 1 Introduction

Boolean rules that encode causal relationships between DTCs. By reinterpreting these rules as a causal discovery problem, it becomes possible to identify potential causes as DTCs for unknown EPs and hence create new rules based on the DTCs as causes of an EP.

**Automated and Explainable Reasoning Systems** Beyond discovering causal relations, the ultimate goal in industrial AI is to enable autonomous reasoning over complex automation tasks. Such a system can not only infer causal structures but also explain, justify, and act upon them to automate manual processes. While causal discovery provides the skeleton of knowledge, it often remains abstract, numerical, or incomplete. Such causal graphs must be translated into interpretable reasoning chains that domain experts can trust and validate. This requires bridging two complementary worlds: data-driven inference from causal discovery algorithms and domain knowledge. Recent advances in LLMs have opened new possibilities for reasoning, automation, and the integration of external knowledge to form intelligent systems. These models can process both structured and unstructured information, including textual descriptions, metadata, documentation, and relational rules, either directly in the prompt (in-context learning) or via retrieval-augmented generation (RAG), making them ideal candidates for reasoning over causal evidence. Yet, using LLMs alone remains insufficient: without grounding in causal structure or domain constraints, they may hallucinate or reason inconsistently. Conversely, causal discovery methods alone provide semantic knowledge but lack the adaptability of LLMs.

This gap motivates a hybrid paradigm that combines the structured and principled outputs of causal discovery algorithms with the natural-language reasoning capabilities of LLMs, often referred to as Causal Machine Learning (CML). By organizing these components into multi-agent systems, each agent can specialize in one task. One inferring causal dependencies, another contextualizes them using metadata and textual descriptions. The result is a collaborative reasoning process where causal evidence is grounded, verified, and articulated in human-readable form. In the automotive industry, they could automatically generate interpretable Boolean rules that describe how diagnostic events combine to form EPs. These rules, which currently require extensive manual expert labor, could then be fully automated. More broadly, multi-agent systems powered by causal discovery could be extended to any domain where reducing LLMs' hallucinations and increasing interpretability are essential, from medical diagnostics and industrial health monitoring to cybersecurity incident analysis.

## 1.3 Contributions

The contributions of this thesis can be summarized as follows.

### 1.3.1 Predictive Sequence Modeling of Vehicle Diagnostics

In the first contribution of this thesis, we explore how modern sequence models can anticipate system failures in vehicles before they occur [91].

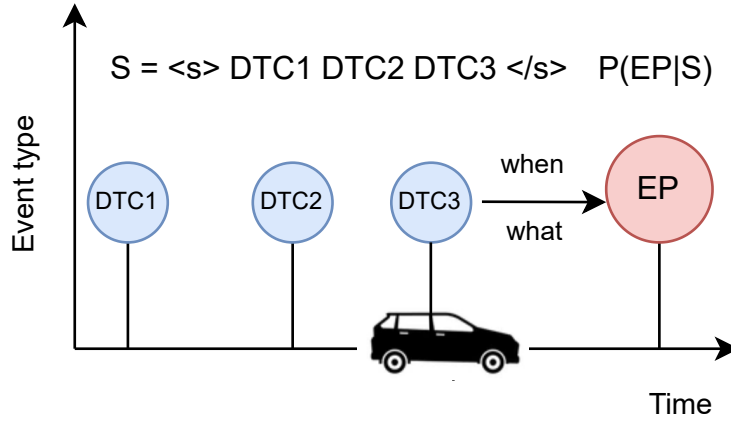


**Figure 1.1: Error Pattern Prediction (when and what).** Based on the past sequence  $S$  of diagnostic trouble codes (DTCs), manufacturers want to prevent error patterns (EPs) from happening by predicting their likelihood and time of occurrence.

**Autoregressive Transformers for Vehicle Event Sequences** We draw an analogy between natural language and vehicular diagnostic data: just as words that form structured sentences convey meaning, DTCs form spatio-temporal sequences encoding the vehicle’s state at each mileage and time. This analogy motivates the use of Transformer-based language models for automotive fault prediction. To this end, we introduce two autoregressive Transformer architectures [150]:

- **CarFormer**, designed to model the generative process of DTC sequences by predicting the following DTC and its time of occurrence.
- **EPredictor**, which extends this formulation to EPs by jointly predicting *what* EP will occur and *when*, given a history of observed DTCs.

Together, these models learn to anticipate vehicle faults in an autoregressive manner, providing both event type and time of occurrence. Despite the complex data distribution of a stochastic process such as the DTCs and EPs appearance, their high event-type cardinality ( $> 10^4$ ), irregular sampling, and unbalanced label distributions, they demonstrate robust performance across multiple metrics, outperforming the classical autoregressive Transformer model. In particular, they could anticipate a given EP appearance with 80% F1-score within an interval of  $58.4 \pm 13.2\text{h}$  when predicting the time of occurrence.

**Predictive Maintenance Metric for Autoregressive Models** We introduce the Confident Predictive Maintenance Window (CPMW), a novel evaluation protocol that measures how early in an observed sequence of events (DTCs) a model can issue a confident outcomes (EPs) prediction. Unlike accuracy-at-end-of-sequence metrics, CPMW

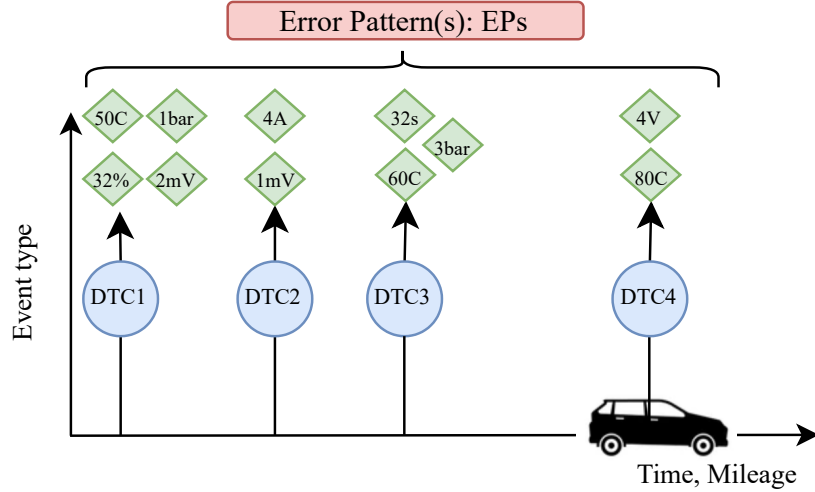


**Figure 1.2: Error Pattern Prediction using Multimodal Sequences.** Past diagnostic trouble codes only provide limited information about complex and overlapping error patterns. In addition, domain experts rely on environmental conditions (e.g., temperature, voltage, humidity, ...) to identify more accurately error patterns.

rewards early, high-confidence predictions, directly reflecting the operational value of predictive maintenance.

**Offline Error Pattern Prediction using Multimodal Learning** While modern diagnostic systems primarily rely on sequences of vehicular DTCs, they overlook valuable contextual information such as raw sensory data (e.g., temperature, humidity, and pressure) known as environmental conditions. Experts often use such sensory information to separate overlapping EPs that might share the same DTCs in their Boolean rule definition. To this end, we introduce **BiCarFormer**, a bidirectional multimodal Transformer that integrates environmental sensor data with DTC sequences. Through special fusion mechanisms, BiCarFormer learns interdependencies between discrete diagnostic events and environmental conditions, improving predictive performance compared to standalone bidirectional Transformers (+9% precision on average) and enabling more interpretable predictions through attention scores interpretation.

### 1.3.2 Multi-Label Causal Discovery in High-Dimensional Event Sequences

In the second part of this thesis, we move from predicting events to understanding why they occur. While the introduced autoregressive models capture the temporal regularities of diagnostic sequences, they remain fundamentally correlational. We introduce two causal discovery framework for discrete sequences, each one targeting *sample-* and *population-level*, that is, discovering causal relationships on respectively one sequence or a multitude.

**Sample-Level** To address this challenge, we introduce OSCAR (One-Shot Causal AutoRegressive discovery). OSCAR identifies, for each outcome label, the minimal set of causal events (the so-called Markov Boundary) directly from a single observed sequence, as formalized in Table 1.1. We refer to this regime as sample-level causal discovery throughout this thesis to emphasize the key property: the causal graph is inferred from and specific to one individual sequence, without requiring a population of observations<sup>1</sup>. OSCAR reuses the pretrained autoregressive Transformers from Part I as neural autoregressive density estimators (NADEs) to estimate the conditional mutual information (CMI) between events and labels given the past events. They quantify the extent to which each event contributes to a future outcome. This formulation enables efficient, GPU-parallelized computation of causal dependencies. Theoretically grounded under standard assumptions, we show that OSCAR recovers the Markov Boundaries of each label within an associated Bayesian Network [69]. In practice, it also introduces causal indicators that distinguish excitatory and inhibitory effects between events, offering a more nuanced view than deterministic causal graphs [67].

We validate OSCAR on a large-scale vehicular dataset comprising over tens of thousands of DTCs and hundreds of Error Patterns (EPs). Classical constraint-based causal discovery methods fail to scale beyond a few hundred variables whereas OSCAR successfully identifies meaningful causal relations between DTCs and EPs, revealing interpretable causal structures for phenomena such as steering wheel degradation or battery power limitation (Fig. 1.3). In summary, the key contributions of OSCAR are as follows:

- **Sample-level Multi-Label Causal Discovery**, recovering the Markov Boundary of each outcome label from a single observed sequence without requiring a population of observations.
- **NADEs** reuse, repurposing pretrained autoregressive Transformers as neural autoregressive density estimators for conditional mutual information estimation, establishing a formal bridge between Parts I and II of this thesis.
- **Causal indicators**, annotating each discovered dependency with a signed measure of excitatory or inhibitory influence, going beyond binary edge presence.
- **Extreme-scale**, handling 29,100 event types and 474 outcome labels simultaneously a regime where classical constraint-based methods fail entirely.

**Population-level** While OSCAR performs causal discovery at the level of individual sequences (sample-level), real-world systems demand a broader perspective: understanding global causal relationships across the entire observational dataset (population-level). To address this, we introduce CARGO (Causal Aggregation via Robust Graph Operations), a scalable framework that merges sample-level causal graphs into a unified global representation. CARGO treats causal discovery as a two-phase process. In the first phase,

---

<sup>1</sup>This terminology supersedes the label 'one-shot' used in the associated conference publications [93, 89], where 'one-shot' was used informally to mean 'from a single sequence'.

## 1 Introduction

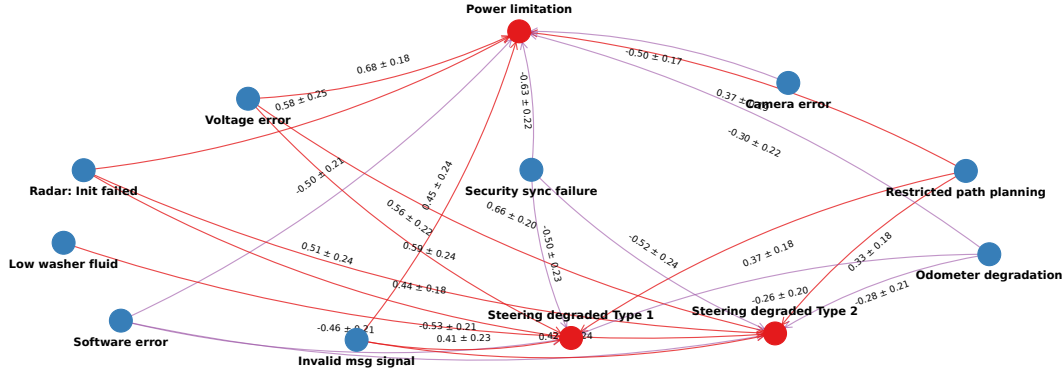


**Figure 1.3: Anonymized Causal Graph.** Example of a sequence of events (DTCs) that lead to a steering wheel degradation and a power limitation as outcome labels. The causal indicators are shown in violet if inhibitory and orange or red if excitatory, depending on the magnitude. The voltage error DTC is the biggest causal driver for the power limitation EP while the security sync failure seems to have the biggest inhibitory effect on all EP.

OSCAR extracts sample-level causal graphs. In the second phase, CARGO aggregates these causal graphs based on the frequencies of edge appearances across labels using a novel adaptive frequency-based fusion strategy. Motivated by long-tail distributions in labeled data, the edges are retained based on their frequency of appearance and the number of available samples per label. This aggregation process enables the recovery of global Markov Boundaries for each label while filtering out spurious relations caused by noise, sparsity, or rare events. Empirical evaluation demonstrates that CARGO not only scales where classical algorithms fail, but also increases the accuracy and recall compared to using OSCAR alone. The ablation studies confirm the robustness of its aggregation phase across multiple thresholding and scoring strategies. In summary:

- **Adaptive frequency-based fusion**, aggregating sample-level graphs into a global structure via a label-frequency-aware thresholding strategy motivated by the long-tail distribution of EP samples.
- **Linear scalability**, processing 300,000 sequences with 29,100 event types on modern GPUs where quadratic constraint-based methods fail.
- **Global Markov Boundary recovery**, with theoretical guarantees under mild assumptions.

### 1.3.3 Scalable Sample-Level Causal Discovery in Event Sequences

Multi-label causal discovery methods are limited to local structure learning, ignoring the dense information of inter-event dependencies. To fully diagnose complex phenomena like cascading vehicle failures, we must recover the complete causal graph. This presents a significantly more challenging scenario due to the combinatorial explosion of possible

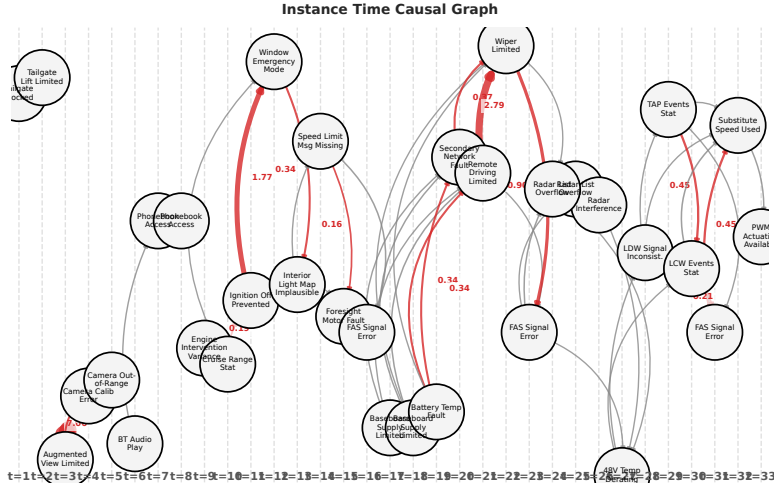


**Figure 1.4: Anonymized Instance-Time Causal Graph for Diagnostic Defect Cascade.** Temporal evolution of a diagnostic defect cascade in a vehicle ( $|\mathcal{X}| \approx 29, 100$ ). TRACE effectively captures causal relationships, revealing distinct **error clusters** at different time steps (e.g., initial sensor failures at  $t = 3$  triggering mechanical faults at  $t = 12$ , battery at issue  $t = 17$ ). This enables actionable root-cause analysis by isolating the specific onset of a failure mechanism and its strength using the conditional mutual information.

edge connections, as opposed to simple events-to-outcome relationships. We therefore introduce TRACE (Temporal Reconstruction via Autoregressive Causal Estimation), a framework that uses the density estimation capabilities of autoregressive models to recover the causal graph from a single sequence. By treating the event stream as a high-order Markov chain, TRACE employs an autoregressive model to perform scalable conditional independence testing via its learned distributions. TRACE inherits OSCAR’s linear scalability with the vocabulary size, extending it to event-to-event dependencies. Our results show that causal structure becomes identifiable well before the autoregressive model fully converges during the pretraining. In summary:

- **Sample-Level Event-to-Event Causal Discovery**, we propose TRACE, to the best of our knowledge, the first framework designed to recover the summary causal graph from a single high-dimensional sequence by amortizing the learning of dynamics via a pre-trained AR model. This addresses a substantially underexplored area in causal discovery.
- **Backbone Agnosticism**, the framework strictly decouples *density estimation* (Phase 1) from *causal discovery* (Phase 2). Consequently, TRACE can leverage any state-of-the-art autoregressive backbone (e.g., Transformers, Mamba, RNNs).
- **Linear Complexity in High Dimensions**, TRACE scales linearly with the vocabulary size, bypassing the combinatorial explosion of constraint-based structural learning.

Causal Scope	Events-to-Outcome (DTCs $\rightarrow$ Error Pattern)	Event-to-Event (DTCs $\rightarrow$ DTCs)
Sample-Level (Single Sequence)	<p><b>OSCAR</b></p> <p>One-Shot Multi-Label Causal Discovery</p> <p>Markov Boundary per label from a single sequence</p> <p><i>Chapter 6</i></p>	<p><b>TRACE</b></p> <p>Scalable Amortized Causal Discovery</p> <p>Instance-time causal graph from a single sequence</p> <p><i>Chapter 8</i></p>
Population-Level (Full Dataset)	<p><b>CARGO</b></p> <p>Graph Aggregation for Causal Discovery</p> <p>Global Markov Boundaries via adaptive graph fusion</p> <p><i>Chapter 7</i></p>	<p><b>Open Problem</b></p> <p>Population-level summary causal graph over event types/outcomes</p> <p>Requires aggregation of instance-time and summary graphs with acyclicity constraints</p> <p><i>Future work</i></p>

**Table 1.1: The four regimes of causal discovery in discrete event sequences**, defined by the cross-product of *causal scope* (single-sequence inference vs. population-level aggregation) and *dependency type* (events-to-outcome vs. event-to-event). The three shaded contributions of this thesis — **OSCAR**, **TRACE**, and **CARGO** — share a common backbone: pretrained autoregressive Transformers repurposed as neural autoregressive density estimators (NADEs) for conditional mutual information estimation. The remaining cell, population-level event-to-event discovery, constitutes an open problem and a direct avenue for future work.

- **Identifiability under Generative Approximation**, we theoretically establish that causal identifiability is achievable for any autoregressive model that sufficiently approximates the data-generating process. We derive error bounds for the identifiability, proving that the causal graph is recoverable up to a noise floor determined by the model’s convergence.
- **Real-World Applicability**, we empirically validate TRACE on synthetic structural causal models with challenging vocabulary, memory requirements, and apply it to vehicle diagnostic logs, demonstrating its practical utility in industrial settings.

### 1.3.4 Automated Causal Reasoning with Multi-Agent Systems for Error Pattern Rule Automation

To fully automate the construction of EPs, we introduce CAREP for Causal Automated Reasoning for Error Patterns, a multi-agent system for the automatic synthesis of EP rules in high-dimensional automotive event sequences. It comprises three agents:

- a **Causal Discovery Agent** that estimates candidate causes and causal indicators for each unknown EP using OSCAR and CARGO,
- a **Contextual Information Agent** that incorporates DTC descriptions, known EP rules, and metadata to simulate expert knowledge,
- an **Orchestrator Agent** that coordinates the two agents to synthesize five plausible rules for these EPs, alongside a natural language explanation.

Through its agent-based design, CAREP translates causal evidence and contextual information into symbolic rules, along with their explanations, so that engineers can use them directly for vehicle fault analysis. To evaluate CAREP, we masked a random subset of the known rules and tested the framework’s ability to identify them. Results show that CAREP consistently outperforms LLM-only baselines by a large margin when reconstructing the rule, going up to 83% precision in recovering the correct elements in the rule, while offering interpretable explanations at scale.

Finally, the reuse of the same pretrained model, first as a predictor in Part I, then as a density estimator in Part II, and finally as the causal backbone of CAREP in Part III, forms the conceptual spine of the thesis and the unifying insight of this work.

### 1.3.5 Software

In addition to the theoretical, methodological and architectural contributions presented in this dissertation, a significant effort has been dedicated to practical and scalable software. The core algorithmic frameworks have been formalized and open-sourced as a Python library named `seq2cause` [87]<sup>2</sup>.

Released under the permissive MIT License and publicly available via the Python Package Index (PyPI), `seq2cause` provides a universal, plug-and-play pipeline designed to transform standard autoregressive sequence models such as Transformers into robust causal discovery frameworks. This software contribution not only ensures the reproducibility of the experiments detailed in the subsequent chapters but also equips the broader machine learning community with a practical, open-source implementation to uncover causal mechanisms in complex, event-driven systems.

---

<sup>2</sup><https://pypi.org/project/seq2cause/>

## 1.4 List of Publications

Most parts of this thesis have been published in the academic literature and presented at international conferences. The following list gives an overview of the publications:

### **Harnessing Event Sensory Data for Error Pattern Prediction in Vehicles: A Language Model Approach.**

[91] Hugo Math, Rainer Lienhart, Robin Schön, Proceedings of the AAAI Conference on Artificial Intelligence, vol. 39, no. 18, pp. 19423–19431, 2025, Philadelphia, USA, February 2025.

### **One-Shot Multi-Label Causal Discovery in High-Dimensional Event Sequences.**

[93] Hugo Math, Robin Schön, Rainer Lienhart, Conference on Neural Information Processing Systems (NeurIPS) Workshop 2025 on CauScien: Uncovering Causality in Science, San Diego, USA, December 2025.

### **Towards Practical Multi-label Causal Discovery in High-Dimensional Event Sequences via One-Shot Graph Aggregation.**

[89] Hugo Math, Rainer Lienhart, Conference on Neural Information Processing Systems (NeurIPS) Workshop 2025 on Structured Probabilistic Inference & Generative Modeling, San Diego, USA, December 2025.

### **Context-Informed Sequence Classification: A Multimodal Approach to Vehicle Diagnostics.**

[88] Hugo Math, Rainer Lienhart, International Conference on Learning Representations (ICLR) Workshop on Time Series in the Age of Large Models, April 2026.

### **Neuro-Symbolic Rule Discovery: Empowering LLMs with Causality for Vehicle Diagnostics.**

[92] Hugo Math, Julian Lorenz and Rainer Lienhart, International Conference on Learning Representations (ICLR) Workshop on Logical Reasoning of Large Language Models, April 2026.

### **TRACE: Scalable Amortized Causal Discovery from Single Sequences via Autoregressive Density Estimation (under review).**

[90] Hugo Math, Rainer Lienhart, under review at the International Conference on Machine Learning (ICML), Seoul, South Korea, *Available on arXiv:2602.01135*, July 2026.

## 1.5 Thesis Outline

This thesis is organized into three main parts. Part I (Chapters 2–4) establishes the modeling foundations. Chapter 2 provides background on event sequence modeling and Transformers. Chapters 3 and 4 present our predictive architectures for DTC sequences, evaluated on large-scale BMW data. Part II (Chapters 5–8) develops three causal discovery frameworks. Chapter 5 provides mathematical foundations. Chapters 6, 7, and 8 present OSCAR, CARGO, and TRACE respectively, with theoretical guarantees and scalability experiments. Part III (Chapters 9–10) moves from causal discovery to automated reasoning and introduces CAREP, a multi-agent system. The thesis concludes in Chapter 10 with a synthesis of the main findings and perspectives for future work. We summarize how predictive modeling, causal discovery, and automated reasoning can be unified into a coherent pipeline for scalable, interpretable diagnostics of vehicle error codes and patterns. Finally, we discuss open challenges and future directions.



## **Part I**

# **Predictive Sequence Modeling**



## 2 Foundations of Event Sequence Modeling

This chapter introduces the formal machinery used throughout the thesis: event sequence modeling, Transformer architectures, and evaluation metrics. We give a formal definition of a sequence of events and common ways of representing them. Then, we highlight challenges of traditional statistical methods and provide a brief introduction to Transformers [150, 26, 121]. We introduce their primary components: positional embedding techniques, feed-forward layers, layer normalization, and the attention mechanism. At the end of this chapter, we investigate various metrics for evaluating language model predictions in classification and regression.

### 2.1 Hawkes Processes

The Hawkes Process [53] has arguably been the most studied modeling technique for the occurrence of discrete events in a sequence, spanning financial and earthquake data [106, 73]. Its key property, the so-called *self-excitation*, is that the occurrence of one event may trigger a series of similar events. For instance, earthquakes trigger aftershocks, stock-market transactions may trigger a chain reaction, or a neuron fires and triggers brain activity elsewhere.

To do so, we model the number of event occurrences up to time  $t$  through a stochastic process  $N(t)$ . In some extensions of the basic Hawkes process, a random variable called a *mark*, which provides auxiliary information such as spatial coordinates or sensory measurements is attached to each event. In the automotive context, a vehicle generates a sequence of discrete events (DTCs), where each arrival is characterized by a timestamp  $t$  and a specific mileage  $m$  acting as the mark. Furthermore, we consider the multivariate setting where multiple Hawkes processes are *mutually exciting*: an occurrence in one event stream increases the probability of future occurrences in other streams. For example, in a social network, a message may trigger further messages from different users.

This cross-excitation is the fundamental mechanism explored in this work. However, scaling these models remains a challenge: when faced with thousands of distinct event types across numerous long sequences, how can we efficiently learn a robust model and reason about the underlying interactions? In Part I, we address the statistical and computational challenges of learning robust models from event sequences.

#### 2.1.1 Background

**Definition 1** (Counting Process). *A stochastic process  $N(t)$ , also noted  $N_t$ , defined for  $t \geq 0$ , is a counting process starting at  $N(0) = 0$  if  $N(t)$  only takes values in  $\{0, 1, 2, \dots\}$*

## 2 Foundations of Event Sequence Modeling

and increases in jumps of size  $+1$ . The random jump times  $t_1, t_2, \dots$  form a point process, with  $0 < t_1 < t_2 < \dots$  and  $t_0 \triangleq 0$ . The counting process can be defined in terms of the point process as:

$$N(t) = \sum_{i=1}^{\infty} \mathbb{I}\{t_i \leq t\} = \sum_{t_i \leq t} 1$$

The *point process* representation enables us to formally define a *marked event sequence* (Def. 3). Although event sequences can refer to multivariate time series as well [52], we abbreviate the term and refer solely to *event sequences* as a discrete sequence of events, such as:

**Definition 2** (Event Sequence). *Let each event be composed of a time of occurrence  $t \in \mathbb{R}^+$  and an event type  $x \in \mathcal{X}$  forming a pair  $(x, t)$ .  $\mathcal{X}$  is a finite set of discrete event types. A sequence of length  $L + 1$  is constructed with multiple pairs of events, such as  $S = \{(x_0, t_0), \dots, (x_L, t_L)\}$  where  $0 < t_1 < \dots < t_L$  with  $t_0 \triangleq 0$ .*

**Definition 3** (Marked Event Sequence). *A Marked Event Sequence is an event sequence (Def. 2) where each event  $x_i$  is augmented with a mark  $m_i \in \mathcal{M}$ . The event is then defined as a triple  $(x_i, t_i, m_i)$ .*

The inclusion of marks is mostly used in Part I and Part III when dealing with the mileage and other sensory or metadata information per event  $x_i$ .

**Definition 4** (Conditional Intensity Function). *The conditional intensity function of  $N(t)$  is defined, for  $t \geq 0$ , by*

$$\lambda^* \triangleq \lim_{\Delta \rightarrow 0} \frac{\mathbb{E}(N(t + \Delta) - N(t) | \mathcal{H}_t)}{\Delta}$$

if the limit exists. Here  $\mathcal{H}_t$  is the history of  $N(t)$  such that  $\mathcal{H}_t \triangleq \{(x_i, t_i) \in \mathcal{X} \times \mathbb{R}^+ | t_i < t\}$ .

**Remark 1.** *In the context of vehicle logs or manufacturing trajectories,  $S$  is a realization of a discrete-event stochastic process. While we acknowledge the Hawkes process framework common in the literature for modeling instantaneous rates as  $\lambda^*(t)$ , our primary interest lies in the conditional dependencies between the event types  $x$  within the sequence.*

### 2.1.2 Self-exciting property

Hawkes [53] defined the counting process (named after him) by specifying its conditional intensity process:

**Definition 5** (Hawkes Process). *A Hawkes process is a counting process  $N(t)$  whose conditional intensity process for  $t \geq 0$  is:*

$$\lambda^*(t) = \lambda + \sum_{t_i < t} \mu(t - t_i)$$

where  $\lambda > 0$  is a background arrival rate and  $\mu : \mathbb{R}^+ \rightarrow \mathbb{R}^+$  is the excitation function.

The excitation function  $\mu$  controls how past event occurrence will affect the rate of future occurrences. A common and simple excitation function is  $\mu(t) = \alpha \exp(-\beta t)$  (exponentially decaying intensity). In this case,  $(N(t), \lambda^*(t))$  is a *Markov process* [69] such that the current intensity  $\lambda(t)$  does not depend on the entire history of events.

### 2.1.3 Mutually Exciting Hawkes Processes

**Definition 6** (Mutually-Exciting Hawkes processes). *Consider  $\mathbf{N}(t) = (N^1(t), \dots, N^{|\mathcal{X}|}(t))$  as a collection of  $|\mathcal{X}|$  counting processes with  $N^k(t)$ 's occurrence times denoted as  $t_1^k, t_2^k$  etc. They are mutually-exciting Hawkes processes if  $N^k(t)$ 's conditional intensity follows:*

$$\lambda_k^*(t) = \lambda + \sum_{j=1}^{|\mathcal{X}|} \sum_{t_i^j < t} \mu_{j,k}(t - t_i^j) \text{ for } k = 1, \dots, |\mathcal{X}|$$

where  $\mu_{j,k}(s) \geq 0$

**Remark 2.** Denote the integrals of the  $\mu_{j,k}$  excitation functions as  $\phi_{j,k} = \int_0^\infty \mu_{j,k}(s) ds$  and the excitation matrix as  $\Phi = (\phi_{j,k}) \in \mathbb{R}^{|\mathcal{X}| \times |\mathcal{X}|}$ . The  $\Phi$  matrix is conventionally treated as an approximation of the causal adjacency matrix of a graph with  $|\mathcal{X}|$  nodes and is typically used to extract causal relationships [161]. The  $|\mathcal{X}|^2$  parameter count renders this approach computationally intractable in our high-dimensional regime. Part II adopts an alternative that avoids this bottleneck.

### 2.1.4 Limitations

**Number of parameters.** The  $N_t^j$  process has either an excitatory effect on  $N_t^k$  ( $\phi_{j,k} > 0$ ) or no effect on  $N_t^k$  ( $\phi_{j,k} = 0$ ) for  $j = k$  or  $j \neq k$ . Importantly, these processes have  $\mathcal{O}(|\mathcal{X}|^2)$  parameters to fit, which is often intractable in practice for many applications [73]. Moreover, the actual number of scalars being optimized in practice is more than  $|\mathcal{X}|^2$ , since there is the base intensity  $\lambda$ , the parameters of the excitation functions  $\mu$  (decay rates) and interaction magnitude. The literature often assumes  $|\mathcal{X}|^2 + |\mathcal{X}|$  [73].

**Optimization.** To understand why the Hawkes process is insufficient for our setting, we first show that the Maximum Likelihood Estimation (MLE) of its parameters is computationally intractable at scale. We therefore seek the parameters (base rate  $\alpha$ , decay  $\beta$ ) that make the observed sequence of events most probable. The likelihood for any point process parametrized by  $\theta$  with observations  $\{t_1, \dots, t_L\}$  within a time horizon  $0 \leq t \leq T$  can be computed as the sum of the log-likelihood for each process:

$$\ln \mathcal{L}(\theta | t_1, \dots, t_L, T) = \sum_{k=1}^{|\mathcal{X}|} \sum_{i=1}^L \ln \lambda_k^*(t_i) - \sum_{k=1}^{|\mathcal{X}|} \int_0^T \lambda_k^*(t) dt \quad (2.1)$$

The full derivation can be found in Appendix A.1.1. Importantly, Eq. 2.1 cannot be computed easily since the sum over all event types  $|\mathcal{X}|$  and the double summation over

all pairs of event  $t_i$  and  $t_j$ , leading to  $\mathcal{O}(|\mathcal{X}|^2 \cdot N(T)^2)$  at worst and  $\mathcal{O}(|\mathcal{X}|^2 \cdot N(T))$  if using exponential decay [73]. This is a regime where classical MLE is computationally prohibitive and statistically prone to overfitting [9, 77]. In contrast, the standard self-exciting Hawkes process with exponential decay leads to  $\mathcal{O}(N(T))$  complexity [73] but implies a greater parametric assumption.

### 2.1.5 The High-Dimensional Discrete Event Stream Regime

While the Mutually-Exciting Hawkes process provides a rigorous theoretical foundation for interacting events, it assumes that maintaining a continuous intensity function  $\lambda_k^*(t)$  for every dimension  $k \in \{1, \dots, |\mathcal{X}|\}$  is computationally feasible. However, in regimes of highly structured data with a large number of discrete events (patient trajectories [105], event logs [30], vehicle diagnostics [91], NLP [129]), representing each continuous intensity function or *stream* separately is inefficient. For instance, in modern automotive diagnostics, the event space cardinality approaches  $|\mathcal{X}| \approx 10^4$ , while the actual event occurrences are sparse due to structural relationship (event  $A$  always excites the occurrence of  $B$  despite the history). We assume such a high-dimensional<sup>1</sup> regime throughout the thesis.

This shift in perspective is crucial. It aligns the problem with *Neural Sequence Modeling* [143] and *Language Modeling* [121], where the focus is on predicting the next token  $x_{i+1}$  from a high-dimensional discrete sequence of words, rather than regressing  $|\mathcal{X}|$  parallel sequences. This justifies our use of autoregressive architectures (in Part I) to approximate the conditional density  $P(x_{i+1} | \mathcal{H})$  and enables the scalable causal discovery techniques developed further in Part II.

## 2.2 Language Models

Although we employ the term event sequence modeling, we define it in the Natural Language Processing (NLP) realm and adopt its terminology (such as tokens, vocabulary). Therefore, we give an overview of the important concepts in NLP as used in this work.

### 2.2.1 Word Level

**Sentence and Words** Before introducing the modeling framework, we formally define the notion of a sentence as a special case of a unit-time event sequence:

**Definition 7** (Sentence as a Unit-Time Event Sequence). *A sentence  $S$  is a special case of an event sequence (Def. 2) characterized by **unit-time arrivals**. Given a vocabulary*

---

<sup>1</sup>Throughout this thesis, high-dimensional refers mainly to the cardinality of the discrete event space  $|\mathcal{X}|$  rather than the ambient dimension of a feature vector in the classical statistical sense. This usage is consistent with the event sequence and causal discovery literature [6, 41], where dimensionality indexes vocabulary size and refers to the number of nodes in a graph. The regime studied here is characterized simultaneously by large  $|\mathcal{X}|$ , long sequence lengths, and large sample counts, all of which contribute to the described regime.

(the event type space  $\mathcal{X}$ ), a sentence  $S$  is a sequence of events defined as:

$$S = (x_i, t_i)_{i=0}^L \quad \text{where } t_i = i, \quad \forall i \in \{0, \dots, L\} \quad (2.2)$$

where events are so-called 'words'.

**Tokenization** To translate words into machine-interpretable data, a step called *tokenization* converts a sequence of words into *tokens*. These tokens can be seen as word fragments. Consequently, a word is often split into smaller units (*sub-word tokenization*) to optimize the compression of a natural language [26] into a fixed-size *vocabulary*. In event sequence modeling, it is common to treat events as whole tokens, since we do not know their underlying semantic structure.

**Language Preprocessing** To obtain all distinct tokens, there is often a preprocessing stage where we iterate over the entire observational dataset  $\mathcal{D} = \{S_0, \dots, S_m\}$  of sequences and sort the different tokens by their frequency, i.e., we obtain a vocabulary with the most common words. The vocabulary is referred to as  $\mathcal{X}$ . The words that do not appear in the vocabulary are replaced by the unknown token, often defined as:  $[UNK]$ . A start-of-sequence token  $\langle S \rangle$  or  $[CLS]$  in BERT [26] is used as  $x_0$ , and an end-of-sequence token  $\langle /S \rangle$  or  $[EOS]$  for  $x_L$  the last word.

### 2.2.2 Word Embeddings

To get a dense representation of our sequence, we embed each token into a  $d$ -dimensional space using a learnable embedding matrix  $\mathbf{W}^e \in \mathbb{R}^{V \times d}$  where  $V = |\mathcal{X}|$  is the number of distinct tokens (vocabulary). To perform this projection in parallel, we create a sequence of one-hot encoded vectors from the tokens  $\{\mathbf{x}_i\}_{i=0}^L$  as  $\mathbf{Y} \in \mathbb{R}^{L \times V}$ . The word embedding  $\mathbf{E}$  is obtained via a linear projection:

$$\mathbf{E} = \mathbf{Y}\mathbf{W}^e \in \mathbb{R}^{L \times d} \quad (2.3)$$

where  $d \ll V$ . Typically,  $W^e$  is learned from scratch, especially adapted for event sequence modeling, where there is no pretrained word embedding.

### 2.2.3 Transformers

Throughout the thesis, we will primarily employ Transformer-based architectures. This architecture underpins the vast majority of modern deep learning, whether in vision [81], time series [4], or language [146]. It relies on several key concepts such as the attention mechanism, feed-forward layers, layer normalization [7], position embeddings, and self-supervised learning. We provide a brief overview of these elements.

### 2.2.3.1 Attention

**Scaled Dot-Product Attention** The majority of research utilizing Transformer models for sequence data employs the architecture introduced by [150]. We define three linear projection matrices  $\mathbf{Q} = \mathbf{U}\mathbf{W}^Q \in \mathbb{R}^{L \times d}$ ,  $\mathbf{K} = \mathbf{U}\mathbf{W}^K \in \mathbb{R}^{L \times d}$ , and  $\mathbf{V} = \mathbf{U}\mathbf{W}^V \in \mathbb{R}^{L \times d}$  which are called respectively *query*, *key*, and *value*.  $\mathbf{W}^Q$ ,  $\mathbf{W}^K$ ,  $\mathbf{W}^V$  are trainable weights. Scaled dot-product attention computes a similarity between queries and keys to weight the importance of each token’s value, allowing the model to focus on relevant parts of the sequence when making predictions. It is computed as:

$$\mathbf{A} = \text{Attention}(\mathbf{Q}, \mathbf{K}, \mathbf{V}) = \text{softmax}\left(\frac{\mathbf{Q}\mathbf{K}^T}{\sqrt{d_k}}\right)\mathbf{V} \quad (2.4)$$

where  $\mathbf{A} \in \mathbb{R}^{L \times L}$  are the attention scores of each token pair  $i, j$ . The softmax is applied row-wise. In the original paper, [150] argue that scaling the  $\mathbf{Q}\mathbf{K}$  dot product enables a better stability of the softmax function since the gradients become extremely small. Therefore the *scaling* factor  $d_k$  is introduced in Eq. 2.4. For *causal* or *autoregressive* Transformers, a lower triangular matrix  $\tilde{\mathbf{A}} \in \{0, -\infty\}^{L \times L}$  is applied additively to the pre-softmax logits of Eq. 2.4, setting future positions to  $-\infty$  to prevent tokens from attending to future tokens [121].

**Multi-Head Attention** In the same paper, [150] extended the single scaled dot-product into a *multi-head attention* (MHA). They divided the attention scores computation into multiple heads to perform multiple attentions in parallel. In this case, the feature dimension  $d$  is divided into  $h$  parallel attention heads of size  $\frac{d}{h} \in \mathbb{N}$ . It is usually done in practice by reshaping the query, key matrices into respectively  $Q \in \mathbb{R}^{L \times \frac{d}{h} \times h}$  and  $K \in \mathbb{R}^{L \times \frac{d}{h} \times h}$  before feeding them to the attention scores calculation:

$$\text{MHA}(\mathbf{Q}, \mathbf{K}, \mathbf{V}) = [\text{head}_1, \dots, \text{head}_h] \cdot \mathbf{W}^O \quad (2.5)$$

with:

$$\text{head}_i = \text{Attention}(\mathbf{Q}_i, \mathbf{K}_i, \mathbf{V}_i) \quad (2.6)$$

where  $\mathbf{Q}_i \in \mathbb{R}^{L \times \frac{d}{h}}$ ,  $\mathbf{K}_i \in \mathbb{R}^{L \times \frac{d}{h}}$ ,  $\mathbf{V}_i \in \mathbb{R}^{L \times \frac{d}{h}}$  and  $\mathbf{W}^O \in \mathbb{R}^{h \times d_V \times d}$  is a learnable projection matrix. The authors show that each head learns different token-to-token relationships from a single sequence.

### 2.2.3.2 Feed-forward Layers

The multi-head-attention scores are processed using a combination of layer normalization, position-wise feed-forward neural network (FFN), and residual connections to ensure a proper gradient flow and to learn the attention scores patterns between tokens:

$$\begin{aligned} \mathbf{U}' &= \text{LayerNorm}(\mathbf{A} + \mathbf{U}) \\ H &= \text{LayerNorm}(\mathbf{U}' + \text{FFN}(\mathbf{U}')) \end{aligned} \quad (2.7)$$

where  $H \in \mathbb{R}^{L \times d}$  is the resulting hidden state. The so-called position-wise FFN layers are typically two layers that project the  $d$ -dimensional input to an intermediate size, often  $4 \times d$ . These FFNs are applied independently for each position:

$$\text{FFN}(\mathbf{U}) = f(\mathbf{U}\mathbf{W}_1 + \mathbf{b}_1)\mathbf{W}_2 + \mathbf{b}_2 \quad (2.8)$$

where  $f$  an activation function (ReLU [2] in the original paper),  $\mathbf{W}_2$  a learnable weight matrix and  $\mathbf{b}_2$  a bias vector. Then, residual connections [54] are applied in Eq. 2.7 to improve gradient flow and training stability. This layer is stacked  $k$  times, leading to a Transformer with  $k$  layers.

### 2.2.3.3 Normalization

The normalization layer helps stabilize the dynamics of the deep neural network’s hidden states [7] by rescaling each output neuron before the activation function. This mitigates the problem of *internal covariance shift* [64], which arises from the fact that the weights of one layer are highly dependent on the outputs of the neurons in the previous layer. Modern Transformers such as LLaMA [146] use root-mean-square (RMS) normalization [168], normalizes each activation by the RMS of the layer’s outputs, omitting the mean-centering step of classical layer normalization.

### 2.2.3.4 Positional Encoding

**Deterministic** Due to the nature of the attention scores, the architecture does not have a sense of ordering, as the input is just an array of vectors. Therefore, [150] added a so-called *positional encoding* to the word embedding vector for each sequential step. This vector comprises a fixed periodic function, such as:

$$\mathbf{PE}_{i,j} := \begin{cases} \sin(i \times \omega_0^{j/d}) & \text{if } j \bmod 2 = 0 \\ \cos(i \times \omega_0^{(j-1)/d}) & \text{if } j \bmod 2 = 1 \end{cases} \quad (2.9)$$

where  $i$  is the index of the  $i$ -th token and  $\omega_0$  the initial frequency (usually  $10^{-4}$ ). Then, it is added to the word embedding to form the input embedding:

$$\mathbf{U} = \mathbf{PE} + \mathbf{E} \quad (2.10)$$

**Learnable** In most PyTorch [110] and Hugging Face [157] implementations of Transformers (e.g., BERT [26], GPT [121]), a learnable positional embedding is obtained via a learnable lookup table  $\mathbf{W}^{\text{PE}} \in \mathbb{R}^{L \times d}$  for each sequential steps  $\{0, 1, 2, \dots, L\}$ . It is added to the word embeddings in Eq. 2.10

### 2.2.3.5 Autoregressive Transformers

Autoregressive or causal Transformers have a causal attention mask applied in Eq. 2.4. They perform the next token prediction via the chain-rule factorization of the joint

## 2 Foundations of Event Sequence Modeling

distribution  $P(X_0, \dots, X_L)$  [15], such as the probability of observing a sequence of event types  $s = (x_0, \dots, x_L)$  is:

$$P(s) = \prod_{i=0}^L p(x_i | x_0, x_1, \dots, x_{i-1}) \quad (2.11)$$

where  $p(x)$  is the probability mass function, i.e.,  $P(X = x)$ . These models are trained using next-token prediction [121], by minimizing the negative log-likelihood of observing sequences.

### 2.3 Metrics

We measure the prediction of language models using common classification metrics that are interpretable and anchored in the machine learning domain. We also define our own metric later in Chapter 3 for predictive maintenance.

#### 2.3.1 Next-Event Prediction

Next-event prediction is often evaluated using the Accuracy of the inferred next event [172, 179, 77]. However, in the presence of class imbalance, Accuracy alone can be misleading [171]. Therefore, we include Precision and Recall to provide a general view of model performance.

**Accuracy** is defined as the proportion of correct predictions among the total number of cases examined:

$$ACC = \frac{TP + TN}{TP + TN + FP + FN} \quad (2.12)$$

**Precision** (or positive predictive value) quantifies the reliability of the positive predictions, measuring the proportion of inferred events that are correctly identified:

$$P = \frac{TP}{TP + FP} \quad (2.13)$$

**Recall** (or sensitivity) measures the completeness of the discovery, capturing the proportion of actual positive events that were recovered by the model:

$$R = \frac{TP}{TP + FN} \quad (2.14)$$

#### 2.3.2 Next-Time Prediction

**Mean Absolute Error** MAE is the average of the absolute difference between the actual  $t_i$  and predicted values  $\hat{t}_i$ :

$$MAE = \frac{1}{m} \sum_{i=0}^m |t_i - \hat{t}_i| \quad (2.15)$$

For instance, if one finds an MAE of  $5h$ , it indicates that the model has, on average, an error of 5 hours when predicting the time of occurrence. Eq. 2.15 weighs all errors equally, making it less sensitive to outliers.

**Root Mean Square Error** or RMSE, adds a square function inside the sum, averages across all points, and takes the square root:

$$\text{RMSE} = \sqrt{\frac{1}{m} \sum_{i=0}^m (t_i - \hat{t}_i)^2} \quad (2.16)$$

Unlike MAE, RMSE is more sensitive to outliers as it disproportionately penalizes larger errors. Nevertheless, RMSE remains less interpretable as the scaling of values changes.

## 2.4 Dataset

This thesis uses proprietary BMW vehicle datasets. Due to confidentiality constraints, we will briefly describe the dataset in terms of its nature, dimensions, and scale, but no information can be given regarding the intrinsic values and vehicles or customer information. All mentioned GitHub repositories contain synthetic or anonymised data only; no BMW data or mappings are included.

### 2.4.1 Vehicular Fault Sequences

A vehicular fault sequence is commonly referred to as an event sequence, where each event includes an error code and a timestamp. If specified, the vehicle’s mileage at the time the error code was triggered can be included as  $m_i$ , forming a marked event sequence (Def. 3). In addition to that, the dataset is joined with error patterns (EPs) per sequence. In most of our experiments we have labeled sequences, where the labels are the EPs. Let  $\mathcal{D} = \{S_i^{(1)}, \dots, S_i^{(m)}\}$  be a dataset of multi-labeled sequences  $S_i^{(k)} = (\{(x_0, t_0), \dots, (x_L, t_L)\}, \mathbf{y})$  where  $\mathbf{y} \in \{0, 1\}^{|\mathcal{Y}|}$  is a multi-one hot vector (multiple EPs can happen per sequence). For each chapter, we will recall the used dataset and its characteristics, such as the number of distinct DTCs  $|\mathcal{X}|$  and EPs  $|\mathcal{Y}|$ , the number of sequences, and their average lengths. An overview of the notations can be found in Table 2.1.

#### 2.4.1.1 Diagnostic Trouble Code: DTCs

Diagnostic data is generated by various *Electronic Control Units* (ECU) in a vehicle at irregular intervals. Diagnostic data differs substantially from raw sensor data since they are categorical. We construct a *Diagnostic Trouble Code* (DTC) indicating the precise error from 3 pieces of information arriving at the same timestamp and mileage: (1) the ID number of the ECU, (2) an error code (*Base-DTC*), and (3) a *Fault-Byte*. A single DTC token comprises these three elements:

$$\text{DTC} = \text{ECU}|\text{Base-DTC}|\text{Fault-Byte} \quad (2.17)$$

Notation	Description
$x$	Discrete event type, in our case a DTC.
$d$	Absolute mileage of the vehicle in km.
$m$	Mileage of the vehicle in km since the first DTC ( $x_0$ ) occurred in a sequence $S$ such as $m_i = d_i - d_0$
$ts$	Unix timestamp attached to each DTC.
$t$	Number of hours passed since the first DTC occurred in a sequence. More specifically, $t_i$ is defined as $t_i = ts_i - ts_0$ .
$S$	Sequence of triplets (event type, time, mileage) defined as $S = \{(x_i, t_i, m_i)\}_{i=0}^L$ of length $L$ with index starting from 0.
$S_l$	Multi-labeled sequence of triplets (event type, time, mileage) leading to an outcome defined as $S_l = \{(x_i, t_i, m_i), \mathbf{y}\}_{i=0}^L$ of length $L$ with index starting from 0 and $\mathbf{y} \in \{0, 1\}^{ \mathcal{Y} }$ .
$S^{(i)}$	The $i$ -th sequence in a dataset $\mathcal{D}$ .
$S_l^{(i)}$	The $i$ -th multi-labeled sequence in a dataset $\mathcal{D}$ .
$s$	Sequence of length $L$ containing only the event types, e.g., $(x_0, x_1, \dots, x_L)$ .
$i \in \{0, \dots, L\}$	index of element in (event) sequence.

**Table 2.1:** List of dataset symbols and their respective meanings for the datasets used in this thesis.

#### 2.4.1.2 Error Patterns

Error patterns (EPs) are a higher-level abstraction of DTC sequences to characterize specific vehicle faults. They are defined as Boolean combinations over DTCs. When denoting *error pattern*, we refer to it as their intrinsic name (e.g., a precise battery defect, a PCB fault), while when denoting *error pattern rules*, we refer directly to the Boolean combinations that define this error pattern. An example of an EP rule for ( $y_1$ )

based on some diagnosis trouble codes ( $x_i$ ) is shown in Eq. 2.18 such as:

$$y_1 = x_1 \ \& \ x_5 \ \& \ x_8 \ \& \ (x_{12} \ | \ x_3) \ \& \ !x_{10} \ \& \ !x_{20} \quad (2.18)$$

A tangible EP example for a battery failure could be:

$$(\text{voltage drop} \ \& \ \text{temp high}) \ | \ (\text{charging error} \ \& \ \text{!battery replaced}) \quad (2.19)$$



## 3 Error Pattern Prediction from Vehicle Diagnostic Event Sequences

Anticipating both *what* error pattern will occur and *when* it will appear is an important step toward predictive maintenance and improved vehicle safety. In this chapter, we present an approach that draws an analogy between natural language processing and modeling multivariate vehicle event streams. Similar to words in a sentence, DTCs unfold as sequences over time, enriched with contextual information such as mileage and time of occurrence. To capture these dependencies, we introduce two autoregressive Transformer-based architectures: *CarFormer*, an autoregressive Transformer trained with a novel self-supervised strategy, and *EPredictor*, a decoder that jointly predicts the type and timing of future EPs. This chapter is based on the following publication, with some text passages directly taken from it:

**Harnessing Event Sensory Data for Error Pattern Prediction in Vehicles: A Language Model Approach.** [91] Hugo Math, Rainer Lienhart, Robin Schön. *Proceedings of the AAAI Conference on Artificial Intelligence*, vol. 39, no. 18, pp. 19423–19431, 2025, Philadelphia, USA, February 2025.

Our experimental evaluation demonstrates that these models can address the challenges of high event-type cardinality, unbalanced code frequencies, and limited labeled data. On average, with sequences of 160 error codes, the proposed approach achieves an F1 score of 80% for predicting the next error pattern using only half of the sequence. It estimates the time of occurrence with a mean absolute error of  $58.4 \pm 13.2$  hours. These results show that autoregressive Transformers can anticipate vehicle failures before they occur, laying the foundation for reliable predictive maintenance in large vehicle fleets.

### 3.1 Introduction

A central challenge in vehicle diagnostics lies in predicting both *what* kind of error will manifest and *when* it is likely to occur. Unlike individual DTCs, which may be noisy or repetitive (e.g., due to recurring electrical glitches or software updates), EPs characterize entire fault sequences, such as engine or battery failures. Fig. 1.1 illustrates this setting, where the task is to infer, given a past sequence of DTCs, the probability distribution over future EPs and their expected time of occurrence.

Recent research has begun to address predictive maintenance using DTC sequences, for instance, with recurrent neural networks (RNNs) [50] or Transformer-based architectures [49] that aim to predict the next DTC. However, focusing solely on the next DTC

is insufficient for two reasons. First, minor or noisy DTCs can obscure critical patterns, making it difficult to distinguish between trivial and critical faults. Second, as the event vocabulary grows often into the tens of thousands, the accuracy of next-token prediction deteriorates rapidly, much like in natural language modeling with large vocabularies and long sequences [8].

Historically, Hawkes Processes and their neural variants have advanced the state of the art in event modeling for next event and time prediction tasks [53, 31, 131]. Transformer-based models like BERT [26] and GPT-3 [18] have gained overwhelming popularity due to their attention-based architecture, flexibility, parallelization, and state-of-the-art performance in sequence modeling. Consequently, models adapted to discrete-time sequences using Transformers have emerged naturally [172, 179, 136], achieving state-of-the-art performance in next-event prediction benchmarks. Inspired by the analogy between natural language processing and vehicle event streams, we adopt this perspective for DTCs and EPs: DTCs play the role of words, while EPs correspond to a sentence label (e.g., sequence classification for sentiment analysis).

Formally, we represent a DTC sequence as a sentence of the form

$$" < s > DTC_1 DTC_2 \dots DTC_n < /s > "$$

We make several modifications to the vanilla Transformer from [150], incorporating continuous-time and mileage positional embeddings as additional context. Using two distinct training phases, we introduce CarFormer, a pretrained model acting as an encoder and EPredictor, a decoder Transformer-based model that generates a probability distribution over a set of error patterns for each event step  $i$  to determine *what* EPs will most likely happen and estimates a time for *when* it will occur.

## 3.2 Background

### 3.2.1 Transformers for Event Streams

**Time Embedding** Time embedding replaces the traditional positional encoding, which grants the Transformer model positional information of each token within the sequence, as shown previously. This time embedding is defined deterministically with periodic functions exactly like in [150]:

$$\mathbf{P}_{i,j} := \begin{cases} \sin(t_i \times \omega_0^{j/d}) & \text{if } j \bmod 2 = 0 \\ \cos(t_i \times \omega_0^{(j-1)/d}) & \text{if } j \bmod 2 = 1 \end{cases} \quad (3.1)$$

where  $i$  is the index of the  $i$ -th event,  $\omega_0$  is the frequency (usually  $10^{-4}$  [150]).

**Event-Type Embedding** To get a dense representation of our sequence, we embed each event into a  $d$ -dimensional space using an embedding matrix  $\mathbf{L}^{V \times d}$  where  $V = |\mathcal{X}|$  is the number of distinct events. As it is done for word embeddings in Eq. 2.3, we create a sequence of one-hot encoded vectors from the event types  $\{x_i\}_{i=0}^L$  as  $\mathbf{Y} \in \mathbb{R}^{L \times V}$ . The event-type embedding  $\mathbf{E}$  is defined as  $\mathbf{E} = \mathbf{Y}\mathbf{L} \in \mathbb{R}^{L \times d}$  and the input embedding  $\mathbf{U}$  as  $\mathbf{U} = \mathbf{E} + \mathbf{P} \in \mathbb{R}^{L \times d}$ .

### 3.3 Dataset Description

**Overview** We encode each DTC uniquely by a single token to predict the next token directly. In this chapter, we use an anonymized vehicular DTC sequence dataset of  $1.7 \times 10^6$  sequences with, on average, 150 DTCs per sequence. Each sequence belongs to a unique vehicle and the dataset is focused on a specific BMW model range. An overview of the DTC elements<sup>1</sup> can be found in Table 3.1.

Data	# of values	Description
DTC	8710	Diagnostic Trouble Code
ECU	61	Electronic Control Unit
Base-DTC	7726	Error Code
Fault-Byte	2	Binary Value

**Table 3.1:** Number of Distinct values of the DTC elements

To obtain a full marked event sequence  $S = \{(x_i, t_i, m_i)\}_{i=0}^L$  (Def. 3), we obtain the last known timestamp  $ts_L$  and mileage  $d_L$  and select all DTCs that are no further than: (1) a given period in the past ( $ts_L - ts_i \leq 30$  days) and (2) a given distance in the past ( $d_L - d_i \leq 300$ km). Table 2.1 explains the different data notation.

#### 3.3.1 Time and Mileage

We plot the distribution of  $t_i$  and  $m_i$  in Fig. 3.1. We observe peaks at zero on both distributions due to truncation and missing values.

To feed our model with the time  $t$  feature, we need a scaling method to mitigate the left-tail skew. Using  $\log(t + 1)$  is a natural choice. At the same time, we want

<sup>1</sup>DTC composition defined in 2.4.1.1

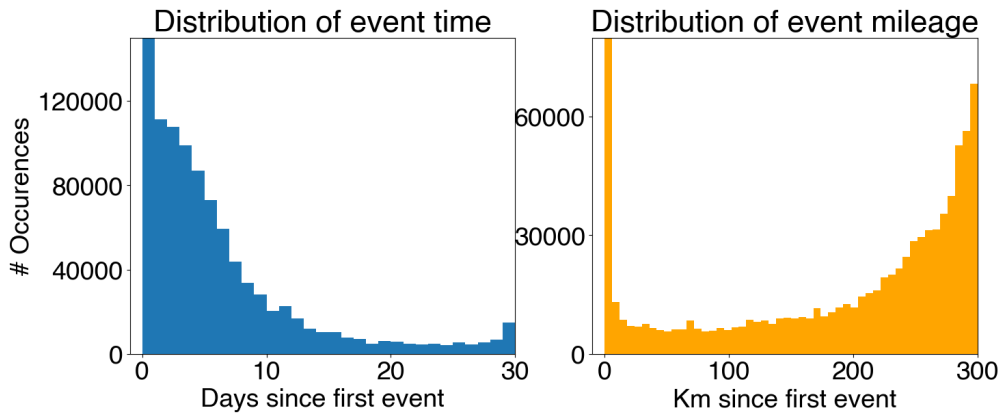


**Figure 3.1: Time and Mileage Distribution.** Distribution of  $t_i$  and  $m_i$  (relative time and mileage) in our dataset.

to approximately map  $t$  into the range of  $[-1, 1]$ . Therefore, we apply the following non-linear function  $f_t : \mathbb{R}^+ \rightarrow \mathbb{R}$  to  $t$ :

$$t' = f_t(t) = \log(t + 1) - 1 \quad \forall t \in \mathbb{R}^+ \quad (3.2)$$

In TPPs the time is usually represented as inter-event time or its logarithm[131, 31], making our approach anchored in the literature.

## 3.4 Methodology

We introduce the following two models: *CarFormer* and *EPredictor* for autoregressive DTC and EP prediction.

### 3.4.1 CarFormer

The CarFormer model can be seen in Fig. 3.2. We now describe the main architectural ideas.

#### 3.4.1.1 Embeddings

CarFormer uses four different embeddings to capture the spatial and temporal dependencies of irregular event appearance. These embeddings differ from the positional embedding  $\mathbf{P}$  used in TPPs [179], [174], and next-DTC prediction studies [49], [50]. We embed both time  $t$  and mileage  $m$  and use a rotation matrix to induce absolute and relative event positions such as:

- **Event-type embedding**  $\mathbf{E} \in \mathbb{R}^{L \times d}$  is obtained like described in section 3.2.1.
- **Absolute time embedding**  $\mathbf{T} \in \mathbb{R}^{L \times d}$  is constructed on-the-fly at each forward pass by a linear transformation  $t_{i,j} = t'_i w_j + b_j$  where  $w_j, b_j$  are learnable parameters and  $t'_i$  is the scaled time at event step  $i$ .
- **Mileage embedding**  $\mathbf{M} \in \mathbb{R}^{L \times d}$  is obtained via a learnable lookup table  $\mathbf{W}^{m_{\max} \times d}$  where  $m_{\max} = 300(\text{km})$ . Each row  $\mathbf{w}_m \in \mathbb{R}^d$  corresponds to the learnable embedding vector for the discrete mileage  $m$ . The continuous mileage  $m_i \in \mathbb{R}^+$  is cast to an integer value  $m = \lfloor m_i \rfloor$ . We attempted to leverage the continuous mileage by appropriately linearly interpolating the embeddings  $w_m$  and  $w_{m+1}$ , but the time complexity increased without observing any benefits.
- **Rotary Position Embedding (RoPE)**  $\mathbf{R}_{\Theta}^d$  Due to the permutation invariance of the Transformer model and the scattered time  $t$ , we still need to integrate positional event information. To do so,  $\mathbf{Q}, \mathbf{K}$  are rotated using the orthogonal matrix  $\mathbf{R}_{\Theta}^d$  from [142] as a function of the absolute event position  $i$  in the sequence  $S$ . This method has two advantages: (1) it is not learnable (less likely to overfit), and (2) it integrates natively the relative position instead of altering  $\mathbf{A}$  with a learnable bias like in [130].

Unlike some papers suggesting using only a time embedding plus an event embedding [179], [172], we argue that, like in [136], encoding solely the position with a time embedding leads to inefficient sequential learning for our Transformer model and leads to an early plateau in our pretraining. We make the distinction between our event-type embedding  $\mathbf{E}$  and the other information per event (time and mileage), which we call context embedding  $\mathbf{CE} = \mathbf{T} + \mathbf{M}$ .

**Continuous Time Mileage Aware Attention** We modify the vanilla Transformer from [150] by (1) adding the context embedding to the projected event-type embedding at every layer [146], and then (2) a Rotary Position Embedding (RoPE) [142] is applied to both query  $\mathbf{Q}$  and key  $\mathbf{K}$ :

$$\mathbf{Q} = \mathbf{R}_{\Theta}^d(\mathbf{W}^Q\mathbf{E} + \mathbf{CE}),$$

$$\mathbf{K} = \mathbf{R}_{\Theta}^d(\mathbf{W}^K\mathbf{E} + \mathbf{CE})$$

where<sup>2</sup>  $\Theta = \{\theta_i = \theta_0^{-2(i-1)/d}, i \in [1, 2, \dots, d/2]\}$ ,  $\theta_0 = 10^4$ . More specifically, the inner product between query  $\mathbf{q}_m$  and key  $\mathbf{k}_n$  takes the event-type embedding  $\mathbf{e}_m, \mathbf{e}_n$  where  $m - n$  is their relative position with context  $\mathbf{CE}_m$  and  $\mathbf{CE}_n$ :

$$\begin{aligned} \mathbf{q}_m^T \mathbf{k}_n &= (\mathbf{R}_{\Theta, m}^d(\mathbf{W}_q \mathbf{e}_m + \mathbf{CE}_m))^T \mathbf{R}_{\Theta, n}^d(\mathbf{W}_k \mathbf{e}_n + \mathbf{CE}_n) \\ &= \mathbf{e}_m^T \mathbf{W}_q \mathbf{R}_{\Theta, n-m}^d \mathbf{W}_k \mathbf{e}_n + \mathbf{e}_m^T \mathbf{W}_q \mathbf{R}_{\Theta, n-m}^d \mathbf{CE}_n + \\ &\quad \mathbf{CE}_m^T \mathbf{R}_{\Theta, n-m}^d \mathbf{W}_k \mathbf{e}_n + \mathbf{CE}_m^T \mathbf{R}_{\Theta, n-m}^d \mathbf{CE}_n \\ &= (1): \text{query-to-key} + (2): \text{query-to-ce} \\ &\quad (3): \text{ce-to-key} + (4): \text{ce-to-ce} \end{aligned} \tag{3.3}$$

where  $\mathbf{R}_{\Theta, n-m}^d = (\mathbf{R}_{\Theta, m}^d)^T \mathbf{R}_{\Theta, n}^d$  is a sparse orthogonal matrix. The terms provide (1) standard attention capturing similarity between token embeddings, (2) query attending to the spatiotemporal information of the other token (vice versa for (3)) and (4) the interaction of the spatiotemporal information only of both token only. Consequently, they provide a richer query and key representations when computing the attention scores. The final the attention scores is computed as:

$$\mathbf{A} = \text{softmax} \left( \frac{(\mathbf{R}_{\Theta}^d(\mathbf{W}^Q\mathbf{E} + \mathbf{CE}))(\mathbf{R}_{\Theta}^d(\mathbf{W}^K\mathbf{E} + \mathbf{CE}))^T}{\sqrt{3d}} \right) \tag{3.4}$$

Adding  $\mathbf{CE}$  after the projection to query and key can be seen as a refinement of  $\mathbf{Q}, \mathbf{K}$  by  $\mathbf{T}, \mathbf{M}$ , providing additional context to the attention scores. We also add a scaling factor of 3 to compensate for the additional terms<sup>3</sup> in Eq. 3.3.

<sup>2</sup>Note the reciprocal relationship between the standard PE frequency  $\omega_0$  and the RoPE base  $\theta_0$

<sup>3</sup>Verified empirically in the ablation experiments (Table 3.3) via the *rotcross-key-value-scaled-ce-2* model.

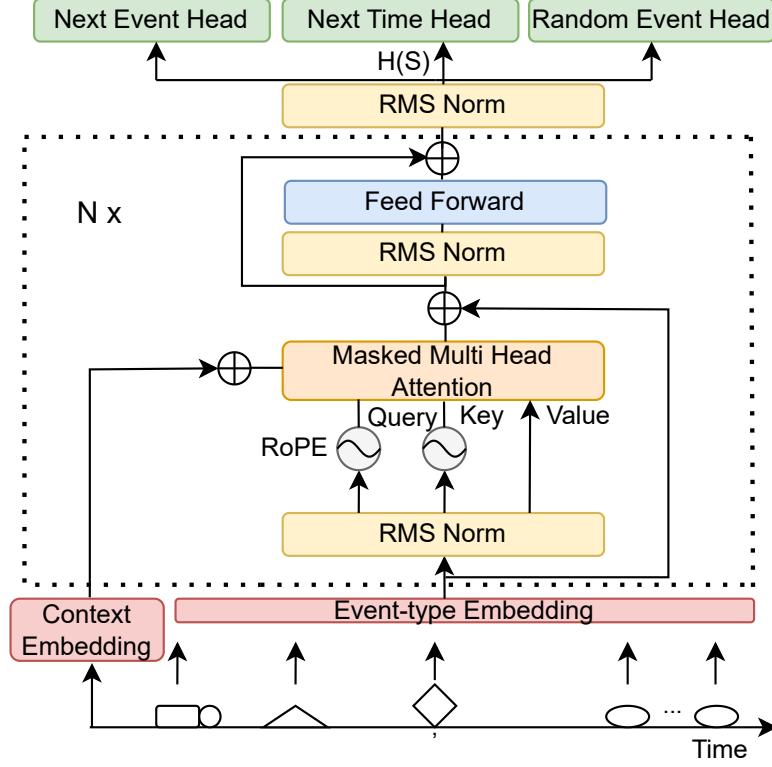


**Figure 3.2: CarFormer Architecture.** A Transformer architecture is used alongside spatio-temporal embeddings (*context embedding*) injected to the query and key. A RoPE is then applied to induce the relative position of the DTCs. Three predictive heads are used to learn the complex dynamics of the DTC sequences.

### 3.4.1.2 Multi-Task Learning

**Next-Event Prediction.** We use a standard language modeling objective which aims to minimize the cross-entropy loss between our output distribution  $\hat{x}_i$  generated by our model’s *Next Event Head* and the next event  $x_{i+1}$ . [136] used a BERT [26] model trained on a masked event modeling task, which is commonly used for bidirectional models. However, they simultaneously applied a causal mask, resulting in a loss of the bidirectional property. We argue that, by doing so, we lose substantial sample efficiency; thus, we will retain a standard next-token prediction.  $\hat{x}_i$  is the probability distribution produced by the *Next Event Head*, which integrates an RMS normalization [168] and one linear layer. The cross-entropy loss between  $\hat{x}_i$  and  $x_{i+1}$  (= a one-hot vector in  $\{0, 1\}^V$ ) is obtained by:

$$\mathcal{L}_c := - \sum_{i=0}^L \sum_{j=0}^V x_{i+1,j} \log(\hat{x}_{i,j}) (1 - \delta_{i,r}) \quad (3.5)$$

where  $\delta_{i,r}$  is the Kronecker delta, iff event type  $x_i$  belongs to the set of random event types  $R$  and 0 otherwise.

**Next Event Time Prediction.** In addition, we compute the Huber loss [65] between the estimated inter-event time  $\Delta \hat{t}'_i$  for the event  $x_i$  and the ground truth  $\Delta t'_i = f_t(t_{i+1}, 10) - f_t(t_i, 10)$  to deal with outliers and prevent exploding gradients with  $\beta = 1$ ,  $\epsilon_i = \Delta \hat{t}'_i - \Delta t'_i$ .

$$\mathcal{L}_t := \sum_{i=0}^L (1 - \delta_{i,r}) \begin{cases} 0.5\epsilon_i^2 & \text{if } |\epsilon_i| < \beta, \\ (|\epsilon_i| - 0.5) & \text{otherwise,} \end{cases} \quad (3.6)$$

$t'$  is obtained using a log, hence we are essentially computing a kind of Mean Squared Logarithmic Error (MSLE) but with a  $\beta$ , useful to stabilize training and help convergence.

**Random Event Prediction.** Finally, a binary classifier that predicts whether an event was true or randomly generated is added. This choice is motivated by several papers [136, 38] stating that a model should learn when an event does not happen to reinforce the negative evidence of no observable events within each inter-event. At each step  $i$ , a random event is injected with probability  $p$ . If a random event is successfully injected, the process continues until a failure occurs (i.e., the event is not injected). This allows for multiple random events to be injected in a row, allowing for more complexity. The  $\mathcal{L}_r$  loss is defined as the binary cross-entropy loss between the probability distribution  $\hat{y}_i^r$  generated by our *Random Event Head* and the ground truth  $y_i^r$  at event step  $i$ :

$$\mathcal{L}_r := - \sum_{i=0}^{|R|} y_i^r \log(\hat{y}_i^r) + (1 - y_i^r) \log(1 - \hat{y}_i^r) \quad (3.7)$$

**Total Loss.** The total loss is defined as follows:

$$\mathcal{L} = \frac{1}{L - |R|} (\mathcal{L}_c + k_1 \mathcal{L}_t) + k_2 \frac{1}{|R|} \mathcal{L}_r \quad (3.8)$$

where  $k_1, k_2$  are trade-off between the different losses,  $L$  the sequence length,  $R$  the set of random events injected in  $S$ .

### 3.4.2 EPredictor

We now describe the architecture of EPredictor in detail (Fig. 3.3). We motivate this problem formulation and leverage the autoregressive property of CarFormer to introduce EPredictor.

#### 3.4.2.1 Limitations of Next-Event Prediction

Predicting only the next DTC in a sequence of DTC faults has inherent limitations and remains a difficult task. For instance, in [49], they used DTCs, whose ECU, Base-DTC, and Fault-Byte data have a cardinality of 83, 419, and 64, respectively, and only report a 81% top-5 accuracy for next DTC prediction. This is because DTCs are not always correlated nor have causal links. Instead, we are also using repair and warranty data to

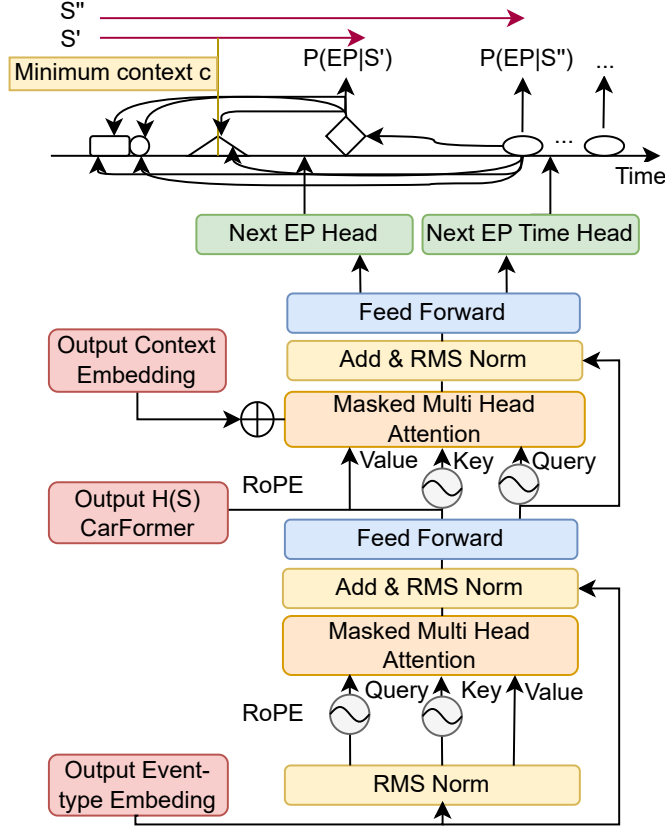


**Figure 3.3: EPredictor Architecture.** The hidden state  $H(S)$  is extracted from CarFormer and fed to the second attention layer as value and key. The event-type embedding  $E$  is fed into the first layer after being normalized, and the context embedding  $CE$  carrying the spatio-temporal information is added directly after the RoPE application to the keys and queries of the second layer.

predict more important events, such as EPs (error patterns). Repair and warranty data differ from DTCs since they are defined after observing all DTCs and characterizing a whole sequence  $S$  and not an individual event  $x_i$ .

### 3.4.2.2 Multi-Label Event Prediction

We define that error pattern  $y$  occurs at index  $i = L$  in a sequence  $S$ . Note that multiple EPs can occur at the same time. We can now define a supervised multi-label classification learning problem of predicting EPs. Multi-label classification has attracted growing attention in the context of event prediction. [174] uses an LSTM for fault detection. More recently, [135] treats concurrent event predictions as a multi-label classification problem and models such data using a Transformer architecture.

To define the multi-label event prediction task with  $N$  labels ( $\equiv$ EPs), we reuse each  $S = \{(x_i, t_i, m_i)\}_{i=0}^L$  and attach a binary vector  $\mathbf{y} \in [0, 1]^N$  to indicate the EPs occurring

at time  $t_L$ . Importantly,  $\mathbf{y}$  is invariant per sequence  $S$ , meaning for all events within  $S$  the ground truth  $\mathbf{y}$  will be the same. By applying a causal mask to both CarFormer and EPredictor, we enable predictive maintenance, since tokens can only attend to previous tokens, as shown in Figure 3.3.

With EPredictor, we leverage the *seq2seq* nature of Transformers, where CarFormer outputs a sequence  $H(S)$  of tokens encoded in a high-dimensional space  $d$ , positioning tokens with similar characteristics nearby. Then, this hidden representation  $H(S)$  is fed into EPredictor, which acts as an autoregressive multi-label classifier for EPs. We approach EP prediction as a machine translation task. By utilizing the contextualized hidden states  $H(S)$  from CarFormer as key and value (i.e., through *cross-attention*), this effectively transitions our model from a "seq2seq" to a "dte2errorpattern" framework.

### 3.4.2.3 Imbalanced Labels

In our case, and in most real-world problems, EPs are highly imbalanced across the dataset, which makes the event prediction task considerably more challenging, especially when the least frequent classes are the most important to detect [174]. In natural language processing, traditional upsampling methods involve perturbing  $S$  by shuffling and replacing tokens. However, in event data, we cannot afford to lose spatial and temporal information. Therefore, we inject random events  $(x_i, m_i, t_i)$  with the same probability of  $p = 0.05$  as in Section 3.4.1.2 and reuse the associated Algorithm. We upsample the different EP classes to a minimum of  $\theta_1 = 6000$  and downsample the most popular ones to a maximum of  $\theta_2 = 12000$ . We also drop classes below 100 appearances across the dataset.

### 3.4.2.4 Losses

We define a minimum context  $c = 30$  which acts as a "minimum history" of DTCs to retain. The *Next EP Head* outputs a vector of probabilities  $\hat{y}_i = \text{sigmoid}(\text{MLP}_c(H_i))$  for each history  $\{H_1, \dots, H_i\}$ ,  $i \in c, \dots, L$  where  $H_i \in \mathbb{R}^d$  is the generated hidden representation from EPredictor at step  $i$ . For the regression task we forecast the time until the EP(s) occurrence  $\Delta \hat{t}'_i = \text{MLP}_t(H_i)$  where the ground truth is  $\Delta t'_i = f_t(t_L, 30) - f_t(t_i, 30)$ . Formally, we define our binary cross-entropy loss over the  $N$  possible EPs for one step  $i$  as follows:

$$\mathcal{L}_i^{ep} := -\frac{1}{N} \sum_{j=1}^N y_j \log(\hat{y}_{i,j}) + (1 - y_j) \log(1 - \hat{y}_{i,j}) \quad (3.9)$$

The total loss across  $S$  with  $L$  events and context  $c$  is:

$$\mathcal{L}^{ep} := \frac{1}{L - c + 1} \sum_{i=c}^L \mathcal{L}_i^{ep} \quad (3.10)$$

We use the Huber loss [65] and define  $\epsilon_i = \Delta \hat{t}'_i - \Delta t'_i$ , with  $\beta = 1$  thus:

$$\mathcal{L}^t := \frac{1}{L - c} \sum_{i=c}^L \begin{cases} 0.5\epsilon_i^2 & \text{if } |\epsilon_i| < \beta, \\ |\epsilon_i| - 0.5 & \text{otherwise,} \end{cases} \quad (3.11)$$

Our final loss to minimize is then:  $\mathcal{L} = \mathcal{L}^{ep} + \gamma\mathcal{L}^t$

## 3.5 Experiments

We implemented CarFormer and EPredictor models using PyTorch, the code is publicly available<sup>4</sup>. Training details are included in the Appendix A.1.2.

### 3.5.1 Ablation I: CarFormer Embeddings

Multiple CarFormer models with different embedding choices were evaluated on next-token prediction accuracy (ACC) and on the regression task using mean absolute percentage error (MAPE) and root mean square error (RMSE) to determine the best-performing CarFormer model. The different choices were *rot* (RoPE), *time* (absolute time embedding added to the input  $\mathbf{U}$ ), *mileage* (also added to  $\mathbf{U}$ ), *m2c*, and *c2m* are additional dot-products ([55]). In our case, we are more interested in the next-event prediction task, thus we are willing to sacrifice some MAPE % over the ACC (%).

Model	ACC(%)	MAPE(%)	RMSE
<b>rot-ce</b>	<b>22.64</b>	3.2	0.04770
time	21.48	<b>2.9</b>	<b>0.04762</b>
time-mileage	21.38	3.0	0.04785
time-c2m-m2c	21.58	3.5	0.04794
time-m2c	21.52	3.6	0.04823
GPT	19.89	-	-

**Table 3.2:** Overall prediction performance of CarFormer with different embeddings. Best results are in bold.

Using only *time* gave the best MAPE (2.9) but not the best ACC (21.48), suggesting that other features might improve the model predictions. For the mileage integration, our intuition was that doing an early summation of the two embeddings ( $\mathbf{T}, \mathbf{M}$ ) seemed to denature the input  $\mathbf{U}$  (ACC of *time-mileage* < ACC of *time*), but the mileage of the vehicle could help differentiate between different DTCs. We tried to modify the attention dot products, which seemed to help the ACC a bit (*time-c2m-m2c*, *time-m2c*), but increased the MAPE drastically. So we fused it with **CE** directly in  $\mathbf{Q}, \mathbf{K}$ . Then, by applying a RoPE to the transformed input, the ACC increased while preserving the RMSE, leading to the best performing model in terms of ACC, namely: *rot-ce*.

### 3.5.2 EPredictor Experiments

We evaluate multi-labeled classification using the micro-F1 score [171]. To better understand and enhance our model’s predictive maintenance capabilities, we introduce

<sup>4</sup><https://github.com/Mathugo/AAAI2025-CarFormer-EPredictor>

Model	F1	MAPE	MAE	CPMWAUC <sub>f1</sub> ↑	CPMWAUC <sub>mae</sub> ↓
rotcross-query-key-ce-1-2	82.69	32.45	0.0268	52.80	0.888
rotcross-query-key-ce-2	82.69	<b>31.18</b>	0.0254	56.61	0.882
rotcross-query-ce-2	82.69	<b>31.18</b>	0.0254	53.00	0.884
rotcross-key-value-ce-2	<b>84.38</b>	33.47	0.0263	65.06	0.904
<b>rotcross-key-value-scaled-ce-2</b>	<b>84.38</b>	31.44	<b>0.0252</b>	<b>67.63</b>	<b>0.874</b>
rotnocross-ce-1-2	80.74	37.61	0.0275	42.95	0.927
cross-speed	83.53	34.73	0.0260	49.28	0.877
cross-mixffn	83.41	33.37	0.0270	54.39	0.891
time-cross-query	83.34	35.89	0.0275	45.71	0.896

**Table 3.3:** EPredictor evaluation results with different model architectures on the test set (no up- nor down-sampling). The MAPE and F1 are shown in (%)

the concept of *Confident Predictive Maintenance Window (CPMW)*, which represents the interval within which our model can make reliable predictive maintenance predictions (similar to the "prediction window" described in [116]). We quantify this with the *CPMW Area Under Curve (CPMWAUC)*. The F1 score, MAE, and MAPE have been calculated on average for all observations in Table 3.3, and additionally for each history  $H_t^i$  in Fig. 3.4 to understand how each model performs with different numbers of observations. To monitor the predictive maintenance capability of each model, the CPMWAUC<sub>f1</sub> and CPMWAUC<sub>mae</sub> were computed.

### 3.5.3 Ablation II: EPredictor Architecture & CPMW

**Embedding Architecture and Cross-attention** We explored several architectural changes and their impact on the CPMW: we applied a RoPE (*rot*), a cross-attention with *query* or *key* or *value* to the second multi-head attention block (*cross*), added the context embedding **CE** (*ce*) to layer 1 and/or 2, applied a scaling factor of  $\sqrt{3d}$  to **Q**, **K** as shown in Eq. 2.4 (*scale*), injected a relative matrix **S<sub>rel</sub>** into the attention scores (*speed*), and applied a mixed feed-forward network (*mixffn*) [159] to the mileage embedding. The *time* model refers to **T**, which is also added to **E**. Finally, we trained a model with and without the *Random Event Head*.

**Results** Our experiments revealed several key insights: By applying a *cross* attention, we can see improvement in all metrics (*rotnocross-ce-1-2*), which is consistent with the machine translation analogy "*dtc2errorpattern*". The best cross-attention results were obtained when  $H(S)$  was used as the *key-value*. Adding the mileage via an MLP layer (*cross-mixffn*) seemed to help the MAPE (-2.5%), the CPMWAUC<sub>f1</sub>(+9) and also the CPMWAUC<sub>mae</sub>(-0.005) compared to *time-cross-query* model, suggesting that mileage is beneficial for both tasks. This is consistent since EPs are also dependent on the traveled distances between DTCs and the different stationary behavior of the vehicle. Furthermore, models incorporating a RoPE (*rot*) performed significantly better in both regression and classification tasks, as in the pre-training, highlighting the performance of RoPE in machine translation tasks [142]. Adding **CE** to the last layer (*ce-2*) yielded

### 3 Error Pattern Prediction from Vehicle Diagnostic Event Sequences

the best results, as opposed to adding it to both layers (*ce-1-2*). Surprisingly, doing feature engineering on  $\mathbf{T}, \mathbf{M}$  with a *speed* matrix  $\mathbf{S}_{\text{rel}}$  did not help the metrics, which could indicate some missing modalities (e.g., mileage) during training, thus  $\mathbf{CE}$  is more adapted for real-world scenarios. We monitored the need for our *Random Event Head* and noticed +1.2% in the F1 Score and +10.1 in the  $\text{CPMW}_{f_1}$ .

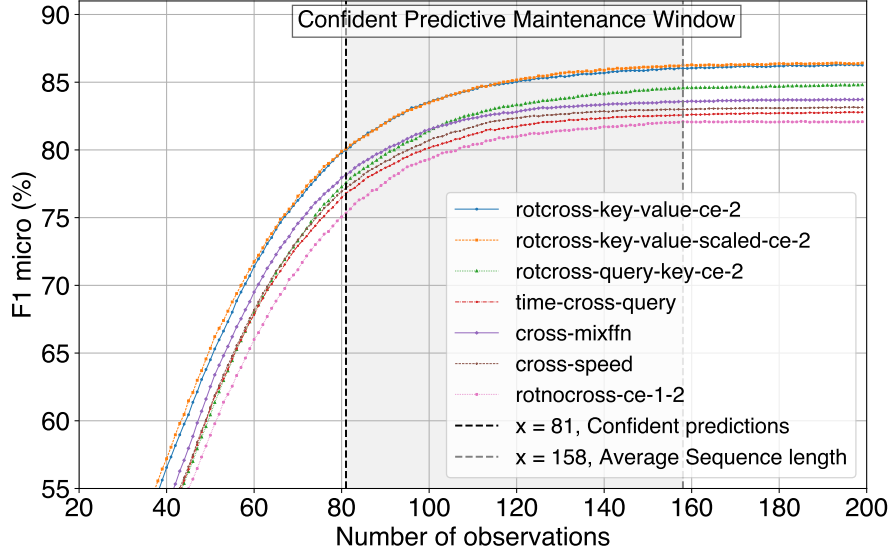


**Figure 3.4: Classification Performance Comparison Between Architectural Changes.** F1 Score comparison with multiple EPredictor architectures as a function of the number of observations. This answers *what* EP is most likely to occur.

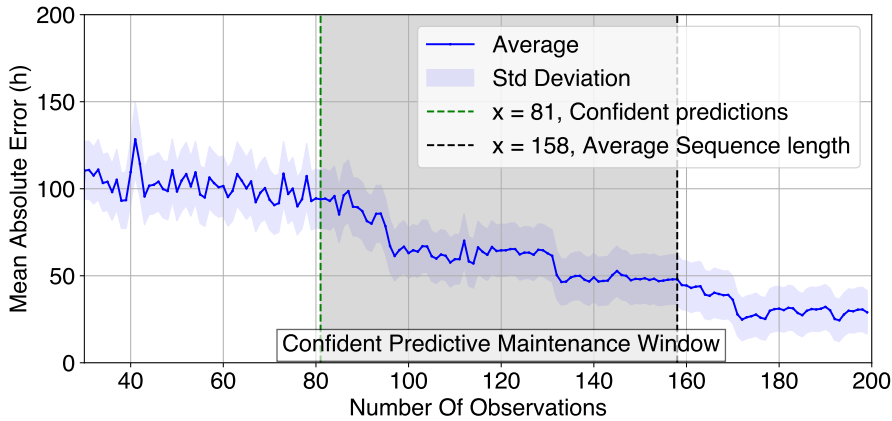


**Figure 3.5: Regression Error As a Function of the Number of Observations.** Evolution of the MAE as a function of the number of observations for the best performing model, this effectively tests for *when* an EP is most likely to occur.

When taking the best performing model (*rotcross-key-value-scaled-ce-2*), the model entered the CPMW after 81 observations, i.e., **half of the sequence**. Within this window,

the model obtained an error of  $\approx 65 \pm 14\text{h}$  when estimating the time of EP occurrence (Figure 3.5), highlighting the model’s predictive capability within the CPMW. Otherwise, the average absolute error across all observations was approximately  $58.4 \pm 13.2\text{h}$ . By experimenting with these modifications, we aimed to identify the optimal architecture for predictive maintenance. The findings reveal that cross-attention, context embedding in the second layer, and scaled attention significantly improve performance within the CPMW.

### 3.6 Summary

This chapter presented a novel approach to predictive maintenance in vehicles by modeling diagnostic event sequences as a language. By introducing two Transformer-based architectures, *CarFormer* and *EPredictor*, we demonstrated that it is possible to jointly forecast both *when* and *what* error patterns are likely to occur, even in the presence of highly unbalanced, irregular, and high-cardinality diagnostic data. Our results show that autoregressive modeling of DTC sequences provides a powerful means to capture the temporal and contextual dependencies underlying vehicle faults. The proposed framework effectively reconciles traditional event sequence modeling and large-scale fault prediction, moving toward a unified, data-driven foundation for predictive maintenance. Beyond its experimental performance, the proposed system has clear practical implications. In principle, once deployed, *EPredictor* can operate in real-world scenarios by continuously analyzing DTC streams and estimating the probability and timing of forthcoming error patterns. When a sufficiently confident prediction is made, the vehicle can proactively notify the user of a potential critical fault and recommend a visit to a service center. Such a system has the potential to enhance vehicle safety, reduce maintenance costs, and ultimately support the broader vision of intelligent and self-diagnostic automotive systems. The pretrained *CarFormer* and *EPredictor* backbones are directly applicable for a broad range of downstream tasks, including sequence clustering, anomaly detection, and causal discovery, as demonstrated in the subsequent parts of this thesis.

### 3.7 Outlook

Several limitations remain. First, predictive performance is sensitive to the quality and convergence of *CarFormer*’s pretraining; a poorly trained backbone degrades *EPredictor* accordingly. Second, the CPMW metric shows that reliable predictions require observing approximately half the sequence, which may be too late for certain use cases. Third, the highly imbalanced distribution of error patterns means that rare but critical EPs remain harder to detect, despite the upsampling strategy employed. These constraints motivate the following chapter, which incorporates additional modalities to improve the classification of overlapping and rare error patterns.



## 4 Multimodal Sequence Modeling for Error Pattern Classification

Chapter 3 demonstrated that DTC sequences alone provide a strong predictive signal, but highlighted a key failure mode: error patterns sharing identical Boolean DTC rules cannot be disambiguated from the event stream alone. Chapter 4 addresses this limitation directly, by introducing environmental sensor data as a complementary modality. Contextual information such as raw sensory data (e.g., temperature, humidity, and pressure) is beneficial for engineers to classify sequences of error codes into vehicle failures. Yet, it introduces unique challenges due to its complexity and the noisy nature of real-world data. This chapter is based on the following publication:

**Context-Informed Sequence Classification: A Multimodal Approach to Vehicle Diagnostics.** [88] Hugo Math, Rainer Lienhart, International Conference on Learning Representations (ICLR) Workshop on Time Series in the Age of Large Models, April 2026.

This chapter introduces BiCarFormer: a multimodal approach to multi-label sequence classification of error codes into EPs that integrates DTC sequences and environmental conditions. BiCarFormer is a bidirectional Transformer model tailored for vehicle event sequences, employing embedding fusions and a co-attention mechanism to capture the relationships between diagnostic codes and environmental data.

### 4.1 Introduction

Diagnostic experts routinely find it necessary to incorporate contextual information as complex EPs seem to overlap in their rule definition (Eq. 2.18). Prior work relies only on DTCs to infer either the next DTCs (using Transformers [150, 49] and RNNs [50]). While environmental data can enhance the classification or clustering of EPs, it poses integration challenges due to its volume, variability, and ultimately high dimensionality. Modern time series foundation models (TSFMs) such as Chronos [4] operate on one modality and on a continuous event sequence. Vehicle data is intrinsically multimodal, consisting of continuous signals (voltage, RPM) interleaved with discrete event codes (DTCs), a modality mix that purely continuous TSFMs struggle to integrate. Our goal is to uncover the appearance of DTCs and environmental conditions that correlate with certain EPs. We demonstrate that our approach significantly improves the multi-label sequence classification of EPs, outperforming traditional models that rely solely on DTCs [49, 50] and classical Transformers such as BERT [26]. We further explain classification

predictions by interpreting cross-attention scores. We show that BiCarFormer learns to detect fluctuations of quantized continuous values, despite encoding different units and thousands of different environmental conditions. We emphasize the implications of real-world data to the proposed method and its potential further applications.

## 4.2 Related Work

### 4.2.1 Failure Detection in Vehicles

Historically, machine learning models have been employed to detect machine failures. It includes techniques based on correlation [175], Bayesian networks [72], decision tree models [138], and more recently neural state-space models [56] to predict machine failures or remaining useful life (RUL). These methods rely on historical data to identify patterns and predict potential failures. Bayesian networks can model the probabilistic dependencies among various components of the vehicle. Some papers explore the use of Deep Neural Networks (DNNs). For example, [178] uses a combination of convolutional, fully connected, and Transformer modules within one architecture for the classification of machine event logs.

In Chapter 3, we suggested using the warranty data of vehicles to create a supervised learning problem where we attach EPs to each DTC sequence. We further model these multivariate vehicle event sequences and focus on classifying error patterns to benchmark the proposed methods.

### 4.2.2 Multimodal Fusion & Learning

Introducing other modalities in a Transformer model has been extensively studied [162, 99]. One common and simple way to fuse two token embeddings  $\mathbf{X}_A \in \mathbb{R}^{L_a \times d}$  and  $\mathbf{X}_B \in \mathbb{R}^{L_b \times d}$  from modality A and B (assumed to be sequences) is via *early summation*. Specifically, *token-wise weighted summing* of multiple embeddings at the input level is defined as:

$$\mathbf{U} = \alpha \mathbf{X}_a \oplus \beta \mathbf{X}_b \quad (4.1)$$

In MedBERT [122], the authors summed three types of embeddings (diagnostic codes, the order, and the position of each visit) to form input  $\mathbf{U}$ . This method has several advantages: it is simple to integrate into a Transformer and does not significantly alter the computation. However, the different tokens need to be aligned or projected to a latent space if  $L_a \neq L_b$ , and it is not clear how one should weigh the different embeddings when summing using  $\alpha, \beta$ . For example, BERT uses an early summation of its token embedding  $\mathbf{E}$  and its position  $\mathbf{PE}$  such that  $\mathbf{U} = \mathbf{E} + \mathbf{PE}$ .

In the diagnostic domain, DTC-TranGRU [49] uses three separate DTC components embeddings that they concatenate along  $d$  to form a global DTC embedding  $\mathbf{D} \in \mathbb{R}^{L \times d}$  (we refer to this method as *early concatenation*).

$$\mathbf{U} = \text{concat}(\mathbf{X}_a, \mathbf{X}_b) \in \mathbb{R}^{L \times (d_b + d_a)} \quad (4.2)$$

This enables finer-grained integration of additional features by selecting their embedding sizes,  $d_a$  and  $d_b$ . It also preserves the distinct characteristics of each feature by maintaining separate dimensions, thus potentially learning more nuanced representations and interactions in the deeper attention layers. However, it usually requires more computation since we concatenate along  $d$ , resulting in more parameters [162] for the point-wise feed-forward layers and the projection matrices. It also does not work well with low cardinality features such as token type ids from BERT [26] because it will only span across a very small size in the hidden dimension  $d$ , thus early summation is preferable for this case.

By combining embeddings at an early stage, models can learn a unified representation that captures the interactions between different features. This can be particularly useful if the features are highly correlated. These methods are used in a wide variety of domains, in particular in medicine [122, 132] with electronic health records (EHR). When dealing with complex modalities such as audio or images that are not necessarily aligned, the attention mechanism of Transformers [150] is usually used for fusion. Late fusion in Transformers usually involves encoding the different modalities through independent Transformer encoders to extract high-level representations  $\mathbf{Z}_a, \mathbf{Z}_b$ :

$$\begin{aligned}\mathbf{Z}_a &= Tf_a(X_a) \in \mathbb{R}^{L_a \times d} \\ \mathbf{Z}_b &= Tf_b(X_b) \in \mathbb{R}^{L_b \times d}\end{aligned}$$

Then, these representations can be concatenated and encoded via another third Transformer (*Hierarchical Attention*) to output a fused representation using multi-head attention:

$$\mathbf{Z} = Tf(\text{concat}(\mathbf{Z}_a, \mathbf{Z}_b)) \in \mathbb{R}^{L_a \times (d_a + d_b)}$$

One can also fuse  $\mathbf{Z}_a, \mathbf{Z}_b$  with similarity products like in CLIP [120]. The CLIP model introduces a new self-supervised multimodal learning task where the model learns which caption goes with which image and demonstrates SOTA performance for 30 different existing computer vision datasets. The problem with this method is its limited cross-modal interaction, where we first encode separately the modalities to fuse them later. Perhaps the model would benefit from learning multimodal dependencies earlier in the architecture.

At the other end, middle fusion (or *mid fusion*) methods involve *cross-attention* and more generally *co-attention* mechanisms. In ViLBERT [81] and LXMBERT [144], the attention models enable computation of the attention scores  $\mathbf{A}$  as a function of the image and text input. For example, using  $\mathbf{X}_a$  as query  $\mathbf{Q}_a$  and  $\mathbf{X}_b$  as  $\mathbf{K}_b, \mathbf{V}_b$ , we can compute the resulting  $\mathbf{C}_{a \rightarrow b} \in \mathbb{R}^{L_a \times d}$  and vice versa (one input attends to another). In *co-attention* both inputs attend to each other by computing two attentions simultaneously ( $\mathbf{C}_{a \rightarrow b}, \mathbf{C}_{b \rightarrow a}$ ), which enables multimodal learning in both ways. One caveat to these methods is that by not projecting  $\mathbf{X}_a, \mathbf{X}_b$  into a fixed attention scores matrix but computing a new  $\mathbf{A} \in \mathbb{R}^{L_a \times L_b}$ , if  $L_b \gg L_a$ , we drastically increase the computational overhead due to the quadratic time complexity  $O(L^2)$  of the *vanilla* attention. We also get two hidden representations for each modality:  $\mathbf{H}_a, \mathbf{H}_b$ .

The product  $QK^T$  carries most of the computation, thus one may consider selecting specific query and key multiplications, resulting in a sparse attention variant like LongFormer [14], or BigBird [167]. These models use a sliding, global, and random attention combination, reducing  $O(L^2)$  to a linear complexity of  $O(w \times L)$  for LongFormer. Another method is to project the keys and values into a lower-dimensional space, like in Linformer [152], or use a multimodal bottleneck Transformer [99] to compute the cross-attention partially in a restricted latent space. Feature fusion in event sequence models has received comparatively little attention in the literature. The majority of papers aim at fusing the time  $t_i$  information per event type  $x_i$  by performing an *early summation* [178, 172, 179] to integrate the time component, sometimes omitting the positional embedding for the time embedding [179], sometimes summing both [136, 77], or not taking it into account [49].

### 4.3 Dataset Extension with Environmental Conditions

We extend the Chapter 3 dataset with 5 million sequences, containing an average of  $L \approx 150 \pm 90$  DTCs per sequence from different BMW model ranges. Each sequence  $S_{raw}$  belongs to a unique vehicle. In  $S_{raw}$ , each DTC occurrence is attached additionally with a small sequence  $S_e^{(i)} = \{(d_j, v_j, c_j)\}_{j=0}^{L_e^{(i)}}$  of environmental conditions, respectively with elements description, value, and unit.

These elements construct a single event  $(x_i, t_i, m_i, S_e^{(i)})$ . To obtain a complete marked event sequence  $S_{raw} = \{(x_i, t_i, m_i, S_e^{(i)})\}_{i=0}^L$  (Def. 3), we apply the same 30-day, 300-km observation window as in Chapter 3. We then split  $S_{raw}$  into two distinct sequences:  $S = \{(x_i, t_i, m_i)\}_{i=0}^L$  for the DTCs, and  $S_e = \{(d_i, v_i, c_i)\}_{i=0}^{L_e}$  for only the environmental conditions with length  $L_e \approx 2275 \pm 2310$ , making it highly unaligned with  $S$  and orders of magnitude longer. An overview of the elements is provided in Table 4.1 as well as the number of distinct values for each feature in Table 4.2.

#### 4.3.1 Integration

Incorporating sensory information efficiently, such as temperature or pressure value alongside discrete codes, remains an open problem [178, 49]. Intuitively, it might seem

Notations	Description
$S_e$	Sequence of environmental conditions triplets defined as $S_e = \{(d_i, v_i, c_i)\}_{i=0}^{L_e}$ of length $L_e \gg L$
$d$	Environmental condition description, e.g., temperature increase, vehicle speed, pressure increase
$v$	Environmental condition value can be int, float, string, null
$c$	Environmental condition unit, e.g., A, V, bar, °C, sec

**Table 4.1:** New symbols introduced in this chapter. For base DTC notation, see Table 2.1

### 4.3 Dataset Extension with Environmental Conditions

trivial to rely on temperature for diagnosing a specific defect in a vehicle engine or a voltage measurement in a battery to identify a cell failure. Experts often analyze this data to make decisions about EPs in vehicles. However, the integration of environmental conditions comes with three significant challenges:

1. *Dimensionality*: descriptions have a high cardinality ( $> 10^3$ ) and values can be multi-types: strings, Booleans, integers, floats, or NaN.
2. *Variability*: differs across each DTC: e.g., we cannot be certain that we will observe 'temperature' for DTC1 and 'pressure' for DTC2.
3. *Volume*: there are multiple environmental conditions per DTC, which can be redundant, noisy, and duplicated across the sequence  $S_e$ .

The *Dimensionality* problem increases model complexity and often necessitates extensive data engineering. The *Variability* makes integration into a machine learning model challenging, and lastly, the *Volume* requires substantial data infrastructure to manage environmental conditions, since it is often several times the size of DTC data and significantly increases the sequence length, a known challenge in Transformers [77]. We partially address these challenges by:

- removing *null* values, units, or descriptions.
- removing duplicates per DTC: the same  $(d, v, c)$  triplet occurring multiple times within the same  $S_e^{(i)}$  is removed, retaining only one instance. This significantly reduced redundancy and noise in the data, though we still observed  $L_e \approx 2275 \pm 2310$  triplets per  $S_e$ . One caveat of this approach is the *nonalignment* of environmental conditions and DTC when multiple DTCs occur at the same  $t_i$ . In such cases, we drop subsequent environmental conditions after the first occurrence.
- selecting the top-18 most popular units.

To ingest the resulting  $S_e$  into a Transformer, we map our continuous values  $v \in \mathbb{R}^+$  into discrete *tokens* [162] with a limited vocabulary. Therefore, we search for the optimal bins for each unit  $c$ . A variation of the Greenwald-Khanna algorithm [45] up to a maximum of 4000 tokens per unit  $u$  to limit a potential  $18 \times \theta = 72000$  values. In practice, they overlap and do not reach the maximum (Table 4.2).

Data	# of values	Description
DTC	22,137	Diagnostic Trouble Code
ECU	132	Electronic Control Unit
Base-DTC	17,044	Error Code
Fault-Byte	2	Binary Value
E. Condition Description	2,559	(See Table 1: $d$ )
E. Condition Value	3,288	(See Table 1: $v$ )
E. Condition Unit	18	Most popular units: $u$

**Table 4.2:** Number of distinct values after filtering for each feature.

## 4.4 BiCarFormer

### 4.4.1 DTC Embeddings

We use a Bidirectional Transformer model [26] that we train with mask language modeling. Each DTC element is embedded in a specific feature space, namely: *ECU* ( $\mathbf{D}_{ecu} \in \mathbb{R}^{L \times d_{ecu}}$ ), *Base-DTC* ( $\mathbf{D}_{base} \in \mathbb{R}^{L \times d_{base}}$ ), and the *Fault-Byte* ( $\mathbf{D}_f \in \mathbb{R}^{L \times d}$ ) using separate lookup tables. The first two are concatenated along the feature dimension, like in [49], and  $\mathbf{D}_f$  is added to the result like a token type id in BERT [26]. This reduces the vocabulary size and trainable parameters compared to [91] and ensures that the embeddings with high cardinality are preserved independently, thus capturing more relationships between the *ECU*, the *Base-DTC*, and the *Fault-byte*. We obtain the input DTC embedding  $\mathbf{D} \in \mathbb{R}^{L \times d}$ :

$$\mathbf{D} = \text{concat}(\mathbf{D}_{base}, \mathbf{D}_{ecu}) + \mathbf{D}_f$$

During the pretraining phase, we mask only the Base-DTC token, since it provides the primary information.

### 4.4.2 Positional Embeddings

Understanding the positioning of failure events in both the temporal and spatial (mileage) dimensions is beneficial for predictive maintenance. Failure events in our dataset exhibit spatial and temporal patterns (Figure 4.1), which could indicate stationary behavior of the vehicle or recurring temporal failures [91]. Prior work, such as [178], employs adaptive binning to discretize time in long event sequences. However, given our moderate sequence length (258 DTCs with 30-day and 300-km intervals), binning is unnecessary. Additionally, lookup table embeddings, often used in discrete event modeling, would be computationally expensive, introduce unnecessary parameters, and fail to preserve meaningful distance relationships in  $\mathbb{R}^+$ .

We adopt a continuous time embedding [172] which is the deterministic positional encoding introduced in Chapter 3 (Eq. 3.1). We do it similarly to create a mileage embedding  $\mathbf{M} \in \mathbb{R}^{L \times d/2}$ . Both embeddings,  $\mathbf{T}$ ,  $\mathbf{M}$ , are concatenated along the feature dimension to form a unified positional representation. This preserves their independent contributions and prevents interference when fused with  $\mathbf{D}$ . Our final fused input  $\mathbf{U} \in \mathbb{R}^{L \times d}$  is given by:

$$\mathbf{U} = \text{concat}(\mathbf{D}_{base}, \mathbf{D}_{ecu}) + \mathbf{D}_f + \text{concat}(\mathbf{T}, \mathbf{M}) \quad (4.3)$$

### 4.4.3 Environmental Embeddings

To better capture relationships between the different environmental conditions elements ( $d, v, u$ ), we create three distinct learnable embeddings: (1) the description of the environmental conditions  $\mathbf{D}_e \in \mathbb{R}^{L_e \times d_d}$  (2) the discretized value  $\mathbf{V}_e \in \mathbb{R}^{L_e \times d_v}$  (3) its unit  $\mathbf{U}_e \in \mathbb{R}^{L_e \times d}$ . We use a mix of early summation and concatenation to fuse these embeddings at the input level and obtain the total environmental conditions embedding

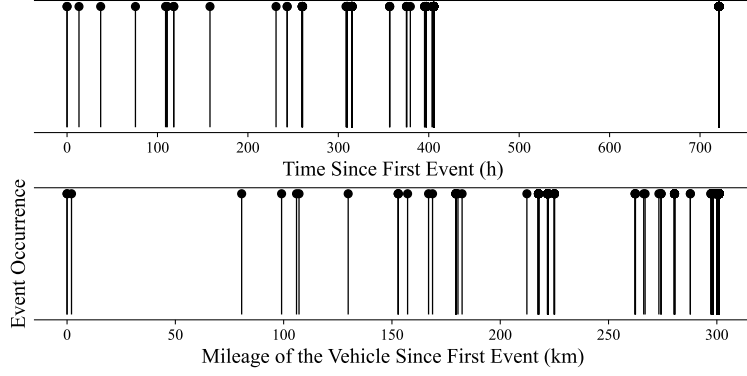


**Figure 4.1: Spatio-temporal Point Process Representation of a Vehicle.** Spatial (mileage) and Temporal (time) point process representation of events from a vehicle. Bold vertical lines indicate multiple events occurring at the same time  $t_i$  or mileage  $m_i$ .

$$\mathbf{E} \in \mathbb{R}^{L_e \times d}.$$

$$\mathbf{E} = \text{concat}(\mathbf{V}_e, \mathbf{D}_e) + \mathbf{U}_e$$

To fuse the environmental conditions, we cannot simply align them with their respective DTC to perform an early token-wise summation or concatenation with  $\mathbf{D}$ . Given that we utilize real-world data (noisy, redundant) and perform rigorous data filtering, there are too many missing environmental conditions for each DTC. Consequently, we chose to create a separate sequence  $S_e$  that is much longer than  $S$ , where we will concatenate all environmental conditions and fuse them into one embedding  $\mathbf{E}$ . This straightforward method is flexible, and  $\mathbf{E}$  can be employed in a middle fusion manner inside the attention mechanism [162].

#### 4.4.4 Co-attention for Vehicle Event Sequences

The overall architecture of BiCarFormer is shown in Figure 4.2. Our architecture is directly inspired by the co-attention mechanism of ViLBERT [81], which enables multimodal learning by computing attention scores conditioned on each modality. Two multi-head attention layers are processing  $S$  and  $S_e$ , resulting in two attention scores computation conditioned on:  $\mathbf{D}$  (DTCs) and  $\mathbf{E}$  (environmental conditions) fused embeddings. We apply a RoPE (Rotary Position Encoding) [142] like in the previous chapter, on two sets of queries and keys (one for each cross-attention) to induce the absolute and relative position of tokens (Figure 4.2).

More specifically, the fused input embedding vectors  $\mathbf{u}_m \in \mathbb{R}^d$  and  $\mathbf{e}_n \in \mathbb{R}^d$  from token positions  $m, n$  are projected through weights  $\mathbf{W}_q, \mathbf{W}_k, \mathbf{W}_v$ . The query and key are given by applying two different RoPE [142]:

$$\mathbf{q}_m = e^{im\theta_u} \mathbf{W}_q \mathbf{u}_m \quad (4.4)$$

$$\mathbf{k}_n = e^{in\theta_e} \mathbf{W}_k \mathbf{e}_n \quad (4.5)$$

#### 4 Multimodal Sequence Modeling for Error Pattern Classification

where  $\theta_u = \text{diag}(\theta_1, \dots, \theta_{d/2})$  with  $\theta_i = \theta_{0,u}^{-2i/d}$ ,  $\theta_{0,u} = 5000$ . Same for  $\theta_e$  but with  $\theta_{0,e} = 80000$  due to  $L_e \gg L$ . We use an alignment function [17]  $f : \mathbb{R} \rightarrow [0, 1]$  to produce the attention weights between two tokens:

$$\begin{aligned} a(\mathbf{u}_m, \mathbf{e}_n, m, n) &= f(\mathbf{q}_m^T \mathbf{k}_n) = a_{dtc \rightarrow env} \\ &= f\left(\mathbf{u}_m^T \mathbf{W}_q^T e^{i(n\theta_e - m\theta_u)} \mathbf{W}_k \mathbf{e}_n\right) \end{aligned} \quad (4.6)$$

We also compute Eq. 4.6 for  $a_{env \rightarrow dtc} = a(\mathbf{e}_m, \mathbf{u}_n, n, m)$  with separate weights for  $\mathbf{q}_m, \mathbf{k}_n$ . Finally, two cross-attended context vectors are produced:

$$\mathbf{c}_{dtc \rightarrow env}(m) = \sum_{n=1}^{L_e} a_{dtc \rightarrow env}(m, n) \mathbf{v}_{e,n} \in \mathbb{R}^d \quad (4.7)$$

$$\mathbf{c}_{env \rightarrow dtc}(n) = \sum_{m=1}^L a_{env \rightarrow dtc}(n, m) \mathbf{v}_{u,m} \in \mathbb{R}^d \quad (4.8)$$

where values  $\mathbf{v}_u, \mathbf{v}_e$  are obtained from  $\mathbf{V}_e = \mathbf{W}_v^e \mathbf{E}, \mathbf{V}_u = \mathbf{W}_v^u \mathbf{D}$ . We tried two different alignment functions  $f$  [17] for Eq. 4.6. The widely used *softmax* and *1.5-entmax*

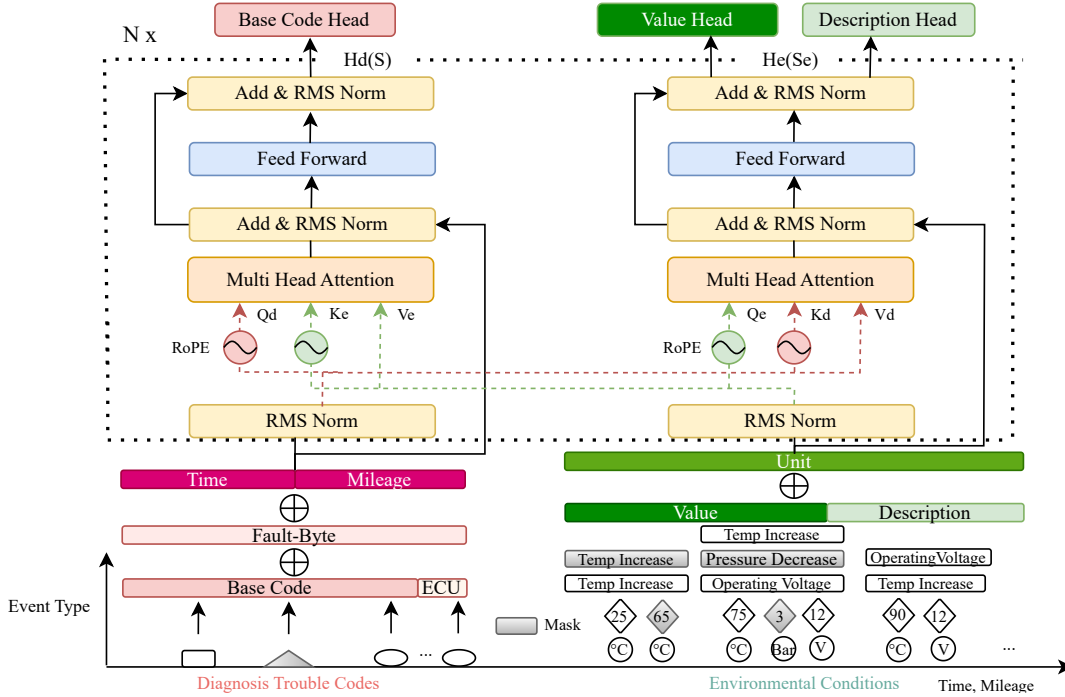


**Figure 4.2: BiCarFormer Architecture.** Both parallel Transformers are computing cross-attention scores conditioned on each modality  $\mathbf{Q}, \mathbf{K}, \mathbf{V}$ . Two final representations are generated for each modality: DTC ( $\mathbf{H}_d$ ) and environmental conditions ( $\mathbf{H}_e$ ). Multiple hierarchical embeddings are defined at the input level to account for DTC-specific features (ECUs, Fault-Bytes, Base-Code).

[115]. The standard *softmax* outputs dense attention scores, which might take too many environmental conditions into account. Since our input data is noisy and redundant, we would like to extract salient information; a sparse alignment function seems like an intuitive choice. However, in practice, we did not find a benefit using 1.5-entmax in the pretraining and classification where we observed a 30% slowdown in iterations per second. Consequently, we retained the *softmax*. As a consequence, two hidden states  $\mathbf{H}_d \in \mathbb{R}^{L \times d}$  and  $\mathbf{H}_e \in \mathbb{R}^{L_e \times d}$  (Figure 4.2) for each modality are computed after fully connected layers, residual connections and root-mean-squared normalizations [168, 146].

#### 4.4.5 Multimodal Learning

To reinforce the relationship between DTC events and environmental conditions, we not only mask the DTC but also the environmental conditions  $(d, v)$  and let the unit unmask to reduce training complexity. This enables multimodal learning by reconstructing  $S_e$  using  $S$  and vice versa. As a result, BiCarFormer learns to benefit from this extra modality, which can be confirmed by inspecting the cross entropy loss of the *Base-DTC* classification:  $\mathcal{L}_{\text{dtc}}$  where using both modalities helps to reduce the pretraining loss (Appendix. A.2). However, due to multitasking, the losses are less stable and may require gradient clipping and a smaller learning rate to stabilize training. BiCarFormer is trained with three cross-entropy losses balanced by static coefficients:  $\alpha = 0.5, \beta = 0.3, \gamma = 0.2$ :

$$\mathcal{L} = \alpha \mathcal{L}_{\text{dtc}} + \beta \mathcal{L}_{\text{value}} + \gamma \mathcal{L}_{\text{description}} \quad (4.9)$$

## 4.5 Experiments

### 4.5.1 Settings

We evaluated our model against established Transformer architectures, including BERT [26] (without the Next Sentence Prediction task) and DTC-TranGRU [49]. Since DTC-TranGRU is autoregressive [49], we trained it using next-token prediction and three separate heads, each classifying one of the three DTC components. To assess each model’s performance, we focused on multi-label classification of error patterns in the downstream task. For BERT and BiCarFormer we masked 15% of the tokens during the pretraining. The different models comprised approximately 25 million parameters, with the same hidden size  $d = 600$ , ensuring a fair comparison. For our downstream task of multi-label sequence classification, we used either the [CLS] token to perform classification or in the case of the BiCarFormer, the  $[CLS]_{\text{dtc}}$  and  $[CLS]_{\text{env}}$  after simply concatenating them along the feature dimension  $d$  and fusing with a small *MLP*. We used the [EOS] token for DTC-TranGRU rather than the [CLS]. Each classifier has 3,461,160 trainable parameters and consists of a small MLP with layer normalization, residual connections, and a sigmoid activation. We froze all backbones during classification. The dataset was partitioned into training, validation, and testing sets, adhering to a ratio of 75%, 15%, and 15%, respectively, with about 360 labeled error patterns. For the pretraining, we used a learning rate of  $10^{-4}$  with a cosine scheduler and warm-up of 2000 steps for all

models. We used the AdamW optimizer [79] with  $\beta_1$  set to 0.9 and  $\beta_2$  to 0.999. We applied a weight decay of 0.1 and a percentile gradient clipping of 5. Finally, we trained on an NVIDIA A10G GPU using FP16 with a batch size of 32 for the pretraining and 192 for the classifiers.

#### 4.5.2 Metrics

The evaluations were conducted across 360 different error patterns. To measure classification performance, we employed multiple metrics, namely AUROC (Area Under the Receiver Operating Characteristic), Precision, Recall, and F1 Score [108]. The last three were computed using a confidence threshold of 0.8. The metrics were aggregated using different averaging: micro, macro, and sample. Micro computes metrics broadly and favors frequent classes. It provides an overall picture of model performance, but it does not reflect the performance *per-class* or *per-instance*. In contrast, macro averaging treats all classes equally by computing metrics independently for each class and averages the results. In multi-label classification, the focus is often on *per-instance* performance rather than *per-class* performance. This means we prioritize the overall quality of multi-label predictions for each instance, rather than optimizing for the accuracy of individual labels in isolation. For this, the sample averaging computes metrics *per-instance* and then averages across all samples.

#### 4.5.3 Multi-label Classification Performance Analysis

Table 4.3 presents a comparative analysis of BiCarFormer against established sequence-to-sequence models for multi-label error pattern classification. Multi-label classification is particularly challenging due to the varying complexity of error patterns, where a single instance may be associated with multiple diagnostic trouble codes (DTCs) and environmental conditions. DTC-TranGRU [49] underperforms, particularly in *per-class* and *per-instance* evaluations, likely due to the limitations of masked attention mechanisms

Micro and Macro Averaging			
Model	AUROC (Micro)	F1 Score (Micro)	F1 Score (Macro)
<b>BiCarFormer</b>	<b>0.809</b>	<b>0.77</b>	<b>0.71</b>
DTC-TranGRU [49]	0.602	0.36	0.28
BERT [26]	0.768	0.71	0.63
Sample Averaging			
Model	Precision (Sample)	Recall (Sample)	F1 Score (Sample)
<b>BiCarFormer</b>	<b>0.68</b>	<b>0.62</b>	<b>0.64</b>
DTC-TranGRU [49]	0.23	0.19	0.20
BERT [26]	0.59	0.53	0.55

**Table 4.3:** Downstream evaluation of multi-label error pattern classification. Each model has the same number of parameters (25M). Results are grouped by averaging type (micro/macro vs. sample).

and model architecture. These constraints make it difficult for the model to capture long-range dependencies in the input sequence, leading to a lower AUROC (0.602) and poor F1 scores (Micro: 0.36, Macro: 0.28, Sample: 0.2). While BERT [26] is already achieving relatively high AUROC and F1 Micro, BiCarFormer significantly enhances the AUROC (Micro) by +4%, and the F1 Score (Micro) by +6%.

The improvement of BiCarFormer is especially visible for *per-class* averaging. When dealing with many error patterns, some are more difficult to distinguish due to their natural complexity and overlaps. BiCarFormer, however, better differentiates rare classes, suggesting an improved capacity to generalize across a diverse range of error patterns. This is confirmed in this experiment, where we see the gaps in classification performance when averaging across classes, with a +8% F1 Macro compared to BERT. This means that classes with small instances, usually hard to classify using only the DTCs, can be better differentiated using environmental conditions. Finally, *per-instance* precision and recall are the biggest improvement with +9% in F1 Score, Precision, and Recall compared to BERT. These results confirm that BiCarFormer effectively leverages this additional information and highlights the predictive improvement compared to standard Transformers.

#### 4.5.4 Cross-Attention Scores Interpretations

We would like to understand how the co-attention mechanism enables multimodal learning and enhances downstream tasks. We took a random test sample with a specific battery issue and ran it on BiCarFormer to analyze the different cross-attention score patterns. Figure 4.4 presents a heat-map visualization of  $\mathbf{A}_{dtc \rightarrow env}$ . This helps us to

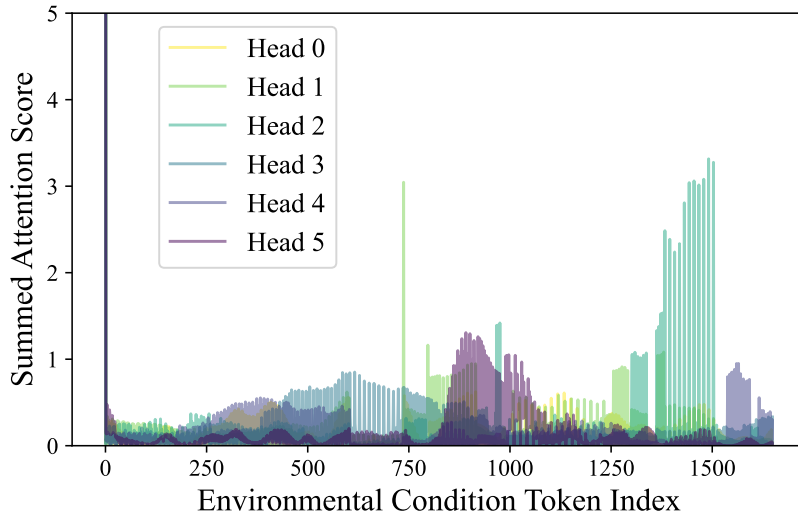


**Figure 4.3: Attention Distribution between Environmental Condition Tokens.** Amount of attention received by each environmental condition token from the DTCs. The y-axis was truncated to improve clarity as well as the number of heads printed. We take  $\mathbf{A}_{dtc \rightarrow env}$  of the last layer.

#### 4 Multimodal Sequence Modeling for Error Pattern Classification

understand general attention patterns from DTCs to environmental conditions. Cross-attention uncovers natural relationships from certain DTCs linked to specific environmental conditions. Consider DTC 190, we can see that this token focuses more on a local series of environmental conditions with unit  $km/h$  rather than other units. Whereas DTC 33 and 485 attend more to  $^{\circ}C$ . This result is attributable to specific environmental conditions that characterize certain DTCs, i.e., the temperature might define DTC1 while DTC2 might indicate a rise in the voltage. Due to the duplicated environmental conditions unit across  $S_e$ , one DTC might attend to the next environmental conditions 'voltage' also later in the sequence, creating these line patterns on Figure 4.4 with DTC 190 & 33 & 485. As a consequence, we notice the local temporal patterns between DTCs and their surrounding environmental conditions (Figure 4.4). Therefore, the initial DTCs should prioritize the initial environmental conditions in  $S_e$ , with an offset resulting from the difference in sequence length between  $L$  and  $L_e$ . For instance, DTC 190 at positions 1 and 6 should prioritize the initial environmental conditions.

We would like to assess whether the DTCs attend to a few key environmental conditions. From the same test sample, Figure 4.3 plots the amount of attention that DTCs give to each of the environmental conditions. We observed different clusters per head. Each head learns to focus on specific environmental conditions, sometimes particular

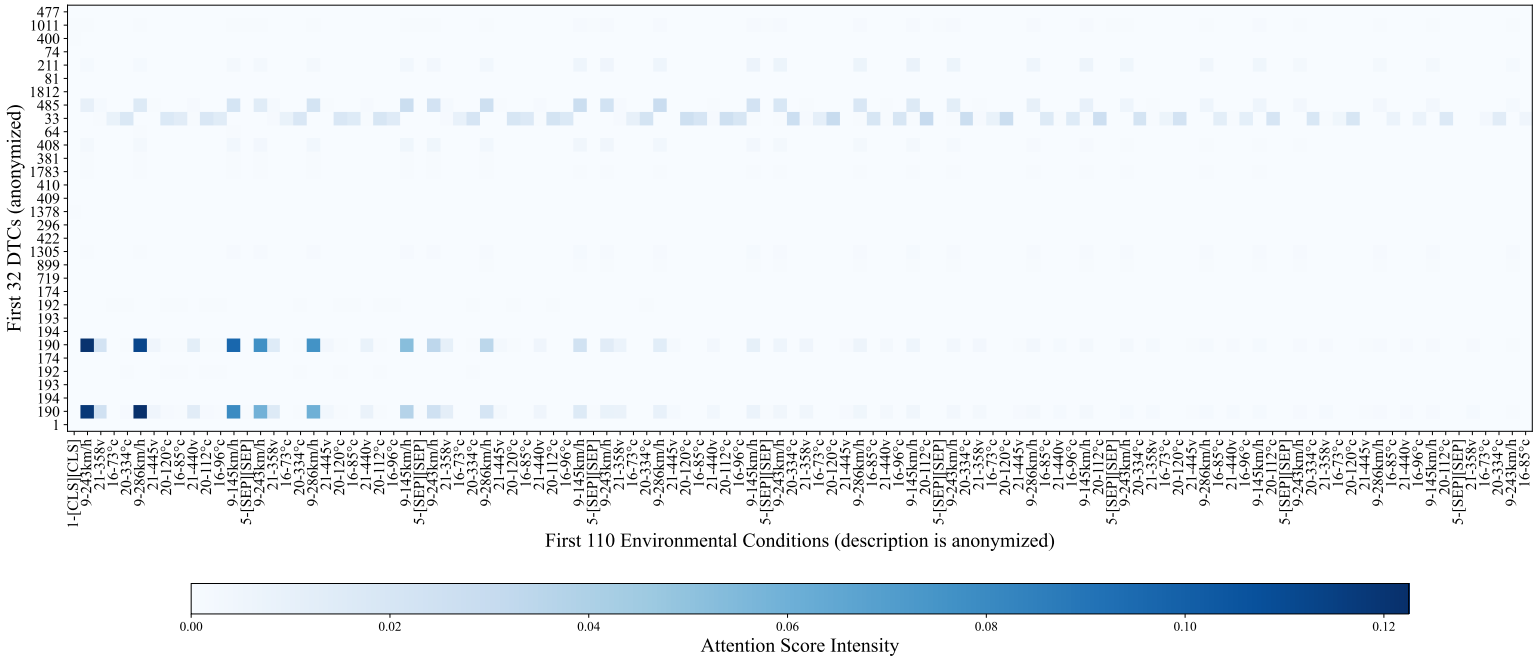


**Figure 4.4: Cross-Attention Scores for  $A_{dtc \rightarrow env}$ .** The DTCs are shown on the y-axis (anonymized), and the environmental conditions with their 3 elements ( $d, v, u$ ) concatenated are shown on the x-axis (the description  $d$  is anonymized). The intensity of each cell reflects the attention weight, where darker shades indicate higher attention values.

indices like *head 1* ( $i \approx 749$  and  $800$ ), and *head 2* ( $i \approx 960$ ). The [CLS] token is traditionally heavily attended. Interestingly, the last part of the sequence seems to be more attended by specific heads:  $i \in [1300, 1500]$ , signaling that we can capture long-range dependencies between DTCs and tokens of environmental conditions even with a big difference in sequence length (i.e., with  $L_e \gg L$ ). Moreover, late environmental conditions might carry a lot of defect signals, which makes sense as the sequence approaches the time of the critical failure event occurring at time  $t_i = t_L$ . Thus, attention scores increase correspondingly.

#### 4.5.5 Error Pattern in Battery Electric Vehicles

With the increasing popularity of *BEV* (battery-electric vehicle), there is a pressing need to diagnose failures in these vehicle types. We take the example of a concrete error pattern, such as a *battery aging*, which is a common phenomenon in electric vehicles. And draw the cumulative attention of e. condition units for the same test sample as before. Since attention heads focus on a certain part of  $S_e$  (Figure 4.3), some should focus on special units (Figure 4.6) such as km/h (*head 0, 4, 9*) while other on  $^{\circ}\text{C}$  (*head 6, 7*) and voltage (*head 1, 2*). Now, more interestingly, we take a head that tends to specialize in one unit like *head 2* for voltage and draw the evolution of the discretized voltage value as a function of their index in  $S_e$  in Figure 4.5. We essentially try to answer if we have a fluctuation of voltage values and a correlated change in the attention pattern. We also draw the associated attention scores received from DTCs and obtain multiple *trigger points* where the voltage value strongly correlates with attention scores.

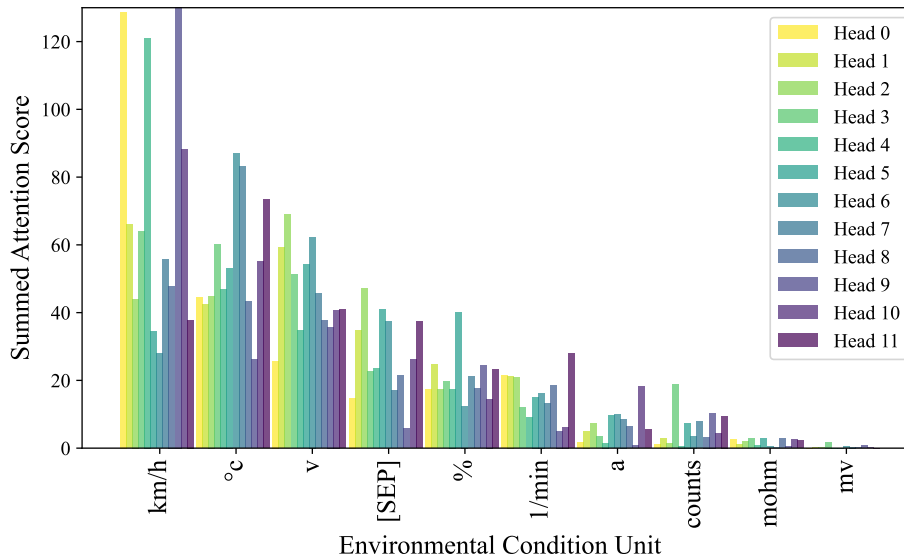


**Figure 4.5: Attention Distribution between Environmental Conditional Units.** Amount of attention received by each environmental unit from the DTCs in a *battery aging* error pattern from a battery electric vehicle. We take  $\mathbf{A}_{dtc \rightarrow env}$  of the last layer and print all heads.

We note that this is not the same depending on the heads; some exhibit exponentially decreasing attention scores shapes, while others exhibit noisy signals. As a consequence, BiCarFormer is able to extract specific fluctuations of continuous voltage values from a tokenized input. Engineers may extract trigger points and analyze how these specific variations affect the vehicle, providing a more explainable result.

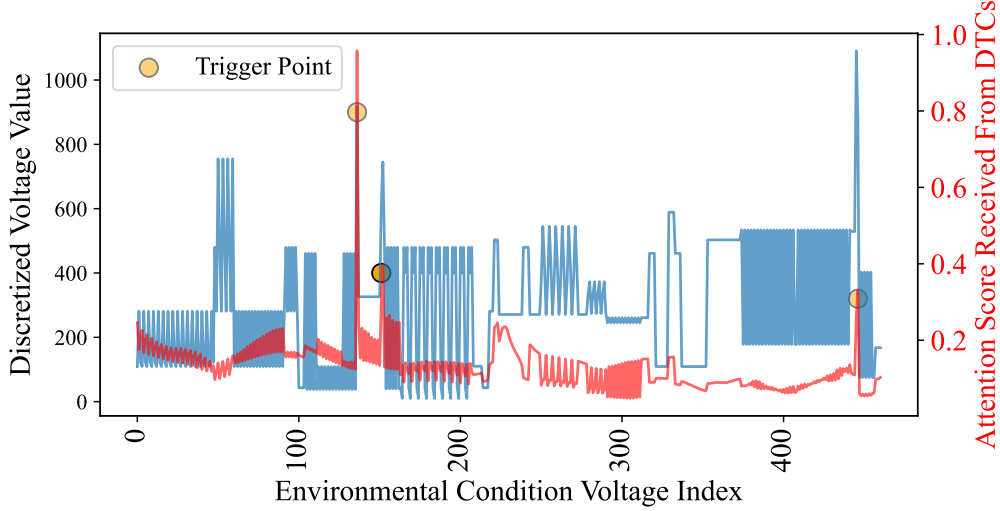


**Figure 4.6: Discretized Voltage and Attention Scores Evolution between Environmental Token Position.** Discretized voltage variation as a function of environmental condition tokens and the associated amount of attention received from DTCs. We only take triplets  $(d, v, u)$  from  $S_e$  with  $u = 'v'$  and extract  $A_{dtc \rightarrow env}$  from the last layer and *head 2*. The sample is taken from a *battery aging* error pattern. BiCarFormer implicitly learns the fluctuation of discretized continuous values to make a prediction.

## 4.6 Applications to Downstream Tasks

Having a separate hidden state for the environmental conditions also enables unsupervised learning in settings where EPs are unavailable. The hidden state  $H_e$  could provide a more accurate dimensionality reduction and observe better decision boundaries between unlabeled EPs using clustering techniques. Also, if provided with domain knowledge, we could directly filter  $S_e$  beforehand to take specific environmental conditions. Our model and overall paradigm enable retention of this architectural choice and reduce the computation by injecting domain knowledge directly into the preprocessing steps. Another possible useful downstream application is explainability. We would like to see the contributions of environmental conditions and DTCs to the EPs classification. Since error patterns are hard-coded defined rules, we could try to derive new rules for unknown error patterns based on feature attribution methods [82], cross-attention scores, perturbation-based methods or multi-label causal discovery with Transformers. BiCar-

Former model classifies EPs a posteriori (offline setting); thus, the inference optimization might not be needed since we do not rely on edge computing capabilities within the vehicles. Nevertheless, due to the quadratic time complexity of cross-attention scores, there is an extensive need to optimize Eq. 4.7, and Eq. 4.8. Alternatives like sparse attention [77, 167, 14], token merging [16] or pooling should be adapted for co-attention in event sequences.

## 4.7 Summary

We introduced BiCarFormer, a bidirectional multimodal Transformer designed to classify error patterns by jointly encoding discrete DTC sequences and continuous environmental conditions. Through a co-attention mechanism and hierarchical embedding fusion, BiCarFormer learns cross-modal dependencies between failure events and their surrounding sensory context. On a real-world automotive dataset comprising 22,137 DTCs and 360 error patterns, BiCarFormer achieves an AUROC of 0.809, a micro F1 score of 0.77, and a sample-level F1 score of 0.64, representing improvements of +4%, +6%, and +9% respectively over a standard BERT baseline trained on DTC sequences alone. The gains are most pronounced in per-class and per-instance evaluations, confirming that environmental conditions provide discriminative signal for rare and overlapping error patterns that share identical DTC rule definitions. Interpretability analysis of the cross-attention scores reveals that individual attention heads specialize in specific environmental units, such as voltage or temperature, and implicitly detect fluctuations in discretized continuous values that correlate with fault onset. This provides an additional layer of transparency beyond what DTC-only models offer. However, two practical limitations merit acknowledgment. First, the quadratic complexity of the co-attention mechanism with respect to the environmental condition sequence length ( $L_e \gg L$ ) constitutes a computational bottleneck for long sequences, motivating future work on sparse or pooled cross-attention variants. Second, BiCarFormer classifies error patterns offline (a posteriori), in contrast to EPredictor’s online, causal-mask-based operation; it is therefore better suited to retrospective diagnostic analysis than real-time on-board deployment.

## 4.8 Outlook

Part I has demonstrated that large-scale Transformers can serve as effective predictive and diagnostic models for high-dimensional vehicle event streams. The introduced models demonstrated that NLP techniques such as word embeddings, positional encoding, and transformer models can be adapted to event sequences to capture the hierarchical dependencies among diagnostic trouble codes (DTCs). The connection is not merely sequential: the autoregressive models of Part I serve as neural density estimators in Part II, a repurposing that distinguishes this thesis from prior work. By interpreting attention scores, automotive engineers can better understand BiCarFormer predictions. However, we must establish cause-and-effect relationships between DTCs and error patterns rigorously, as relying on attention scores alone lacks reliability [155, 11]. While

predictive models enable early fault detection, they remain fundamentally correlational: a high F1 score tells us what will fail and when, but not why. Without understanding the underlying causal mechanisms, any prediction remains fragile, susceptible to distributional shift, and incapable of supporting counterfactual reasoning or root-cause analysis. Establishing such causal relationships requires moving beyond correlation-based models toward methods that explicitly encode the data-generating process. This demands a formal framework for causal discovery, grounded in probability theory and information theory, that is capable of operating on the scale of tens of thousands of event types over multiple samples. Part II introduces precisely this foundation.

## **Part II**

# **Understanding Causal Structures in High-Dimensional Event Sequences**



# 5 Foundations of Causal Discovery and Information Theory

Having established predictive models in Part I, we now turn to understanding. Causal discovery requires measuring statistical dependencies between random variables in graphical models, a task for which information theory provides the right tools. We therefore introduce the related background, including the common definitions and modeling techniques required for Part II.

Let  $\mathbf{U}$  denote the set of all (discrete) random variables. We define the event set  $\mathbf{X} = \{X_1, \dots, X_n\} \subset \mathbf{U}$ , and the label set  $\mathbf{Y} = \{Y_1, \dots, Y_l\} \subset \mathbf{U}$ . When explicitly said, event  $X_i^{(t_i)}$  represent the occurrence of  $X_i$  at step  $i$  and time  $t_i$  and similarly for  $Y_i^{(t_i)}$ . We use this notation to improve clarity, since we mainly deal with stationary stochastic systems (Assumption 2).

## 5.1 Information Theory

In this section, we present the primary mathematical tools from probability and information theory that we will use in Part II.

### 5.1.1 Marginal, Conditional, and Relative Entropy

#### 5.1.1.1 Definitions

**Definition 8** (Entropy). *The entropy [129] of a discrete random variable  $X$  with a probability mass function  $p(x) = P(X = x)$  is defined by*

$$H(X) = - \sum_{x \in \mathcal{X}} p(x) \log p(x) \quad (5.1)$$

It can be thought of as the amount of surprise of the random variable  $X$  and thus quantifies its uncertainty. We measure it in *nats* as we use cross-entropy loss in PyTorch [110] which are calculated in *nats*.

**Definition 9** (Conditional Entropy). *We can define the conditional entropy as the entropy of a random variable given another random variable*

$$H(Y|X) = - \sum_{x \in \mathcal{X}, y \in \mathcal{Y}} p(x, y) \log \frac{p(x, y)}{p(x)} \quad (5.2)$$

This can also be written as a function of the posterior  $p(y|x)$  using the chain rule of probability:

$$H(Y|X) = - \sum_{x \in \mathcal{X}, y \in \mathcal{Y}} p(x)p(y|x) \log p(y|x) = -\mathbb{E}_{p(x,y)} \log p(Y|X) \quad (5.3)$$

It can be thought of as the remaining uncertainty in  $Y$  when we already know  $X$ .

**Definition 10** (Relative Entropy). *The relative entropy is defined as the distributional difference or Kullback-Leibler-Divergence ( $D_{KL}$ ) [23] between two probability distribution  $P$  and  $Q$ :*

$$D_{KL}(P||Q) = \sum_{x \in \mathcal{X}} p(x) \log \frac{p(x)}{q(x)} \quad (5.4)$$

It is an asymmetric “distance” measure between two probability distributions.

**Definition 11** (Joint Entropy). *The joint entropy  $H(X, Y)$  of a pair of discrete random variables  $(X, Y)$  with joint distribution  $P(X, Y)$  is defined as:*

$$H(X, Y) = - \sum_{x \in \mathcal{X}} \sum_{y \in \mathcal{Y}} p(x, y) \log p(x, y) \quad (5.5)$$

which is also the expected value of  $\log p(x, y)$ :

$$H(X, Y) = -\mathbb{E}_{p(x,y)} \log p(X, Y)$$

**Definition 12** (Information Gain). *The information gain  $I_G$  of a random variable  $Y$  obtained from an observation of the realization of  $X = x$  is defined as*

$$I_G(Y, x) = H(Y) - H(Y|x) \quad (5.6)$$

*It can also be written as a distributional difference*

$$I_G(Y, x) = D_{KL}(P(Y|X = x)||P(Y)) \quad (5.7)$$

Information gain is used to construct decision trees [119]. It will be our primary tool for performing causal discovery from posterior distributions.

### 5.1.1.2 Properties

We now list the key properties regarding the different types of entropy.

**Lemma 1** (Non-negativity of the entropy). *[23] The entropy of a random variable is always non-negative*

$$H(X) \geq 0$$

**Lemma 2** (Chain Rule). *[23] We can decompose the joint entropy into a sum of marginal and conditional entropy*

$$H(X, Y) = H(X) + H(Y|X)$$

**Lemma 3** (Conditioning reduces entropy). [23] *Conditioning the entropy of a random variable  $X$  on multiple random variables reduces its entropy*

$$H(X) \geq H(X|Y) \geq H(X|Y, Z) \geq \dots \geq 0$$

**Lemma 4** (Bounded). [23] *The entropy of a random variable  $X$  is bounded by the log of its support, where  $|\mathcal{X}|$  denotes the cardinality of  $X$*

$$\log |\mathcal{X}| \geq H(X)$$

*This follows from the fact that  $H(X)$  is concave in  $p$  and is non-negative.*

## 5.1.2 Mutual Information and its variants

### 5.1.2.1 Definitions

**Definition 13** (Mutual Information). *The reduction in uncertainty due to another random variable is called the mutual information (MI) [23]. For two random variables  $X, Y$  with joint probability mass function  $p(x, y)$ , it is given as the relative entropy between the joint distribution  $P(X, Y)$  and the product distribution  $P(X)P(Y)$*

$$I(Y, X) = D_{KL}(P(X, Y) || P(X)P(Y)) = \sum_{x \in \mathcal{X}, y \in \mathcal{Y}} p(x, y) \log \frac{p(x, y)}{p(x)p(y)} \quad (5.8)$$

*It can also be defined as the difference between  $H(Y)$  and  $H(Y|X)$*

$$I(Y, X) = H(Y) - H(Y|X) \quad (5.9)$$

*Consequently, the mutual information  $I(Y, X)$  is the reduction in uncertainty of  $X$  due to the knowledge of  $Y$ . We write  $I(Y, X)$  for mutual information, the semicolon notation  $I(X; Y)$  is equivalent. We now define the conditional mutual information (CMI), which is the reduction in uncertainty of  $X$  due to the knowledge of  $Y$  given  $Z$ .*

**Definition 14** (Conditional Mutual Information). *The conditional mutual information of random variables  $X$  and  $Y$  given  $Z$  is defined by*

$$I(Y, X|Z) = H(Y|Z) - H(Y|X, Z) \quad (5.10)$$

$$= \mathbb{E}_{p(x, y, z)} \log \frac{p(X, Y|Z)}{p(X|Z)p(Y|Z)} \quad (5.11)$$

$Z$  can be also multiple random variables such as  $\mathbf{Z} = \{X_0, X_1, \dots, X_i\}$ . This notation will be particularly used in this Part II. Now that we have defined the conditional mutual information, we can define conditional independence between random variables.

**Definition 15** (Conditional Independence). *Variables  $X$  and  $Y$  are said to be conditionally independent given a variable set  $\mathbf{Z}$ , if  $P(X, Y|\mathbf{Z}) = P(X|\mathbf{Z})P(Y|\mathbf{Z})$ , denoted as  $X \perp Y|\mathbf{Z}$ . Inversely,  $X \not\perp Y|\mathbf{Z}$  denotes the conditional dependence. Using the conditional mutual information [23] to measure the independence relationship, this implies that*

$$I(X, Y|\mathbf{Z}) = 0 \Leftrightarrow X \perp Y|\mathbf{Z}$$

### 5.1.2.2 Properties

**Lemma 5** (Symmetry of Mutual Information). *In its standard definition, the MI is symmetric:*

$$I(Y, X) = I(X, Y) = H(Y) - H(Y|X) = H(X) - H(X|Y)$$

**Lemma 6** (Non-negativity of mutual information). *For any two random variable  $X, Y$ ,*

$$I(Y, X) \geq 0 \tag{5.12}$$

*It is also the case for the conditional mutual information:*

$$I(X, Y|Z) \geq 0 \tag{5.13}$$

## 5.2 Graphical Models

Graphical models [69] provide a simple way to represent probabilistic dependencies across random variables. For instance, a physician must infer the most likely diagnoses, given the patient’s symptoms, test results, genetics, and symptom evolution. A diagnostic expert might want to evaluate the causes of defects in a vehicle based on the series of diagnostic trouble codes that preceded it.

### 5.2.1 Bayesian Networks

#### 5.2.1.1 Motivation

Our goal is to represent the joint distribution  $P$  over the set of random variables  $\mathbf{U} = \{X_0, \dots, X_n, Y_1, \dots, Y_c\}$ . To reduce the specification of every possible random variable assignment, the independence properties in the distribution can be used to represent distributions via directed acyclic graphs [69], i.e., graphs that have oriented edges and no cycles.

Bayesian Networks [114] have served as a modeling technique for a variety of decision problems and benefit from the extensive literature on causal discovery associated with such directed acyclic graphs (DAGs). In particular, we build upon Pearl’s model of causality, which assumes that the underlying causal structure is in the form of a directed acyclic graph (DAG) [113]. Such a graph describes the causal relationships between event types.

#### 5.2.1.2 Definitions

**Definition 16** (Bayesian Network). *[114] Let  $P$  denote the joint distribution over a variable set  $\mathbf{U}$  of a directed acyclic graph (DAG)  $\mathcal{G}$ . The triplet  $\langle \mathbf{U}, \mathcal{G}, P \rangle$  constitutes a Bayesian Network (BN) if it satisfies the Markov condition: every random variable is independent of its non-descendant variables given its parents in  $\mathcal{G}$ . Each node  $X_i \in \mathbf{U}$*

represents a random variable. The directed edge  $(X_i \rightarrow X_j)$  encodes a probabilistic dependence. The joint probability distribution can be factorized as

$$P(X_0, \dots, X_n) = \prod_{i=0}^n P(X_i | Pa_{\mathcal{G}}(X_i)) \quad (5.14)$$

with  $Pa_{\mathcal{G}}(X_i)$  the parents of node  $X_i$  in  $\mathcal{G}$ .

We now define I-maps, which will help us identify graphs that represent the same set of conditional independence.

**Definition 17** (I-maps). [69] Let  $P$  be a distribution over  $\mathcal{X}$ , we define  $\mathcal{I}(P)$  to be the set of independence assertions of the form  $X \perp Y | Z$  that hold in  $P$

We can rewrite the statement that  $P$  satisfies the local independencies associated with the graph  $\mathcal{G}$  as  $\mathcal{I}(\mathcal{G}) \subseteq \mathcal{I}(P)$ . The graph  $\mathcal{G}$  encodes a set of conditional independencies  $\mathcal{I}(\mathcal{G})$ , where each element corresponds to a conditional independence relation  $X \perp Y | Z$ , meaning that  $X$  and  $Y$  are conditionally independent given the variable  $Z$  (Def. 15).

**Definition 18** (Faithfulness). [140] Given a BN  $\langle \mathbf{U}, \mathcal{G}, P \rangle$ ,  $\mathcal{G}$  is faithful to  $P$  if and only if every conditional independence present in  $P$  is entailed by  $\mathcal{G}$  i.e.,  $\mathcal{I}(\mathcal{G}) \subseteq \mathcal{I}(P)$  and the Markov condition holds.  $P$  is faithful if and only if there exist a DAG  $\mathcal{G}$  such that  $\mathcal{G}$  is faithful to  $P$ .

That is, the conditional independencies in  $P$  correspond exactly to those implied by the DAG.

**Definition 19** (Markov Equivalence Class). Two distinct graphs  $\mathcal{G}, \mathcal{G}'$  are said to belong to the same Markov Equivalence Class (MEC) if they have the same set of conditional independencies, i.e.,  $\mathcal{I}(\mathcal{G}) = \mathcal{I}(\mathcal{G}')$ .

Causal Discovery algorithm often recovers not the exact graph  $\mathcal{G}$  but rather an MEC [21, 139, 41], since orienting the edges is perilous and involves, in general, domain knowledge or additional assumptions.

**Definition 20** (Markov Boundary). [148] In a faithful BN  $\langle \mathbf{U}, \mathcal{G}, P \rangle$ , for a set of variables  $\mathbf{Z} \subset \mathbf{U}$  and label  $Y \in \mathbf{U}$ , if all other variables  $X \in \{\mathbf{X} - \mathbf{Z}\}$  are independent of  $Y$  conditioned on  $\mathbf{Z}$ , and any proper subset of  $\mathbf{Z}$  does not satisfy the condition, then  $\mathbf{Z}$  is the Markov Boundary of  $Y$ :  $\mathcal{MB}(Y)$ .

Many local structure learning (LSL) algorithms seek a reduced Bayesian Network in the form of the *Markov Boundary*. This serves primarily for feature selection [76].

## 5.3 Tasks

### 5.3.1 Causal Discovery

Causal discovery aims to recover the underlying causal structure among a set of random variables  $\mathbf{X} = \{X_0, \dots, X_n\}$  from observational data and or interventions [113]. Formally, the goal is to identify a directed acyclic graph (DAG)  $\mathcal{G} = (\mathbf{X}, E)$  whose edges

encode the direct causal relations such that the joint distribution  $P(\mathbf{X})$  satisfies the Markov condition with respect to  $\mathcal{G}$  (Definition 16). Depending on the assumptions and available information, the tasks consist of recovering either:

- The **full DAG**  $\mathcal{G}$ ,
- A **Markov Equivalence Class (MEC)** (Def. 19),
- Or the **Markov Boundary** of selected target variables (Def. 20),

Each representation offers a different level of identifiability. In high-dimensional settings such as error codes in vehicles, recovering the complete DAG is often infeasible; Many methods, therefore, focus on local structures (Markov Boundaries) or on equivalence classes of DAGs.

### 5.3.1.1 Assumptions

To enable identifiability, causal discovery algorithms typically rely on classical assumptions [139] such as:

- **Causal Sufficiency:** all relevant common causes of observed variables are themselves observed.
- **Faithfulness** (Def. 18): The conditional independencies in  $P$  correspond exactly to those implied by the DAG.
- **(Causal) Markov Condition:** A variable is conditionally independent of its non-descendants given its parents in the causal graph.

These assumptions vary across domains and settings. In temporal data, a time direction is present and greatly simplifies the edge orientations [41]. Violations of these assumptions (hidden confounders, cycles, non-stationarity) are common in practice due to the inaccurate recording of events, hidden confounders, and so forth.

### 5.3.1.2 Classes of Causal Discovery Algorithms

**Constraint-Based Methods.** These algorithms determine graph structure by performing a series of conditional independence tests (Def. 15). They are mostly employed in tabular data where a lot of data samples are presents with a few number of variables. Examples include PC [139], and local structure learning methods such as IAMB [147], MBB-BY-MBB [160], or HITON [3].

**Granger Methods.** In temporal data, Granger [44] causality is commonly employed to assess pairwise dependencies [161, 118]. It is based on the assumption that *causes precede effects and should improve the predictability of the effect*. Recently, [51] proposed a Granger-inspired causal discovery framework in multivariate time series using

an encoder-decoder architecture. Their method achieves state-of-the-art root-cause identification via autoregressive modeling of structured time series. [118] explores Granger causality under low-resolution temporal data using Hawkes processes [53] and shows gains in F1 across time granularities. However, their setup also assumes relatively small event vocabularies. However, their setup also assumes relatively small event vocabularies. CASCADE [24] recovers DAGs from temporal event data under a Poisson process assumption but is limited to smaller event spaces ( $\sim 200$  types). All these approaches remain limited and are applied in poor experimental settings in which the number of variables (or events) does not reflect real-world and industrial applications. Additionally, Granger causality refers more to probabilistic causation [33] than Pearl causality [114]. It is often considered a relatively weak notion of causality that excludes instantaneous and inhibitory effects and is usually unable to discover true causal dependencies. In Granger causality, baking a cake is causal to a birthday.

**Score-Based Methods.** These methods search over graph structures to maximize a scoring function (e.g., Bayesian Information Criterion: BIC or BDeu). The Greedy Equivalence Search (GES) [21] is the most popular method and relies on decomposable, score-equivalent metrics (Definitions 26–28). Since we benchmark criteria in Chapter 7, we need to define their properties formalized by [21].

**Optimization-Based and Neural Structural Learning Methods.** A recent line of work formulates causal discovery as a continuous optimization problem, enabling gradient-based learning of DAG structures. The NOTEARS framework [177] introduced a smooth acyclicity constraint that relaxes the discrete DAG search into a differentiable objective, making it possible to learn graph structures via standard gradient descent. Then, GOLEM [101] proposed a more scalable likelihood-based formulation, while DAG-GNN [166] leveraged variational autoencoders and graph neural networks.

**Temporal and Point-Process-Based Models.** In sequential domains, Hawkes Processes and Temporal Point Processes model temporal causation via excitation kernels [73]. In Part I we show that the excitation matrix  $\Phi \in \mathbb{R}^{|\mathcal{X}| \times |\mathcal{X}|}$  was used as a proxy for causality. These approaches impose parametric assumptions and are interesting to discover causal relationships between different event streams [173], rather than a single high-dimensional one like in vehicle fault sequences.

### 5.3.2 Multi-Label Causal Discovery

In multi-label settings, the objective is to recover the direct causes of each label  $Y_j$  among a large set of events  $\mathbf{X}$ . Instead of estimating the complete graph, one seeks the Markov Boundary:  $\mathcal{MB}(Y_j) \subseteq \mathbf{X}$ .

### 5.3.3 Evaluation Metrics for Multi-Label Causal Discovery

In the multi-label setting (events-to-outcome), we aim to identify the set of direct temporal causes  $\mathcal{P}_j \subseteq \mathcal{X}$  for each outcome label  $y_j$ . Following the Markov assumption, this set corresponds to the Markov Boundary  $\mathcal{MB}(Y_j)$  of the label. We evaluate the alignment between the ground-truth boundary  $\mathcal{MB}(Y_j)$  and the inferred boundary  $\widehat{\mathcal{MB}}(Y_j)$ .

#### 5.3.3.1 Set-Based Metrics

To measure the local recovery of the causal neighborhood for each label, we utilize the following metrics:

- **Precision** ( $P$ ) quantifies the reliability of the inferred causes, measuring the proportion of discovered event types that are true causal parents:

$$P = \frac{|\widehat{\mathcal{MB}}(Y_j) \cap \mathcal{MB}(Y_j)|}{|\widehat{\mathcal{MB}}(Y_j)|}$$

- **Recall** ( $R$ ) (or Sensitivity) measures the completeness of the discovery, capturing the proportion of the true causal mechanism recovered by the model:

$$R = \frac{|\widehat{\mathcal{MB}}(Y_j) \cap \mathcal{MB}(Y_j)|}{|\mathcal{MB}(Y_j)|}$$

- **F1-Score** ( $F_1$ ) provides the harmonic mean of precision and recall. It is our primary metric for causal discovery, as it penalizes both the hallucination of spurious causes and the omission of weak causal signals:

$$F_1 = 2 \cdot \frac{P \cdot R}{P + R}$$

### 5.3.4 Evaluation Metrics for Event-to-Event Causal Discovery

For global structure recovery (Chapter 8), we reconstruct the full event-type adjacency matrix  $\hat{A} \in \{0, 1\}^{|\mathcal{X}| \times |\mathcal{X}|}$ . Unlike set-based evaluation, graph-based evaluation must account for the structural topology of the system.

### 5.3.5 Structural Hamming Distance (SHD)

The Structural Hamming Distance is the standard metric for comparing two causal graphs  $\mathcal{G}$  and  $\hat{\mathcal{G}}$ . It counts the minimum number of edge operations (additions, deletions, or orientation reversals) required to transform the estimated graph into the ground truth. In our directed temporal setting, where orientation is fixed by time, SHD reduces to the  $L_1$  distance between the flattened adjacency matrices:

$$\text{SHD}(A, \hat{A}) = \sum_{i=1}^{|\mathcal{X}|} \sum_{j=1}^{|\mathcal{X}|} |A_{ij} - \hat{A}_{ij}|$$

## 6 Sample-Level Multi-Label Causal Discovery

Building upon the predictive foundations established in the previous chapter, where autoregressive Transformer models were used to anticipate *when* and *what* error patterns occur, we now turn to a complementary and equally essential question: *why* these failures arise. We observe that autoregressive models trained on next-event prediction already encode the conditional distributions required by information theory metrics such as information gain (Def. 12), potentially usable for conditional independence testing in a graphical model. We therefore reuse the pretrained CarFormer and EPredictor weights, without fine-tuning, as NADEs. Consequently, in this chapter we address the challenge of causal discovery in large-scale event sequences, in which outcomes, such as error patterns, emerge from preceding diagnostic events in a single sample during inference (*sample-level*). It is based on the following publication:

### **One-Shot Multi-Label Causal Discovery in High-Dimensional Event Sequences.**

[93] Hugo Math, Robin Schön, Rainer Lienhart, Conference on Neural Information Processing Systems (NeurIPS) Workshop on CauScien: Uncovering Causality in Science, San Diego, USA, December 2025.

### 6.1 Introduction

Understanding causal relations among diagnostic events is a crucial next step toward interpretable and automated reasoning in large-scale event-driven systems. Causal discovery in sequential data has broad relevance across domains such as healthcare [122, 57], cybersecurity [85], flight operations [83], and vehicle diagnostics [116]. Although recent progress in sequence modeling, particularly through Transformers [150, 121, 146] has improved our ability to capture temporal dependencies, most methods remain focused on prediction rather than explanation. Traditional causal discovery methods, such as constraint-based or Granger-causal approaches [44], face severe computational bottlenecks when applied to industrial-scale event data [76, 165, 52, 41]. Their reliance on repeated conditional independence tests grows combinatorially with the number of event types, rendering them impractical for modern diagnostic systems.

Interpreting attention weights as a measure of causality is a promising direction [100, 124] but lacks theoretical guarantees and often admits strong parametric assumptions as in [124]. Some authors strongly criticize the reliance on attention scores, arguing that they provide no explanatory value [155]. On the other hand, repurposing Transformers as neural density estimators [63, 96] offers a promising direction, enabling the modeling

of sequences using graphical models [69] and the use of the learned joint probability distribution.

Nevertheless, all of these methods often aim to recover a single global causal graph. A representation that is not only difficult to interpret for a lot of different events but also misaligned with how practitioners reason about causality in practice. In industrial and operational settings, reasoning about causality typically occurs at the *sample-level*: given a single temporal sequence of observed events, one seeks to identify the specific causes leading to an outcome such as a system failure, defect, or disease with one sample during inference. For instance, in vehicle diagnostics, engineers may ask: “*Which diagnostic events most likely caused this particular error pattern?*” This local, sample-level perspective motivates a more efficient, explainable form of causal discovery that can operate directly on individual event sequences in a *one-shot* manner.

To address this underexplored problem this chapter introduces OSCAR, to the best of our knowledge, the first sample-level causal discovery method that extends the predictive modeling framework of the previous chapter toward causal reasoning. OSCAR performs a single-pass, fully parallelized causal extraction on GPUs and recovers an interpretable causal graph with quantified causal indicators and uncertainty measures. This enables practical multi-label causal discovery at a scale previously unattainable, supporting thousands of event types and hundreds of outcome labels simultaneously. This chapter, therefore, marks a conceptual shift: from purely predictive modeling to causal understanding, laying the foundation for the automated reasoning systems developed in the following chapters.

## 6.2 Related Work

### 6.2.1 Neural Autoregressive Density Estimation

Neural autoregressive density estimators (NADEs) were initially introduced for density estimation via chain-rule factorization of the joint distribution [15], later extended through recurrent architectures [22, 58] and Transformers [150]. These models are trained using next-token prediction by minimizing the negative log-likelihood of observing the sequence  $s = (x_1, \dots, x_L)$ . Recall that the joint probability  $P(s)$  can be expressed using the chain rule as in Eq. 2.11. Recent work has explored autoregressive models as tools for causal inference. For example, [39] leverages density estimators to simulate interventions and compute average treatment effects. [63] shows that autoregressive language models can approximate sequential Bayesian networks (Fig. 6.2), treating the model itself as a statistical engine for causal inference. These findings motivate our use of pretrained Transformers to estimate conditional mutual information (Def. 14) between events and labels.

Specifically, we repurposed these models as neural autoregressive density estimators (NADEs) for both the events and labels, allowing us to quickly estimate the conditional probabilities of the next event  $x_i$  and labels  $\mathbf{y}$  given past events  $(x_1, \dots, x_{i-1})$ .

## 6.2.2 Transformers as Causal Learners

Transformer-based models have gained growing attention in causal discovery literature. [103] showed that when trained on sequences generated from in-context Markov chains, they can implicitly learn latent causal graphs, where attention weights align with the adjacency matrix of the actual causal structure. For sequential data, [124] analyzes self-attention under the assumption that data is generated by a linear-Gaussian structural causal model (SCM) [140]. They relate the covariance of endogenous variables to attention scores and apply conditional independence (CI) tests to the final layer’s outputs to recover a partial ancestral graph. Our work builds on this idea by leveraging Transformers but focuses on multi-label event sequences. The terminology ‘one-shot’ is used here to distinguish this regime from ‘zero-shot’ approaches, as inference requires a single sequence from the target domain.

## 6.2.3 Multi-label Causal Discovery

Multi-label causal discovery seeks to identify the Markov Boundary or  $\mathcal{MB}$  (Def. 20) of each label, i.e., its minimal set of parents, children, and spouses—such that the label is conditionally independent of all other variables given its  $\mathcal{MB}$  [148]. This boundary constitutes an optimal feature set for tasks such as explainable modeling and feature selection under the faithfulness assumption.

However, rather than learning the full joint causal graph, which is known to be NP-hard [20]—*we focus on recovering local causal structure* (LCS) [165]: discovering minimal sub-graphs from inputs to labels within a single sequence. This formulation makes the problem tractable in high dimensions and better suited for real-world production scenarios. Unlike event-to-event causal learning, multi-label causal discovery remains unexplored in event sequences [41, 52], yet its potential applications are broad across various domains.

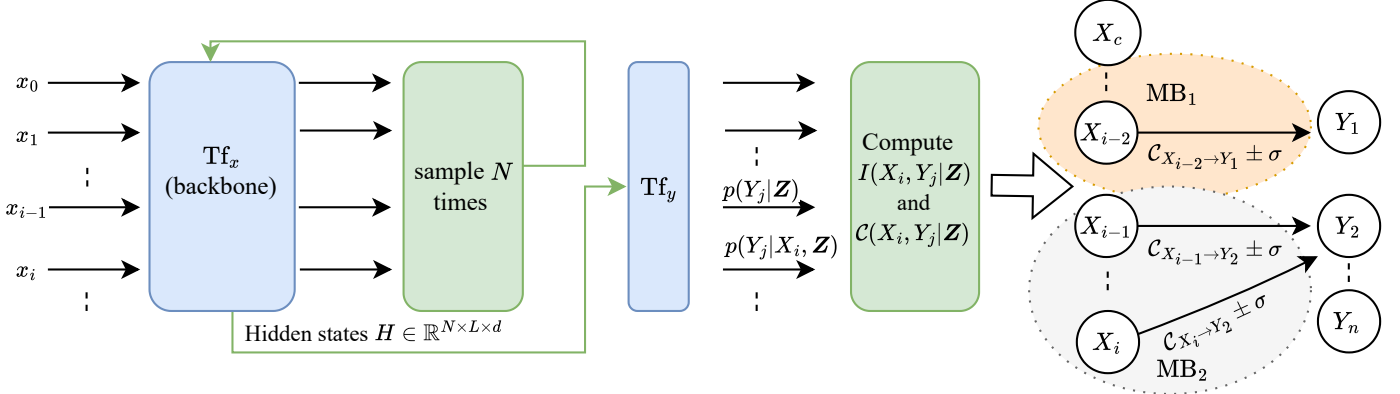
## 6.3 Methodology

Fig. 6.1 depicts OSCAR, our introduced one-shot causal autoregressive discovery method for event sequences. The lemmas and theorems introduced are directly followed by their proofs.

### 6.3.1 Autoregressive Event Sequence Models.

We begin by repurposing the two Transformer architectures introduced in Part I to perform next event (*CarFormer* as  $\text{Tf}_x$ ) and next labels (*EPredictor* as  $\text{Tf}_y$ ) prediction. These two autoregressive Transformers model the conditional probability distribution of the next events and labels conditioned on the past sequence of observed events  $\mathbf{Z} = (X_1, \dots, X_{i-1}) = S_{<i}$ , the predictive distributions are defined as:

$$P_{\theta_x}(X_i|\mathbf{Z}) \triangleq \text{Softmax}(\mathbf{h}_{i-1}^x) = \text{Tf}_x(S_{<i}) \quad (6.1)$$



**Figure 6.1: The Overview of OSCAR:** One-Shot multi-label Causal AutoRegressive discovery.  $d$  denotes the hidden dimension,  $L$  the sequence length,  $\mathcal{MB}_1, \mathcal{MB}_2$  the Markov Boundary of  $Y_1, Y_2$  respectively. All green and blue areas represent parallelised operations.

$$P_{\theta_y}(Y|X_i, \mathbf{Z}) \triangleq \text{Sigmoid}(\mathbf{h}_i^y) = \text{Tf}_y(S_{\leq i}) \quad (6.2)$$

Here,  $\mathbf{h}_{i-1}^x, \mathbf{h}_i^y \in \mathbb{R}^d$  are the logits produced by the two Transformer heads of  $\text{Tf}_x$  and  $\text{Tf}_y$  parametrized by  $\theta_x, \theta_y$ . The majority of  $\text{Tf}_x$  (except the heads) serves as a backbone for  $\text{Tf}_y$ , see Fig. 6.1.

### 6.3.2 Assumptions

Working with causal structure learning from observed data requires several assumptions, notably the causal Markov assumptions [114], which state that a variable is conditionally independent of its non-descendants given its parents. An extended discussion on the impact of assumptions is provided later in Section 6.6. Formally, we assume the following throughout this section:

**Assumption 1** (Temporal Precedence). *Given a perfectly recorded sequence of events  $((x_0, t_0), \dots, (x_L, t_L))$  with labels  $(\mathbf{y}_L, t_L)$  and monotonically increasing time of occurrence  $0 \leq t_1 \leq \dots \leq t_L$ , an event  $x_i$  is allowed to influence any subsequent event  $x_j$  such that  $t_i \leq t_j$  and  $i < j$ . Formally, the graph  $\mathcal{G} = (\mathbf{U}, \mathbf{E})$ ,  $(x_i, x_j) \in \mathbf{E} \implies t_i \leq t_j$  and step  $i < j$*

It allows us to remove ambiguity in causal directionality and orient the BN edges in Fig. 6.2.

**Assumption 2** (Stationary Markovian Dynamic System). [69] *We assume that the probability distribution  $P(Y_j^{(t_{j+1})} | \mathbf{Z}^{(t_j)})$  is the same for all  $t$ . In this case we represent our transition probability  $P(Y_j | \mathbf{Z})$ , so that for any,  $t \geq 0$ , as:*

$$P(Y_j^{(t_{j+1})} = y | \mathbf{Z}^{(t_j)} = z) = P(Y_j = y | \mathbf{Z} = z) \quad (6.3)$$

Stationarity allows us to compute the correct posteriors  $P(Y_j^{(t_i)}|\mathbf{Z}, X_i)$  even at different time step  $t_i$ .

**Assumption 3** (Causal Sufficiency for Labels). *All relevant variables are observed, and there are no hidden confounders affecting the labels.*

**Assumption 4** (Oracle Models). *We assume that two autoregressive Transformer models,  $Tf_x$  and  $Tf_y$ , are trained via maximum likelihood on a dataset of multi-labeled event sequences  $\mathcal{D} = \{S_l^{(1)}, \dots, S_l^{(n)}\}$ , and can perfectly approximate the true conditional distributions of events and labels:*

$$P(X_i|Pa_{\mathcal{G}}(X_i)) = P_{\theta_x}(X_i|Pa_{\mathcal{G}}(X_i)) = Tf_x(S_{<i}) \quad (6.4)$$

$$P(Y_j|Pa_{\mathcal{G}}(Y_j)) = P_{\theta_y}(Y_j|Pa_{\mathcal{G}}(Y_j)) = Tf_y(S_{\leq i}) \quad (6.5)$$

**Assumption 5** (Bounded Lagged Effects). *Once we observed events up to timestamp  $t_i$  and step  $i$  as  $\mathbf{Z} = \{X_0, \dots, X_{i-1}\}$ , any future lagged copy of event  $X_i^{(t_i+\tau)}$  is independent of  $Y_j$  conditioned on  $\mathbf{Z}$ :*

$$Y_j \perp X_i^{(t_i+\tau)} | \mathbf{Z}$$

Where  $\tau = t_{i+1} - t_i$  is a finite bound on the allowed time delay for causal influence.

In other words, we allow the causal influence of event  $X_i$  on  $Y_j$  until the next event  $X_{i+1}$  is observed. We note that this may not hold for data with strong lagged effects (e.g., financial transactions), but it is relevant for log-based and error code-based data.

### 6.3.3 Lemmas

We can derive the Markov Boundary of each label in the Bayesian Network constructed from a multi-labeled sequence (Fig. 6.2).

**Lemma 7** (Markov Boundary Equivalence). *In a multi-label event sequence  $S_l$  and under the temporal precedence assumption A1, the Markov Boundary of each label  $Y_j$  is only its parents such that  $\forall X \in \{\mathbf{U} - Pa_{\mathcal{G}}(Y_j)\}, X \perp Y_j | Pa_{\mathcal{G}}(Y_j) \Leftrightarrow \mathcal{MB}(Y_j) = Pa_{\mathcal{G}}(Y_j)$ .*

*Proof.* Let  $\langle \mathbf{U}, \mathcal{G}, P \rangle$  be the sequential BN composed of the events from the multi-labeled sequence. Following the temporal precedence assumption A1, the labels  $\mathbf{y}_L$  can only be caused by past events  $(x_0, \dots, x_L)$ ; we assume that labels do not cause any other labels. Thus,  $Y_j$  has no descendants, so no children and spouses. Therefore, together with the Markov Assumption we know that  $\forall X \in \{\mathbf{U} - Pa_{\mathcal{G}}(Y_j)\} : Y_j \perp X | Pa_{\mathcal{G}}(Y_j)$ . Which is the definition of the MB (Def. 20). Consequently  $\mathcal{MB}(Y_j) = Pa_{\mathcal{G}}(Y_j)$ .  $\square$

To recover the causal graph  $\mathcal{G}$ , we must make sure it is identifiable from the observational data.

**Lemma 8** (Identifiability of  $\mathcal{G}$ ). *Assuming the faithfulness condition holds for the true causal graph  $\mathcal{G}$ . Let  $Tf_x$  and  $Tf_y$  be Oracle models perfectly approximating the actual conditional distributions of events and labels, respectively. The joint distribution  $P_{\theta_x, \theta_y}$*

## 6 Sample-Level Multi-Label Causal Discovery

can then be constructed, and any conditional independence detected from the distributions estimated by  $Tf_x$  and  $Tf_y$  corresponds to a conditional independence in  $\mathcal{G}$ :

$$X_i \perp_{\theta_x, \theta_y} Y_j | \mathbf{Z} \implies X_i \perp_{\mathcal{G}} Y_j | \mathbf{Z}.$$

Where  $\perp_{\theta_x, \theta_y}$  denotes the independence entailed by the joint probability  $P_{\theta_x, \theta_y}$ .

*Proof.* We assume that the data is generated by the associated causal graph  $\mathcal{G}$  following the sequential BN from a multi-labeled sequence  $S_l$ . And that the faithfulness assumption holds [114], meaning that all conditional independencies in the observational data are implied by the true causal graph  $\mathcal{G}$ . Given that the Oracle models  $Tf_x$  and  $Tf_y$  are trained to perfectly approximate the true conditional distributions, for any variable  $U_i$  in the graph, we have:

$$P(U_i | \text{Pa}_{\mathcal{G}}(U_i)) = \begin{cases} P(Y_j | \text{Pa}_{\mathcal{G}}(Y_j)) = P_{\theta_y}(Y_j | \text{Pa}_{\mathcal{G}}(Y_j)), & \text{if } U_i \in \mathbf{Y} \\ P(X_i | \text{Pa}_{\mathcal{G}}(X_i)) = P_{\theta_x}(X_i | \text{Pa}_{\mathcal{G}}(X_i)), & \text{otherwise.} \end{cases}$$

The joint distribution  $P_{\theta_x, \theta_y}$  can then be constructed using the chain rule

$$P_{\theta_x, \theta_y}(X_0, \dots, X_i, Y_1, \dots, Y_c) = \prod_{k=0}^i P(X_k | \text{Pa}_{\mathcal{G}}(X_k)) \prod_l^c P(Y_l | \text{Pa}_{\mathcal{G}}(Y_l))$$

By the faithfulness assumption [114], if the conditional independencies hold in the data, they must also hold in the causal graph  $\mathcal{G}$ :

$$X_i \perp Y_j | \mathbf{Z} \implies X_i \perp_{\mathcal{G}} Y_j | \mathbf{Z}$$

Since we can approximate the true conditional distributions, it follows that:

$$X_i \perp_{\theta_x, \theta_y} Y_j | \mathbf{Z} \implies X_i \perp Y_j | \mathbf{Z} \implies X_i \perp_{\mathcal{G}} Y_j | \mathbf{Z}$$

Where  $\perp_{\theta_x, \theta_y}$  denotes the independence entailed by the joint probability  $P_{\theta_x, \theta_y}$ . As a result, the graph  $\mathcal{G}$  can be identified from the observational data.  $\square$

### 6.3.4 Conditional Mutual Information Estimation via Autoregressive Models

OSCAR works like a constraint-based causal discovery algorithm, where the conditioning set of nodes  $\mathbf{Z}$  increases over time as we unfold the Bayesian Network in Fig. 6.2. Specifically, we would like to assess how much additional information an event  $X_i$  occurring at step  $i$  provides about label  $Y_j$  when we already know the past sequence of events  $\mathbf{Z} = S_{<i}$ . We essentially try to answer if:

$$P(Y_j | X_i, \mathbf{Z}) = P(Y_j | \mathbf{Z}) \Leftrightarrow D_{KL}(P(Y_j | X_i, \mathbf{Z}) || P(Y_j | \mathbf{Z})) = 0$$

where  $D_{KL}$  denotes the *Kullback-Leibler divergence* (Def. 10). The distributional difference between the conditionals  $P(Y_j | X_i, \mathbf{Z})$ ,  $P(Y_j | \mathbf{Z})$  is akin to Information Gain  $I_G$  [119] conditioned on past events  $z = \{x_0, \dots, x_{i-1}\}$  (Def. 12):

$$I_G(x_i, Y_j | z) \triangleq D_{KL}(P(Y_j | X_i = x_i, \mathbf{Z} = z) || P(Y_j | \mathbf{Z} = z)) \quad (6.6)$$

Which is equal to the difference between the conditional entropies [23, 119] denoted as  $H$ :

$$I_G(Y_j, x_i | z) = H(Y_j | z) - H(Y_j | x_i, z) \quad (6.7)$$

More generally, we can use the CMI to assess conditional independence (Def. 15), which is simply the expected value of the information gain  $I_G(Y_j, x_i | z)$  such as:

$$I(Y_j, X_i | \mathbf{Z}) \triangleq H(Y_j | \mathbf{Z}) - H(Y_j | X_i, \mathbf{Z}) = \mathbb{E}_{p(z)}[I_G(Y_j, X_i | \mathbf{Z} = z)] \quad (6.8)$$

It can be interpreted as the expected value over all possible context  $\mathbf{Z}$  of the deviation from independence of  $X_i, Y_j$  in this context. To approximate Eq. 6.8, a naive Monte Carlo [29] approximation is performed where we draw  $N$  random variations of the conditioning set  $z^{(l)} = \{x_0^{(l)}, \dots, x_{i-1}^{(l)}\}$ , denoting the  $l$ -th sampled *particle* from  $P_\theta$ <sup>1</sup>:

$$\hat{I}_N(Y_j, X_i | \mathbf{Z}) = \frac{1}{N} \sum_{l=1}^N I_G(Y_j, X_i | \mathbf{Z} = z^{(l)}) \quad (6.9)$$

Under Assumption 4 (Oracle model), the estimator  $\hat{I}_N$  is unbiased with respect to the true distribution  $P$ . Since  $I_G(Y_j, X_i | \mathbf{Z} = z)$  is a difference between conditional entropies (Eq. 6.7), it is thus bounded uniformly [23] by the log of supports (Lemma 4) such as:

$$0 < I_G(Y_j, X_i | \mathbf{Z} = z^{(l)}) = H(Y_j | z^{(l)}) - H(Y_j | X_i, z^{(l)}) \leq H(Y_j) \leq \log |\mathcal{Y}|$$

Thus the posterior variance of  $f_i = I_G(Y_j, X_i | \mathbf{Z} = z^{(l)})$  satisfies  $\sigma_{f_i}^2 \triangleq \mathbb{E}_{p(z)}[f_i^2(p(z))] - I^2(f_i) < +\infty$  [29] then the variance of  $\hat{I}_N(f_i)$  is equal to  $\text{var}(\hat{I}_N(f_i)) = \frac{\sigma_{f_i}^2}{N}$  and from the strong law of large numbers the estimation  $\hat{I}_N$  converges almost surely to the conditional mutual information:

$$\hat{I}_N \xrightarrow[N \rightarrow +\infty]{\text{a.s.}} \mathbb{E}_{p(z)}[I_G(Y_j, X_i | \mathbf{Z} = z)] \triangleq I(f_i). \quad (6.10)$$

<sup>1</sup>Averaging the information gain over multiple sampled past event histories enables tractable computation as we do not need to enumerate over all possible contexts  $\{x_0, x_1, x_2\}, \{x_2, x_1, x_0\}, \{x_1, x_2, x_0\}, \dots$

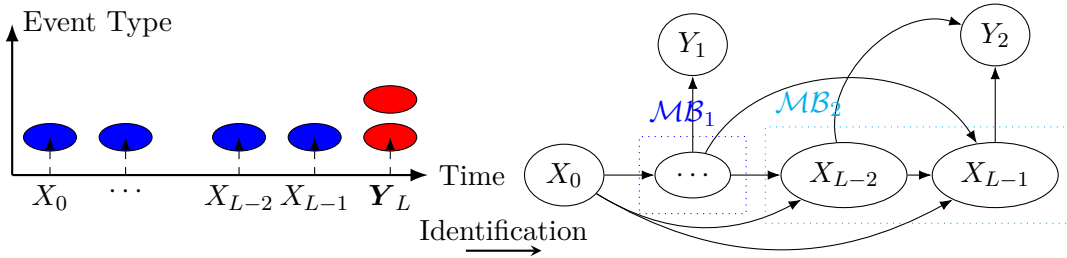


**Figure 6.2: Example of a Causal Graph** extracted from a multi-label event sequence where  $\mathcal{MB}_1$  represents the Markov Boundary of  $Y_1$  and  $\mathcal{MB}_2$  the Markov Boundary of  $Y_2$ .

### 6.3.5 Sequential Markov Boundary Recovery

In practice, a label-specific threshold  $\tau_j \approx 0$  is applied to Eq. 6.9 to identify conditional independence:

$$Y_j \not\perp\!\!\!\perp X_i \mid \mathbf{Z} \Leftrightarrow I(Y_j, X_i \mid \mathbf{Z}) > \tau_j \approx 0 \quad (6.11)$$

$\tau_j$  is dynamically computed for each label based on the mean and standard deviation of the CMI values across the sequence, such that:  $\tau_j = \mu_{Y_j} + k \cdot \sigma_{Y_j}$ , where  $k$  controls the confidence interval. We analyze the effect of  $k$  in Appendix. B.2.

**Theorem 1** (Markov Boundary Identification in Event Sequences). *If  $S_t^{(k)}$  a multi-labeled sequence drawn from a dataset  $\mathcal{D} = \{S_t^1, \dots, S_t^n\}$  where two Oracle Models  $Tf_x$  and  $Tf_y$  were trained on, then under causal sufficiency (A3), bounded lagged effects (A5) and temporal precedence (A1), the Markov Boundary of each label  $Y_j$  in the causal graph  $\mathcal{G}$  can be identified using conditional mutual information for CI-testing.*

*Proof.* By induction over the sequence length  $L$  of the multi-label sequence  $S_t^{(k)}$ , we want to show that under temporal precedence A1, bounded lagged effects A5, causal sufficiency A3, Oracle Models A4 the Markov Boundary of label  $Y_j$  can be identified in the causal graph  $\mathcal{G}$ . Let's define  $\mathcal{M}_j^L$  as the estimated Markov Boundary of  $Y_j$  after observing  $L$  events.

**Base Case  $L = 1$ :** Consider the BN for step  $L = 1$  following the Markov assumption [114] with two nodes  $X_0, Y_j$ . Using  $Tf_x, Tf_y$  as Oracle Models A4, we can express the conditional probabilities for any node  $U$ :

$$P(U \mid \text{Pa}_{\mathcal{G}}(U)) = \begin{cases} P(X_0) = P_{\theta_x}(X_0 \mid [CLS]) & \text{if } U \in \mathbf{X} \\ P(Y_j \mid X_0) = P_{\theta_y}(Y_j \mid X_0) & \text{otherwise} \end{cases} \quad (6.12)$$

Where  $P(\cdot \mid [CLS])$  is considered the marginal distribution. Assuming that P is faithful (Def. 18) to  $\mathcal{G}$ , no hidden confounders bias the estimate (A3) and temporal precedence (A1), we can estimate the CMI 6.8 such that iff  $I(X_0, Y_j \mid \emptyset) > 0 \Leftrightarrow Y_j \not\perp_{\theta_x, \theta_y} X_1 \implies Y_j \not\perp_{\mathcal{G}} X_1$  (Lemma 8).

Since we assume temporal precedence A1, we can orient the edge such that  $X_0$  must be a parent of  $Y_j$  in  $\mathcal{G}$ . Using Lemma 7, we know that  $\text{Pa}_{\mathcal{G}}(Y_j) = \mathcal{MB}(Y_j) \implies X_1 \in \mathcal{MB}(Y_j)$ , thus we must include  $X_0$  in  $M_j^1$ , otherwise not.

**Heredity** For  $L = i$ , we obtained  $M_j^i$  with the sequential BN up to step  $L = i$ . Now for  $L = i + 1$ , the sequential BN has  $i + 2$  nodes denoted as  $\mathbf{U}' = (X_0, \dots, X_i, X_{i+1}, Y_j)$ . Using the Oracle Models A4 and following the Markov assumption [114], we can estimate the following conditional probabilities for any nodes  $U \in \mathbf{U}'$ :

$$P(U \mid \text{Pa}_{\mathcal{G}}(U)) = \begin{cases} P(Y_j \mid \text{Pa}_{\mathcal{G}}(Y_j)) = P_{\theta_y}(Y_j \mid \text{Pa}_{\mathcal{G}}(Y_j)), & \text{if } U \in \mathbf{Y} \\ P(X \mid \text{Pa}_{\mathcal{G}}(X)) = P_{\theta_x}(X \mid \text{Pa}_{\mathcal{G}}(X)), & \text{otherwise.} \end{cases} \quad (6.13)$$

By bounded lagged effects (A5) we know that the causal influence of past  $X_{\leq i}$  on  $Y_j$  has expired. In addition, no hidden confounders (A3) bias the independence testing. Finally, using Eq. 6.8, we can estimate the CMI such that iff  $I(Y_j, X_{i+1} | \mathbf{Z}) > 0 \Leftrightarrow Y_j \not\perp_{\theta_x, \theta_y} X_{i+1} | \mathbf{Z} \implies Y_j \not\perp_{\mathcal{G}} X_{i+1} | \mathbf{Z}$  (Lemma 8).

Since we assume temporal precedence A1, we can orient the edge so that  $X_{i+1}$  must be a parent of  $Y_j$  in  $\mathcal{G}$ . Using Lemma 7, we know that  $\text{Pa}_{\mathcal{G}}(Y_j) = \mathcal{MB}(Y_j) \implies X_{i+1} \in \mathcal{MB}(Y_j)$ . Thus,  $X_{i+1} \in M_j^{i+1}$  which represent the  $\mathcal{MB}(Y_j)$  for step  $i + 1$ .

Finally,  $\mathcal{M}_j^{i+1}$  still recovers the Markov Boundary of  $Y_j$  such that

$$\forall U \in \{\mathbf{U}' - \mathcal{M}_j^{i+1}\}, Y_j \perp U | \mathcal{M}_j^{i+1}$$

□

Intuitively, Theorem 1 states that if our Transformers perfectly approximate the true joint distribution, then testing conditional mutual information at each step is sufficient to recover the Markov Boundary of each label sequentially. By induction, we prove that with bounded lagged effects of the previous events, we can restrict their causal influence and recover the correct  $\mathcal{MB}$  of each label in the associated Bayesian Network (Fig. 6.2).

### 6.3.6 Computation

**Parallelization** A key advantage of our approach is its scalability. Fig. 6.1 shows all parallelized steps on GPUs. Unlike traditional methods whose complexity depends on the event and label cardinality  $|\mathcal{X}|$  and  $|\mathcal{Y}|$  [76], our method is agnostic to both. CMI estimations are independently performed for all positions  $i \in [c, L]$ , with the sampling pushed into the batch dimension and results averaged across particles using Eq. 6.9. This reduces the per-sample computational overhead via batch parallelism from  $\mathcal{O}(\text{BS} \times N \times L)$  sequential forward passes to a single batched forward pass as  $\mathcal{O}(1)$ . A simple PyTorch [110] implementation of OSCAR and a top-k/p sampling is given in Appendix B.1.8. The main computation can be summarized through these simple steps:

```

1 logits_x = tfx(**batch)['prediction_logits']
2 x_hat = F.softmax(logits_x, dim=-1)
3 sampled = topk_p_sampling(batch['input_ids'], x_hat, c=c, n=N)

```

**Listing 6.1:** Step 1: Next-event prediction and sampling.

The next-event Transformer `tfx` produces logits over next event types. We apply top- $k$ /nucleus sampling to expand the batch into  $N$  candidates in parallel. Only the first  $c$  events are sampled.

```

1 out_y = tfy(input_ids=sampled.reshape(-1,L), attention_mask=attention_mask.repeat(
    N, 1))
2 prob_y = torch.sigmoid(out_y['logits']).reshape(bs, N, L-c, -1)
3 prob_y = torch.clamp(prob_y, eps, 1-eps)

```

**Listing 6.2:** Step 2: Next-label prediction.

The label Transformer `tfy` evaluates all samples in one forward pass starting from  $c$ , yielding conditional probabilities  $P(Y_j|\mathbf{Z})$  and  $P(Y_j|X_i, \mathbf{Z})$ . We then calculate the binary  $D_{KL}$ :

```

1 y_z, y_zx = prob_y[..., :-1, :], prob_y[..., 1:, :]
2 cmi = torch.mean(
3     y_zx*torch.log(y_zx/y_z) +
4     (1-y_zx)*torch.log((1-y_zx)/(1-y_z)),
5     dim=1
6 ) # (bs, L, |Y|)

```

**Listing 6.3:** Step 3: Conditional mutual information.

Conditional mutual information is averaged across the sampling dimension, producing a compact  $(bs, L - c, |\mathcal{Y}|)$  tensor:

```

1 mu, std = cmi.mean(dim=1), cmi.std(dim=1)
2 mask = cmi >= (mu + k*std).unsqueeze(1)

```

**Listing 6.4:** Step 4: Dynamic thresholding.

Finally, dynamic per-label thresholds identify causal events by evaluating their values across the sequence length dimension.

**Context** Following the EPredictor architecture seen in Chapter 3, to ensure stable conditional entropy estimates and reliable predictions from `Tfy`, the CMI is computed after observing  $c$  events (*context*). This design choice also enables out-of-the-box parallelization. By sampling  $N$  variations of the prefix sequence  $S_{\leq c}$ , the CMI is independently computed across positions  $i \in [c, L]$ . One caveat is the phenomenon of entropy saturation [129], whereby the conditional entropy  $H(Y_j | \mathbf{Z}_i)$  diminishes as  $\mathbf{Z}_i = S_{\leq i}$  grows longer. Recall the Lemma 3:

$$H(Y_j | X_{i+1}, \mathbf{Z}_i) \leq H(Y_j | X_i, \mathbf{Z}_{i-1}).$$

In other words, once a sufficiently informative context is observed, future uncertainty becomes minimal. Therefore, context  $c$  and sequence length  $L$  must be carefully selected to balance informativeness and computational efficiency. In our experiments, we set  $c = 15$  and  $L = 128$ . An ablation on  $c$  and the quality of the NADEs can be found in the Appendix B.1.3.

## 6.4 Causal Indicator

While deterministic DAGs reveal structural dependencies, they often obscure the *magnitude* and *direction* of influence between variables. In many settings, a small subset of causal events may exert disproportionate influence on the probability of a label. Also, causal relationships can be either *excitatory* or *inhibitory*. That is, the presence of a cause may either increase or decrease the likelihood of its effect.

For instance, if  $P(Y_j | X_i, \mathbf{Z}) < P(Y_j | \mathbf{Z})$  then  $X_i$  negatively influences  $Y_j$ , yet still constitutes a valid causal relationship [113]. Without quantifying the effect direction and strength, such cases may mislead an operator. Given that we can estimate both conditionals  $P(Y_j | X_i, \mathbf{Z})$  and  $P(Y_j | \mathbf{Z})$ , we define the *causal indicator*  $\mathcal{C} \in [-1, 1]$  between an event  $X_i$  and a label  $Y_j$  under causal sufficiency and the context  $\mathbf{Z}$  that we assume fixed for every measurement [35]:

$$\mathcal{C}(Y_j, X_i; \mathbf{Z}) := \mathbb{E}_{p(z)}[P(Y_j = 1 | X_i = 1, \mathbf{Z} = z) - P(Y_j = 1 | X_i = 0, \mathbf{Z} = z)] \quad (6.14)$$

where the expectation is taken over contexts  $z$  sampled from the learned model distribution  $P_\theta$ . This aligns with Eq. 6.9. We compute mean and standard deviations over contexts to provide uncertainty estimates. Eq. 6.14 follows the measure proposed by [33] and is akin to the average causal effect [113]. Here,  $\mathcal{C} > 0$  indicates a positive influence and  $\mathcal{C} < 0$  reflects an inhibitory effect. While several metrics for causal strength exist—including Causal Power [19] and Good’s measure [35], we adopt Eells’ measure for its simplicity of interpretation. An operator can easily read it and get a sense of the rise in likelihood of the label  $Y_j$ . We employ the term *causal indicator* to distinguish it from causal strength measures, which, if using this formulation, can be problematic as pointed out by [67]. Ours serves more as an indication than a strength, which is here the conditional mutual information.

## 6.5 Empirical Evaluation

### 6.5.1 Settings

We used a *g4dn.12xlarge* instance from AWS Sagemaker to run comparisons. It contains 48 vCPUs and 4 NVIDIA T4 GPUs. During inference, we used fp16 for  $Tf_y$  and fp32 for  $Tf_x$ . We used a combination of F1-Score, Precision, and Recall with different averaging [171] to perform the comparisons. The code for OSCAR,  $Tf_x$ ,  $Tf_y$  and the evaluation are provided <sup>2</sup> as well as the anonymized version of the dataset for reproducibility purposes.

### 6.5.2 Vehicle Event Sequences Dataset

We evaluated our method on an anonymized real-world vehicular test set of  $n = 300,000$  sequences. It contains  $|\mathcal{Y}| = 474$  different error patterns and about  $|\mathcal{X}| = 29,100$  different DTCs forming sequences of  $\approx 150 \pm 90$  events. We used 105m parameters backbones as

<sup>2</sup><https://github.com/Mathugo/OSCAR-One-Shot-Causal-AutoRegressive-discovery>

$Tf_x, Tf_y$ . The two NADEs did not see the test set during training. We set the elements of the EP rules (as defined in 2.4.1.2, Eq. 2.18) as the correct Markov Boundary for each label  $y_j$  in the tested sequences. Importantly, the rules are subject to change over time by automotive engineers, contain some noise, and are biased, which makes it more difficult to extract the true  $\mathcal{MB}$ . Further, there is about 12% missing ground truth  $\mathcal{MB}$  rules for certain  $Y_j$ .

### 6.5.3 Comparisons

Although no existing method directly targets one-shot multi-label causal discovery [41], we benchmark OSCAR against local structure learning (LSL) algorithms that estimate global Markov Boundaries. This includes established approaches such as CMB [37], MB-by-MB [151], PCD-by-PCD [164], IAMB [147] from the *PyCausalFS* package [165], as well as the more recent, state-of-the-art MI-MCF [84]. 9 random folds of the test data were created and converted into a multi-one-hot data-frame where one row represents one sequence, and each column represents an event type or label  $(\mathcal{X}, \mathcal{Y})$ . We set the target nodes as the labels with *PyCausalFS*.

### 6.5.4 Results

We first drew  $n = 50,000$  random sequences from our dataset and performed comparisons (Table 6.1). We observed that even under this reduced setup, LSL algorithms failed to compute the Markov Boundaries within a 3-day timeout, far exceeding practical limits for deployment. OSCAR, on the other hand, shows robust classification over a large amount of events (29,100), especially 55% precision, in a matter of minutes. This behavior highlights the current infeasibility of multi-label causal discovery in massive discrete event sequences. This positions OSCAR as a more feasible approach for large-scale sample-level causal discovery in production environments.

To enable at least partial comparison, we further sub-sampled to  $n = 500$  sequences (Table 6.2) to enable a faster computation. However, the number of labels in the test set is approximately the same for  $n = 500$  samples. This resulted in a poor number of CI tests for the baselines. As a result, LSL algorithms output empty  $\mathcal{MB}$  sets after multiple hours. Especially MI-MCF with even 500 samples suffers from its expensive CMI testing. Thus, traditional algorithms suffer from having either too many samples and taking days to compute or too little data to even function.

We illustrate the explainability provided by our method for the task of explaining error patterns observed in a vehicle (Fig. B.3). A concrete use case for OSCAR in this context is to refine or develop new error-pattern rules based on OSCAR output predictions, such as non-common causal variables [158] between labels (*Camera Error* node), thereby improving the automation of quality processes. More examples are given in the Appendix B.1.7.1.

Algorithm	Precision $\uparrow$	Recall $\uparrow$	F1 $\uparrow$	Running Time (min) $\downarrow$
IAMB	-	-	-	> 4320
CMB	-	-	-	> 4320
MB-by-MB	-	-	-	> 4320
PCDbyPCD	-	-	-	> 4320
MI-MCF	-	-	-	> 4320
OSCAR	<b>55.26 <math>\pm</math> 1.42</b>	<b>31.37 <math>\pm</math> 0.82</b>	<b>40.02 <math>\pm</math> 1.03</b>	<b>11.7</b>

**Table 6.1:** Comparisons of  $\mathcal{MB}$  retrieval with  $n = 50,000$  samples,  $|\mathcal{X}| = 29,100$ ,  $|\mathcal{Y}| = 474$  averaged over 6-folds. Classification metrics averaging is 'weighted' and shown as one-shot for OSCAR. The symbol '-' indicates that the algorithm did not output the  $\mathcal{MB}$  within 3 days. Metrics are given in %.

Algorithm	Precision $\uparrow$	Recall $\uparrow$	F1 $\uparrow$	Running Time (min) $\downarrow$
IAMB	0.0 $\pm$ 0.0	0.0 $\pm$ 0.0	0.0 $\pm$ 0.0	129.4
CMB	0.0 $\pm$ 0.0	0.0 $\pm$ 0.0	0.0 $\pm$ 0.0	128.7
PCDbyPCD	0.0 $\pm$ 0.0	0.0 $\pm$ 0.0	0.0 $\pm$ 0.0	129.1
MB-by-MB	0.0 $\pm$ 0.0	0.0 $\pm$ 0.0	0.0 $\pm$ 0.0	140.3
MI-MCF	0.0 $\pm$ 0.0	0.0 $\pm$ 0.0	0.0 $\pm$ 0.0	> 1440
OSCAR	<b>54.78 <math>\pm</math> 2.91</b>	<b>30.39 <math>\pm</math> 2.39</b>	<b>39.92 <math>\pm</math> 2.25</b>	<b>0.14</b>

**Table 6.2:** Comparisons of  $\mathcal{MB}$  retrieval with  $n = 500$  samples over 9 folds.

## 6.6 Limitations

Our approach relies on several assumptions that enable one-shot causal discovery under practical and computational constraints.

**Temporal Precedence** Temporal precedence (A1) simplifies directionality and faithfulness to  $\mathcal{G}$ . However, this relies heavily on precise event time-stamping. Even though we only test  $X_i \rightarrow Y_j$ , this could falsify the conditioning test  $\mathcal{Z}$ .

**Bounded Lagged Effects** The bounded lagged effects (A5) assumption enables us to restrict causal influence and recover the  $\mathcal{MB}$  of each label using Theorem 1. It also makes the computation faster. In most real-world sequences where relevant history is limited, this holds empirically. Nonetheless, in highly delayed causal chains, like financial transactions, some influence may be missed.

**Causal Sufficiency** As with many causal discovery approaches, we assume all relevant variables are observed (A3). Although it constitutes a strong assumption, in high-cardinality domains such as vehicle diagnostics, the volume of recorded events may reduce but not eliminate the risk of hidden confounding.

**Inter-label Effects** By definition, the labels are explained solely by events. While simplifying multi-label causal discovery, this intrinsic assumption could be relaxed in future work by using the *do* operator [113] to perform interventions on common causal variables of multiple labels. For example, our current framework estimates the Markov Boundaries for each label independently. However, inter-label dependencies can exist, particularly when labels share overlapping Markov Boundaries (e.g  $MB_1 = [X_1, X_3]$ ,  $MB_2 = [X_1, X_2]$ ). We aim to investigate a 'Phase 2' for OSCAR, focusing on inter-label dependencies through simulated interventions. For instance, if we consider a sequence of two labels  $Y_1, Y_2$  with the MB above, we could perform counterfactual interventions by applying  $do(X_1 = 0), do(X_3 = 0)$ . We then compute the average change in the likelihood of  $Y_1$ , which, if non-zero, indicates a dependence between  $Y_1$  and  $Y_2$ . [158] points out that the assumptions of these inter-label dependencies are already anchored in the Markov Boundaries; we do the same here.

**NADEs** Leveraging flexible NADEs, we can relax common assumptions about data-generating processes, such as Poisson Processes or SCMs. Finally, as seen in the Abulations B.1.3, the effectiveness of OSCAR hinges on the capacity of  $Tf_x$  and  $Tf_y$  to approximate true conditional probabilities (A4) and provide Oracle CI-test. While assuming Oracle tests is common in the literature [160, 76] and necessary to recover faithful causal structures, this remains a strong assumption. It is valid only to the extent that the models are perfectly trained. In multi-label classification settings, performance may degrade in underrepresented regions of the data distribution. For example, we analyze on a reduced dataset, the performance of OSCAR as a function of the  $MB$  length:

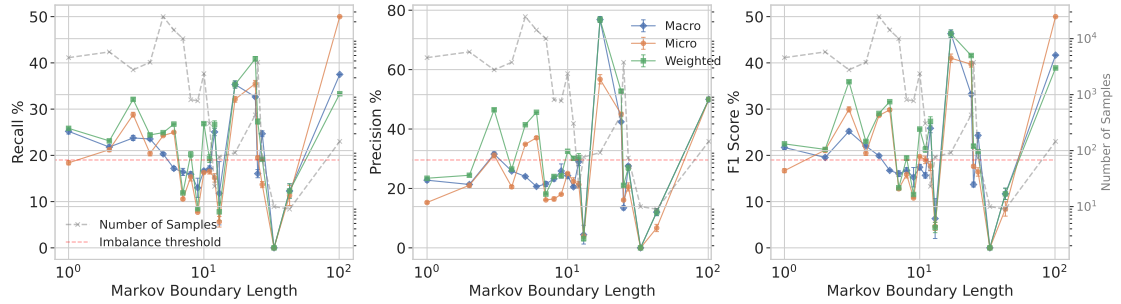


**Figure 6.3: Evolution of the Classification Performance as a Function of the Markov Boundary Length  $|\mathcal{MB}(Y_j)|$  ( $n = 45969$  samples).** We can identify that the Markov Boundary complexity is not the bottleneck but rather the number of samples per class (imbalance threshold), which reduces classification performance.

Fig. 6.3 reveals the classification performance depending on the number of nodes in the ground truth  $MB$ . On the same plot is drawn in grey the number of samples that each  $MB$  length contains (to account for imbalance). We observe that generally, a bigger  $|\mathcal{MB}(Y_j)|$  does not imply a reduction in performance, highlighting the capability of OSCAR to retrieve complex Markov Boundaries in high-dimensional data. However, we observe that past a *certain number of samples* (imbalance threshold in red  $\approx 7 \times 10^2$

samples), the classification metrics are directly correlated with the number of samples per  $|\mathcal{MB}(Y_j)|$ . This indicates that  $Tf_x, Tf_y$  struggle to output proper conditional probabilities, which deteriorates the CI-test when having rare classes. Therefore, when using OSCAR and more generally assumption A4, one should carefully assess class imbalance in the pretraining phase.

## 6.7 Summary

OSCAR extends autoregressive Transformers toward causal discovery by repurposing them as NADEs. The proposed methodology combines theoretical guarantees with parallelized computation on GPUs. Under assumptions, such as temporal precedence, causal sufficiency, and bounded lagged effects, OSCAR can reliably recover the local causal structure underlying each observed sequence, as we have shown. Thanks to its parallelized implementation on GPUs, the approach scales seamlessly to tens of thousands of event types and hundreds of labels, achieving in minutes what traditional constraint-based methods fail to compute within days. By introducing a *causal indicator*, OSCAR further quantifies the direction and magnitude of influence between events and outcomes, making causal discovery not only feasible but also interpretable for practitioners. Applied to a large-scale vehicular dataset, OSCAR demonstrated the ability to uncover the correct EP rules. However, we highlighted the limitations of the assumptions, including the impact of under-training of EPredictor on rare classes, which can, in practice, break the Oracle assumption. Nevertheless, this constitutes an important conceptual change in our overall framework—from predicting *when* and *what* faults will occur, to understanding *why* they arise. Such causal interpretability is essential in many industrial problems, in fault diagnostics but also in production lines where defects arrive sequentially.

## 6.8 Outlook

Chapter 7 addresses a distinct challenge: while OSCAR recovers causal structure within a single observed sequence, practitioners require a consensus causal graph that is stable across the full vehicle fleet. Chapter 7 introduces CARGO, which treats OSCAR’s per-sample outputs as noisy graph samples and recovers a population-level structure via adaptive aggregation.



# 7 Population-Level Multi-Label Causal Discovery

While OSCAR enables interpretable causal reasoning within individual sequences, it is also essential in many real-world systems to recover the global set of causes for each outcome (disease, defect, seismic event) across the entire available data. We aim to recover all the causes of each error pattern to potentially suggest new rules or automate the rules of unknown error patterns. This chapter is based on the following publication:

## **Towards Practical Multi-label Causal Discovery in High-Dimensional Event Sequences via One-Shot Graph Aggregation.**

[89] Hugo Math, Rainer Lienhart. *NeurIPS 2025 Workshop on Structured Probabilistic Inference & Generative Modeling*, San Diego, USA, December 2025.

### 7.1 Introduction

Although the local view of causal relationships enables direct, interpretable causal reasoning within individual sequences, real-world systems such as fleets of vehicles, patient populations, or distributed networks often share underlying causal mechanisms that recur across many realizations. Understanding these global causal dependencies is essential to building coherent diagnostic or decision-making frameworks that generalize beyond a single observation. It remains currently unknown how to perform such population-level causal discovery across industrial-scale event sequences [85, 122, 57, 83, 116] as standard methods are computationally intractable.

To address this, we reinterpret multi-label causal discovery for event sequences as a form of Bayesian model averaging [59, 114], where each sequence is treated as a sample from a local causal model. Specifically, each sequence induces a sample-level causal graph (i.e., a directed acyclic graph (DAG)) [93] inferred from OSCAR. Together, they can be fused to form a unified global structure [28]. This process, known as structural fusion [112], aggregates local graphs into a consensus causal graph over all observed samples. To this end, in this chapter we introduce CARGO: (Causal Aggregation via Robust Graph Operations), a scalable two-phase causal discovery framework.

### 7.2 Related Work

**Bayesian Model Averaging** Fusing BNs has two primary applications: averaging models from different experts to learn a global representation [59], or performing causal discovery in distributed settings with federated learning algorithms [153, 47].

Formally, given a set of Bayesian Networks  $\{B_k\}_{k=1}^m$  with associated DAGs  $\{\mathcal{G}^{(k)} = (\mathbf{V}_k, E_k)\}_{k=1}^m$ ,  $\mathbf{V}_k \in \mathbf{U}$  sharing the same finite set of node  $\mathbf{U}$ , structural fusion aims to construct the DAG  $\mathcal{G}^* = (V, E)$ ,  $V \in \mathbf{U}$ . Multiple fusion methods exist and leverage either the probability distribution  $P$  by doing Bayesian Model Averaging [59] or focus on the structural learning (Fig. 7.1) of  $\mathcal{G}^*$  [126, 112, 40, 117, 47], i.e., only merging the edges  $\{E_k\}_{k=1}^m$  to the correct nodes  $\{\mathbf{V}_k\}_{k=1}^m$ . Bayesian Model Averaging is considered to be an NP-hard [112] problem. We focus on the structural learning and seek the merged edges  $E = \bigcup_{i=1}^m E_i^\sigma$ . The consistent node ordering  $\sigma$  ensures acyclicity. The fused DAG  $\mathcal{G}^*$  is the minimal I-map of the intersection of the conditional independencies across all DAGs  $\mathcal{G}^{(k)} = (\mathbf{V}_k, E_k)_{k=1}^m$ .

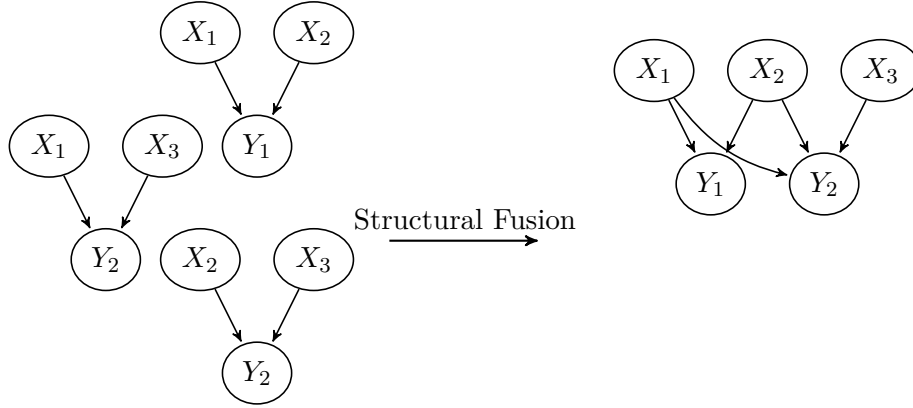


**Figure 7.1: Structural Fusion Example:** individual set of causal graphs  $\{\mathcal{G}^{(k)}\}$  (left) aggregated into a fused DAG for multi-label event sequences (right) using a simple union.

**Greedy Equivalence Search** Greedy equivalence search (GES) [21] is one of the most theoretically sound methods to recover a Markov equivalence class (MEC: Def. 19) of a DAG. Particularly in the context of large samples of data, GES provides theoretical guarantees of reaching the true graph. Formally, GES searches for the MEC of the graph  $\mathcal{G}^*$  from the observational dataset  $\mathcal{D}$  with distribution  $P$ . This defines the optimization problem as:

$$\mathcal{G}^* = \arg_{\mathcal{G}} \max f_s(\mathcal{G}, \mathcal{D}) \quad (7.1)$$

[21] proved that, under parametric assumption, a large number of samples and using the Bayesian Information Criterion (BIC) as criterion  $f_s$ , GES is guaranteed to recover an MEC of  $\mathcal{G}^*$  since it is score equivalent (Def. 27) and locally consistent (Def. 28). Some contemporary works point to decomposing classical causal discovery for high-dimensional datasets into subproblems and graph aggregation. [71] introduce a ring-based distributed algorithm for learning high-dimensional BN, [28] explores a distributed approach for large-scale causal structure learning and [97] for Markov Boundaries.

**Frequency-Based** Multiple heuristics have been developed to merge multiple BNs. One uses an edge frequency cutoff [141], another relies on estimating the proportion of false positive edges and integer linear programming (ILP) [36] or a mix of both: [145]. As pointed out by [36], choosing a frequency cutoff  $\tau$  is particularly challenging. Moreover, under class imbalance and long-tail problem in labeled datasets [169], the theoretical property of frequency approaches, such as the law of large numbers, might not hold.

## 7.3 Methodology

We now explain the two phases of CARGO, which are (1) the one-shot causal discovery (2) graph aggregation using adaptive thresholding. Since we covered already the first phase in Chapter 6, we focus on the graph aggregation phase.

### 7.3.1 Structural Fusion of Markov Boundaries

Let  $\{\mathcal{G}^{(k)} = (\mathbf{V}_k, E_k)\}_{k=1}^m$  be the set of generated DAGs by the Phase 1 from the dataset  $\mathcal{D}$  containing  $m$  i.i.d multi-labeled sequences  $\{S_l^{(k)}\}_{k=1}^m$  drawn from a joint distribution  $P(X, Y)$ . Each graph  $\mathcal{G}^{(k)}$  represents local Markov Boundaries identified within a multi-labeled sequence  $S_l^{(k)}$ . Our objective is to fuse these local graphs into a single, global consensus graph  $\mathcal{G}^* = (\mathbf{U}, E)$  (see Fig. 7.1) with the events always as parents of labels  $Y_j$  such as:

$$\text{Pa}_{\mathcal{G}}(Y_j) \subseteq \{X_0, \dots, X_n\}$$

A naive fusion approach, such as taking the simple union of all edges  $E = \bigcup_{k=1}^m E_k^\sigma$  works if and only if the Oracle models (A4) yield the perfect CI-tests in Phase 1 and thus the

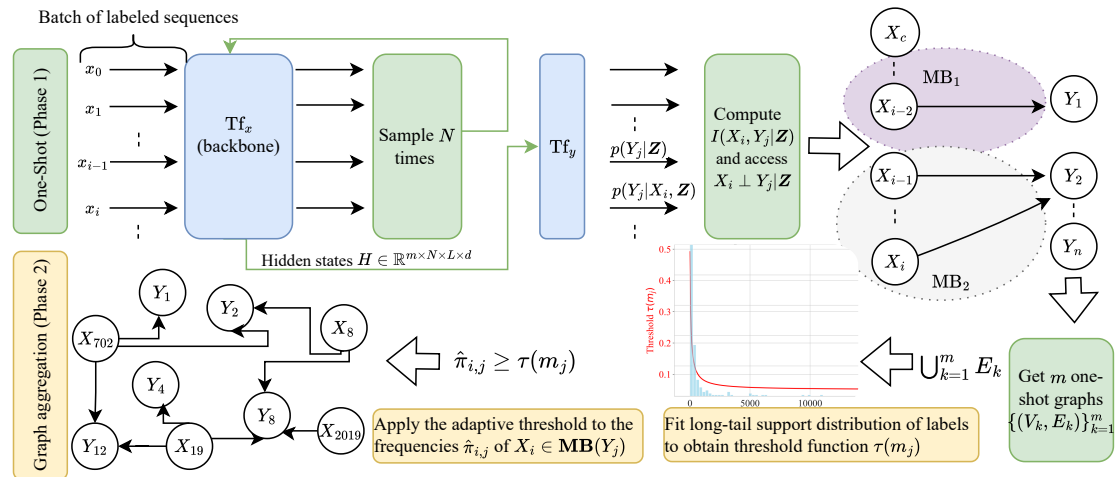


**Figure 7.2: Overview of CARGO.** Phase 1 (One-shot) is on top, and Phase 2 (Adaptive Thresholding) is on the bottom.  $d$  denotes the hidden dimension,  $L$  the sequence length,  $m$  the number of samples and  $\mathcal{MB}_1, \mathcal{MB}_2$  the Markov Boundary of  $Y_1, Y_2$ . All green and blue areas are parallelised.

local graphs  $\mathcal{G}^{(k)}$  are faithful to  $P(X, Y)$  ([112], Theorem 4.). Here, the ordering  $\sigma$  does not matter since we are dealing with Markov Boundaries. Thus,  $\mathcal{G}^*$  is naturally a DAG because we considered previously that outcome labels are solely explained by events, which simplifies acyclicity. We define the Bernoulli variable  $B_{i,j}^k$  for each potential edge  $(X_i \rightarrow Y_j)$  within each sequence  $S_l^{(k)}$ :

$$B_{i,j}^k = \begin{cases} 1 & \text{if the edge } X_i \rightarrow Y_j \text{ is present in } \mathcal{G}^{(k)} \\ 0 & \text{otherwise} \end{cases}$$

Under the Oracle Models assumption (A4), our one-shot discovery phase acts as a perfect conditional independence tester. Consequently, the detection of an edge in a local graph  $\mathcal{G}^{(k)}$  corresponds precisely to a true causal dependency in the global graph  $\mathcal{G}^*$ . The probability of this event  $P(B_{i,j}^k = 1)$  is therefore the true marginal probability of the edge's existence, which we denote as  $\pi_{i,j}$ . The empirical frequency,  $\hat{\pi}_{i,j}(m)$ , of the edge  $(X_i \rightarrow Y_j)$  after observing  $m$  sequences is the sample mean of these i.i.d Bernoulli variables  $\hat{\pi}_{i,j}(m) = \frac{1}{m} \sum_{k=1}^m B_{i,j}^k$ . By the Law of Large Numbers (LLN), as the number of i.i.d sequences  $m$  tends to infinity, the empirical frequency converges in probability to the true expected value of the random variable:

$$\hat{\pi}_{i,j}(m) \xrightarrow{P} \mathbb{E}[B_{i,j}^{(k)}] = \pi_{i,j}$$

Given a sufficiently large number of sequences, the empirical frequency  $\hat{\pi}_{i,j}(m)$  serves as a consistent estimator for the true probability of the edge's existence in the global DAG  $\mathcal{G}^*$ .

### 7.3.2 Aggregation under imperfect CI-tests

The assumption of an Oracle CI-tester, while necessary for initial theoretical guarantees and common in the literature [97], is invariably violated in practice due to factors like model capacity, limited data or class imbalance. The extracted one-shot graphs will most likely violate the independencies in  $\mathcal{G}^{(k)}$  and thus  $\mathcal{G}^*$ . Let us model the performance of our one-shot CI-test for any potential edge  $X_i \rightarrow Y_j$  with the following error rates: (1) False Positive Rate (Type I Error):  $\alpha = P(\text{detect} \mid \text{edge is spurious})$  (2) True Positive Rate (Sensitivity):  $1 - \beta = P(\text{detect} \mid \text{edge is causal})$ . We operate under the reasonable assumption that our one-shot classifier is significantly better than random, which implies that  $1 - \beta \gg \alpha$ . The expected value of our Bernoulli variable  $B_{i,j}^k$  is now:

$$\begin{aligned} \mathbb{E}[B_{i,j}^k] &= P(B_{i,j}^k = 1) \\ &= P(\text{detect} \mid \text{causal})P(\text{causal}) + P(\text{detect} \mid \text{spurious})P(\text{spurious}) \\ &= (1 - \beta)\pi_{ij} + \alpha(1 - \pi_{ij}) \end{aligned}$$

The empirical frequency now converges to this new expectation. For a true edge ( $\pi_{i,j} = 1$ ), the empirical frequency converges to a high value:  $\hat{\pi}_{i,j}(m) \xrightarrow{P} 1 - \beta$  and for spurious edge ( $\pi_{i,j} = 0$ ) it converges to a low value:  $\hat{\pi}_{i,j}(m) \xrightarrow{P} \alpha$ . This reveals the critical role of frequency aggregation as a mechanism for separating signal from noise.

### 7.3.3 Adaptive Fusion for Structural Discovery in Long-Tail Distributions

A primary challenge in real-world causal discovery is the long-tail distribution of outcome labels, where a few "head" labels possess abundant data while the vast majority of "tail" labels are data-sparse [169].

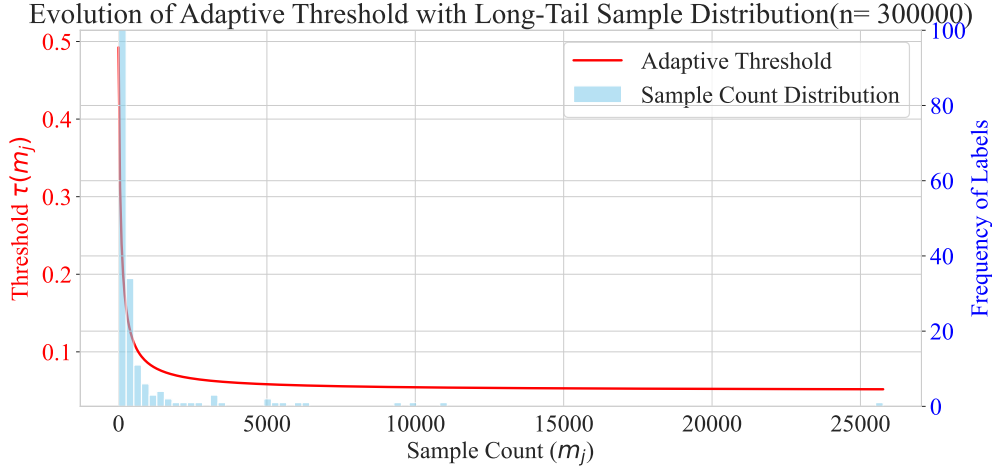


**Figure 7.3: Adaptive Thresholding Function**  $\tau_j(m_j)$  across varying support  $m_j$ , illustrating the logistic decay from  $\tau_{\max}$  to  $\tau_{\min}$ .

To resolve this, we introduce an *adaptive thresholding* strategy (Fig. 7.3) that tailors the edge inclusion criterion to the statistical power available for each label. We define a label-specific threshold  $\tau_j$ , as a logistic decay function of its sample support  $m_j$ :

$$\tau_j(m_j) = (\tau_{\max} - \tau_{\min}) \cdot \frac{1}{1 + e^{k(\log m_j - \log m_0)}} + \tau_{\min} \quad (7.2)$$

This function smoothly interpolates between a user-defined maximum threshold,  $\tau_{\max}$  (prioritizing precision for the tail), and a minimum,  $\tau_{\min}$  (prioritizing recall for the head). The function's behavior is calibrated by the data distribution. Such that decay midpoint  $m_0$  is set to the median of all label supports, providing a robust anchor point against skew. The decay rate  $k$  is made inversely proportional to the log-inter-quartile range of supports such that:

$$k = \frac{2 \log 3}{\log q_{75} - \log q_{25}} \quad (7.3)$$

Consequently, for rare labels with small  $m_j$ , the high variance of the frequency estimate necessitates a high threshold  $\tau_j(m_j)$  that acts as a strong regularizer. For common labels with large  $m_j$ , the LLN guarantees the convergence of  $\hat{\pi}_{i,j}$  to the true edge probability, justifying a lower threshold to capture a more complete causal structure.

## 7.4 Empirical Evaluation

The empirical evaluation of CARGO follows the same experimental setting and dataset configuration introduced in Chapter 6. The implementation is included in Appendix B.2.6. This task is challenging, as it involves handling cumulative noise across sequences from the imperfect CI-tests, managing severe label imbalance, and ensuring that aggregated structures remain both interpretable and statistically valid.

### 7.4.1 Benchmark Against Multi-Label Causal Discovery Methods

**Settings** We benchmark CARGO against a representative set of local structure learning (LSL) algorithms commonly used for Markov Boundary estimation, including CMB [37], MB-by-MB [151], PCD-by-PCD [164], and IAMB [147] from the *PyCausalFS* package [165], as well as the more recent MI-MCF [84]. Each algorithm was evaluated on the same dataset partition used for OSCAR, consisting of six random folds converted into a multi-one-hot representation where each sequence is represented by its observed event types and corresponding label vector  $(\mathcal{X}, \mathcal{Y})$ .

**Results** Table 7.1 shows the performance of the multi-label causal discovery algorithms, the one-shot performance of OSCAR, and the global Markov boundary retrieval of CARGO. Since the evaluation setup is the same, all baseline LSL algorithms failed to compute complete Markov Boundaries within a three-day timeout, as established in Chapter 6. We observe that, even though the imperfect conditional independence tests introduce cumulative errors and the classification task becomes considerably more challenging since, in the global setting, the model aims to recover the underlying global causal rules rather than the more straightforward local rules identifiable within a single sequence, CARGO still achieves a significant performance improvement. As shown in Table 7.1, it surpasses OSCAR by a clear margin across all metrics, e.g., the Precision

Algorithm	Precision $\uparrow$	Recall $\uparrow$	F1 $\uparrow$	Running Time (min) $\downarrow$
IAMB	-	-	-	> 4320
CMB	-	-	-	> 4320
MB-by-MB	-	-	-	> 4320
PCDbyPCD	-	-	-	> 4320
MI-MCF	-	-	-	> 4320
OSCAR (sample-level)	55.3 $\pm$ 1.4	31.3 $\pm$ 0.8	40.0 $\pm$ 1.0	<b>11.7</b>
CARGO (population-level)	<b>60.6 <math>\pm</math> 1.5</b>	<b>45.8 <math>\pm</math> 1.7</b>	<b>45.8 <math>\pm</math> 1.2</b>	11.8

**Table 7.1:** Comparisons of  $\mathcal{MB}$  retrieval with  $m = 50,000$  samples averaged over 6-folds with  $|\mathcal{Y}| = 474, |\mathcal{X}| = 29,100$  nodes. Averaging is 'weighted'. The symbol '-' indicates that the algorithm did not output the **MBs** within 3 days. Metrics are given in %. OSCAR reports only the one-shot performance (Phase 1).

is  $(60.6 \pm 1.5$  vs.  $55.26 \pm 1.42)$  for the one-shot performance, confirming the benefit of graph aggregation for large-scale causal discovery.

### 7.4.2 Ablation on Aggregation Criteria for Phase 2

**Criteria** We provide an Ablation of the different criteria used in the structural fusion of Markov Boundaries. *Union* stands for a simple union over all edges without any removal. *Frequency* or edge voting, counts how often is  $X_i \in \mathcal{MB}(Y_j)$ . Then apply a static frequency threshold  $\tau = [0.05, 0.25, 0.5, 0.8]$ . *MI* uses the mutual information between events and labels as a criterion in a Background Equivalence Search [21]. *Expected FPR* (false positive ratio) [36] describes two beta distributions which are fitted using the distribution of the mutual information  $I(X_i, Y_j)$  extracted from Phase 1. The lower tail is used for outlier detection. Different FPR are chosen  $\beta = [0.01, 0.05, 0.15, 0.2]$ . Detailed definitions can be found in Appendix B.2.2.

**Results** Figure 7.4 illustrates the impact of aggregation choices during Phase 2. A naive *Union* maximizes recall (84% for weighted) but suffers from poor precision. When optimizing a local scoring criterion as the mutual information *BES mi*, it did not enhance

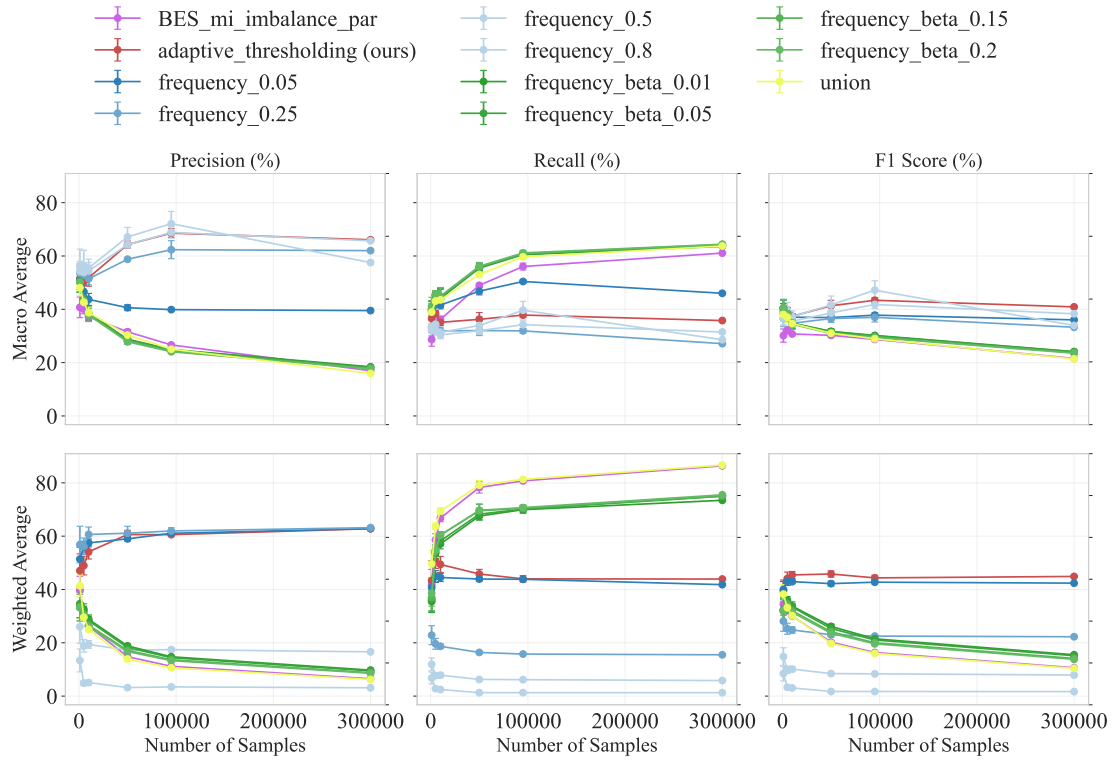


**Figure 7.4: Criterion Ablation for Structural Fusion.** Comparison of different criteria for the structural fusion (Phase 2) as a function of the number of samples  $m$ . With  $|\mathcal{Y}| = 474, |\mathcal{X}| = 29, 100$  nodes.

the performance over a basic *Union* significantly. In contrast, instead of optimizing a score, fitting Beta distributions to detect outliers using their mutual information appears to perform better; hence, *frequency beta* outperforms alternatives, particularly in terms of lower FPR. Experimental results for Frequency approaches with static thresholds corroborate the analysis in Section 7.3.2. Specifically, we observe a trade-off dictated by class support: strict cut-offs ( $\tau \in [0.5, 0.8]$ ) yield the lowest weighted F1-scores, as they penalize classes with large support ( $m_j$ ). Conversely, lowering the threshold ( $\tau \in [0.05, 0.25]$ ) leads to a substantial gain in weighted precision (+40%), but at the expense of macro-averaged metrics (−20% precision), as rare classes become overwhelmed by noise.

Our Adaptive Thresholding criterion bridges this gap by applying conservative thresholds to small supports and lenient thresholds to large supports, effectively leveraging the long-tail distribution. Consequently, it achieves state-of-the-art performance across all metrics, ranking first with F1-scores of 44.88% (weighted) and 40.9% (macro), and precision scores of 62.8% and 66.1%, respectively.

### 7.5 Summary

CARGO completes the population-level events-to-outcome causal discovery cell (Table 1.1). Moving from sample-level to population-level discovery significantly increases the task’s complexity, as it requires the model to recover generalizable causal mechanisms rather than sequence-specific associations. Yet CARGO achieves strong performance (60.6% precision), especially across a remarkable order of magnitude of  $10^4$  event types and  $10^2$  labels, demonstrating both robustness and scalability in real-world automotive diagnostics. It effectively demonstrates that complex causal dependencies can be efficiently inferred from noisy, sparse, and imbalanced data. Under the temporal assumptions, large samples, faithfulness, and a perfect CI-test, CARGO recovers the set of Markov Boundaries. However, we highlighted the practical limitations, in particular long-tail distributions, which will most likely introduce spurious edges due to the imperfect CI tests.

### 7.6 Outlook

OSCAR and CARGO together form a complete pipeline for multi-label causal discovery, identifying, for each outcome label, the set of events that causally drive it. Yet both methods share an important scope restriction: they model events-to-outcome dependencies, treating the causal structure between events themselves as opaque. In many diagnostic scenarios, however, understanding how one DTC causally triggers another is equally essential for root-cause analysis and cascading failure diagnosis, e.g., why does DTC A tend to precede DTC B? This limitation motivates a change in problem formulation: rather than asking which events cause a given label, we now ask how events cause each other. Chapter 8 addresses this more general challenge with TRACE, a framework for scalable sample-level event-to-event causal discovery in discrete sequences.

## 8 Sample-Level Event-to-Event Causal Discovery

Chapters 6 and 7 addressed events-to-outcome causal structure. A complete diagnostic picture additionally requires understanding how events causally influence each other, the event-to-event setting tackled in this chapter. In this setting, it becomes possible to identify root-causes, mediating effects and recover the global causal graphs. We therefore study causal discovery from a single observed sequence of discrete events generated by a stochastic process, as encountered in vehicle logs, manufacturing systems, or patient trajectories. This regime is particularly challenging due to the absence of repeated samples, high dimensionality, and long-range temporal dependencies of the single observation during inference. This chapter is based on the following contribution:

**TRACE: Scalable Amortized Causal Discovery from Single Sequences via Autoregressive Density Estimation under review.**

[90] Hugo Math, Rainer Lienhart, under review to the International Conference on Machine Learning (ICML), Seoul, South Korea, July 2026.

### 8.1 Introduction

Suppose we observe a single realization of a discrete stochastic process, for instance, the symptoms, tests, and disease evolution of a patient [75, 57], a manufacturing line’s tests, or some diagnostic codes generated by a vehicle. Which of these discrete events influences the occurrence of the others?

Contemporary causal discovery algorithms for sequences infer relations across multiple parallel streams (e.g., distinct users or sensors). These methods are ill-suited for recovering causal structure within a single event stream, nor do they scale to the long, noisy, and heterogeneous sequences encountered in modern industrial systems. Moreover, sample-level causal discovery, where discovery must be performed on a specific sample (see Chapter 6) poses a fundamentally harder challenge than population-level discovery, as it requires identifying conditional independencies among event types from a single realization of the process.

In the era of large-scale pretraining, Autoregressive Language Models (AR LMs) [121, 146] have emerged as powerful density estimators, encoding rich conditional distributions over complex contexts to predict the next token [30]. Consequently, there is growing interest in amortized causal discovery [80, 10], where the heavy computational cost is shifted to pretraining a single model that can infer causal structures. We propose to take this a step further by repurposing existing predictive priors rather than training

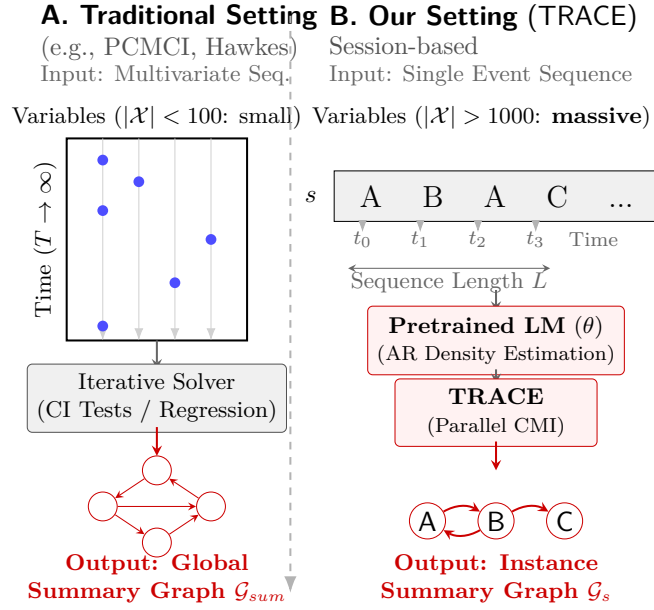


**Figure 8.1: Methodological Shift.** (A) **Traditional Causal Discovery in Sequences** (e.g., PCMCI, Hawkes, Granger) relies on iterative solvers (CI-tests) over long multivariate time series ( $T \rightarrow \infty$ ). (B) **Our TRACE Approach** processes a single sequence (e.g., event logs, user interactions, patient trajectories) through a pretrained autoregressive (AR) model as density estimator to compute the Conditional Mutual Information (CMI) in parallel, enabling scalable causal discovery over massive vocabularies ( $|\mathcal{X}| > 1000$ ).

specialized models. This effectively transforms a production forecaster into a causal discovery engine without the need for task-specific retraining.

## 8.2 Related Work

### 8.2.1 Causal Discovery in Event Sequences

Distinguishing between the multi-stream and single-stream paradigm is key, as they fundamentally address different causal problems (Fig. 8.1). We point out the current methods' limitations in Table 8.1.

**Multiple Streams (Standard).** The most common paradigm considers a long multivariate time series, each corresponding to an individual entity (e.g., sensor, user, or machine). The goal is to uncover how the occurrence of events in one sequence influences the occurrences in others. It is traditionally done via Granger-based [44, 134, 100, 173] (TCDF, CAUSE), constraint-based [125] (PCMCI), functional [62] (VARLiNGAM) or optimization-based methods [109] (DYNOTEARS). Modern information-theoretic variants (NPHC [1], CASCADE [24]) and neural point processes (THP [179], SHTP [118]).

Method Class	Discrete Events	High Dim.	Non-Param.	Lags	Instance-Level	Linear Complexity
Constraint-based (PCMRI, FCI)	×	×	✓	✓	×	×
Score-based (DYNOTEARS)	×	×	×	✓	×	×
Granger (TCDF, CAUSE)	×	×	×	✓	×	×
Noise-based (VarLiNGAM)	×	×	×	✓	×	×
Hawkes / TPP Models (THP, SHP)	✓	×	×	✓	×	×
Info-Theoretic (NPHC, CASCADE)	✓	×	✓	✓	×	×
<b>TRACE (Ours)</b>	✓	✓	✓	✓	✓	✓

**Table 8.1:** Comparison of causal discovery methods. **Discrete Events:** Operates on discrete event sequences (e.g., text, logs) rather than multivariate time series. **High Dim:** Computationally tractable for large vocabularies ( $|\mathcal{X}| > 10^3$ ). **Non-Param.:** Agnostic to the functional form (e.g., linearity) of causal relationships. **Lags:** Models delayed causal effects. **Sample-Level:** Infers a local causal graph specific to a single sequence, rather than a global graph. **Linear Complexity:** Complexity scales linearly with the vocabulary size  $|\mathcal{X}|$ .

As established in Chapters 5 and 6, these methods are limited to small number of nodes in the resulting graph.

**Single Stream (The Sample-Level Regime).** Our setting differs fundamentally (Fig. 8.1) as we operate in the ‘session-based’ regime common to NLP and system logs: we observe many short, independent sequences over a massive vocabulary (often with  $|\mathcal{X}| > 1000$ ). During inference, only one realization of the process is often available. Here, the goal is to understand if event type  $A$  causes type  $B$ . This regime is significantly harder due to the sparsity of specific event pairs in high-dimensional vocabularies and the lack of independent trials during inference. While recent works attempt to interpret attention weights in Transformers as causal graphs [124], this is heavily criticized for being a poor proxy of causality [11].

## 8.3 Methodology

An overview of TRACE can be found in Fig. 8.2. A key advantage of TRACE is its architectural agnosticism. The framework decouples the density estimation (Phase 1) from causal discovery (Phase 2). Consequently, TRACE can leverage any state-of-the-art autoregressive backbone (e.g., Transformers, Mamba, RNNs).

### 8.3.1 Data-Generating Process

We model the *data-generating process* (DGP) as a non-stationary stochastic process<sup>1</sup>  $\{X_t, t \in \mathbb{N}\}$  taking values in a finite, discrete alphabet  $\mathcal{X}$ . We assume that the process

<sup>1</sup>We slightly abuse the notation compared to Chapters 6, 7 by using  $X_t$  instead of  $X_i$  to denote an event occurrence at time step  $t$ . This is more aligned with dynamical systems and stochastic processes literature [69].

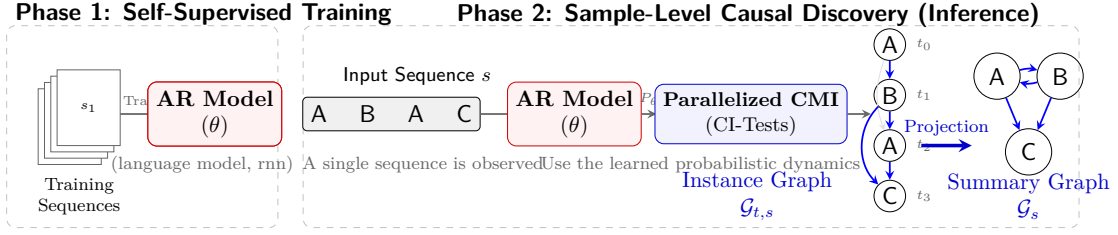


**Figure 8.2: TRACE Methodology. Phase 1 (Training):** An autoregressive (AR) model (e.g., LM, RNN) is pretrained on a corpus of event sequences via next-token prediction to learn the process dynamics ( $P_\theta$ ). **Phase 2 (Inference):** A single sequence  $s$  is passed through the frozen model. We then estimate conditional mutual information (**Parallelized CMI** module) to prune non-causal edges and form the *Instance-Time Causal Graph*  $\mathcal{G}_{t,s}$ . Finally, this graph is projected onto the event types to recover the *Summary Causal Graph*  $\mathcal{G}_s$ .

forms a high-order Markov chain [69] with transition distribution  $P(X_t|X_{<t})$ , where  $X_{<t} = X_{0:t-1} \triangleq \{X_0, \dots, X_{t-1}\}$ . This implies that the past  $X_{0:t-1}$  is not independent of the future  $X_{t+1}$  conditioned on the present  $X_t$ .

### 8.3.2 Sample-Level Causality

Our analysis begins at the level of the specific observed sequence. To bridge the gap between the multinomial realization  $s = (x_0, \dots, x_L)$  and causal structure, we define the Binary Event Process  $\{E_t\}_{t=0}^L$  as

$$E_t \triangleq \mathbb{1}_{X_t=x_t}$$

Here,  $E_t$  is a binary random variable representing the realization of the specific event type observed at time  $t$ . This transformation allows us to represent the causal dependencies specific to this sequence as a DAG, which we term the *Instance-Time Causal Graph*.

**Definition 21** (Instance-Time Causal Graph). *Let  $s$  be a realization of the process  $\{X_t\}$ . The Instance-Time Causal Graph  $\mathcal{G}_{t,s} = (\mathcal{T}, \mathcal{E}_t)$  is a DAG where the nodes  $\mathcal{T} = \{0, \dots, L\}$  correspond to the time steps of the sequence. A directed edge  $(t-k) \rightarrow t$  exists in  $\mathcal{E}_t$  if and only if the realization of the event at  $t-k$  is a cause of the event at  $t$ .*

This graph  $\mathcal{G}_{t,s}$  (illustrated in Fig. 8.2, right) represents the unrolled causal history of the sequence  $s$ .

### 8.3.3 Summary-Level Causality

Operators are often confronted with observing a single sequence during inference to understand generalizable rules (e.g., "Fire causes Smoke") rather than specific timestamps ( $\mathcal{G}_{t,s}$ ). We adapt the terminology from [6] regarding summary causal graph (SCG), which treats the unique event types in  $\mathcal{X}$  as the variables of interest. Therefore, for a single sequence  $s$ , we aim to recover its *Instance Summary Causal Graph*.

**Definition 22** (Instance Summary Causal Graph). *Let  $\mathcal{X}_s \subseteq \mathcal{X}$  be the set of unique event types in  $s$ . The Instance SCG  $\mathcal{G}_s = (\mathcal{X}_s, \mathcal{E}_s)$  is the surjective projection of the Instance Graph  $\mathcal{G}_{t,s}$  onto  $\mathcal{X}_s$ . Specifically, a type-level edge  $u \rightarrow v$  exists in  $\mathcal{G}_s$  if and only if it appears at least once in the instance graph:*

$$u \rightarrow v \in \mathcal{E}_s \iff \exists t, k \text{ s.t. } ((t-k) \rightarrow t) \in \mathcal{E}_t \wedge x_{t-k} = u \wedge x_t = v$$

Hence, our causal discovery objective is to identify the parents  $\text{Pa}_{\mathcal{G}_{t,s}}(t)$  for each node in the sequence (e.g., detecting  $\text{Fire}@t_1 \rightarrow \text{Smoke}@t_2$ ) and aggregate them to reconstruct the instance summary causal graph  $\mathcal{G}_s$  (e.g.,  $\text{Fire} \rightarrow \text{Smoke}$ ), illustrated in Fig. 8.2 (right).

**Remark 3** (Cyclicity in Summary Graphs). *Consistent with the standard literature [6], the summary graph  $\mathcal{G}_s$  is an abstraction of the time-unrolled graph and is therefore permitted to contain cycles.*

### 8.3.4 Autoregressive Density Estimation

TRACE leverages the same density estimation capability as OSCAR (Chapter 6): a pretrained AR model denoted  $\text{Tf}_\theta$  (CarFormer) estimates the next token probabilities  $P_\theta$ . We map it to the binary event process as:

$$P_\theta(E_t = 1 \mid X_{<t} = x_{<t}) = [\text{Softmax}(\text{Tf}_\theta(x_{<t}))]_{x_t} \quad (8.1)$$

The model is trained on a single event stream rather than multi-labeled sequences (Chapter 3). This formulation allows us to utilize the joint distributions learned by the AR model for the structure learning of  $\mathcal{G}_{t,s}$ . Therefore, in contrast to recent works probing causal reasoning abilities of AR models (e.g., language models) via prompting [78, 68], we focus on extracting causal structure from the learned probabilistic dynamics.

### 8.3.5 Assumptions

In particular,  $\mathcal{G}_{t,s}$  implies (1) the *Markov assumption* [114], such that a variable is conditionally independent of its non-descendants given its parents, and (2) *consistency through time* [6]. We give their limitations in Section 8.7. We aim at being more flexible than Chapters 6 and 7. Specifically, we also assume:

**Assumption 6** (Temporal Precedence). *Given a perfectly recorded sequence of events  $((x_1, t_1), \dots, (x_L, t_L))$  and monotonically increasing time of occurrence  $0 \leq t_1 \leq \dots \leq t_L$ , an event  $x_t$  is allowed to influence any subsequent event  $x_{t'}$  such that  $t < t'$ .*

**Assumption 7** (Causal Sufficiency). *All relevant variables are observed, and there are no hidden confounders affecting the events.*

**Assumption 8** ( $\epsilon$ -Oracle Model). *We assume that the AR model  $Tf_\theta$ , trained via maximum likelihood estimation on a dataset generated by the true distribution  $P$ , has converged such that the Kullback-Leibler divergence is bounded by  $\epsilon$ :*

$$D_{KL}(P(X_t | X_{<t}) || P_\theta(X_t | X_{<t})) \leq \epsilon \quad (8.2)$$

And that the total variation distance  $\delta(P, P_\theta) \leq \frac{1}{2}$ . We thus define  $Tf_\theta^\epsilon$  as an  $\epsilon$ -Oracle model.

By Pinsker's inequality, this implies the total variation distance  $\delta(P, P_\theta)$  to be bounded by  $\sqrt{\epsilon/2}$ .

## 8.4 Single Stream Causal Discovery

In this section, similarly to Chapter 6, we describe how we can derive a CI-test to construct the Instance-Time Causal Graph  $\mathcal{G}_{t,s}$  within single streams.

### 8.4.1 Conditional Mutual Information

In a sequence  $s = (x_0, \dots, x_L)$ , we would like to assess how much additional information the realization  $x_t$  ( $E_t = 1$ ) provides about the next event occurrence  $X_{t+1} = x_{t+1}$  when we already know the past observation  $X_{<t}$ . We essentially try to answer whether:

$$P(E_{t+1}|E_t, X_{<t}) = P(E_{t+1}|X_{<t})$$

Similarly to Chapter 6, Information Gain  $I_G$  (Def. 12) characterizes the remaining uncertainty in  $E_{t+1}$  once we know the realization  $e_t$  conditioned on  $x_{<t}$ :

$$\begin{aligned} I_G(E_{t+1}, e_t|x_{<t}) &= D_{KL}(P(E_{t+1}|e_t, x_{<t})||P(E_{t+1}|x_{<t})) \\ &= H(E_{t+1}|x_{<t}) - H(E_{t+1}|e_t, x_{<t}) \end{aligned} \quad (8.3)$$

The conditional independence (CI, Def. 15) between event  $E_t$  and event  $E_{t+1}$  is assessed with the CMI such as:

$$\begin{aligned} I(E_{t+1}, E_t|X_{<t}) &\triangleq H(E_{t+1}|X_{<t}) - H(E_{t+1}|E_t, X_{<t}) \\ &= \mathbb{E}_{e_t, x_{<t}}[I_G(E_{t+1}, e_t|x_{<t})] \end{aligned} \quad (8.4)$$

We thus can deduce the following CI-test, such that:

$$E_{t+1} \not\perp E_t|X_{<t} \Leftrightarrow I(E_{t+1}, E_t|X_{<t}) > 0 \quad (8.5)$$

**Remark 4.** *We condition on the full trajectory  $X_{<t}$  rather than the coarsened binary history  $E_{<t}$  to test for all observed events in the history, thereby blocking potential back-door paths (confounders) that would otherwise remain hidden in the binary projection.*

### 8.4.2 Estimation and Approximation Error

The previous Eq. 8.4 involves an expectation over the distribution of histories  $x_{<t}$ . Since the true distribution  $P$  is unknown, we utilize the  $\epsilon$ -Oracle model  $\text{Tf}_\theta$  as a proxy to simulate  $N$  i.i.d. history particles  $\{x_{<t}^{(l)}\}_{l=1}^N \sim P_\theta(X_{<t})$ . We define the empirical estimator  $\hat{I}_N$  of the CMI as the Monte Carlo estimation:

$$\hat{I}_N(E_{t+1}; E_t | X_{<t}) = \frac{1}{N} \sum_{l=1}^N \underbrace{\mathbb{E}_{e_t \sim P_\theta} [I_G(E_{t+1}, e_t | x_{<t}^{(l)})]}_{f_\theta(x_{<t}^{(l)})} \quad (8.6)$$

**Proposition 1** (Convergence to the  $\epsilon$ -Proxy). *The estimator  $\hat{I}_N$  is a consistent estimator of the  $\epsilon$ -Oracle induced CMI denoted as  $I_\theta$ . By the Strong Law of Large Numbers, as  $N \rightarrow \infty$ :*

$$\hat{I}_N \xrightarrow[N \rightarrow +\infty]{\text{a.s.}} I_\theta(E_{t+1}; E_t | X_{<t})$$

(Proof Sketch) It follows directly from the Strong Law of Large Numbers (SLLN), as the samples are drawn i.i.d. from  $P_\theta$  and the information gain term  $f_\theta(x_{<t}^{(l)})$  is bounded by  $\log 2$ , ensuring finite variance.

*Proof.* The particles  $x_{<t}^{(l)}$  are sampled directly from the model  $\text{Tf}_\theta$ . Let  $f_\theta(x_{<t}^{(l)})$  represents the estimation CMI for a fixed history  $x_{<t}$  and  $I_\theta$  the CMI with the approximated distribution  $P_\theta$ . Expressing this as a difference of conditional entropies:

$$\begin{aligned} 0 &\leq \mathbb{E}_{e_t \sim P_\theta} I_G(E_{t+1}, e_t | x_{<t}^{(l)}) \\ &= H_\theta(E_{t+1} | x_{<t}^{(l)}) - H_\theta(E_{t+1} | E_t, x_{<t}^{(l)}) \\ &\leq H_\theta(E_{t+1}) \leq \log 2. \end{aligned} \quad (8.7)$$

Thus the posterior variance of  $f_\theta(x_{<t}^{(l)})$  satisfies  $\sigma_f^2 \triangleq \mathbb{E}_{x_{<t}} [f_\theta^2(x_{<t})] - I_\theta^2(f_\theta) < +\infty$  [29] then the variance of  $\hat{I}_N(f)$  is equal to  $\text{var}(\hat{I}_N(f)) = \frac{\sigma_f^2}{N}$  and from the strong law of large numbers:

$$\hat{I}_N \xrightarrow[N \rightarrow +\infty]{\text{a.s.}} \mathbb{E}_{e_t \sim P_\theta, x_{<t} \sim P_\theta} [I_G(E_{t+1}, e_t | x_{<t})] \triangleq I_\theta(f_\theta) \quad (8.8)$$

□

Since we know that the estimator  $\hat{I}_N$  converges to the approximated CMI as  $I_\theta$ , we derive an approximation error bound to characterize the remaining noise induced by the imperfect  $\epsilon$ -Oracle model.

**Theorem 2** (Total Error Bound in the  $\epsilon$ -Regime). *Let  $\hat{I}_N$  be the Monte Carlo estimator of the approximated CMI  $I_\theta$ . Assuming the AR model  $P_\theta$  approximates the true DGP  $P$  as an  $\epsilon$ -Oracle model (A8), the asymptotic error of the true CMI  $I$  is bounded by:*

$$\limsup_{N \rightarrow \infty} |I - \hat{I}_N| \leq 2\sqrt{\epsilon/2} \ln(2) + 2(1 + \sqrt{\epsilon/2}) h_b \left( \frac{\sqrt{\epsilon/2}}{1 + \sqrt{\epsilon/2}} \right)$$

## 8 Sample-Level Event-to-Event Causal Discovery

where  $h_b(\cdot)$  is the binary entropy function  $h_b(p) = -p \ln p - (1-p) \ln(1-p)$ .

(*Proof Sketch*) We use the Alicki-Fannes-Winter [156] inequality for the difference between conditional entropies of two distributions with a small total variation distance  $\delta(P, P_\theta)$  corresponding to an  $\epsilon$ -Oracle model.

*Proof.* By definition, the Conditional Mutual Information is the difference of two conditional entropies (Eq. 8.4):

$$I(E_t; E_{t'} | X_{<t}) = H(E_t | X_{<t}) - H(E_t | E_{t'}, X_{<t})$$

Our framework operates in the Teacher Forcing regime. We do not sample the history  $X_{<t}$  from the model's joint distribution. Instead, we estimate the CMI conditioned on the observed history  $x_{<t}^{(l)}$ . Consequently, the relevant error metric is the per-step conditional divergence at time  $t$ , given the fixed history.

Let  $\Delta = |I - I_\theta|$  be the CMI estimation error. By the triangle inequality:

$$\Delta \leq \underbrace{|H_P(E_t | X_{<t}) - H_\theta(E_t | X_{<t})|}_{\text{Term A}} + \underbrace{|H_P(E_t | E_{t'}, X_{<t}) - H_\theta(E_t | E_{t'}, X_{<t})|}_{\text{Term B}}$$

We apply the sharp continuity bound for conditional entropy in classical systems ([156], Lemma 2). Let  $\rho$  and  $\sigma$  be the true and model distributions respectively. Let  $\delta = |(P(E_t|\cdot) - P_\theta(E_t|\cdot))|_1$  be the total variation distance. Since the target variable  $E_t$  is binary ( $d_A = 2$ ), the bound is:

$$|H_\rho - H_\sigma| \leq \delta \ln(d_A) + (1 + \delta) h_b\left(\frac{\delta}{1 + \delta}\right)$$

From Assumption 8,  $\delta \leq \frac{1}{2}$ . Substituting  $d_A = 2$  (so  $\ln 2$  in nats since we are using cross-entropy loss in PyTorch [110]):

$$|H_P(E_t | X_{<t}) - H_\theta(E_t | X_{<t})| \leq \delta \ln(2) + (1 + \delta) h_b\left(\frac{\delta}{1 + \delta}\right)$$

Term B represents the same entropy difference conditioned on an augmented set  $\{E_{t'}, X_{<t}\}$ . Since the target dimension  $d_A$  remains 2, the same bound applies. Summing the terms:

$$|I - I_\theta| \leq 2\delta \ln(2) + 2(1 + \delta) h_b\left(\frac{\delta}{1 + \delta}\right)$$

Substituting the Pinsker upper bound  $\delta = \sqrt{\epsilon/2}$  and noting that the right-hand side ( $h_b(x)$ ) is monotonically increasing in  $\delta$ , we obtain the final bound in terms of the oracle score  $\epsilon$ :

$$|I - I_\theta| \leq 2\sqrt{\epsilon/2} \ln(2) + 2(1 + \sqrt{\epsilon/2}) h_b\left(\frac{\sqrt{\epsilon/2}}{1 + \sqrt{\epsilon/2}}\right) \quad (8.9)$$

Finally, we decompose the total error into estimation variance and approximation bias using the triangle inequality:

$$|\hat{I}_N - I| = |(\hat{I}_N - I_\theta) + (I_\theta - I)| \leq \underbrace{|\hat{I}_N - I_\theta|}_{\text{Estimation Error}} + \underbrace{|I_\theta - I|}_{\text{Approximation Bias}} \quad (8.10)$$

Given that  $\hat{I}_N$  is a consistent estimator of the model's internal CMI,  $I_\theta$  (Prop. 1). By the Strong Law of Large Numbers,  $\hat{I}_N \xrightarrow{a.s.} I_\theta$  as  $N \rightarrow \infty$  the stochastic estimation error vanishes, leaving only the irreducible approximation bias:

$$\limsup_{N \rightarrow \infty} |\hat{I}_N - I| \leq 0 + |I - I_\theta|$$

We thus obtain the final bound in terms of the oracle score as:

$$\limsup_{N \rightarrow \infty} |\hat{I}_N - I| \leq 2\sqrt{\epsilon/2} \ln(2) + 2(1 + \sqrt{\epsilon/2})h_b \left( \frac{\sqrt{\epsilon/2}}{1 + \sqrt{\epsilon/2}} \right)$$

This confirms that minimizing the cross-entropy loss ( $\epsilon$ ) directly minimizes the upper bound on structural causal error using the CMI as causal strength.  $\square$

Crucially, this bound implies that as the AR model approaches the true distribution ( $\epsilon \rightarrow 0$ ), the causal identification error vanishes.

### 8.4.3 Identifiability

Standard Faithfulness [139] relies on Oracle CI-tests returning exact zeros, an unrealistic premise under finite samples and imperfect density estimation. We instead adopt a variant of Strong Faithfulness [149], which requires valid causal associations to exceed a detection threshold  $\tau$  (i.e.,  $I > \tau$ ). Crucially, in our setting, this lower bound  $\tau$  is by the estimator's bias (Theorem 2) (if we assume  $N \rightarrow +\infty$ ).

**Definition 23** ( $\epsilon$ -Strong Faithfulness). *Let  $\tau_\epsilon$  be the asymptotic approximation error bound of the model (Theorem 2). A distribution  $P$  is  $\epsilon$ -**Strongly Faithful** to a causal graph  $\mathcal{G}$  with respect to the estimator  $P_\theta$  if, for every active edge  $E_t \rightarrow E_{t'}$  with  $t < t'$ , the **true** CMI satisfies:*

$$I(E_t; E_{t'} | X_{<t}) > 2\tau_\epsilon \quad (8.11)$$

Identifiability is guaranteed provided the true causal signal dominates the model's approximation error (verified experimentally in Appendix B.3.3.2).

**Lemma 9** (Identifiability of the Instance-Time Causal Graph). *Let  $\hat{I}_N$  be the consistent Monte Carlo estimator of the CMI derived from the  $\epsilon$ -Oracle model  $P_\theta$ . Under the assumption of  $\epsilon$ -Strong Faithfulness (Def. 23), the instance-time causal graph  $\mathcal{G}_{t,s}$  is identifiable with probability 1 as  $N \rightarrow \infty$ .*

*Proof.* Let  $\Delta = |\hat{I}_N - I|$  be the total estimation error. From Theorem 2, we have a finite bound corresponding to a noise floor  $\tau_\epsilon$  such as  $\limsup_{N \rightarrow \infty} \Delta \leq \tau_\epsilon$ .

We analyze the two cases for binary classification of the edge  $E_{ij}$ :

**Case 1: No Edge ( $H_0$ ).** If the edge is absent,  $I = 0$ . The estimator is bounded by the noise floor:

$$\begin{aligned} 0 &\leq |\hat{I}_N - I| \leq \tau_\epsilon \\ &\iff 0 \leq \hat{I}_N \leq \tau_\epsilon \end{aligned}$$

The CI-test is rejected (Correct Rejection).

**Case 2: Active Edge ( $H_1$ ).** If the edge exists, by Definition 23,  $I = 2\tau_\epsilon + \gamma$  for some  $\gamma > 0$ . We have:

$$\begin{aligned} |\hat{I}_N - I| &= \Delta \\ \implies -\Delta &\leq \hat{I}_N - I \leq \Delta \\ \implies I - \Delta &\leq \hat{I}_N \leq \Delta + I \\ \implies 2\tau_\epsilon + \gamma - \tau_\epsilon &\leq \hat{I}_N \leq \Delta + I \\ \implies \tau_\epsilon + \gamma &\leq \hat{I}_N \leq \Delta + I \end{aligned} \tag{8.12}$$

$$\implies \tau_\epsilon < \hat{I}_N \tag{8.13}$$

Since  $\gamma > 0$  we have  $\hat{I}_N > \tau_\epsilon$ . The estimator detects an edge (Correct Detection). Thus the graph is identifiable.  $\square$

#### 8.4.4 Lagged Effects via Simulated Interventions

To evaluate the lagged effects of an event  $E_t$  on  $E_{t'}$  with  $t < t'$ , we control for the intermediate events, so-called *mediators*  $\mathbf{M} = X_{t+1:t'-1}$  by simulating a Controlled Direct Effect (CDE) [113] of  $E_t$  on  $E_{t'}$ .

**Definition 24** (Randomized Interventional Do-Operator). *Let  $\mathbf{M} = X_{t+1:t'-1}$  be the set of intermediate events between cause  $E_t$  and effect  $E_{t'}$ . We define the intervention  $do(\mathbf{M} \sim Q)$  as the expectation over counterfactual realizations sampled from a proposal  $Q$  (e.g., Uniform over  $|\mathcal{X}|$ ) and average this effect for  $N$  particles  $m^{(l)}$  as with the Monte Carlo estimation (Eq. 8.6) such as:*

$$\begin{aligned} P(E_{t'} | do(\mathbf{M} \sim Q), X_{<t}) &\triangleq \mathbb{E}_{\mathbf{M} \sim Q} [P(E_{t'} | \mathbf{M}, X_{<t})] \\ &\approx \frac{1}{N} \sum_{l=1}^N P(E_{t'} | \mathbf{m}^{(l)}, X_{<t}) \end{aligned} \tag{8.14}$$

**Remark 5.** *This effectively marginalizes out the intermediate causal mechanisms only if we assume that there are no hidden confounders (Assumption 3).*

Using the previous definition, we modify Eq. 8.3 to detect lagged information gain from  $E_t$  to  $E_{t'}$ , namely  $I_G^L$ :

**Definition 25** (Lagged Information Gain). Let  $E_t$  be the cause,  $E_{t'}$  be the effect ( $t < t'$ ) and  $\mathbf{M} = X_{t+1:t'-1}$  the set of intermediate events. The Lagged Information Gain  $I_G^{\mathcal{L}}$  is defined:

$$I_G^{\mathcal{L}}(E_{t'}; e_t | x_{<t}) \triangleq D_{\text{KL}}\left(P(E_{t'} | \text{do}(\mathbf{M} \sim Q), x_{<t}) \parallel P(E_{t'} | \text{do}(\mathbf{M} \sim Q), e_t, x_{<t})\right) \quad (8.15)$$

Under the do-operator, conditioning on the realized  $e_t$  is still admissible since the intervention affects  $M$  only (the intermediates).

## 8.5 Algorithm: Parallel Causal Discovery

TRACE uses a series of parallelizable tensor operations on GPUs. Instead of iterating sequentially,  $I_G^{\mathcal{L}}$  is evaluated for all candidate edges simultaneously. We start from an unknown  $\mathcal{G}_{un}$  representing the single stream and iteratively remove edges based on the CMI estimation  $\hat{I}_N$  to obtain  $\mathcal{G}_{t,s}$ . An overview of the process can be found in Fig. 8.3.

We introduce Theorem 3, which guarantees the soundness of our algorithm when returning the strong instance-time causal graph.

**Theorem 3** (Soundness of TRACE for the Instance-Time Causal Graph). Let  $\mathcal{G}_{t,s}$  be the Instance-Time Causal Graph of a sequence  $s$  generated by a stochastic process. Assume the underlying distribution  $P$  is  $\epsilon$ -Strongly Faithful to  $\mathcal{G}_{t,s}$  (Def. 23) and that TRACE uses a consistent CMI estimator  $\hat{I}_N$  with threshold  $\tau_\epsilon$  (Lemma 9) and the corresponding  $\epsilon$ -Oracle Model  $P_\theta$ . Then, under Causal Sufficiency (A7) and Temporal Precedence (A6), it recovers the correct Instance-Time Causal Graph  $\mathcal{G}_{t,s}$  asymptotically as  $N \rightarrow \infty$ .

(Proof Sketch) By induction, we show that for each sequential step  $t$ , we can recover the potential causes  $E_{<t}$  of the effect event  $E_t$  using the consistent CMI estimator (Prop. 1)

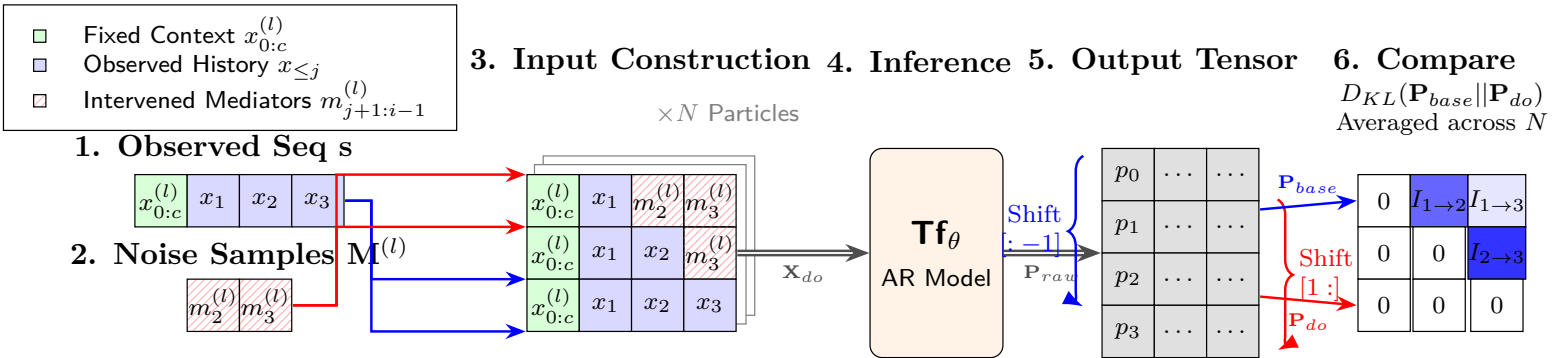


**Figure 8.3: Overview of TRACE Parallel CI-tests.** We construct a single broadcasted tensor  $\mathbf{X}_{do}$  where each row  $j$  incrementally fixes the history  $x_{<j}$  while randomizing the future (staircase pattern). The model processes this tensor in parallel to produce raw probabilities  $\mathbf{P}_{raw}$  (grey). We then compute the Causal Mutual Information by comparing adjacent rows: the distribution at row  $j - 1$  serves as the baseline ( $\mathbf{P}_{base}$ , blue) for the intervention at row  $j$  ( $\mathbf{P}_{do}$ , red).

which generates a  $\epsilon$ -Strong Faithful CI-test (Lemma 9) and control for lagged effects using (Def. 25). By temporal precedence (A6) and causal sufficiency (A7), we can conclude that no other events will affect the effect event  $E_t$  and thus verify the heredity.

*Proof.* We proceed by induction on the time index  $t \in \{1, \dots, L\}$  knowing temporal precedence (Assumption 1).

**Goal:** We show that for every  $t$ , the estimated parent set  $\widehat{Pa}(x_t)$  is exactly the true parent set  $Pa(x_t)$  in the instance-time causal graph  $\mathcal{G}_{t,s}$ .

**Base Case ( $t = 1$ ):** Consider the first event  $x_1$ . By the temporal precedence and causal sufficiency (Assumption 3),  $x_1$  has no ancestors in the observed sequence. Thus, the true parent set is  $Pa(x_1) = \emptyset$ . The TRACE algorithm evaluates candidates  $e_{1-k}$  for  $k \geq 1$ . Since no such events exist in the sequence, the candidate set is empty. TRACE returns  $\widehat{Pa}(E_1) = \emptyset$ . Thus,  $\widehat{Pa}(E_1) = Pa(E_1)$ .

**Heredity:** Assume that for all time steps  $j < t$ , the algorithm has correctly identified the local structure (though note that the decision for  $e_t$  depends only on the history  $x_{<t}$ , not on previous graph decisions). We consider the event  $E_t$ . With the full variant, the algorithm iterates through all valid past events  $E_{t-k} \in E_{<t}$  as candidate parents. For each candidate, we apply the decision rule based on the estimator  $\hat{I}_N$  (Def. 23) assuming that no hidden confounders alters the CI-tests (Assumption 3):

- **Case 1:  $E_{t-k}$  is a True Parent ( $E_{t-k} \in Pa(E_t)$ ).** By the  $\epsilon$ -Strong Faithfulness assumption (Def. 23), the true conditional mutual information satisfies  $I > 2\tau_\epsilon$ . By Lemma 9 (Identifiability), this ensures that the estimator satisfies  $\hat{I}_N > \tau_\epsilon$  asymptotically. Consequently, TRACE **accepts** the edge.
- **Case 2:  $E_{t-k}$  is Not a Parent ( $E_{t-k} \notin Pa(E_t)$ ).** By the Causal Markov Condition, conditioned on the history  $x_{<t}$  (which contains the true parents),  $E_t$  is independent of non-descendants. Thus,  $I(E_t; E_{t-k} | X_{<t}) = 0$ . By Lemma 9, the estimator is bounded by the noise floor:  $\hat{I}_N \leq \tau_\epsilon$ . Consequently, TRACE **rejects** the edge.

Since the algorithm makes the correct decision for every candidate  $E_{t-k}$  individually, the resulting set  $\widehat{Pa}(E_t)$  is identical to  $Pa(E_t)$ .

**Conclusion:** By induction,  $\widehat{Pa}(E_t) = Pa(E_t)$  for all  $t = 1, \dots, L$ . Since the graph  $\mathcal{G}_{t,s}$  is defined by the union of these parent sets, TRACE recovers  $\mathcal{G}_{t,s}$  exactly. Consequently, by Def. 22, TRACE recovers the instance summary causal graph  $\mathcal{G}_s$ .  $\square$

### 8.5.1 Scalability of TRACE

To parallelize the Monte-Carlo estimation (Eq. 8.4) and counterfactual sampling (Eq. 8.15) we avoid computing the CMI for the full trajectory  $x_{0:t-1}$  but a truncated version, called *context* as

$$x_{<t} \approx x_{0:c} \text{ for } c < t \text{ and } 0 < c \ll L$$

We argue that truncating the history in this way enables parallelized CI-tests on GPUs. In all experiments, we set  $c = \max(0.1L, 20)$ . Although it might break Markovianity for

long sequence, empirical results show robustness to this truncation. We provide ablation to unseen sequence lengths during training and show our method to be robust to high delayed effects in Fig 8.5.

**Sparse Approximation** For each time step  $t$ , we must perform  $t$  CI-tests (one for every potential lag per step). For a sequence of length  $L$ , the total number of CI-tests is given by  $\sum_{t=1}^L t = \frac{L(L+1)}{2}$  which grows quadratically with the sequence length. As a result, even on multiple GPUs, inference becomes computationally intractable.

To solve this, we propose a *sparse variant* for which we bound the lagged effects of previous events on future events up to a memory  $m$  (Assumption 9). Thus the DGP  $\{X_t\}$  becomes an  $m$ -order Markov chain. With  $m \ll L$ , TRACE scales linearly with the sequence length  $L$ . The memory complexity transitions from:

$$\mathcal{O}(N \cdot (L - c) \cdot L \cdot |\mathcal{X}|) \xrightarrow{\text{Bounded Memory}} \mathcal{O}(N \cdot m \cdot L \cdot |\mathcal{X}|)$$

## 8.6 Experiments

We evaluate TRACE on synthetic linear Structural Causal Models (SCMs) and real-world vehicle logs. All baselines utilize the same frozen backbone to evaluate the contribution of the inference mechanism. TRACE is implemented in Python. A more complete protocol description can be found in Appendix B.3.2 as well as additional ablations.

### 8.6.1 Settings

**Synthetic Linear-SCM** We validate TRACE on sequences generated by linear SCMs with controllable memory  $m$ , sequence length  $L$ , and vocabulary size  $|\mathcal{X}|$ . Our evaluation proceeds in two phases: (1) We train a standard AR LM (LLaMA architecture [146]) on the SCM and validate the training by monitoring the oracle scores  $\hat{\epsilon}$  (Eq. B.6, normalized  $\epsilon$ ) (2) We then apply TRACE to recover the summary causal graph of each single observation. To evaluate performance, we perform atomic interventions by uniformly randomizing  $E_t$  and measuring the average KL divergence over 10 counterfactual between post-intervention and observational distributions of  $E_{t'}$ . If the divergence is above  $\tau > 0.05$ , an edge  $E_t \rightarrow E_{t'}$  exists in  $\mathcal{G}_{t,s}$ . We then report the Precision, Recall, and Structural Hamming Distance (SHD) against this ground truth.

We benchmark TRACE against four distinct baseline types:

- **Neural Granger:** A Granger-causal discovery method that uses the same AR Model as TRACE but computes the difference in probability rather than the CMI to detect causality.
- **Attention:** We train a BERT [26] model on the same SCM with the same model capacity and training steps as  $\text{Tf}_\theta$  and extract the attention scores at the deepest layer. A threshold  $\tau = 0.02$  is applied to get the adjacency matrix.
- **Saliency (Input  $\times$  Gradient):** A local sensitivity baseline that estimates feature importance by computing the gradient of the target token’s log-probability with respect to the input embeddings [137].

- **Shapley Value Sampling:** An axiomatic attribution method rooted in cooperative game theory [82]. Shapley values estimate the *average marginal contribution* of a token  $x_t$  to the prediction of  $x_\nu$  by sampling permutations of the input history.
- **Naive baselines:** A random guesser that predicts edges ( $X_j \rightarrow X_i$ ) with a fixed probability  $\rho = 0.01$  and a frequency baseline that assumes the top- $k$  most frequent event types are universal causes for all other events. These tests reveal whether the task is non-trivial.

### 8.6.2 Comparative Analysis

As detailed in Table 8.2, TRACE establishes state-of-the-art performance for causal discovery on discrete sequences generated from single streams and outperforms the strongest baseline by over 0.20 F1 Score. While attention scores alone fail to distinguish correlation from causation (F1 0.50), the Neural Granger baseline achieves a respectable F1 of 0.69 but suffers from high variance (SHD  $100.2 \pm 14.6$ ). Saliency methods, traditional in NLP, also fail to distinguish causal links between events, especially with poor precision 0.51. This disparity highlights a critical insight: **measuring the CMI is a far more robust signal of causality** than monitoring the probability fluctuation of a single target token (Granger) or relying on metrics that are not anchored in causal discovery (Saliency, attention scores).

Method	SHD ( $\downarrow$ )	F1 ( $\uparrow$ )	Precision ( $\uparrow$ )
Random	218.8 $\pm$ 3.2	0.01 $\pm$ 0.00	0.04 $\pm$ 0.01
Frequency	723.0 $\pm$ 6.7	0.09 $\pm$ 0.00	0.06 $\pm$ 0.00
Attention (BERT)	321.0 $\pm$ 15	0.50 $\pm$ 0.01	0.35 $\pm$ 0.01
Saliency (Input x Gradient LLaMA)	160.2 $\pm$ 6.55	0.67 $\pm$ 0.01	0.51 $\pm$ 0.01
Shapley Value Sampling (LLaMA)	148.0 $\pm$ 5.09	0.60 $\pm$ 0.01	0.55 $\pm$ 0.01
Neural Granger (LLaMA)	100.2 $\pm$ 14.6	0.69 $\pm$ 0.04	0.71 $\pm$ 0.04
<b>TRACE (LLaMA)</b>	<b>28.6<math>\pm</math>2.8</b>	<b>0.91<math>\pm</math>0.01</b>	<b>0.89<math>\pm</math>0.01</b>

**Table 8.2: Identifiability Comparison.** Comparison of causal discovery performance on synthetic SCMs with  $|\mathcal{X}| = 1000$ ,  $L = 64$ ,  $\epsilon = 0.05$ ,  $\tau = 3.10^{-5}$ ,  $N = 128$ . **TRACE** significantly outperforms local (Saliency) and global (Granger/Shapley) baselines, achieving over 20 points higher F1 while maintaining high precision. Results across 10 runs are reported.

### 8.6.3 Scalability and Robustness Analysis

**Breaking the Curse of Dimensionality** Standard causal discovery algorithms suffer from combinatorial explosions when the variable count or state space increases. In Fig. 8.4, we challenge TRACE with massive vocabularies to validate its scalability to massive event types. Remarkably, we observe that **discovery performance is invari-**

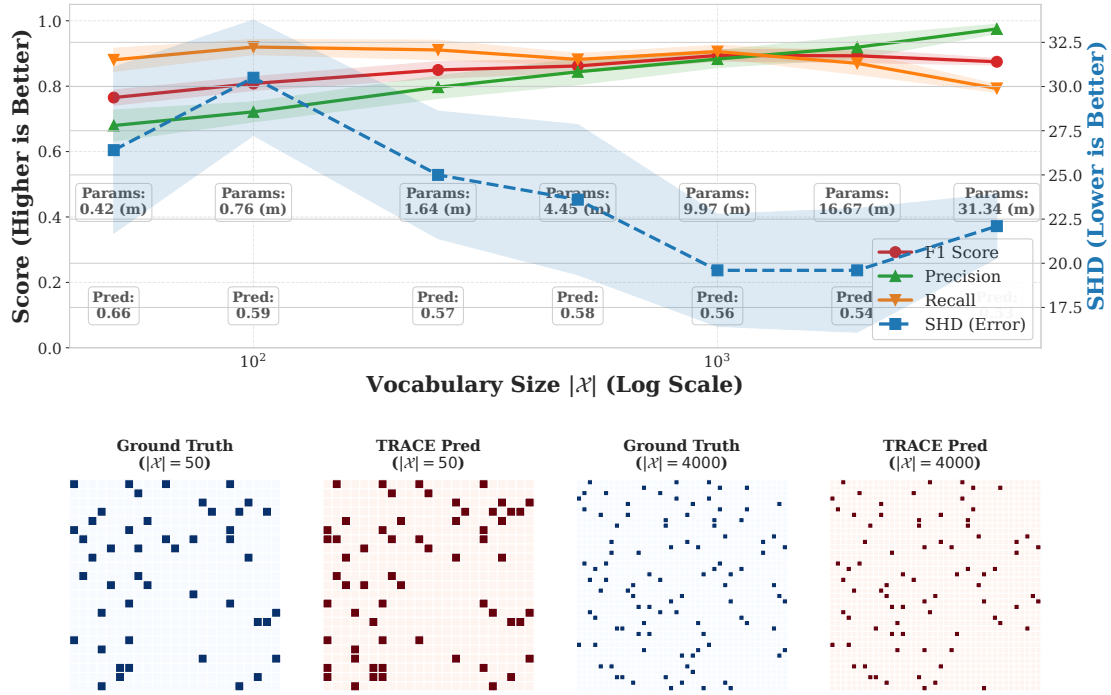


**Figure 8.4: Scalability to High-Dimensional Event Spaces.** Evaluation of structural identifiability across exponentially growing vocabulary sizes. **Top:** Evolution of discovery metrics. TRACE exhibits **performance invariance**, maintaining F1  $\approx 0.81$  even as the combinatorial search space explodes. **Bottom:** Visual examples of recovered summary graphs  $\mathcal{G}_s$  at scale. Shannon redundancy as  $(Pred = 1 - H(P)/H_{max})$  confirm that TRACE succeeds even in high-entropy regimes. ( $\hat{\epsilon} = 0.01, L = 64, N = 64, \tau = 10^{-4}$ ).

**ant to the vocabulary size  $|\mathcal{X}|$ .** The F1 score remains stable at  $\approx 0.81$  even as the search space grows exponentially and the underlying SCM entropy increases. This confirms a key advantage of our approach: by leveraging a pre-trained AR model, TRACE enables causal discovery over massive event vocabularies at scales that were infeasible before.

**Unseen Sequence Lengths** We evaluate TRACE’s ability to scale to unseen sequence length during training of the AR Model, as well as the maximum GPU memory consumption for the *Full* and the *Sparse* variant, which computes up to  $m$  lagged effects per event. As shown in Fig. 8.5 (b), the sparse variant of TRACE achieves linear memory scaling, whereas the full variant exhibits quadratic memory growth. For the classification metrics, we observe a quick degradation in Recall as the sequence length exceeds the training window. Therefore, the model’s ability to identify all causal links diminishes as the temporal context becomes increasingly out-of-distribution. Precision remains remarkably high and stable ( $\approx 0.95$ ) across all tested lengths. This suggests that the

## 8 Sample-Level Event-to-Event Causal Discovery

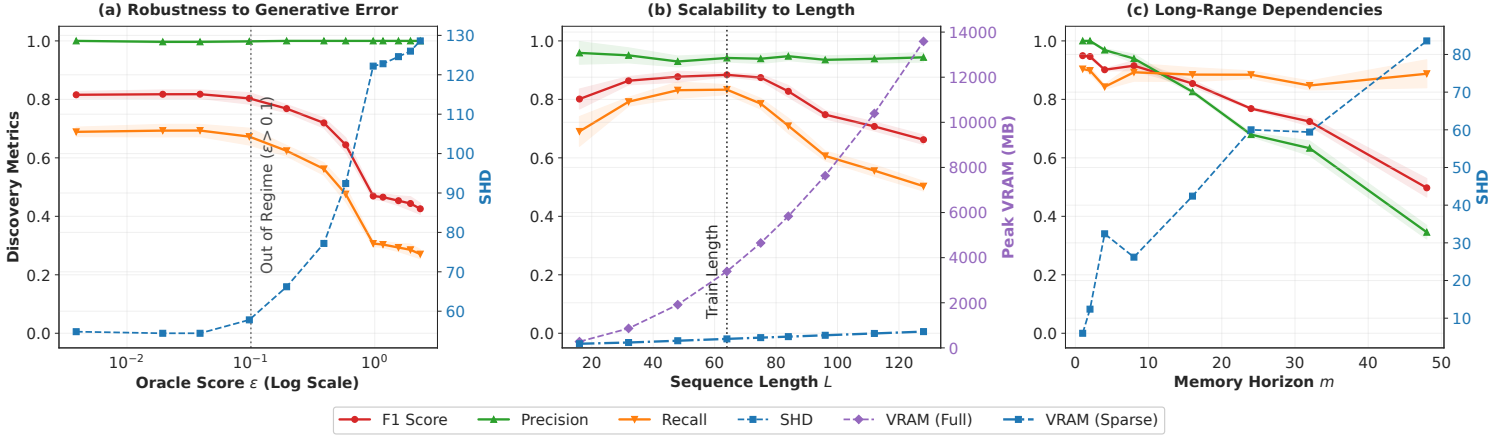


**Figure 8.5: Robustness and Scalability Analysis** ( $|\mathcal{X}| = 1000, N = 128, \tau = 10^{-4}, L = 64$ ). Evolution of causal discovery performance (F1, Precision, Recall, SHD). **(a) Robustness to Generative Error:** Performance as a function of the model’s oracle score  $\epsilon$ . TRACE exhibits a phase transition, recovering structure even for imperfect models ( $\epsilon < 0.1$ ) and maintaining high Precision even as fidelity degrades. **(b) Scalability to Length:** Performance and GPU memory usage vs. sequence length  $L$ . The **Sparse** variant demonstrates linear memory scaling ( $O(mL)$ ), enabling inference on sequences far exceeding the training length ( $L = 64$ ), whereas the Full variant scales quadratically. **(c) Long-Range Dependencies:** Robustness to increasing delayed-effects  $m$ . TRACE maintains  $F1 > 0.8$  even as dependencies span one third of the sequence ( $m = 20$ ), confirming the method’s ability to capture distant causal mechanisms.

model becomes more conservative with longer sequences. This **conservative failure mode** is highly desirable and further supported by Fig. 8.5 (a).

**Identifiability Precedes Convergence.** A central question is whether the AR model must be perfect ( $\epsilon \rightarrow 0$ ) to recover causal structure. Fig. 8.5 (a) reveals a critical finding: **exact convergence is not a necessary condition for identifiability**. We observe a distinct phase transition where the coarse-grained causal graph is recovered early in the training dynamics ( $\epsilon \approx 0.1$ ), before the model masters fine-grained transition probabilities. TRACE exhibits a **conservative failure mode**. As approximation error  $\epsilon$  increases, the model defaults to “blindness” (lower Recall) rather than “hallucination” (lower Precision), maintaining near-perfect precision ( $> 0.95$ ) even in high-entropy regimes. This suggests that model uncertainty manifests as a failure to detect weak signals rather than the generation of false positives—a desirable property for safety-critical applications.

**Deep Temporal Dependencies.** In Fig. 8.5 (c), we stress-test the method by extending the memory horizon of the underlying SCM up to  $m = 48$ . TRACE maintains high stability ( $F1 > 0.80$ ) up to  $m = 20$ , confirming that our parallelized intervention

mechanism effectively **captures long-range dependencies**. While precision naturally softens as the number of events behind detected increases, hence necessitating a bigger threshold  $\tau$ .

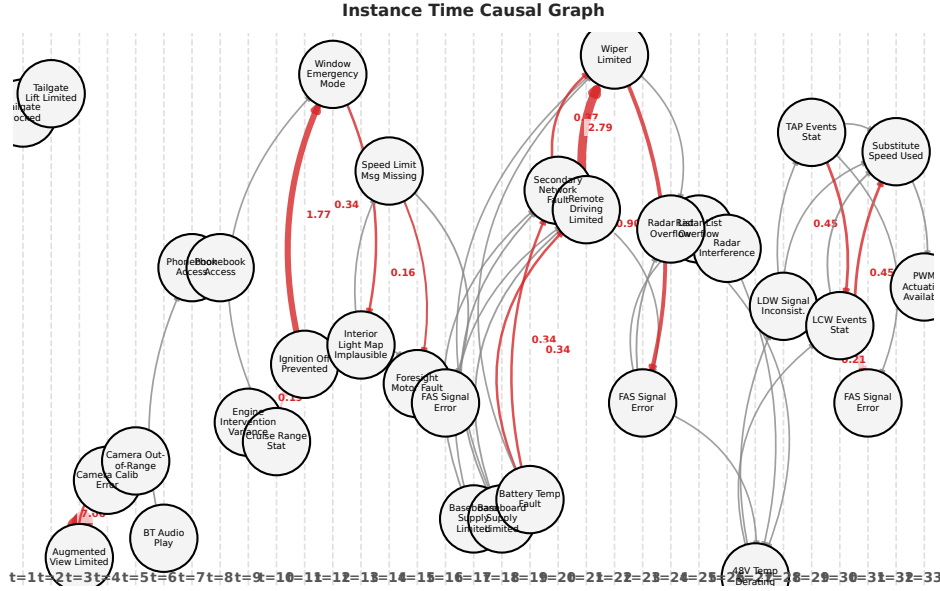


**Figure 8.6: Instance-Time Causal Graph.** Temporal evolution of a diagnostic defect cascade in a vehicle ( $|\mathcal{X}| \approx 29, 100$ ). TRACE effectively captures causal relationships, revealing distinct **error clusters** at different time steps (e.g., initial sensor failures at  $t = 3$  triggering mechanical faults at  $t = 12$ , battery at issue  $t = 17$ ). This enables actionable root-cause analysis by isolating the specific onset of a failure mechanism and their strength using the CMI  $\hat{I}_N$

### 8.6.4 Application to Vehicles Diagnostics

To evaluate TRACE, we use the same dataset as in Chapters 6 and 7. The training loss reported of  $Tf_x$  is  $\mathcal{L}_{AR} = 1.91$  nats. We apply TRACE to analyze complex electrical cascades, specifically focusing on battery and sensor degradation scenarios as shown in Fig. 8.6 with  $\mathcal{G}_{t,s}$  and in Fig. B.8 with  $\mathcal{G}_s$ . In standard approaches, these events are often collapsed into a static correlation graph, obscuring the order of operations and their causal relationship.

## 8.7 Limitations

We now include a discussion regarding the main assumptions taken in this chapter.

### 8.7.1 Causal Sufficiency

A fundamental assumption in causal discovery is *Causal Sufficiency* (Assumption 3)—the premise that no unobserved confounders influence the system. Since TRACE relies on pre-trained backbones which may have learned from noisy or incomplete data, we empirically evaluate the robustness of TRACE under controlled violations of causal sufficiency, focusing on two realistic forms of hidden confounding.

**Measurement Error (Noise Injection).** In Fig. 8.7(a), we simulate measurement error by randomly replacing valid tokens in the history with noise ( $P_{noise}$ ). While Recall naturally degrades as the true causal parents are obscured, **Precision remains high** ( $> 0.8$ ) even when 40% of the context is corrupted. This confirms that TRACE does not hallucinate false edges from noisy inputs; if the causal signal  $X \rightarrow Y$  is destroyed by measurement error, the model assigns  $CMI \approx 0$  rather than hallucinating a spurious link.

**Missing Intermediaries (Temporal Drops).** In the same Fig. 8.7(b), we simulate missing data by randomly dropping time steps, effectively hiding intermediate nodes in the causal chain ( $X \rightarrow Z_{hidden} \rightarrow Y$ ). This is a more critical scenario where the Markov conditioning sets are incomplete as intermediate causal nodes are unobserved. We observe that TRACE is robust to moderate data loss ( $P_{drop} < 0.2$ ).

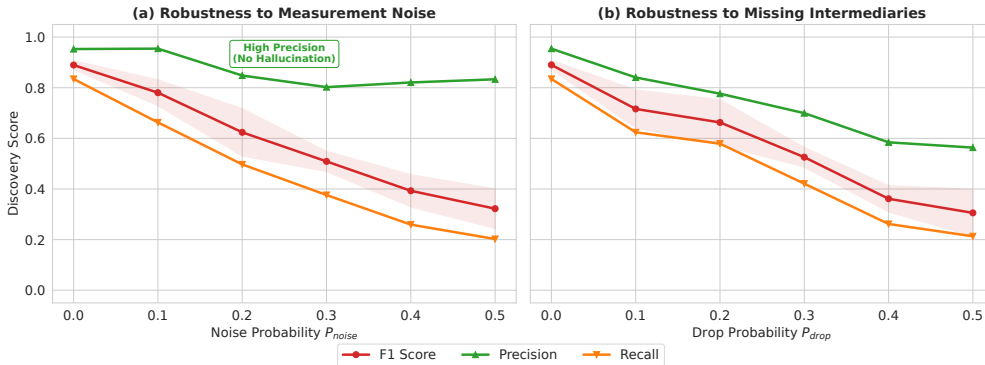


**Figure 8.7: Robustness to Hidden Confounding.** Evaluation of TRACE under violations of causal sufficiency. **(a)** Measurement Error: Random noise is injected into the context. Precision stays high, indicating resistance to hallucination. **(b)** Temporal Drops: Time steps are randomly deleted, thus conditioning sets are broken. TRACE still recovers structure despite missing intermediaries but the discovery scores quickly decrease.

### 8.7.2 Temporal Precedence & Instantaneous Effects

TRACE assumes that causal influence respects temporal precedence, which means observations are perfectly recorded over time and therefore does not model instantaneous

causal effects between events occurring at the same time index. This assumption is standard in sequential causal discovery and ensures that the recovered causal graph is acyclic and identifiable in the single observed sequence setting.

From a theoretical standpoint, instantaneous effects are not identifiable from a single observed trajectory without additional parametric assumptions, repeated samples, or access to interventions. In practice, apparent simultaneity often *arises from time discretization*, logging resolution, or batching effects. TRACE interprets such cases *through the earliest observable temporal ordering*, yielding a conservative but identifiable causal structure. As a result, the recovered summary graph captures directed causal influence with positive temporal delay, rather than true simultaneity.

### 8.7.3 Consistency Through Time

TRACE operates in a one-shot regime, where causal structure must be inferred from a single observed trajectory rather than from repeated i.i.d. samples *during inference*. To make this statistically meaningful, we assume *consistency through time*: the causal mechanisms governing the generation of events are invariant across time indices. In other words, causal directionality does not reverse over time. For instance, if  $A \rightarrow B$ , it is subsequently assumed that  $B \not\rightarrow A$ .

This assumption is strictly weaker than stationarity [6]. While the marginal distribution of  $\{X_t\}$  may vary over time, the underlying causal dependencies—encoded by the directed edges of the instance-time causal graph remain stable. This form of causal invariance is standard in sequential settings and underlies the validity of summary causal graphs that collapse time-indexed relations into event-to-event dependencies (Def. 22).

### 8.7.4 Amortization

TRACE leverages amortized causal discovery, shifting the computational burden to the self-supervised pretraining of an autoregressive model. However, because the base entropy of the true data-generating process is rarely known in practice, the generative error  $\epsilon$  cannot be directly deduced from the cross-entropy loss. This makes identifying the optimal model capacity and training duration challenging; as a practical heuristic, we recommend slight over-parameterization and extended training. Furthermore, while TRACE achieves linear scaling during inference with respect to sequence length and vocabulary size ( $|\mathcal{X}|$ ), this efficiency does not account for the prerequisite pretraining phase, which scales non-linearly with  $|\mathcal{X}|$ .

## 8.8 Summary

We presented TRACE, a framework for single-sequence causal discovery in high-dimensional discrete event streams. By repurposing a pretrained autoregressive model as a conditional density estimator, TRACE recovers the instance-time and summary causal graphs without any task-specific retraining, scaling *linearly* with the event vocabulary size, a regime that renders classical constraint-based algorithms intractable.

Our comparative analysis demonstrates that measuring causal influence via conditional mutual information (CMI) is fundamentally more discriminative than attribution-based alternatives: TRACE achieves an F1 score of  $0.91 \pm 0.01$ , outperforming the strongest attribution baseline (Shapley value sampling, 0.60) by more than 30 points and Neural Granger causality (0.69) by over 20 points. Critically, this gap is not merely a matter of model capacity, all methods share the same pretrained backbone, but reflects a fundamental distinction between *correlation* (captured by saliency and Granger-type scores) and *causal dependence* (captured by the CMI under controlled interventions). This result provides direct empirical evidence that causal structure learning is necessary for reliable discovery in event sequences, and cannot be replaced by post-hoc attribution.

On the theoretical side, Theorem 2 establishes a finite bound on the gap between the estimated CMI  $\hat{I}_N$  and the true causal strength  $I$ , showing that this gap is governed exclusively by the model’s cross-entropy approximation error  $\epsilon$ . Lemma 9 then guarantees that the instance-time causal graph is identifiable with probability 1 as  $N \rightarrow \infty$ , provided the true causal signal exceeds the noise floor  $\tau_\epsilon$  induced by  $\epsilon$ , a condition we term  $\epsilon$ -Strong Faithfulness. Taken together, these results confirm that structural identifiability is achievable under imperfect density estimation, and that minimizing the pretraining cross-entropy loss directly tightens the causal identification bound. TRACE thus represents a principled, GPU-scalable step toward causal discovery in real-world, high-dimensional event streams, where both the scale and the noise level of data preclude oracle-level approximations.

## 8.9 Outlook

The discovery frameworks presented in this part OSCAR, CARGO, and TRACE collectively establish a scalable pipeline for uncovering causal structures in high-dimensional single-event streams. Several frontiers nonetheless remain open.

**Toward MDL-grounded Causal Scoring.** A conceptually significant direction concerns the theoretical foundations of the causal scoring function underlying TRACE. At its core, TRACE decides whether event  $E_t$  causes  $E_{t'}$  by measuring how much knowing  $E_t$  reduces uncertainty about  $E_{t'}$ , given the observed history—a quantity formalized as the conditional mutual information (CMI). This choice is empirically effective, yet it can be given a deeper justification through the lens of the *Minimum Description Length* (MDL) principle [123, 46].

MDL is a general principle of model selection grounded in information theory: given a dataset, the best explanation is the one that leads to the shortest description of the data [46]. Concretely, one compares two descriptions of the same observations, a model  $M$  and the data encoded *given* that model and selecting the model minimizing their combined length  $L(M) + L(\mathcal{D} | M)$ . Applied to causal discovery, this principle instantiates *causal minimality*: the true causal graph is the simplest one that fully accounts for the observed dependencies, and any additional edge would only increase the total description length without improving the fit. MDL-based methods have been successfully

applied to causal inference in discrete data [24] and, most closely related to the present setting, to learning Granger-causal networks in TPP [66].

TRACE’s approximation error bound (Theorem 2) reveals a direct structural parallel with these ideas. Cross-entropy *is* a compression objective: a model achieving a lower cross-entropy provides a shorter expected code for the data under Shannon’s source-coding theorem [23]. Minimizing  $\epsilon$  during pretraining therefore simultaneously tightens the noise floor  $\tau_\epsilon$ , sharpens the identifiability threshold, and, in the language of MDL, corresponds to finding a more compact two-part description of the event sequence. Formalizing this connection constitutes a promising theoretical direction.

**Unified Event-to-Event and Events-to-Outcome Discovery.** A unified framework supporting simultaneous recovery of both event-to-event and events-to-outcome causal dependencies within a single sequence would provide a more complete picture of system dynamics. As indicated by the open cell in Table 1.1, the population-level counterpart of TRACE remains an open problem, requiring new aggregation strategies and, likely, explicit acyclicity constraints to reconcile instance-time graphs across sequences.

**From Causal Graphs to Actionable Rules.** Despite providing a robust causal backbone, the numerical and graphical representations produced by TRACE remain a silent language for the domain expert. Causal graphs identify statistical dependencies but do not inherently capture the symbolic logic—such as Boolean combinations of events— or the contextual nuance required for formal diagnostic standards. There remains a substantial gap between numerical causal evidence and the actionable rules that practitioners can validate and trust. Part III closes this methodological arc. By transitioning from causal discovery to automated reasoning, it embeds the causal structures recovered by OSCAR, CARGO within a multi-agent framework powered by (LLMs). As a result, the system synthesizes interpretable Boolean rules alongside natural language explanations, effectively transforming raw causal evidence into human-interpretable diagnostic expertise.



## **Part III**

# **From Causal Discovery to Automated Reasoning**



## 9 Multi-Agent Causal Reasoning System for Error Pattern Automation

While Part I focused on learning event representations and Part II on uncovering causal dependencies, Part III explores how these causal insights can be operationalized. It is based on the following contribution:

### **Neuro-Symbolic Rule Discovery: Empowering LLMs with Causality for Vehicle Diagnostics.**

[92] Hugo Math, Julian Lorenz and Rainer Lienhart. International Conference on Learning Representations (ICLR) Workshop on Logical Reasoning of Large Language Models, April 2026.

LLMs and overall agentic systems have demonstrated the capacity to integrate heterogeneous information sources for structured reasoning tasks. From this perspective, we introduce CAREP: (Causal Automated Reasoning for Error Patterns), a multi-agent reasoning system that leverages the causal structures discovered by OSCAR and CARGO to generate interpretable EP rules with their natural language explanation automatically. CAREP integrates three coordinated agents: (1) a *causal discovery agent* that refines DTC-EP relationships using the underlying causal graphs, (2) a *contextual information agent* that enriches reasoning with semantic and metadata knowledge, and (3) an *orchestrator agent* that synthesizes candidate Boolean rules and produces transparent reasoning traces.

We evaluated both the capacity of LLMs and CAREP to generate accurate Boolean rules (i.e., correct DTCs) and the accuracy of those rules based on their truth tables relative to the ground truth. CAREP demonstrates the ability to automatically infer accurate and human-readable EP rules, outperforming purely language-model-based baselines while providing interpretability. This framework thus completes the methodological trajectory of the thesis, transforming predictive modeling into causal discovery and finally into automated causal reasoning.

### 9.1 Introduction

Beyond causality, automation requires interpretability. Presenting unexplained rules is risky in safety-critical domains such as the automotive industry or in medical data. Large Language Models (LLMs) [107, 25, 146] have recently demonstrated emergent capabilities in planning, explanation, abduction, reasoning, and in-context learning [27, 170]. Especially when using Chain-of-Thought [154] (CoT) to guide them through step-by-step reasoning processes. Since CoT is not grounded in the external world, it is

limited in its ability to reason reactively or update its knowledge, thereby propagating factual hallucinations and errors throughout the reasoning process. ReAct [163] goes further by creating a *reason to act* and *act to reason* framework where the LLM has access to external environments (e.g., Wikipedia) to incorporate additional information into the reasoning.

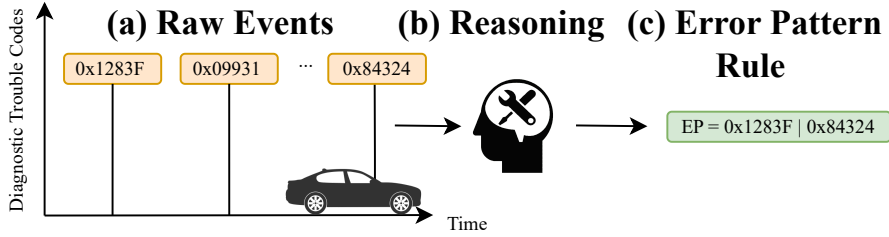


**Figure 9.1: Illustration of Error Pattern Automation in Modern Vehicles.** (a) A vehicle with an unknown defect generates a sequence of Diagnostic Trouble Codes (DTCs) over time. (b) A domain expert analyzes the DTCs and the vehicle’s metadata (e.g., model, descriptions). (c) Provide a Boolean rule to identify this error pattern.

Through retrieval-augmented generation (RAG), external memory access, and context injection [74], LLMs can use raw text as references to improve question answering. Importantly, although causal graphs provide a theoretically grounded, valuable source of information, they alone rarely yield a complete, interpretable rule. A DTC may be discovered as a strong causal parent of an EP, but paired with the textual metadata can reveal whether the DTC reflects a root cause, a downstream effect, or an irrelevant side-symptom. LLMs offer a practical computational mechanism for integrating these heterogeneous evidence sources, resolving contradictions, and translating causal signals into symbolic form through the Boolean expression of an EP.

Nevertheless, a single model is often insufficient to handle the diverse subtasks involved in automation. The growing paradigm of *agentic systems* [128, 176, 61] highlights how specialized agents, each with distinct capabilities, can collaborate through structured dialogues or planning loops. This opens the door to human-interpretable, automated causal reasoning in complex industrial pipelines [32]. For example, often referred to as causal machine learning (CML), it offers a more nuanced and interpretable approach to black box models and has found interesting applications [48]. That is, for LLMs, as noted by [95], they are sensitive and fragile without semantic or neuro-symbolic knowledge. For tasks requiring the selection of correct tokens, accuracy decreases exponentially with the number of tokens, making them unsuitable for high-dimensional event sequences alone.

## 9.2 Related Work

### 9.2.1 Multi-Agent Fault Diagnosis

The application of multi-agent systems for industrial diagnostics and failure analysis has become a prominent research area. [98] established an early framework using an agent-based inference engine to provide efficient and reliable assistance for vehicle failure diagnosis. In the domain of autonomous safety, [86] proposed an explainable system designed to interpret complex vehicle accidents, emphasizing the need for transparent decision-making. More recently, the scope of agentic systems has expanded to the manufacturing sector. [111] introduced an agentic AI framework for "self-healing" production lines capable of autonomous root cause analysis and fault correction. While these works share the goal of automating diagnostics through agents, CAREP distinguishes itself by addressing four critical challenges:

- **Extreme Cardinality:** CAREP is specifically designed for large-scale event streams containing over 29,100 unique DTC types, a scale where traditional inference engines, causal inference and discovery typically struggle.
- **Causal Integration:** It integrates a dedicated causal discovery agent (utilizing OSCAR and CARGO) to filter irrelevant events before reasoning begins.
- **Metadata Integration:** Through embedding models, the metadata is integrated as references and used by a contextual information agent.
- **Symbolic Synthesis:** Unlike systems that provide static alerts, CAREP automates the synthesis of symbolic Boolean rules (Error Patterns) alongside natural language reasoning traces, effectively translating raw statistical evidence into actionable human-readable expertise.

### 9.2.2 Error Pattern Rule Automation

The creation of EPs (Fig. 9.1) has emerged as production and vehicle manufacturing have become increasingly complex. As demonstrated in the foundations, to identify new defects, experts analyze the diagnostic trouble code (DTC) sequence for each vehicle. Intuitively, this reasoning task is not trivial. Experts must draw on their prior observations and knowledge of specific DTCs that may cause each EP. That is where the Boolean operators are useful. They allow us to construct different rules to characterize precise EPs. It sometimes requires the absence of certain DTCs (! NOT) to separate overlapping EPs. Or the presence of multiple DTCs at the same time (& AND) or a particular culprit (| OR). Therefore, the different operators (&, |, !) involve different statistical perspectives. Intuitively, the ! operator measures inhibitory strength [35], where the likelihood of observing  $y_1$  will be lowered if we observe  $x_{10}$  (Fig 9.1). On the other hand, & and | are more associated with excitatory events that will raise the likelihood of an EP. Knowing only the causes of an EP is not sufficient to elaborate a new rule. It is necessary to have indicators that quantify how DTCs are related to one another and

to EPs. Finally, rules are subject to change and are dynamically updated by a domain expert based on the new incoming data. As a result, automating a rule is a complex, dynamic problem.

### 9.3 Methodology

Let  $\mathcal{D} = \{S_l^1, \dots, S_l^m\}$  be a dataset of multi-labeled sequences. Each label  $y_j$  is defined as a Boolean rule between some events  $\{x_i\}_i, x \in \mathcal{X}$ . Such that if in a sequence  $S_l^{(k)}$ , the Boolean rule is true for some label  $y_j$ , then it is present in  $S_l^{(k)}$ .  $\mathcal{D}$  contains multiple labels with unknown Boolean rules denoted as  $y^{un} \in \mathcal{Y}$ . We aim to find the unknown rule of each label  $y^{un}$  using the observed sequences in  $D$ .

The general architecture of CAREP is shown in Fig. 9.2. The agentic system outputs a reasoning explanation for each estimated error pattern rule. To increase prediction’s plurality, CAREP outputs 5 rules per EP with different levels of confidence (high, medium, low) that are reflected in the provided explanation. Each agent receives a system prompt that specifies their task and uses CoT [154]. The orchestrator is responsible for structuring comprehensive, traceable reasoning for each rule based on the other agents’ outputs. We now examine each component separately.

#### 9.3.1 Causal Discovery

**Population-Level Causal Graphs** We explicitly model the unknown error patterns  $y^{un}$  as the target in the autoregressive classifier  $\text{Tf}_y$ ’s (EPredictor) output logits<sup>1</sup>. This forms a supervised unknown class learning strategy and enables us to extract the posteriors  $P_{\theta_y}(Y = y^{un}|\cdot)$ . To provide new causes for each unknown EPs, we employ OSCAR ( $k = 2.75, N = 64$ ) and CARGO to extract causal relationships from the dataset  $\mathcal{D}$ . As a result, we get as output a collection of DAGs as  $\{\mathcal{G}_j^*\}_j^c$ , representing unknown error pattern aggregated causal relationships, alongside causal indicators.

**Average Causal Effect** We reuse the causal indicator defined in the one-shot phase in Eq. (6.14) as *ACE* (Average Causal Effect). This indicates, on average, how much the DTC increased or decreased the likelihood of an error pattern. We report its expected value as the mean and its standard deviation over the sampled particles  $z^{(l)}$  used in the Monte Carlo estimation of Eq. (6.9):

$$\hat{C}_\mu(Y_j, X_i) \triangleq \frac{1}{N} \sum_{l=1}^N P(Y_j = 1 | X_i = 1, Z = z^{(l)}) - P(Y_j = 1 | Z = z^{(l)}) \quad (9.1)$$

$$\hat{C}_\sigma(Y_j, X_i) \triangleq \sqrt{\frac{1}{N} \sum_{l=1}^N (P(Y_j = 1 | X_i = 1, Z = z^{(l)}) - \hat{C}_\mu(Y_j, X_i))^2} \quad (9.2)$$

<sup>1</sup>The training labels are used but the Boolean rule is generated at inference time.

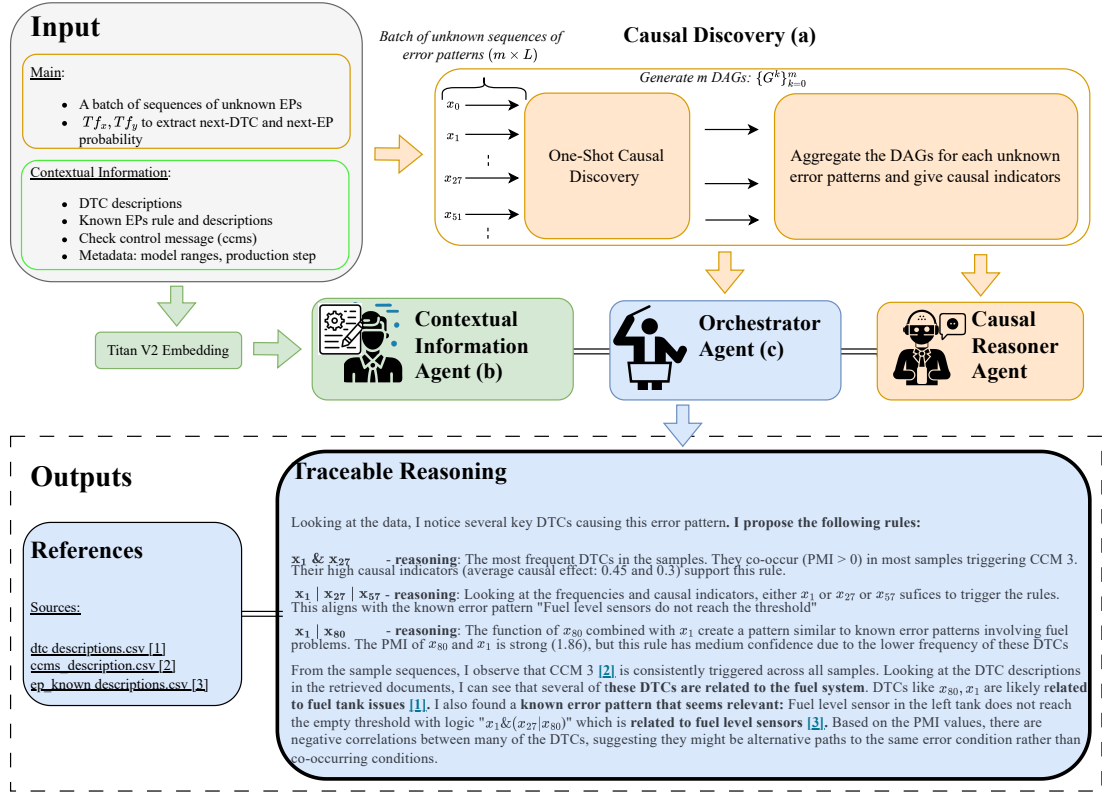


**Figure 9.2: CAREP: A Causal Reasoning Agentic System for Error Pattern Automation.** (a) Represents the causal discovery phase, where we extract candidate DTC causes for the unknown error pattern alongside causal indicators. It then feeds the causal reasoner agent. (b) The descriptions and metadata are extracted through a Titan V2 Embeddings and fed into the contextual information agent. (c) The orchestrator agent manages the two agents and provides traceable reasoning to explain why the unknown error pattern may match these rules.

**Co-occurrence** The different Boolean operators in the defined EP rules in Eq. (2.18) imply different statistical perspectives. In the previous section, we captured the elements in the rule, i.e., the set of DTC causes for a given label. However, we should also provide co-occurrence estimates of event pairs to properly address the OR, AND, and NOT operators. Traditionally, Point-wise Mutual Information (PMI) [23] is used to measure co-occurrence strength. It is defined as:

$$pmi(x_i, x_j) = \log \frac{p(x_i, x_j)}{p(x_i)p(x_j)} \quad (9.3)$$

where  $p(x_i), p(x_j)$  are probability mass functions.

Along with the previous empirical frequency of event  $x_i$  in the set of causes of label  $y_j$ , denoted as  $\hat{\pi}_{i,j}$ , we also compute empirical joint frequencies of pairs of events within the same label-specific graph  $\mathcal{G}_j^*$ . Formally, given a collection of DAGs  $\{(\mathbf{V}_k, E_k)\}_{k=1}^m$ , the

marginal and joint empirical probabilities are estimated as

$$\hat{p}(x_i | y_j) = \frac{1}{m_j} \sum_{k=1}^m \mathbb{1}\{X_i \in \mathbf{V}_k, Y_j \in \mathbf{V}_k\},$$

$$\hat{p}(x_i, x_\ell | y_j) = \frac{1}{m_j} \sum_{k=1}^m \mathbb{1}\{X_i \in \mathbf{V}_k, X_\ell \in \mathbf{V}_k, Y_j \in \mathbf{Y}_k\},$$

where  $m_j$  denotes the number of samples in  $\mathcal{D}$  where label  $Y_j$  is present, and  $\mathbb{1}\{\cdot\}$  is the indicator function.

The PMI between two events  $x_i$  and  $x_\ell$  conditioned on a label  $y_j$  is then given by:

$$\widehat{pmi}(x_i, x_\ell | y_j) = \log \frac{\hat{p}(x_i, x_\ell | y_j)}{\hat{p}(x_i | y_j) \hat{p}(x_\ell | y_j)}. \quad (9.4)$$

Intuitively,  $\widehat{pmi}(x_i, x_\ell | y_j) > 0$  indicates that events  $x_i$  and  $x_\ell$  co-occur more often than expected under independence, while a negative value suggests mutual exclusivity.

### 9.3.2 Contextual Information

We add to each explanation of  $y^{un}$  contextual information about the description of DTCs, EPs, and the known error pattern rules. These descriptions are processed into embedding vectors using a *Titan V2 Embedding*<sup>2</sup> from AWS Bedrock. They are then used as a Retrieval-Augmented Generation (RAG) [74] system, in which the contextual information agent queries are matched against the description embeddings generated by the embedding model. It is incorporated into the context of the contextual information and orchestrator agents.

Now, directly in the prompt (*in-context learning* [27]), we randomly inject 10 DTC sequences that exhibit the same unknown EP we aim to identify. As well as metadata, such as the vehicle model range and the triggered message printed on the board (check control message: CCM). The overall data inputs are shown in Fig. 9.2, and the JSON input to the orchestrator is shown in Appendix. B.9.

## 9.4 Experiments

### 9.4.1 Evaluation Metrics

This task requires multiple levels of evaluation. Suppose that we have an automated method to extract a Boolean rule  $R^*$  for each unknown EP  $y^{un}$  in a batch of sequences. We then want to evaluate how good this generated rule is compared to the ground truth.

Hence, we distinguish between two evaluation types: (1) *structural*, where we compare the Boolean rules directly as a classification set, and (2) *semantic*, where we compare the corresponding truth-tables of the estimated Boolean expressions to the truth-table of the ground truth using the Sympy package [94].

<sup>2</sup><https://aws.amazon.com/de/blogs/aws/amazon-titan-text-v2-now-available-in-amazon-bedrock-optimized-for-improving-rag/>

$x_1$	$x_2$	Ground Truth ( $x_1$ & $x_2$ )	Predicted Rule ( $x_1$   $x_2$ )
0	0	0	0
0	1	0	1
1	0	0	1
1	1	1	1

**Table 9.1:** Illustrative truth table for semantic evaluation. The accuracy using the predicted rule is 50%.

#### 9.4.1.1 Structural Evaluation

Specifically, for (1) we evaluate: *Are the DTCs in the estimated rules correct?* For this, we divide the estimated sets and ground truth using the Boolean operators as separators and perform a standard multi-label classification:

$$dtc1 \ \& \ dtc2 \ \& \ !dte5 \ | \ dtc3 \ \implies [dte1, dtc2, dtc3, dtc5]$$

This evaluation is the same as the one described in Part II for the causal discovery algorithms recovering Markov Boundaries, i.e., sets of causes of an EP.

#### 9.4.1.2 Semantic Evaluation

For (2) we enumerate all possible assignments of the present Boolean variables and compute the truth table of the estimated rules and the ground truth to express: *Is the rule logically correct?* We calculate the accuracy, precision, recall, F1 of the predicted value of the truth tables (e.g., Tab 9.1).

### 9.4.2 Settings

We used the same experimental setup and dataset as in Chapters 6 and 7. We created 5 folds of 50,000 sequences and randomly masked 20 different EPs with at least  $n \geq 100$  sequences. We set their masked rule as the ground truth for each label  $y_j^{un}$  and average the results across the five folds. We used a combination of F1-Score, Precision, and Recall with different averaging methods [171] to compare with LLM-only baselines.

### 9.4.3 Comparison

We compared CAREP against multiple LLMs, such as Claude Sonnet 3.5 and 3.7<sup>3</sup>, GPT4.1 and GPT4.1 mini<sup>4</sup>. We further investigated whether smaller LLMs [13] with fewer parameters impacted the evaluation. The LLMs are compared using only the observed DTC sequences and their descriptions, hence in Fig. 9.2 the orange region is removed. We also added CAREP without the causal indicators. We then performed the structural and semantic evaluation of the generated Boolean rules presented in the

<sup>3</sup><https://www.anthropic.com/news/claude-3-7-sonnet>

<sup>4</sup><https://openai.com/index/gpt-4-1/>

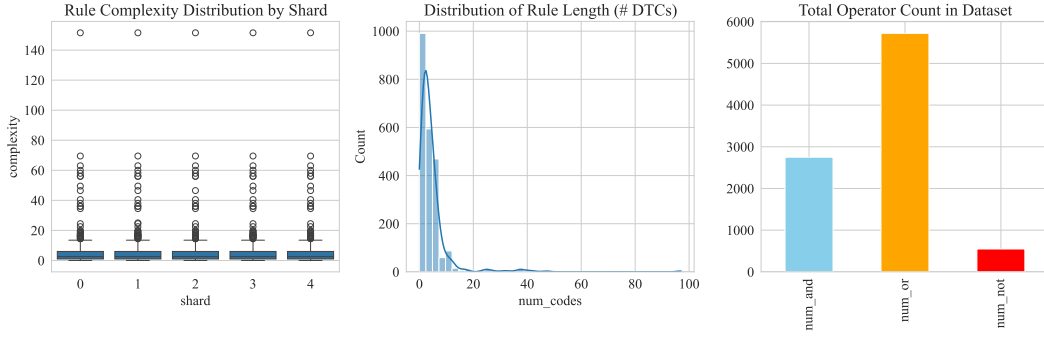


**Figure 9.3: Analysis of Ground Truth Error Patterns.** (Left) **Complexity Distribution by Fold:** The consistency of rule complexity scores across fold confirms a balanced data split strategy. (Middle) **Rule Length Histogram:** The distribution of Diagnostic Trouble Codes (DTCs) per rule reveals a long-tail nature, with some complex rules involving over 20 unique codes. (Right) **Operator Frequency:** The significant presence of logical NOT ( $\neg$ ) and OR ( $\vee$ ) operators highlights the non-trivial, inhibitory causal structures.

foundation chapter. The top-3 and top-5 metrics are computed from the five estimates, ordered by decreasing confidence (high, medium, low), to provide a clearer picture. We average the metrics across labels (macro average).

#### 9.4.4 Results

Figure 9.4 reports the performance of our method CAREP against multiple LLM baselines (Claude Sonnet 3.5/3.7, GPT4.1, and GPT4.1 mini). CAREP consistently outperforms all standalone LLMs across both evaluation protocols. The ground-truth EP rules used for evaluation were manually defined by diagnostic experts and may contain noise or inconsistencies. Results should be interpreted accordingly.

**Semantic evaluation** In terms of truth-table agreement, CAREP substantially improves over LLMs in capturing the logical structure of error patterns. CAREP achieves a *Recall@1* of 0.70, compared to 0.25 for the best-performing baseline (Claude Sonnet 3.7). Precision and F1 scores follow the same trend, showing that CAREP’s causal discovery step yields more faithful Boolean rules rather than over-generalized expressions. Interestingly, LLMs still reach  $\approx 0.50$  semantic *Accuracy@5*, indicating that DTCs’ observations and descriptions alone allow them to approximate the ground truth partially. However, they lack the consistency and reliability required for deployment that CAREP provides.

**Structural evaluation** When evaluating whether the predicted rules include the correct DTCs, CAREP’s advantage becomes even more pronounced. For *Precision@1*, CAREP achieves 0.78 versus only 0.25 for Claude Sonnet 3.7 and 0.05 for GPT4.1 mini. Similar margins are observed in F1 and accuracy. GPT4.1 and mini, in particular, perform

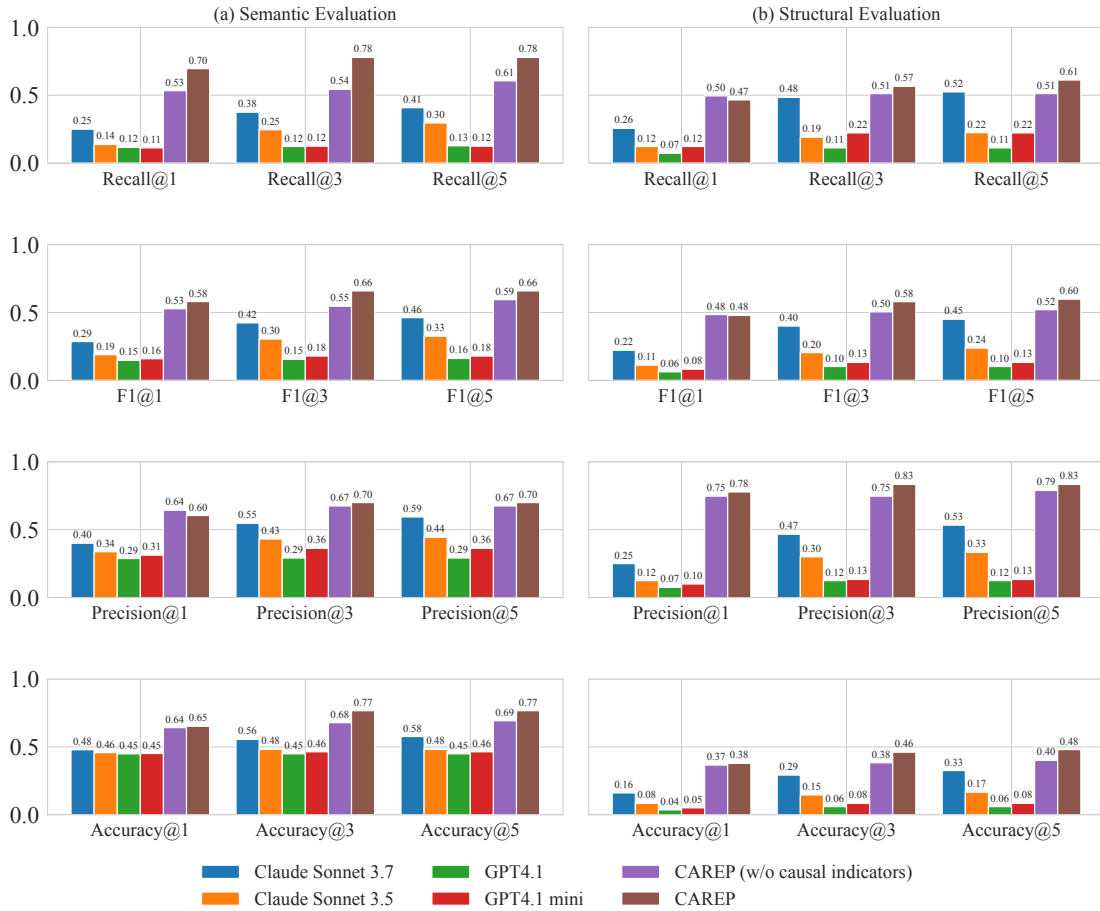


**Figure 9.4: Performance Comparison of CAREP Against Standalone LLMs.** (a) Semantic evaluation represents how well the estimated error pattern rules fit the ground truth in terms of Boolean expression. (b) Structural evaluation or multi-label classification reveals if the estimated rules contain the correct DTCs.

poorly ( $F1@1 < 0.1$ ), demonstrating that without causal discovery, LLMs fail to correctly identify the true DTCs present in the error pattern rules. In addition, unlike OSCAR and CARGO which were evaluated previously using only the structural evaluation, CAREP benefits from the contextual information and the multiple output Boolean rules since it obtains 75%  $Precision@1$  and 83%  $Precision@5$  contrary to 60%  $Precision$  (Table 7.1) for CARGO and 55% for OSCAR.

## 9.5 Summary

We introduced CAREP, a multi-agent causal-reasoning framework that automates the discovery of error pattern rules from large-scale event sequences of error codes. By combining causal discovery, RAG systems, and agents, CAREP consistently outper-

Method	Precision $\uparrow$	Recall $\uparrow$	F1 $\uparrow$	Time (min) $\downarrow$
<i>Phase 1: Sample-Level Causal Discovery (OSCAR)</i>				
Instance Graph $\mathcal{G}^{(i)}$	$55 \pm 1.4$	$31 \pm 0.8$	$40 \pm 1.0$	<b>11.7</b>
<i>Phase 2: Population-Level Causal Discovery (CARGO)</i>				
Consensus Graph $\mathcal{G}_y^*$	$61 \pm 1.5$	$46 \pm 1.7$	$46 \pm 1.2$	11.8
<i>Phase 3: CAREP (End-to-End)</i>				
<b>CAREP</b>	<b><math>83 \pm 1.1</math></b>	<b><math>60 \pm 1.3</math></b>	<b><math>61 \pm 1.1</math></b>	12

**Table 9.2: Ablation of causal discovery performance across the pipeline stages:** (1) Local Discovery, (2) Global Aggregation, and (3) The complete framework (CAREP). The baselines are evaluated using the structural (does the rule contain the correct variables, ignoring the logic). 'Time' represents cumulative runtime. By adding semantic information (metadata) and LLMs' reasoning, CAREP adds a significant prediction margin in selecting the correct *causes* of an outcome (EP).

forms state-of-the-art LLM baselines while producing interpretable reasoning traces essential for safety-related deployment. The ablation across the three pipeline stages (Table 9.2) confirms that neither causal structure alone nor language reasoning alone is sufficient: the performance gap between CARGO and CAREP demonstrates that contextual grounding is indispensable for correct Boolean rule synthesis. We emphasize, however, that CAREP is designed as an assistive tool rather than a fully autonomous decision-maker. Given the high-stakes nature of automotive diagnostics, unsupervised rule deployment carries inherent risks; therefore, human experts must remain in the loop to validate and supervise the system's outputs. The methods and findings of this chapter therefore conclude the full pipeline of this thesis, from raw event-sequence modeling through causal structure recovery to symbolic rule generation, leaving the question of how to scale, adapt, and generalize this pipeline as the central open problem motivating the directions below.

## 9.6 Outlook

Several directions offer high potential for extending CAREP toward a more general and robust automated reasoning system. A first and most immediate direction is to replace the events-to-outcome causal backbone (OSCAR and CARGO) with a *unified causal graph* that jointly encodes event-to-event and events-to-outcome dependencies, the open cell of Table 1.1. Such a graph would allow CAREP to reason not only about which DTCs cause a given error pattern, but also about the cascading sequence of fault propagation leading to it. Incorporating event-to-event causal edges from TRACE into CAREP's causal discovery agent is a natural first step; the richer structural evidence would enable the orchestrator agent to synthesize temporally ordered Boolean rules, capturing not just the presence but the sequential ordering of causes, a property that current EP rules do not yet cover. Scaling this to the full population-level setting, where a unified DAG

over both event types and outcome labels is aggregated across a fleet, constitutes the primary research goal of the *seq2cause* project [87].

A second direction concerns the language backbone of the reasoning agents. The current CAREP implementation relies on general-purpose LLMs that lack the specialized knowledge of automotive subsystems, DTC taxonomy, descriptions and diverse technical jargon. Domain-adapted language models, pretrained or continuously fine-tuned on automotive documentation, service manuals, and fault-knowledge bases would reduce hallucination rates and improve the semantic fidelity of generated rules, particularly for rare error patterns where contextual retrieval alone is insufficient.







# 10 Conclusion and Outlook

This thesis demonstrated that high-dimensional discrete event sequences, long treated as intractable by statistical models and causal discovery methods, can be systematically modeled, causally analyzed, and transformed into interpretable diagnostic knowledge using a unified pipeline of autoregressive Transformers, information-theoretic causal tests, and multi-agent reasoning.

## 10.1 Conclusion

This thesis aimed to address one of the core challenges in modern industrial systems: transforming massive, high-dimensional event streams into interpretable and actionable knowledge for practitioners and researchers. By focusing on the automotive domain, a setting that epitomizes complexity, scale, and safety-critical constraints, we progressively built a pipeline that evolves from sequence modeling to causal discovery and, finally, to automated reasoning for error pattern automation.

In Part I, we demonstrated that event sequences, such as diagnostic trouble codes (DTCs), can be modeled as a language. By introducing CarFormer and EPredictor, we showed that Transformer-based architectures can accurately learn spatio-temporal dependencies in irregular, unbalanced event streams and forecast both when and what failures are likely to occur. We also showed that incorporating additional modalities, such as sensor readings, improves predictive performance with BiCarFormer, a bidirectional Transformer model. This laid the foundation for predictive maintenance systems capable of real-time, self-diagnostic behavior.

In Part II, we moved beyond prediction to understanding. We introduced three complementary frameworks for causal discovery in sequences: OSCAR and TRACE, which perform sample-level causal discovery using autoregressive Transformers as density estimators, and CARGO, which aggregates these sample-level graphs into coherent global causal graphs. A key technical insight underpinning this is the functional duality between prediction and causal discovery: an autoregressive model trained to predict the next event implicitly learns the joint distribution of the sequence, and can therefore be directly reused, without any fine-tuning, as a neural density estimator for conditional mutual information estimation. Critically, the teacher-forcing mechanism of sequence-to-sequence training (i.e., conditioning on observed rather than model-generated history) allows all  $N$  conditional log-probabilities required for a CMI estimate to be computed in a single forward pass, collapsing what would otherwise be  $N$  sequential inference calls into a single vectorized operation and making the approach tractable on the scale of tens of thousands of distinct events. Together, they enable, for the first time, causal discovery in sequences with a considerable number of distinct events and labels, exceeding

tens of thousands of DTCs and hundreds of error patterns in our experiments. These data settings have not been explored in the literature and remain a major obstacle to the adoption of causal discovery in large-scale datasets. These three methods are anchored in modern parallelization of algorithms on GPUs, where Transformers and more generally autoregressive models are the fundamental starting point. The methods are implemented within common frameworks such as Hugging Face and PyTorch. This results in three practical causal discovery methods that practitioners can deploy alongside their event sequence model, and scale its infrastructure using only GPUs. In addition, they are theoretically grounded in causal discovery and probability theory. We proved both experimentally and theoretically that a perfect oracle model is not required to recover the causal graph and provided the soundness of our approaches under several assumptions. We analyzed the limitations of such assumptions and proposed robust methods, such as adaptive thresholding for aggregating graphs with imbalanced label distributions.

Finally, in Part III, we transitioned toward automating error patterns in vehicles, a complex reasoning task. We highlighted how we could build an entire framework powered by efficient causal discovery, contextual information retrieval, and LLMs to reason over dense, multimodal inputs. We show that a multi-agent-based system (CAREP) can generate plausible rules that are highly similar to those created by domain experts. Beyond their direct automotive applications, the methods proposed in this dissertation have broader implications. The combination of autoregressive modeling, scalable causal inference, and multi-agent reasoning opens new pathways for domains such as healthcare, cybersecurity, and industrial process monitoring, wherever complex event-driven systems demand reliable and explainable decision support.

It is important to acknowledge the assumptions and limitations that bound these contributions. The causal discovery frameworks developed in Part II rely on causal sufficiency, the absence of hidden confounders, which may not hold in all industrial deployments where unmeasured variables influence observed events. The evaluation of CAREP in Part III is conducted against EP rules that were themselves constructed by domain experts; while this provides a practical benchmark, it introduces a degree of circularity that future work should address through independent validation. Finally, all experiments are conducted on proprietary BMW data, which, while ensuring industrial relevance, limits direct reproducibility; the open-source seq2cause library and accompanying synthetic datasets are provided to partially mitigate this constraint.

In summary, this dissertation establishes a clear progression from statistical learning to causal understanding and automated reasoning. By integrating large-scale modeling with causal discovery and agent-based frameworks, we provided a unified foundation for the next generation of autonomous systems—ones capable not just of prediction, but of interpretable, causally-aware decision-making across science and industry.

## 10.2 Outlook

The work presented in this thesis brings together sequence modeling, causal discovery, and multi-agent reasoning into a unified framework for automated fault understanding in industrial-scale event sequences. While the proposed methods demonstrate strong performance in automotive diagnostics and point toward a new paradigm for large-scale event understanding, many open problems remain, both theoretical and practical. These challenges define a rich landscape for future research that extends far beyond the automotive domain.

### 10.2.1 Toward a Unified Causal Graph over Events and Outcomes

Table 1.1 organizes the causal discovery landscape of this thesis along two axes: causal scope (sample-level vs. population-level) and dependency type (events-to-outcome vs. event-to-event). Three of the four cells are addressed by the contributions of this thesis (OSCAR, TRACE, and CARGO), yet the fourth cell, population-level event-to-event discovery, remains perhaps the most scientifically important open problem. Filling the open cell requires aggregating instance-time causal graphs produced by TRACE across thousands of sequences into a single, general consistent summary graph over event types. This is the natural event-to-event counterpart of CARGO, and its realization faces three non-trivial obstacles. First, instance-time graphs encode when a causal edge fires within a specific sequence, making naive frequency-based aggregation sensitive to temporal inconsistencies across sequences of varying length and context. Second, enforcing acyclicity constraints on a graph with tens of thousands of nodes after aggregation is computationally demanding and requires careful post-processing beyond what CARGO’s Phase 2 currently provides. Third, robust uncertainty quantification over aggregated edges, such as distinguishing persistent structural causes from spurious co-occurrences driven by rare events demands principled statistical thresholding at a scale that has not yet been studied. However, filling this cell individually still leaves the deeper problem unresolved: the two dependency types are not independent. In practice, a DTC may causally trigger another DTC (event-to-event), which in turn causes an error pattern (events-to-outcome), forming a causal chain that spans both columns of Table 1.1 simultaneously. At the sample-level, OSCAR and TRACE can in principle be run jointly on the same sequence, but their outputs, a Markov Boundary per label and an instance-time causal graph over events are not currently unified into a single coherent object. At the population-level, the problem compounds: one would require a mixed graph that simultaneously encodes directed edges between event types and directed edges from event types to outcome labels, with consistent semantics across both. We refer to this as the joint population-level causal graph, and it constitutes the most ambitious open problem in this line of work. Such a graph would allow a practitioner to trace a complete causal path from a root-cause DTC, through intermediate triggering events, to the final error pattern entirely from observational data, without any manual rule definition. Addressing this problem will require extending the aggregation framework of CARGO to handle heterogeneous node types (events and labels), developing acyclicity constraints that respect the asym-

metry between the two node classes, and designing evaluation protocols that go beyond current set-based and Hamming-distance metrics. The seq2cause library is architected with this unification in mind, and we consider the joint population-level causal graph the single most impactful direction for future research emerging from this thesis.

### 10.2.2 Toward Multimodal and Multi-Resolution Causal Discovery

Throughout this thesis, causal discovery primarily operates on discrete event streams possibly with outcomes. Yet modern vehicles, like many stochastic systems, generate multimodal data, including environmental conditions, textual descriptions, or camera-based observations. Extending causal discovery to this multimodal setting, by combining discrete events with continuous signals, images, or text, would enable richer causal graphs that can explain failures through finer-grained interactions. Foundations from multimodal Transformers, contrastive pretraining, and cross-modal attention could support such expansion. A promising direction is causal fusion learning, where causal edges are allowed to form across modalities and at multiple temporal resolutions (millisecond sensor bursts vs. day-level DTCs), similar to summary graphs in time series [5]. This would help address phenomena such as cascading failures arising from the joint interaction of software and hardware subsystems, and enrich the EP rules by incorporating environmental conditions.

### 10.2.3 Unseen Domain and Continuous Learning

A central challenge for deploying intelligent diagnostic systems in real-world environments is their ability to generalize beyond the distribution from which they were trained. Vehicles evolve across software versions, model years, component suppliers, and even regional driving conditions. Models trained once and deployed indefinitely, whether sequence predictors, causal discovery frameworks, or multi-agent reasoning systems, inevitably face degradation as the data distribution drifts. Such a system needs to continuously learn from new data while retaining previously acquired knowledge.

This opens a rich avenue for future research at the intersection of continual learning and multi-agent adaptation. Classical continual learning methods based on regularization, replay, or architectural expansion [43] provide the first building blocks, but remain insufficient for highly structured, relational tasks such as diagnostic rule synthesis. More recent theoretical developments, such as the “Nested Learning” perspective [12], challenge the assumption that deep architectures inherently build hierarchical abstractions, suggesting instead that models must be explicitly encouraged to discover stable mechanisms that persist across contexts. They use different updating frequencies of neurons across layers, mimicking brain oscillations.

Future systems may therefore incorporate continual updates during Transformers’ training and enable smooth, continuous synthesis of EP rules, with agents detecting when new vehicles introduce unseen failure modes, unseen DTC combinations, or entirely novel clusters of behaviors. Multi-agent architectures are particularly promising in this setting: one agent may monitor distribution shift, another may propose updated causal

graphs for new domains. Beyond adaptation, such systems could also identify *when* previously learned EP rules should be revised, pruned, or merged, enabling long-term autonomous maintenance of diagnostic knowledge bases.

#### 10.2.4 Industrial Foundation Models

Recent progress in large language models raises the question of whether analogous foundation models for event sequences can be developed. Such models would unify sequence modeling, forecasting, causal inference, anomaly detection, and reasoning capabilities across domains such as healthcare, cybersecurity, aviation, and industrial operations. The introduced Transformer-based architectures, coupled with causal discovery tools, could serve as stepping stones toward such foundation models. Pretraining on large-scale, heterogeneous event-log corpora, comparable to natural-language corpora, would enable these models to generalize across systems and support in-context learning, zero-shot, or few-shot diagnostics on unseen devices, procedures, or scenarios. It is essential to strike a balance between the world of words and events through adapted pretraining and fine-tuning tasks. Recent approaches adapt diffusion models for discrete data [127]. This could help build more robust bidirectional models rather than traditional left-to-right models [104], particularly for sequence classification and machine translation tasks.



# List of Figures

1.1	<b>Error Pattern Prediction (when and what).</b> Based on the past sequence $S$ of diagnostic trouble codes (DTCs), manufacturers want to prevent error patterns (EPs) from happening by predicting their likelihood and time of occurrence. . . . .	5
1.2	<b>Error Pattern Prediction using Multimodal Sequences.</b> Past diagnostic trouble codes only provide limited information about complex and overlapping error patterns. In addition, domain experts rely on environmental conditions (e.g., temperature, voltage, humidity, ...) to identify more accurately error patterns. . . . .	6
1.3	<b>Anonymized Causal Graph.</b> Example of a sequence of events (DTCs) that lead to a steering wheel degradation and a power limitation as outcome labels. The causal indicators are shown in violet if inhibitory and orange or red if excitatory, depending on the magnitude. The voltage error DTC is the biggest causal driver for the power limitation EP while the security sync failure seems to have the biggest inhibitory effect on all EP. . . . .	8
1.4	<b>Anonymized Instance-Time Causal Graph for Diagnostic Defect Cascade.</b> Temporal evolution of a diagnostic defect cascade in a vehicle ( $ \mathcal{X}  \approx 29, 100$ ). TRACE effectively captures causal relationships, revealing distinct <b>error clusters</b> at different time steps (e.g., initial sensor failures at $t = 3$ triggering mechanical faults at $t = 12$ , battery at issue $t = 17$ ). This enables actionable root-cause analysis by isolating the specific onset of a failure mechanism and its strength using the conditional mutual information. . . . .	9
3.1	<b>Time and Mileage Distribution.</b> Distribution of $t_i$ and $m_i$ (relative time and mileage) in our dataset. . . . .	31
3.2	<b>CarFormer Architecture.</b> A Transformer architecture is used alongside spatio-temporal embeddings ( <i>context embedding</i> ) injected to the query and key. A RoPE is then applied to induce the relative position of the DTCs. Three predictive heads are used to learn the complex dynamics of the DTC sequences. . . . .	34

3.3 **EPredictor Architecture.** The hidden state  $H(S)$  is extracted from CarFormer and fed to the second attention layer as value and key. The event-type embedding  $\mathbf{E}$  is fed into the first layer after being normalized, and the context embedding  $\mathbf{CE}$  carrying the spatio-temporal information is added directly after the RoPE application to the keys and queries of the second layer. . . . . 36

3.4 **Classification Performance Comparison Between Architectural Changes.** F1 Score comparison with multiple EPredictor architectures as a function of the number of observations. This answers *what* EP is most likely to occur. . . . . 40

3.5 **Regression Error As a Function of the Number of Observations.** Evolution of the MAE as a function of the number of observations for the best performing model, this effectively tests for *when* an EP is most likely to occur. . . . . 40

4.1 **Spatio-temporal Point Process Representation of a Vehicle.** Spatial (mileage) and Temporal (time) point process representation of events from a vehicle. Bold vertical lines indicate multiple events occurring at the same time  $t_i$  or mileage  $m_i$ . . . . . 49

4.2 **BiCarFormer Architecture.** Both parallel Transformers are computing cross-attention scores conditioned on each modality  $\mathbf{Q}, \mathbf{K}, \mathbf{V}$ . Two final representations are generated for each modality: DTC ( $\mathbf{H}_d$ ) and environmental conditions ( $\mathbf{H}_e$ ). Multiple hierarchical embeddings are defined at the input level to account for DTC-specific features (ECUs, Fault-Bytes, Base-Code). . . . . 50

4.3 **Attention Distribution between Environmental Condition Tokens.** Amount of attention received by each environmental condition token from the DTCs. The y-axis was truncated to improve clarity as well as the number of heads printed. We take  $\mathbf{A}_{dtc \rightarrow env}$  of the last layer. . . . . 53

4.4 **Cross-Attention Scores for  $\mathbf{A}_{dtc \rightarrow env}$ .** The DTCs are shown on the y-axis (anonymized), and the environmental conditions with their 3 elements  $(d, v, u)$  concatenated are shown on the x-axis (the description  $d$  is anonymized). The intensity of each cell reflects the attention weight, where darker shades indicate higher attention values. . . . . 54

4.5 **Attention Distribution between Environmental Conditional Units.** Amount of attention received by each environmental unit from the DTCs in a *battery aging* error pattern from a battery electric vehicle. We take  $\mathbf{A}_{dtc \rightarrow env}$  of the last layer and print all heads. . . . . 55

4.6	<b>Discretized Voltage and Attention Scores Evolution between Environmental Token Position.</b> Discretized voltage variation as a function of environmental condition tokens and the associated amount of attention received from DTCs. We only take triplets $(d, v, u)$ from $S_e$ with $u = 'v'$ and extract $\mathbf{A}_{dtc \rightarrow env}$ from the last layer and <i>head 2</i> . The sample is taken from a <i>battery aging</i> error pattern. BiCarFormer implicitly learns the fluctuation of discretized continuous values to make a prediction. . . .	56
6.1	<b>The Overview of OSCAR: One-Shot multi-label Causal AutoRegressive discovery.</b> $d$ denotes the hidden dimension, $L$ the sequence length, $\mathcal{MB}_1, \mathcal{MB}_2$ the Markov Boundary of $Y_1, Y_2$ respectively. All green and blue areas represent parallelised operations. . . . .	72
6.2	<b>Example of a Causal Graph</b> extracted from a multi-label <i>event</i> sequence where $\mathcal{MB}_1$ represents the Markov Boundary of $Y_1$ and $\mathcal{MB}_2$ the Markov Boundary of $Y_2$ . . . . .	75
6.3	<b>Evolution of the Classification Performance as a Function of the Markov Boundary Length <math> \mathcal{MB}(Y_j) </math></b> ( $n = 45969$ samples). We can identify that the Markov Boundary complexity is not the bottleneck but rather the number of samples per class ( <i>imbalance threshold</i> ), which reduces classification performance. . . . .	82
7.1	<b>Structural Fusion Example:</b> individual set of causal graphs $\{\mathcal{G}^{(k)}\}$ (left) aggregated into a fused DAG for multi-label event sequences (right) using a simple union. . . . .	86
7.2	<b>Overview of CARGO.</b> Phase 1 (One-shot) is on top, and Phase 2 (Adaptive Thresholding) is on the bottom. $d$ denotes the hidden dimension, $L$ the sequence length, $m$ the number of samples and $\mathcal{MB}_1, \mathcal{MB}_2$ the Markov Boundary of $Y_1, Y_2$ . All green and blue areas are parallelised. . . . .	87
7.3	<b>Adaptive Thresholding Function <math>\tau_j(m_j)</math></b> across varying support $m_j$ , illustrating the logistic decay from $\tau_{\max}$ to $\tau_{\min}$ . . . . .	89
7.4	<b>Criterion Ablation for Structural Fusion.</b> Comparison of different criteria for the structural fusion (Phase 2) as a function of the number of samples $m$ . With $ \mathcal{Y}  = 474,  \mathcal{X}  = 29, 100$ nodes. . . . .	91
8.1	<b>Methodological Shift. (A) Traditional Causal Discovery in Sequences</b> (e.g., PCMCI, Hawkes, Granger) relies on iterative solvers (CI-tests) over long multivariate time series ( $T \rightarrow \infty$ ). <b>(B) Our TRACE Approach</b> processes a single sequence (e.g., event logs, user interactions, patient trajectories) through a pretrained autoregressive (AR) model as density estimator to compute the Conditional Mutual Information (CMI) in parallel, enabling scalable causal discovery over massive vocabularies ( $ \mathcal{X}  > 1000$ ). . . . .	94

8.2 **TRACE Methodology. Phase 1 (Training):** An autoregressive (AR) model (e.g., LM, RNN) is pretrained on a corpus of event sequences via next-token prediction to learn the process dynamics ( $P_\theta$ ). **Phase 2 (Inference):** A single sequence  $s$  is passed through the frozen model. We then estimate conditional mutual information (**Parallelized CMI** module) to prune non-causal edges and form the *Instance-Time Causal Graph*  $\mathcal{G}_{t,s}$ . Finally, this graph is projected onto the event types to recover the *Summary Causal Graph*  $\mathcal{G}_s$ . . . . . 96

8.3 **Overview of TRACE Parallel CI-tests.** We construct a single broadcasted tensor  $\mathbf{X}_{do}$  where each row  $j$  incrementally fixes the history  $x_{\leq j}$  while randomizing the future (staircase pattern). The model processes this tensor in parallel to produce raw probabilities  $\mathbf{P}_{raw}$  (grey). We then compute the Causal Mutual Information by comparing adjacent rows: the distribution at row  $j - 1$  serves as the baseline ( $\mathbf{P}_{base}$ , blue) for the intervention at row  $j$  ( $\mathbf{P}_{do}$ , red). . . . . 103

8.4 **Scalability to High-Dimensional Event Spaces.** Evaluation of structural identifiability across exponentially growing vocabulary sizes. **Top:** Evolution of discovery metrics. TRACE exhibits **performance invariance**, maintaining  $F1 \approx 0.81$  even as the combinatorial search space explodes. **Bottom:** Visual examples of recovered summary graphs  $\mathcal{G}_s$  at scale. Shannon redundancy as ( $Pred = 1 - H(P)/H_{max}$ ) confirm that TRACE succeeds even in high-entropy regimes. ( $\hat{\epsilon} = 0.01, L = 64, N = 64, \tau = 10^{-4}$ ). . . . . 107

8.5 **Robustness and Scalability Analysis** ( $|\mathcal{X}| = 1000, N = 128, \tau = 10^{-4}, L = 64$ ). Evolution of causal discovery performance (F1, Precision, Recall, SHD). **(a) Robustness to Generative Error:** Performance as a function of the model’s oracle score  $\epsilon$ . TRACE exhibits a phase transition, recovering structure even for imperfect models ( $\epsilon < 0.1$ ) and maintaining high Precision even as fidelity degrades. **(b) Scalability to Length:** Performance and GPU memory usage vs. sequence length  $L$ . The **Sparse** variant demonstrates linear memory scaling ( $O(mL)$ ), enabling inference on sequences far exceeding the training length ( $L = 64$ ), whereas the Full variant scales quadratically. **(c) Long-Range Dependencies:** Robustness to increasing delayed-effects  $m$ . TRACE maintains  $F1 > 0.8$  even as dependencies span one third of the sequence ( $m = 20$ ), confirming the method’s ability to capture distant causal mechanisms. . . . . 108

8.6 **Instance-Time Causal Graph.** Temporal evolution of a diagnostic defect cascade in a vehicle ( $|\mathcal{X}| \approx 29, 100$ ). TRACE effectively captures causal relationships, revealing distinct **error clusters** at different time steps (e.g., initial sensor failures at  $t = 3$  triggering mechanical faults at  $t = 12$ , battery at issue  $t = 17$ ). This enables actionable root-cause analysis by isolating the specific onset of a failure mechanism and their strength using the CMI  $\hat{I}_N$  . . . . . 109

8.7	<b>Robustness to Hidden Confounding.</b> Evaluation of TRACE under violations of causal sufficiency. (a) Measurement Error: Random noise is injected into the context. Precision stays high, indicating resistance to hallucination. (b) Temporal Drops: Time steps are randomly deleted, thus conditioning sets are broken. TRACE still recovers structure despite missing intermediaries but the discovery scores quickly decrease. . . . .	110
9.1	<b>Illustration of Error Pattern Automation in Modern Vehicles.</b> (a) A vehicle with an unknown defect generates a sequence of Diagnostic Trouble Codes (DTCs) over time. (b) A domain expert analyzes the DTCs and the vehicle’s metadata (e.g., model, descriptions). (c) Provide a Boolean rule to identify this error pattern. . . . .	118
9.2	<b>CAREP: A Causal Reasoning Agentic System for Error Pattern Automation.</b> (a) Represents the causal discovery phase, where we extract candidate DTC causes for the unknown error pattern alongside causal indicators. It then feeds the causal reasoner agent. (b) The descriptions and metadata are extracted through a Titan V2 Embeddings and fed into the contextual information agent. (c) The orchestrator agent manages the two agents and provides traceable reasoning to explain why the unknown error pattern may match these rules. . . . .	121
9.3	<b>Analysis of Ground Truth Error Patterns.</b> (Left) <b>Complexity Distribution by Fold:</b> The consistency of rule complexity scores across fold confirms a balanced data split strategy. (Middle) <b>Rule Length Histogram:</b> The distribution of Diagnostic Trouble Codes (DTCs) per rule reveals a long-tail nature, with some complex rules involving over 20 unique codes. (Right) <b>Operator Frequency:</b> The significant presence of logical NOT ( $\neg$ ) and OR ( $\vee$ ) operators highlights the non-trivial, inhibitory causal structures. . . . .	124
9.4	<b>Performance Comparison of CAREP Against Standalone LLMs.</b> (a) Semantic evaluation represents how well the estimated error pattern rules fit the ground truth in terms of Boolean expression. (b) Structural evaluation or multi-label classification reveals if the estimated rules contain the correct DTCs. . . . .	125
A.1	<b>Confident Predictive Maintenance Window Evolution</b> with and w/o the random head. . . . .	169
A.2	<b>Pretraining Loss Comparison.</b> Base-DTC classification loss comparison with and without multimodal learning. . . . .	169
B.1	<b>Ablation of the Number of Particles <math>N</math>.</b> Results are reported using 1-sigma error bar. . . . .	173
B.2	<b>Sensitivity Analysis.</b> Evolution of the one-shot F1 Score, Precision, and Recall as a function of coefficient $k$ . Results are reported using 1-sigma error bar. . . . .	174

List of Figures

B.3 Example of a sequence of events (DTCs) that lead to an emergency antenna dysfunction as outcome labels. The inhibitory strengths are shown in pink and causal strengths in orange and red . . . . . 175

B.4 Example of a sequence of events (DTCs) that lead to an airbag and tire pressure malfunctions as outcome labels. The inhibitory strengths are shown in pink and causal strengths in orange and red . . . . . 175

B.5 **Ablation of the Number of Particles  $N$ .** Evolution of causal discovery performance as a function of the number of particles  $N$  at  $|\mathcal{X}| = 1000, m = 6$  . . . . . 183

B.6 **Sensitivity Analysis.** Classification metrics relative to the filtering threshold  $\tau$  with  $|\mathcal{X}| = 1000, \epsilon = 0.04, c = 6, m = 6, L = 64, N = 128$ . . . 184

B.7 **The Scaling Law of Causal Identifiability.** We perform a sensitivity analysis across vocabulary sizes  $|\mathcal{X}| \in \{100, \dots, 2000\}$  to find the optimal filtering threshold  $\tau_{opt}$  (maximizing F1-score) with  $\epsilon = 0.04$ . The result reveals a power-law relationship  $\tau_{opt} \propto |\mathcal{X}|^{-0.96}$ . . . . . 185

B.8 **Instance Summary Causal Graph.** The global causal structure  $\mathcal{G}_s$  aggregated from TRACE inferences over the validation set. While the instance graph (Fig. 8.6) details *when* events occur, this summary graph captures the invariant mechanism types. The density of the graph highlights the complexity of modern vehicle architectures, where high-degree nodes often represent central control units (e.g., ECU, Battery Management) that propagate cascading faults. The conditional mutual information is reported as causal strength. . . . . 185

B.9 **Input Examples Given to the Agentic System.** The *potential causes* are output by the causal discovery algorithm. For instance, *DTC3* is a cause of *unknown EP* and has an Average Causal Effect (*ACE*) of 0.7, i.e., it increases the likelihood of observing the EP on average by 70% (Eq. (9.1)). Examples of defective vehicles exhibiting this error pattern are provided in the *DTC samples*. . . . . 186

# List of Tables

1.1	<b>The four regimes of causal discovery in discrete event sequences</b> , defined by the cross-product of <i>causal scope</i> (single-sequence inference vs. population-level aggregation) and <i>dependency type</i> (events-to-outcome vs. event-to-event). The three shaded contributions of this thesis — <b>OS-CAR</b> , <b>TRACE</b> , and <b>CARGO</b> — share a common backbone: pretrained autoregressive Transformers repurposed as neural autoregressive density estimators (NADEs) for conditional mutual information estimation. The remaining cell, population-level event-to-event discovery, constitutes an open problem and a direct avenue for future work. . . . .	10
2.1	List of dataset symbols and their respective meanings for the datasets used in this thesis. . . . .	26
3.1	Number of Distinct values of the DTC elements . . . . .	31
3.2	Overall prediction performance of CarFormer with different embeddings. Best results are in bold. . . . .	38
3.3	EPredictor evaluation results with different model architectures on the test set (no up- nor down-sampling). The MAPE and F1 are shown in (%)	39
4.1	New symbols introduced in this chapter. For base DTC notation, see Table 2.1 . . . . .	46
4.2	Number of distinct values after filtering for each feature. . . . .	47
4.3	Downstream evaluation of multi-label error pattern classification. Each model has the same number of parameters (25M). Results are grouped by averaging type (micro/macro vs. sample). . . . .	52
6.1	Comparisons of $\mathcal{MB}$ retrieval with $n = 50,000$ samples, $ \mathcal{X}  = 29,100$ , $ \mathcal{Y}  = 474$ averaged over 6-folds. Classification metrics averaging is 'weighted' and shown as one-shot for OSCAR. The symbol '-' indicates that the algorithm did not output the $\mathcal{MB}$ within 3 days. Metrics are given in %.	81
6.2	Comparisons of $\mathcal{MB}$ retrieval with $n = 500$ samples over 9 folds. . . . .	81
7.1	Comparisons of $\mathcal{MB}$ retrieval with $m = 50,000$ samples averaged over 6-folds with $ \mathcal{Y}  = 474$ , $ \mathcal{X}  = 29,100$ nodes. Averaging is 'weighted'. The symbol '-' indicates that the algorithm did not output the $\mathcal{MB}$ s within 3 days. Metrics are given in %. OSCAR reports only the one-shot performance (Phase 1). . . . .	90

List of Tables

8.1 Comparison of causal discovery methods. **Discrete Events:** Operates on discrete event sequences (e.g., text, logs) rather than multivariate time series. **High Dim:** Computationally tractable for large vocabularies ( $|\mathcal{X}| > 10^3$ ). **Non-Param.:** Agnostic to the functional form (e.g., linearity) of causal relationships. **Lags:** Models delayed causal effects. **Sample-Level:** Infers a local causal graph specific to a single sequence, rather than a global graph. **Linear Complexity:** Complexity scales linearly with the vocabulary size  $|\mathcal{X}|$ . . . . . 95

8.2 **Identifiability Comparison.** Comparison of causal discovery performance on synthetic SCMs with  $|\mathcal{X}| = 1000, L = 64, \epsilon = 0.05, \tau = 3.10^{-5}, N = 128$ . **TRACE** significantly outperforms local (Saliency) and global (Granger/Shapley) baselines, achieving over 20 points higher F1 while maintaining high precision. Results across 10 runs are reported. . . . . 106

9.1 Illustrative truth table for semantic evaluation. The accuracy using the predicted rule is 50%. . . . . 123

9.2 **Ablation of causal discovery performance across the pipeline stages:** (1) Local Discovery, (2) Global Aggregation, and (3) The complete framework (CAREP). The baselines are evaluated using the structural (does the rule contain the correct variables, ignoring the logic). 'Time' represents cumulative runtime. By adding semantic information (metadata) and LLMs' reasoning, CAREP adds a significant prediction margin in selecting the correct *causes* of an outcome (EP). . . . . 126

B.1 Ablations of the performance of Phase 1 (One-shot **MB** retrieval) as a function of different NADEs with  $n = 50,000$  and  $n = 500$  samples, averaged over 5-folds. Classification metrics use weighted averaging. Metrics are given in %. . . . . 172

B.2 One-shot classification performance and elapsed time (sec) across different sampling methods. Best results are in **bold**, and equal performance are in underline. . . . . 172

## Bibliography

- [1] Massil Achab, Emmanuel Bacry, Stéphane Gaïffas, Iacopo Mastromatteo, and Jean-François Muzy. “Uncovering causality from multivariate hawkes integrated cumulants”. In: *J. Mach. Learn. Res.* 18.1 (Jan. 2017), pp. 6998–7025. ISSN: 1532-4435.
- [2] Abien Fred Agarap. “Deep Learning using Rectified Linear Units (ReLU)”. In: *arXiv e-prints*, arXiv:1803.08375 (Mar. 2018), arXiv:1803.08375. DOI: 10.48550/arXiv.1803.08375. arXiv: 1803.08375 [cs.NE].
- [3] C.F. Aliferis, Ioannis Tsamardinos, and A Statnikov. “HITON: A Novel Markov Blanket Algorithm for Optimal Variable Selection”. In: *AMIA ... Annual Symposium proceedings / AMIA Symposium. AMIA Symposium 2003* (Feb. 2003), pp. 21–5.
- [4] Abdul Fatir Ansari, Lorenzo Stella, Caner Turkmen, Xiyuan Zhang, Pedro Mercado, Huibin Shen, Oleksandr Shchur, Syama Sundar Rangapuram, Sebastian Pineda Arango, Shubham Kapoor, Jasper Zschiegner, Danielle C. Maddix, Hao Wang, Michael W. Mahoney, Kari Torkkola, Andrew Gordon Wilson, Michael Bohlke-Schneider, and Yuyang Wang. *Chronos: Learning the Language of Time Series*. 2024. arXiv: 2403.07815 [cs.LG]. URL: <https://arxiv.org/abs/2403.07815>.
- [5] Charles K. Assaad, Emilie Devijver, and Eric Gaussier. “Discovery of extended summary graphs in time series”. In: *Proceedings of the Thirty-Eighth Conference on Uncertainty in Artificial Intelligence*. Ed. by James Cussens and Kun Zhang. Vol. 180. Proceedings of Machine Learning Research. PMLR, 2022, pp. 96–106. URL: <https://proceedings.mlr.press/v180/assaad22a.html>.
- [6] Charles K. Assaad, Emilie Devijver, and Eric Gaussier. “Survey and Evaluation of Causal Discovery Methods for Time Series”. In: *J. Artif. Int. Res.* 73 (May 2022). ISSN: 1076-9757. DOI: 10.1613/jair.1.13428. URL: <https://doi.org/10.1613/jair.1.13428>.
- [7] Jimmy Lei Ba, Jamie Ryan Kiros, and Geoffrey E. Hinton. *Layer Normalization*. 2016. arXiv: 1607.06450 [stat.ML]. URL: <https://arxiv.org/abs/1607.06450>.
- [8] Gregor Bachmann and Vaishnavh Nagarajan. “The Pitfalls of Next-Token Prediction”. In: *ICLR 2024 Workshop: How Far Are We From AGI*. 2024. URL: <https://openreview.net/forum?id=v9L38gCohh>.

## Bibliography

- [9] Emmanuel Bacry, Martin Bompaire, Stéphane Gaffas, and Jean-Francois Muzy. “Sparse and low-rank multivariate Hawkes processes”. In: *Journal of Machine Learning Research* 21.50 (2020), pp. 1–32. URL: <http://jmlr.org/papers/v21/15-114.html>.
- [10] Vahid Balazadeh, Hamidreza Kamkari, Valentin Thomas, Junwei Ma, Bingru Li, Jesse C. Cresswell, and Rahul Krishnan. “CausalPFN: Amortized Causal Effect Estimation via In-Context Learning”. In: *The Thirty-ninth Annual Conference on Neural Information Processing Systems*. 2025. URL: <https://openreview.net/forum?id=RblaNJGx8C>.
- [11] Jasmijn Bastings and Katja Filippova. “The elephant in the interpretability room: Why use attention as explanation when we have saliency methods?” In: *Proceedings of the Third BlackboxNLP Workshop on Analyzing and Interpreting Neural Networks for NLP*. Ed. by Afra Alishahi, Yonatan Belinkov, Grzegorz Chrupala, Dieuwke Hupkes, Yuval Pinter, and Hassan Sajjad. Online: Association for Computational Linguistics, Nov. 2020, pp. 149–155. DOI: 10.18653/v1/2020.blackboxnlp-1.14. URL: <https://aclanthology.org/2020.blackboxnlp-1.14/>.
- [12] Ali Behrouz, Meisam Razaviyayn, Peilin Zhong, and Vahab Mirrokni. “Nested Learning: The Illusion of Deep Learning Architectures”. In: *The Thirty-ninth Annual Conference on Neural Information Processing Systems*. 2025. URL: <https://openreview.net/forum?id=nbMeRvNb7A>.
- [13] Peter Belcak, Greg Heinrich, Shizhe Diao, Yonggan Fu, Xin Dong, Saurav Muralidharan, Yingyan Celine Lin, and Pavlo Molchanov. *Small Language Models are the Future of Agentic AI*. 2025. arXiv: 2506.02153 [cs.AI]. URL: <https://arxiv.org/abs/2506.02153>.
- [14] Iz Beltagy, Matthew E. Peters, and Arman Cohan. *Longformer: The Long-Document Transformer*. 2020. arXiv: 2004.05150 [cs.CL]. URL: <https://arxiv.org/abs/2004.05150>.
- [15] Yoshua Bengio and Samy Bengio. “Modeling High-Dimensional Discrete Data with Multi-Layer Neural Networks”. In: *Advances in Neural Information Processing Systems*. Ed. by S. Solla, T. Leen, and K. Müller. Vol. 12. MIT Press, 1999. URL: [https://proceedings.neurips.cc/paper\\_files/paper/1999/file/e6384711491713d29bc63fc5eeb5ba4f-Paper.pdf](https://proceedings.neurips.cc/paper_files/paper/1999/file/e6384711491713d29bc63fc5eeb5ba4f-Paper.pdf).
- [16] Daniel Bolya, Cheng-Yang Fu, Xiaoliang Dai, Peizhao Zhang, Christoph Feichtenhofer, and Judy Hoffman. “Token Merging: Your ViT But Faster”. In: *The Eleventh International Conference on Learning Representations*. 2023. URL: <https://openreview.net/forum?id=JroZRarw7Eu>.
- [17] Gianni Brauers and Flavius Frasincar. “A General Survey on Attention Mechanisms in Deep Learning”. In: *IEEE Trans. on Knowl. and Data Eng.* 35.4 (Apr. 2023), pp. 3279–3298. ISSN: 1041-4347. DOI: 10.1109/TKDE.2021.3126456. URL: <https://doi.org/10.1109/TKDE.2021.3126456>.

- [18] Tom Brown, Benjamin Mann, Nick Ryder, Melanie Subbiah, Jared D Kaplan, Prafulla Dhariwal, Arvind Neelakantan, Pranav Shyam, Girish Sastry, Amanda Askell, Sandhini Agarwal, Ariel Herbert-Voss, Gretchen Krueger, Tom Henighan, Rewon Child, Aditya Ramesh, Daniel Ziegler, Jeffrey Wu, Clemens Winter, Chris Hesse, Mark Chen, Eric Sigler, Mateusz Litwin, Scott Gray, Benjamin Chess, Jack Clark, Christopher Berner, Sam McCandlish, Alec Radford, Ilya Sutskever, and Dario Amodei. “Language Models are Few-Shot Learners”. In: *Advances in Neural Information Processing Systems*. Ed. by H. Larochelle, M. Ranzato, R. Hadsell, M.F. Balcan, and H. Lin. Vol. 33. Curran Associates, Inc., 2020, pp. 1877–1901. URL: [https://proceedings.neurips.cc/paper\\_files/paper/2020/file/1457c0d6bfc4967418bfb8ac142f64a-Paper.pdf](https://proceedings.neurips.cc/paper_files/paper/2020/file/1457c0d6bfc4967418bfb8ac142f64a-Paper.pdf).
- [19] Patricia Cheng. “From Covariation to Causation: A Causal Power Theory”. In: *Psychological Review* 104.2 (1997), pp. 367–405. DOI: 10.1037/0033-295x.104.2.367.
- [20] David Maxwell Chickering. “Learning Bayesian Networks is NP-Complete”. In: *Learning from Data: Artificial Intelligence and Statistics V*. Ed. by Doug Fisher and Hans-J. Lenz. New York, NY: Springer New York, 1996, pp. 121–130. ISBN: 978-1-4612-2404-4. DOI: 10.1007/978-1-4612-2404-4\_12. URL: [https://doi.org/10.1007/978-1-4612-2404-4\\_12](https://doi.org/10.1007/978-1-4612-2404-4_12).
- [21] David Maxwell Chickering. “Optimal structure identification with greedy search”. In: *J. Mach. Learn. Res.* 3.null (Mar. 2003), pp. 507–554. ISSN: 1532-4435. DOI: 10.1162/153244303321897717. URL: <https://doi.org/10.1162/153244303321897717>.
- [22] Kyunghyun Cho, Bart van Merriënboer, Caglar Gulcehre, Dzmitry Bahdanau, Fethi Bougares, Holger Schwenk, and Yoshua Bengio. “Learning Phrase Representations using RNN Encoder–Decoder for Statistical Machine Translation”. In: *Proceedings of the 2014 Conference on Empirical Methods in Natural Language Processing (EMNLP)*. Ed. by Alessandro Moschitti, Bo Pang, and Walter Daelemans. Doha, Qatar: Association for Computational Linguistics, Oct. 2014, pp. 1724–1734. DOI: 10.3115/v1/D14-1179. URL: <https://aclanthology.org/D14-1179/>.
- [23] T.M. Cover. *Elements of Information Theory*. Wiley series in telecommunications and signal processing. Wiley-India, 1999. ISBN: 9788126508143. URL: <https://books.google.de/books?id=3yGJrqyanyYC>.
- [24] Joscha Cüppers, Sascha Xu, Musa Ahmed, and Jilles Vreeken. “Causal Discovery from Event Sequences by Local Cause-Effect Attribution”. In: *Advances in Neural Information Processing Systems* 37 (2024).
- [25] DeepSeek-AI. *DeepSeek-R1: Incentivizing Reasoning Capability in LLMs via Reinforcement Learning*. 2025. arXiv: 2501.12948 [cs.CL]. URL: <https://arxiv.org/abs/2501.12948>.

## Bibliography

- [26] Jacob Devlin, Ming-Wei Chang, Kenton Lee, and Kristina Toutanova. “BERT: Pre-training of Deep Bidirectional Transformers for Language Understanding”. In: *North American Chapter of the Association for Computational Linguistics*. 2019. URL: <https://api.semanticscholar.org/CorpusID:52967399>.
- [27] Qingxiu Dong, Lei Li, Damai Dai, Ce Zheng, Jingyuan Ma, Rui Li, Heming Xia, Jingjing Xu, Zhiyong Wu, Baobao Chang, Xu Sun, Lei Li, and Zhifang Sui. “A Survey on In-context Learning”. In: *Proceedings of the 2024 Conference on Empirical Methods in Natural Language Processing*. Ed. by Yaser Al-Onaizan, Mohit Bansal, and Yun-Nung Chen. Miami, Florida, USA: Association for Computational Linguistics, Nov. 2024, pp. 1107–1128. DOI: 10.18653/v1/2024.emnlp-main.64. URL: <https://aclanthology.org/2024.emnlp-main.64/>.
- [28] Shuyu Dong, Michèle Sebag, Kento Uemura, Akito Fujii, Shuang Chang, Yusuke Koyanagi, and Koji Maruhashi. “DCILP: A Distributed Approach for Large-Scale Causal Structure Learning”. In: *AAAI-25, Sponsored by the Association for the Advancement of Artificial Intelligence, February 25 - March 4, 2025, Philadelphia, PA, USA*. Ed. by Toby Walsh, Julie Shah, and Zico Kolter. AAAI Press, 2025, pp. 16345–16353. DOI: 10.1609/AAAI.V39I15.33795. URL: <https://doi.org/10.1609/aaai.v39i15.33795>.
- [29] Arnaud Doucet, Nando de Freitas, and Neil Gordon. “An Introduction to Sequential Monte Carlo Methods”. In: *Sequential Monte Carlo Methods in Practice*. Ed. by Arnaud Doucet, Nando de Freitas, and Neil Gordon. New York, NY: Springer New York, 2001, pp. 3–14. ISBN: 978-1-4757-3437-9. DOI: 10.1007/978-1-4757-3437-9\_1. URL: [https://doi.org/10.1007/978-1-4757-3437-9\\_1](https://doi.org/10.1007/978-1-4757-3437-9_1).
- [30] Felix Draxler, Yang Meng, Kai Nelson, Lukas Laskowski, Yibo Yang, Theofanis Karaletsos, and Stephan Mandt. “Transformers for Mixed-type Event Sequences”. In: *The Thirty-ninth Annual Conference on Neural Information Processing Systems*. 2025. URL: <https://openreview.net/forum?id=MtwsRjPZhf>.
- [31] Nan Du, Hanjun Dai, Rakshit Trivedi, Utkarsh Upadhyay, Manuel Gomez-Rodriguez, and Le Song. “Recurrent Marked Temporal Point Processes: Embedding Event History to Vector”. In: *Proceedings of the 22nd ACM SIGKDD International Conference on Knowledge Discovery and Data Mining*. KDD ’16. New York, NY, USA: Association for Computing Machinery, 2016, pp. 1555–1564. ISBN: 9781450342322. DOI: 10.1145/2939672.2939875. URL: <https://doi.org/10.1145/2939672.2939875>.
- [32] Hao Duong Le, Xin Xia, and Zhang Chen. “Multi-Agent Causal Discovery Using Large Language Models”. In: *arXiv e-prints*, arXiv:2407.15073 (July 2024), arXiv:2407.15073. DOI: 10.48550/arXiv.2407.15073. arXiv: 2407.15073 [cs.AI].
- [33] Ellery Eells. *Probabilistic Causality*. Cambridge Studies in Probability, Induction and Decision Theory. Cambridge University Press, 1991.

- [34] Angela Fan, Mike Lewis, and Yann Dauphin. “Hierarchical Neural Story Generation”. In: *Proceedings of the 56th Annual Meeting of the Association for Computational Linguistics (Volume 1: Long Papers)*. Ed. by Iryna Gurevych and Yusuke Miyao. Melbourne, Australia: Association for Computational Linguistics, July 2018, pp. 889–898. DOI: 10.18653/v1/P18-1082. URL: <https://aclanthology.org/P18-1082/>.
- [35] Branden Fitelson and Christopher Hitchcock. “Probabilistic Measures of Causal Strength”. In: *Causality in the Sciences* (Jan. 2010). DOI: 10.1093/acprof:oso/9780199574131.003.0029.
- [36] Holger Fröhlich and Gunnar W. Klau. “Reconstructing Consensus Bayesian Network Structures with Application to Learning Molecular Interaction Networks”. In: *German Conference on Bioinformatics 2013*. Ed. by Tim Beißbarth, Martin Kollmar, Andreas Leha, Burkhard Morgenstern, Anne-Kathrin Schultz, Stephan Waack, and Edgar Wingender. Vol. 34. Open Access Series in Informatics (OASICS). Dagstuhl, Germany: Schloss Dagstuhl – Leibniz-Zentrum für Informatik, 2013, pp. 46–55. ISBN: 978-3-939897-59-0. DOI: 10.4230/OASICS.GCB.2013.46. URL: <https://drops.dagstuhl.de/entities/document/10.4230/OASICS.GCB.2013.46>.
- [37] Tian Gao and Qiang Ji. “Local Causal Discovery of Direct Causes and Effects”. In: *Advances in Neural Information Processing Systems*. Ed. by C. Cortes, N. Lawrence, D. Lee, M. Sugiyama, and R. Garnett. Vol. 28. Curran Associates, Inc., 2015. URL: [https://proceedings.neurips.cc/paper\\_files/paper/2015/file/fcdf25d6e191893e705819b177cddea0-Paper.pdf](https://proceedings.neurips.cc/paper_files/paper/2015/file/fcdf25d6e191893e705819b177cddea0-Paper.pdf).
- [38] Tian Gao, Dharmashankar Subramanian, Karthikeyan Shanmugam, Debarun Bhattacharjya, and Nicholas Mattei. “A Multi-Channel Neural Graphical Event Model with Negative Evidence”. In: *Proceedings of the AAAI Conference on Artificial Intelligence* 34 (Apr. 2020), pp. 3946–3953. DOI: 10.1609/aaai.v34i04.5810.
- [39] Sergio Garrido, Stanislav Borysov, Jeppe Rich, and Francisco Pereira. “Estimating causal effects with the neural autoregressive density estimator”. In: *Journal of Causal Inference* 9.1 (2021), pp. 211–228. DOI: doi:10.1515/jci-2020-0007. URL: <https://doi.org/10.1515/jci-2020-0007>.
- [40] Jinwoo Go and Tobin Isaac. “Robust Expected Information Gain for Optimal Bayesian Experimental Design Using Ambiguity Sets”. In: *The 38th Conference on Uncertainty in Artificial Intelligence*. 2022. URL: <https://openreview.net/forum?id=HU9Ix08oqlc>.
- [41] Chang Gong, Chuzhe Zhang, Di Yao, Jingping Bi, Wenbin Li, and YongJun Xu. “Causal Discovery from Temporal Data: An Overview and New Perspectives”. In: *ACM Comput. Surv.* 57.4 (Dec. 2024). ISSN: 0360-0300. DOI: 10.1145/3705297. URL: <https://doi.org/10.1145/3705297>.

## Bibliography

- [42] Ian Goodfellow, Yoshua Bengio, and Aaron Courville. *Deep learning*. Vol. 1. MIT Press, 2016.
- [43] Ian J. Goodfellow, Mehdi Mirza, Xia Da, Aaron C. Courville, and Yoshua Bengio. “An Empirical Investigation of Catastrophic Forgetting in Gradient-Based Neural Networks”. In: *CoRR* abs/1312.6211 (2013). URL: <https://api.semanticscholar.org/CorpusID:12730344>.
- [44] C W J Granger. “Investigating Causal Relations by Econometric Models and Cross-Spectral Methods”. In: *Econometrica* 37.3 (July 1969), pp. 424–438. URL: <https://ideas.repec.org/a/ect/emetrp/v37y1969i3p424-38.html>.
- [45] Michael Greenwald and Sanjeev Khanna. “Space-efficient online computation of quantile summaries”. In: *SIGMOD Rec.* 30.2 (May 2001), pp. 58–66. ISSN: 0163-5808. DOI: 10.1145/376284.375670. URL: <https://doi.org/10.1145/376284.375670>.
- [46] Peter Grunwald. *A tutorial introduction to the minimum description length principle*. 2004. arXiv: math/0406077 [math.ST]. URL: <https://arxiv.org/abs/math/0406077>.
- [47] Xianjie Guo, Kui Yu, Lin Liu, and Jiuyong Li. “FedCSL: A Scalable and Accurate Approach to Federated Causal Structure Learning”. In: *Proceedings of the AAAI Conference on Artificial Intelligence* 38.11 (Mar. 2024), pp. 12235–12243. DOI: 10.1609/aaai.v38i11.29113. URL: <https://ojs.aaai.org/index.php/AAAI/article/view/29113>.
- [48] Ishansh Gupta, Adriana Martinez, Sergio Correa, and Hendro Wicaksono. “A comparative assessment of causal machine learning and traditional methods for enhancing supply chain resiliency and efficiency in the automotive industry”. In: *Supply Chain Analytics* 10 (2025), p. 100116. ISSN: 2949-8635. DOI: <https://doi.org/10.1016/j.sca.2025.100116>. URL: <https://www.sciencedirect.com/science/article/pii/S2949863525000160>.
- [49] Abdul Basit Hafeez, Eduardo Alonso, and Atif Riaz. “DTC-TranGru: Improving the performance of the next-DTC Prediction Model with Transformer and GRU”. In: *Proceedings of the 39th ACM/SIGAPP Symposium on Applied Computing* (2024). URL: <https://api.semanticscholar.org/CorpusID:269951398>.
- [50] Abdul Basit Hafeez, Eduardo Alonso, and Aram Ter-Sarkisov. “Towards Sequential Multivariate Fault Prediction for Vehicular Predictive Maintenance”. In: *2021 20th IEEE International Conference on Machine Learning and Applications (ICMLA)*. 2021, pp. 1016–1021. DOI: 10.1109/ICMLA52953.2021.00167.
- [51] Xiao Han, Saima Absar, Lu Zhang, and Shuhan Yuan. “Root Cause Analysis of Anomalies in Multivariate Time Series through Granger Causal Discovery”. In: *The Thirteenth International Conference on Learning Representations*. 2025. URL: <https://openreview.net/forum?id=k38Th3x4d9>.

- [52] Uzma Hasan, Emam Hossain, and Md Osman Gani. “A Survey on Causal Discovery Methods for I.I.D. and Time Series Data”. In: *Transactions on Machine Learning Research* (2023). Survey Certification. ISSN: 2835-8856. URL: <https://openreview.net/forum?id=YdMrdhGx9y>.
- [53] ALAN G. Hawkes. “Spectra of some self-exciting and mutually exciting point processes”. In: *Biometrika* 58.1 (Apr. 1971), pp. 83–90. ISSN: 0006-3444. DOI: 10.1093/biomet/58.1.83. eprint: <https://academic.oup.com/biomet/article-pdf/58/1/83/602628/58-1-83.pdf>. URL: <https://doi.org/10.1093/biomet/58.1.83>.
- [54] Kaiming He, Xiangyu Zhang, Shaoqing Ren, and Jian Sun. “Deep Residual Learning for Image Recognition”. In: *Proceedings of 2016 IEEE Conference on Computer Vision and Pattern Recognition*. CVPR ’16. Las Vegas, NV, USA: IEEE, June 2016, pp. 770–778. DOI: 10.1109/CVPR.2016.90. URL: <http://ieeexplore.ieee.org/document/7780459>.
- [55] Pengcheng He, Xiaodong Liu, Jianfeng Gao, and Weizhu Chen. “DeBERTa: Decoding-enhanced BERT with Disentangled Attention”. In: *International Conference on Learning Representations*. 2021. URL: <https://openreview.net/forum?id=XPZLaotutsD>.
- [56] Rui He, Zhigang Tian, and Mingjian Zuo. “Machine prognostics under varying operating conditions based on state-space and neural network modeling”. In: *Mechanical Systems and Signal Processing* 182 (2023), p. 109598. ISSN: 0888-3270. DOI: <https://doi.org/10.1016/j.ymsp.2022.109598>. URL: <https://www.sciencedirect.com/science/article/pii/S0888327022006896>.
- [57] Weijie He, Xiaohao Mao, Chao Ma, Yu Huang, José Miguel Hernández-Lobato, and Ting Chen. “BSODA: A Bipartite Scalable Framework for Online Disease Diagnosis”. In: *Proceedings of the ACM Web Conference 2022*. WWW ’22. New York, NY, USA: Association for Computing Machinery, 2022, pp. 2511–2521. ISBN: 9781450390965. DOI: 10.1145/3485447.3512123. URL: <https://doi.org/10.1145/3485447.3512123>.
- [58] Sepp Hochreiter and Jürgen Schmidhuber. “Long Short-Term Memory”. In: *Neural Comput.* 9.8 (Nov. 1997), pp. 1735–1780. ISSN: 0899-7667. DOI: 10.1162/neco.1997.9.8.1735. URL: <https://doi.org/10.1162/neco.1997.9.8.1735>.
- [59] Jennifer A. Hoeting, David Madigan, Adrian E. Raftery, and Chris T. Volinsky. “Bayesian model averaging: a tutorial”. In: *Statistical Science* 14.4 (1999), pp. 382–417.
- [60] Ari Holtzman, Jan Buys, Li Du, Maxwell Forbes, and Yejin Choi. “The Curious Case of Neural Text Degeneration”. In: *International Conference on Learning Representations*. 2020. URL: <https://openreview.net/forum?id=rygGQyrFvH>.

## Bibliography

- [61] Kexin Huang, Serena Zhang, Hanchen Wang, Yuanhao Qu, Yingzhou Lu, Yusuf Roohani, Ryan Li, Lin Qiu, Junze Zhang, Yin Di, Shruti Marwaha, Jennefer Carter, Xin Zhou, Matthew Wheeler, Jon Bernstein, Mengdi Wang, Peng He, Jingtian Zhou, Michael Snyder, and Jure Leskovec. *Biomni: A General-Purpose Biomedical AI Agent*. June 2025. DOI: 10.1101/2025.05.30.656746.
- [62] Aapo Hyvärinen, Kun Zhang, Shohei Shimizu, and Patrik O. Hoyer. “Estimation of a Structural Vector Autoregression Model Using Non-Gaussianity”. In: *Journal of Machine Learning Research* 11.56 (2010), pp. 1709–1731. URL: <http://jmlr.org/papers/v11/hyvarinen10a.html>.
- [63] Daniel Jiwoong Im, Kevin Zhang, Nakul Verma, and Kyunghyun Cho. *Using Deep Autoregressive Models as Causal Inference Engines*. 2024. arXiv: 2409.18581 [cs.LG]. URL: <https://arxiv.org/abs/2409.18581>.
- [64] Sergey Ioffe and Christian Szegedy. “Batch normalization: accelerating deep network training by reducing internal covariate shift”. In: *Proceedings of the 32nd International Conference on International Conference on Machine Learning - Volume 37*. ICML’15. Lille, France: JMLR.org, 2015, pp. 448–456.
- [65] Aryan Jadon, Avinash Patil, and Shruti Jadon. “A Comprehensive Survey of Regression Based Loss Functions for Time Series Forecasting”. In: *ArXiv abs/2211.02989* (2022). URL: <https://api.semanticscholar.org/CorpusID:253383974>.
- [66] Amirkasra Jalaldoust, Katerina Hlaváčková-Schindler, and Claudia Plant. “Causal Discovery in Hawkes Processes by Minimum Description Length”. In: *Thirty-Sixth AAAI Conference on Artificial Intelligence; Thirty-Fourth Conference on Innovative Applications of Artificial Intelligence; The Twelveth Symposium on Educational Advances in Artificial Intelligence*. Proceedings of the ... National Conference on Artificial Intelligence 6. AAAI Press, June 2022, pp. 6978–6987. ISBN: 978-1-57735-876-3. DOI: 10.48550/arXiv.2206.06124.
- [67] Dominik Janzing, David Balduzzi, Moritz Grosse-Wentrup, and Bernhard Schölkopf. “Quantifying causal influences”. In: *The Annals of Statistics* (Mar. 2012). DOI: 10.1214/13-AOS1145.
- [68] Emre Kiciman, Robert Ness, Amit Sharma, and Chenhao Tan. “Causal Reasoning and Large Language Models: Opening a New Frontier for Causality”. In: *Transactions on Machine Learning Research* (2024). Featured Certification. ISSN: 2835-8856. URL: <https://openreview.net/forum?id=mqoxLkX210>.
- [69] D. Koller and N. Friedman. *Probabilistic Graphical Models: Principles and Techniques*. Adaptive computation and machine learning. MIT Press, 2009. ISBN: 9780262013192. URL: <https://books.google.co.in/books?id=7dzpHCHzNQ4C>.
- [70] Alexander Kraskov, Harald Stögbauer, and Peter Grassberger. “Estimating mutual information”. In: *Phys. Rev. E* 69 (6 June 2004), p. 066138. DOI: 10.1103/PhysRevE.69.066138. URL: <https://link.aps.org/doi/10.1103/PhysRevE.69.066138>.

- [71] Jorge D. Laborda, Pablo Torrijos, José M. Puerta, and José A. Gámez. “A Ring-Based Distributed Algorithm for Learning High-Dimensional Bayesian Networks”. In: *Symbolic and Quantitative Approaches to Reasoning with Uncertainty: 17th European Conference, ECSQARU 2023, Arras, France, September 19–22, 2023, Proceedings*. Berlin, Heidelberg: Springer-Verlag, 2023, pp. 123–135. ISBN: 978-3-031-45607-7. DOI: [10.1007/978-3-031-45608-4\\_10](https://doi.org/10.1007/978-3-031-45608-4_10). URL: [https://doi.org/10.1007/978-3-031-45608-4\\_10](https://doi.org/10.1007/978-3-031-45608-4_10).
- [72] Helge Langseth and Luigi Portinale. “Bayesian networks in reliability”. In: *Reliability Engineering & System Safety* 92.1 (2007), pp. 92–108. ISSN: 0951-8320. DOI: <https://doi.org/10.1016/j.res.2005.11.037>. URL: <https://www.sciencedirect.com/science/article/pii/S0951832005001985>.
- [73] Patrick J. Laub, Young Lee, Philip K. Pollett, and Thomas Taimre. “Hawkes Models and Their Applications”. In: *Annual Review of Statistics and Its Application* 12. Volume 12, 2025 (2025), pp. 233–258. ISSN: 2326-831X. DOI: <https://doi.org/10.1146/annurev-statistics-112723-034304>. URL: <https://www.annualreviews.org/content/journals/10.1146/annurev-statistics-112723-034304>.
- [74] Patrick Lewis, Ethan Perez, Aleksandra Piktus, Fabio Petroni, Vladimir Karpukhin, Naman Goyal, Heinrich Küttler, Mike Lewis, Wen-tau Yih, Tim Rocktäschel, Sebastian Riedel, and Douwe Kiela. “Retrieval-augmented generation for knowledge-intensive NLP tasks”. In: *Proceedings of the 34th International Conference on Neural Information Processing Systems*. NIPS ’20. Red Hook, NY, USA: Curran Associates Inc., 2020. ISBN: 9781713829546.
- [75] Jing Li, Botong Wu, Xinwei Sun, and Yizhou Wang. “Causal Hidden Markov Model for Time Series Disease Forecasting”. In: *2021 IEEE/CVF Conference on Computer Vision and Pattern Recognition (CVPR) (2021)*, pp. 12100–12109. URL: <https://api.semanticscholar.org/CorpusID:232417085>.
- [76] Jundong Li, Kewei Cheng, Suhang Wang, Fred Morstatter, Robert P. Trevino, Jiliang Tang, and Huan Liu. “Feature Selection: A Data Perspective”. In: *CoRR* abs/1601.07996 (2016). arXiv: 1601.07996. URL: <http://arxiv.org/abs/1601.07996>.
- [77] Zhuoqun Li and Mingxuan Sun. “Sparse Transformer Hawkes Process for Long Event Sequences”. In: *Machine Learning and Knowledge Discovery in Databases: Research Track*. Ed. by Danai Koutra, Claudia Plant, Manuel Gomez Rodriguez, Elena Baralis, and Francesco Bonchi. Cham: Springer Nature Switzerland, 2023, pp. 172–188. ISBN: 978-3-031-43424-2.
- [78] Stephanie Long, Tibor Schuster, and Alexandre Piché. “Can Large Language Models Build Causal Graphs?”. In: *NeurIPS 2022 Workshop on Causality for Real-world Impact*. 2022. URL: <https://openreview.net/forum?id=LQQoJGw8JD1>.

## Bibliography

- [79] Ilya Loshchilov and Frank Hutter. “Decoupled Weight Decay Regularization”. In: *International Conference on Learning Representations*. 2019. URL: <https://openreview.net/forum?id=Bkg6RiCqY7>.
- [80] Sindy Löwe, David Madras, Richard Zemel, and Max Welling. “Amortized Causal Discovery: Learning to Infer Causal Graphs from Time-Series Data”. In: *Proceedings of the First Conference on Causal Learning and Reasoning*. Ed. by Bernhard Schölkopf, Caroline Uhler, and Kun Zhang. Vol. 177. Proceedings of Machine Learning Research. PMLR, 2022, pp. 509–525. URL: <https://proceedings.mlr.press/v177/lowe22a.html>.
- [81] Jiasen Lu, Dhruv Batra, Devi Parikh, and Stefan Lee. “ViLBERT: pretraining task-agnostic visiolinguistic representations for vision-and-language tasks”. In: *Proceedings of the 33rd International Conference on Neural Information Processing Systems*. Red Hook, NY, USA: Curran Associates Inc., 2019.
- [82] Scott M. Lundberg and Su-In Lee. “A unified approach to interpreting model predictions”. In: *Proceedings of the 31st International Conference on Neural Information Processing Systems*. NIPS’17. Red Hook, NY, USA: Curran Associates Inc., 2017, pp. 4768–4777. ISBN: 9781510860964.
- [83] Qian Luo, Lin Zhang, Zhiwei Xing, Huan Xia, and Zhao-Xin Chen. “Causal Discovery of Flight Service Process Based on Event Sequence”. In: *Journal of Advanced Transportation* 2021.1 (2021), p. 2869521. DOI: <https://doi.org/10.1155/2021/2869521>. eprint: <https://onlinelibrary.wiley.com/doi/pdf/10.1155/2021/2869521>. URL: <https://onlinelibrary.wiley.com/doi/abs/10.1155/2021/2869521>.
- [84] Lin Ma, Liang Hu, Yonghao Li, Weiping Ding, and Wanfu Gao. “MI-MCF: A Mutual Information-Based Multilabel Causal Feature Selection”. In: *IEEE Transactions on Neural Networks and Learning Systems* (2025), pp. 1–15. DOI: 10.1109/TNNLS.2025.3556128.
- [85] Liam Daly Manocchio, Siamak Layeghy, Wai Weng Lo, Gayan K. Kulatilleke, Mohanad Sarhan, and Marius Portmann. “FlowTransformer: A transformer framework for flow-based network intrusion detection systems”. In: *Expert Systems with Applications* 241 (2024), p. 122564. ISSN: 0957-4174. DOI: <https://doi.org/10.1016/j.eswa.2023.122564>. URL: <https://www.sciencedirect.com/science/article/pii/S095741742303066X>.
- [86] Yasmin Mansy, Nourhan Ehab, and Amr ElMougy. “The Problem of Many Vehicles: An Explainable System for Autonomous Multi-agent Accidents”. In: *Intelligent Systems and Applications*. Ed. by Kohei Arai. Cham: Springer Nature Switzerland, 2024, pp. 38–58. ISBN: 978-3-031-66431-1.
- [87] Hugo Math. *seq2cause: A Python Package for Causal Discovery in Sequences from Autoregressive Models*. <https://pypi.org/project/seq2cause/>. Version 0.1.2. 2026.

- [88] Hugo Math and Rainer Lienhart. “Context-Informed Sequence Classification: A Multimodal Approach to Vehicle Diagnostics”. In: *1st ICLR Workshop on Time Series in the Age of Large Models*. 2026. URL: <https://openreview.net/forum?id=G4iAE9x0pb>.
- [89] Hugo Math and Rainer Lienhart. “Towards Practical Multi-label Causal Discovery in High-Dimensional Event Sequences via One-Shot Graph Aggregation”. In: *NeurIPS 2025 Workshop on Structured Probabilistic Inference & Generative Modeling*. 2025. URL: <https://openreview.net/forum?id=1HZfpuDVeW>.
- [90] Hugo Math and Rainer Lienhart. *TRACE: Scalable Amortized Causal Discovery from Single Sequences via Autoregressive Density Estimation*. 2026. arXiv: 2602.01135 [cs.LG]. URL: <https://arxiv.org/abs/2602.01135>.
- [91] Hugo Math, Rainer Lienhart, and Robin Schön. “Harnessing Event Sensory Data for Error Pattern Prediction in Vehicles: A Language Model Approach”. In: *Proceedings of the AAAI Conference on Artificial Intelligence* 39.18 (Apr. 2025), pp. 19423–19431. DOI: 10.1609/aaai.v39i18.34138. URL: <https://ojs.aaai.org/index.php/AAAI/article/view/34138>.
- [92] Hugo Math, Julian Lorenz, and Rainer Lienhart. “Neuro-Symbolic Rule Discovery: Empowering LLMs with Causality for Vehicle Diagnostics”. In: *ICLR 2026 Workshop on Logical Reasoning of Large Language Models*. 2026. URL: <https://openreview.net/forum?id=M5ZszfsJxm>.
- [93] Hugo Math, Robin Schön, and Rainer Lienhart. “One-Shot Multi-Label Causal Discovery in High-Dimensional Event Sequences”. In: *NeurIPS 2025 Workshop on CauScien: Uncovering Causality in Science*. 2025. URL: <https://openreview.net/forum?id=z7NT8vGWC2>.
- [94] Aaron Meurer, Christopher P. Smith, Mateusz Paprocki, Ondřej Čertík, Sergey B. Kirpichev, Matthew Rocklin, AMiT Kumar, Sergiu Ivanov, Jason K. Moore, Sartaj Singh, Thilina Rathnayake, Sean Vig, Brian E. Granger, Richard P. Muller, Francesco Bonazzi, Harsh Gupta, Shivam Vats, Fredrik Johansson, Fabian Pedregosa, Matthew J. Curry, Andy R. Terrel, Štěpán Roučka, Ashutosh Saboo, Isuru Fernando, Sumith Kulal, Robert Cimrman, and Anthony Scopatz. “SymPy: symbolic computing in Python”. In: *PeerJ Computer Science* 3 (Jan. 2017), e103. ISSN: 2376-5992. DOI: 10.7717/peerj-cs.103. URL: <https://doi.org/10.7717/peerj-cs.103>.
- [95] Seyed Iman Mirzadeh, Keivan Alizadeh, Hooman Shahrokhi, Oncel Tuzel, Samy Bengio, and Mehrdad Farajtabar. “GSM-Symbolic: Understanding the Limitations of Mathematical Reasoning in Large Language Models”. In: *The Thirteenth International Conference on Learning Representations*. 2025. URL: <https://openreview.net/forum?id=AjXkRZIVjB>.

## Bibliography

- [96] Farhad Moghimifar, Afshin Rahimi, Mahsa Baktashmotlagh, and Xue Li. “Learning Causal Bayesian Networks from Text”. In: *Proceedings of the 18th Annual Workshop of the Australasian Language Technology Association*. Ed. by Maria Kim, Daniel Beck, and Meladel Mistica. Virtual Workshop: Australasian Language Technology Association, Dec. 2020, pp. 81–85. URL: <https://aclanthology.org/2020.alta-1.9/>.
- [97] Ehsan Mokhtarian, Sina Akbari, AmirEmad Ghassami, and Negar Kiyavash. “A Recursive Markov Boundary-Based Approach to Causal Structure Learning”. In: *Proceedings of The KDD’21 Workshop on Causal Discovery*. Ed. by Thuc Duy Le, Jiuyong Li, Greg Cooper, Sofia Triantafyllou, Elias Bareinboim, Huan Liu, and Negar Kiyavash. Vol. 150. Proceedings of Machine Learning Research. PMLR, Aug. 2021, pp. 26–54. URL: <https://proceedings.mlr.press/v150/mokhtarian21a.html>.
- [98] Salama A. Mostafa, Aida Mustapha, Ahmed Abdulbasit Hazeem, Shihab Hamad Khaleefah, and Mazin Abed Mohammed. “An Agent-Based Inference Engine for Efficient and Reliable Automated Car Failure Diagnosis Assistance”. In: *IEEE Access* 6 (2018), pp. 8322–8331. DOI: 10.1109/ACCESS.2018.2803051.
- [99] Arsha Nagrani, Shan Yang, Anurag Arnab, Aren Jansen, Cordelia Schmid, and Chen Sun. “Attention bottlenecks for multimodal fusion”. In: *Proceedings of the 35th International Conference on Neural Information Processing Systems*. NIPS ’21. Red Hook, NY, USA: Curran Associates Inc., 2024. ISBN: 9781713845393.
- [100] Meike Nauta, Doina Bucur, and Christin Seifert. “Causal Discovery with Attention-Based Convolutional Neural Networks”. English. In: *Machine Learning and Knowledge Extraction* 1.1 (Jan. 2019), pp. 312–340. ISSN: 2504-4990. DOI: 10.3390/make1010019.
- [101] Ignavier Ng, AmirEmad Ghassami, and Kun Zhang. “On the role of sparsity and DAG constraints for learning linear DAGs”. In: *Proceedings of the 34th International Conference on Neural Information Processing Systems*. NIPS ’20. Red Hook, NY, USA: Curran Associates Inc., 2020. ISBN: 9781713829546.
- [102] Toan Q. Nguyen and Julian Salazar. “Transformers without Tears: Improving the Normalization of Self-Attention”. In: *Proceedings of the 16th International Conference on Spoken Language Translation*. Ed. by Jan Niehues, Rolando Cattoni, Sebastian Stüker, Matteo Negri, Marco Turchi, Thanh-Le Ha, Elizabeth Salesky, Ramon Sanabria, Loic Barrault, Lucia Specia, and Marcello Federico. Hong Kong: Association for Computational Linguistics, Nov. 2019. URL: <https://aclanthology.org/2019.iwslt-1.17>.
- [103] Eshaan Nichani, Alex Damian, and Jason D. Lee. “How transformers learn causal structure with gradient descent”. In: *Proceedings of the 41st International Conference on Machine Learning*. ICML’24. Vienna, Austria: JMLR.org, 2024.

- [104] Shen Nie, Fengqi Zhu, Zebin You, Xiaolu Zhang, Jingyang Ou, Jun Hu, JUN ZHOU, Yankai Lin, Ji-Rong Wen, and Chongxuan Li. “Large Language Diffusion Models”. In: *The Thirty-ninth Annual Conference on Neural Information Processing Systems*. 2025. URL: <https://openreview.net/forum?id=KnqiC0znVF>.
- [105] Siddhartha Nuthakki, Sunil Neela, Judy W. Gichoya, and Saptarshi Purkayastha. “Natural language processing of MIMIC-III clinical notes for identifying diagnosis and procedures with neural networks”. In: *CoRR* abs/1912.12397 (2019). arXiv: 1912.12397. URL: <http://arxiv.org/abs/1912.12397>.
- [106] Yoshihiko Ogata et al. “Statistical studies of the occurrence of small earthquakes: I. A point process model for earthquake sequences”. In: *Annals of the Institute of Statistical Mathematics* 30.1 (1978), pp. 379–395.
- [107] OpenAI. “GPT-4 Technical Report”. In: *ArXiv* abs/2303.08774 (2023). URL: <https://arxiv.org/abs/2303.08774>.
- [108] Juri Opitz. “A Closer Look at Classification Evaluation Metrics and a Critical Reflection of Common Evaluation Practice”. In: *Transactions of the Association for Computational Linguistics* 12 (June 2024), pp. 820–836. ISSN: 2307-387X. DOI: 10.1162/tacl\_a\_00675. eprint: [https://direct.mit.edu/tacl/article-pdf/doi/10.1162/tacl\\_a\\_00675/2465598/tacl\\_a\\_00675.pdf](https://direct.mit.edu/tacl/article-pdf/doi/10.1162/tacl_a_00675/2465598/tacl_a_00675.pdf). URL: [https://doi.org/10.1162/tacl\\_a\\_00675](https://doi.org/10.1162/tacl_a_00675).
- [109] Roxana Pamfil, Nisara Sriwattanaworachai, Shaan Desai, Philip Pilgerstorfer, Konstantinos Georgatzis, Paul Beaumont, and Bryon Aragam. “DYNOTEARS: Structure Learning from Time-Series Data”. In: *Proceedings of the Twenty Third International Conference on Artificial Intelligence and Statistics*. Ed. by Silvia Chiappa and Roberto Calandra. Vol. 108. Proceedings of Machine Learning Research. PMLR, 2020, pp. 1595–1605. URL: <https://proceedings.mlr.press/v108/pamfil120a.html>.
- [110] Adam Paszke, Sam Gross, Francisco Massa, Adam Lerer, James Bradbury, Gregory Chanan, Trevor Killeen, Zeming Lin, Natalia Gimelshein, Luca Antiga, Alban Desmaison, Andreas Köpf, Edward Yang, Zach DeVito, Martin Raison, Alykhan Tejani, Sasank Chilamkurthy, Benoit Steiner, Lu Fang, Junjie Bai, and Soumith Chintala. “PyTorch: an imperative style, high-performance deep learning library”. In: *Proceedings of the 33rd International Conference on Neural Information Processing Systems*. Red Hook, NY, USA: Curran Associates Inc., 2019.
- [111] Kevin Patel. “Agentic AI for Self-Healing Production Lines: Autonomous Root Cause Analysis and Correction”. In: *Journal of Information Systems Engineering and Management* 10 (June 2025), pp. 661–682. DOI: 10.52783/jisem.v10i52s.10772.
- [112] Jose M. Peña. “Finding consensus Bayesian network structures”. In: *J. Artif. Int. Res.* 42.1 (Sept. 2011), pp. 661–687. ISSN: 1076-9757.
- [113] Judea Pearl. *Causality: Models, Reasoning and Inference*. 2nd. USA: Cambridge University Press, 2009. ISBN: 052189560X.

## Bibliography

- [114] Judea Pearl. *Probabilistic Reasoning in Intelligent Systems: Networks of Plausible Inference*. San Francisco, CA, USA: Morgan Kaufmann Publishers Inc., 1988. ISBN: 1558604790.
- [115] Ben Peters, Vlad Niculae, and André F. T. Martins. “Sparse Sequence-to-Sequence Models”. In: *Proceedings of the 57th Annual Meeting of the Association for Computational Linguistics*. Ed. by Anna Korhonen, David Traum, and Lluís Màrquez. Florence, Italy: Association for Computational Linguistics, July 2019, pp. 1504–1519. DOI: 10.18653/v1/P19-1146. URL: <https://aclanthology.org/P19-1146/>.
- [116] Parivash Pirasteh, Slawomir Nowaczyk, Sepideh Pashami, Magnus Löwenadler, Klas Thunberg, Henrik Ydreskog, and Peter Berck. “Interactive feature extraction for diagnostic trouble codes in predictive maintenance: A case study from automotive domain”. In: *Proceedings of the Workshop on Interactive Data Mining. WIDM’19*. New York, NY, USA: Association for Computing Machinery, 2019. ISBN: 9781450362962. DOI: 10.1145/3304079.3310288. URL: <https://doi.org/10.1145/3304079.3310288>.
- [117] José M. Puerta, Juan A. Aledo, José A. Gámez, and Jorge D. Laborda. “Efficient and accurate structural fusion of Bayesian networks”. In: *Information Fusion* 66 (2021), pp. 155–169. ISSN: 1566-2535. DOI: <https://doi.org/10.1016/j.inffus.2020.09.003>. URL: <https://www.sciencedirect.com/science/article/pii/S156625352030364X>.
- [118] Jie Qiao, Ruichu Cai, Siyu Wu, Yu Xiang, Keli Zhang, and Zhifeng Hao. “Structural Hawkes processes for learning causal structure from discrete-time event sequences”. In: *Proceedings of the Thirty-Second International Joint Conference on Artificial Intelligence. IJCAI ’23*. Macao, P.R.China, 2023. ISBN: 978-1-956792-03-4. DOI: 10.24963/ijcai.2023/633. URL: <https://doi.org/10.24963/ijcai.2023/633>.
- [119] J. R. Quinlan. “Induction of Decision Trees”. In: *Machine Learning* 1 (1986), pp. 81–106.
- [120] Alec Radford, Jong Wook Kim, Chris Hallacy, Aditya Ramesh, Gabriel Goh, Sandhini Agarwal, Girish Sastry, Amanda Askell, Pamela Mishkin, Jack Clark, Gretchen Krueger, and Ilya Sutskever. “Learning Transferable Visual Models From Natural Language Supervision”. In: *Proceedings of the 38th International Conference on Machine Learning*. Ed. by Marina Meila and Tong Zhang. Vol. 139. Proceedings of Machine Learning Research. PMLR, July 2021, pp. 8748–8763. URL: <https://proceedings.mlr.press/v139/radford21a.html>.
- [121] Alec Radford and Karthik Narasimhan. *Improving Language Understanding by Generative Pre-Training*. 2018. URL: <https://api.semanticscholar.org/CorpusID:49313245>.

- [122] Laila Rasmy, Yang Xiang, Ziqian Xie, Cui Tao, and Degui Zhi. “Med-BERT: pretrained contextualized embeddings on large-scale structured electronic health records for disease prediction”. In: *NPJ Digital Medicine* 4 (2020). URL: <https://api.semanticscholar.org/CorpusID:218889776>.
- [123] J. Rissanen. “Paper: Modeling by shortest data description”. In: *Automatica* 14.5 (Sept. 1978), pp. 465–471. ISSN: 0005-1098. DOI: 10.1016/0005-1098(78)90005-5. URL: [https://doi.org/10.1016/0005-1098\(78\)90005-5](https://doi.org/10.1016/0005-1098(78)90005-5).
- [124] Raanan Yehezkel Rohekar, Yaniv Gurwicz, and Shami Nisimov. “Causal Interpretation of Self-Attention in Pre-Trained Transformers”. In: *Thirty-seventh Conference on Neural Information Processing Systems*. 2023. URL: <https://openreview.net/forum?id=DS4rKySlYC>.
- [125] Jakob Runge, Peer Nowack, Marlene Kretschmer, Seth Flaxman, and Dino Sejdinovic. “Detecting and quantifying causal associations in large nonlinear time series datasets”. In: *Science Advances* 5.11 (2019), eaau4996. DOI: 10.1126/sciadv.aau4996. eprint: <https://www.science.org/doi/pdf/10.1126/sciadv.aau4996>. URL: <https://www.science.org/doi/abs/10.1126/sciadv.aau4996>.
- [126] José del Sagrado and Serafin Moral. “Qualitative Aggregation of Bayesian Networks”. In: *Data Fusion and Perception*. Ed. by Giacomo Della Riccia, Hans-Joachim Lenz, and Rudolf Kruse. Vienna: Springer Vienna, 2001, pp. 91–108. ISBN: 978-3-7091-2580-9. DOI: 10.1007/978-3-7091-2580-9\_5. URL: [https://doi.org/10.1007/978-3-7091-2580-9\\_5](https://doi.org/10.1007/978-3-7091-2580-9_5).
- [127] Subham Sekhar Sahoo, Marianne Arriola, Aaron Gokaslan, Edgar Mariano Marroquin, Alexander M Rush, Yair Schiff, Justin T Chiu, and Volodymyr Kuleshov. “Simple and Effective Masked Diffusion Language Models”. In: *The Thirty-eighth Annual Conference on Neural Information Processing Systems*. 2024. URL: <https://openreview.net/forum?id=L4uaAR4ArM>.
- [128] Ranjan Sapkota, Konstantinos Roumeliotis, and Manoj Karkee. *AI Agents vs. Agentic AI: A Conceptual Taxonomy, Applications and Challenges*. May 2025. DOI: 10.48550/arXiv.2505.10468.
- [129] Claude Elwood Shannon. “Prediction and Entropy of Printed English”. In: *Bell System Technical Journal* 30 (Jan. 1951), pp. 50–64. URL: <http://languagelog.ldc.upenn.edu/myl/Shannon1950.pdf>.
- [130] Peter Shaw, Jakob Uszkoreit, and Ashish Vaswani. “Self-Attention with Relative Position Representations”. In: *Proceedings of the 2018 Conference of the North American Chapter of the Association for Computational Linguistics: Human Language Technologies, Volume 2 (Short Papers)*. Ed. by Marilyn Walker, Heng Ji, and Amanda Stent. New Orleans, Louisiana: Association for Computational Linguistics, June 2018, pp. 464–468. DOI: 10.18653/v1/N18-2074. URL: <https://aclanthology.org/N18-2074>.

## Bibliography

- [131] Oleksandr Shchur, Ali Caner Türkmen, Tim Januschowski, and Stephan Günemann. “Neural Temporal Point Processes: A Review”. In: *International Joint Conference on Artificial Intelligence*. 2021. URL: <https://api.semanticscholar.org/CorpusID:233181707>.
- [132] Benjamin Shickel, Brandon Silva, Tezcan Ozrazgat-Baslanti, Yuanfang Ren, Kia Khezeli, Ziyuan Guan, Patrick J. Tighe, Azra Bihorac, and Parisa Rashidi. “Multi-dimensional patient acuity estimation with longitudinal EHR tokenization and flexible transformer networks”. In: *Frontiers in Digital Health* 4 (2022). DOI: 10.3389/fdgth.2022.1029191. URL: <https://par.nsf.gov/biblio/10401752>.
- [133] Shohei Shimizu, Patrik O. Hoyer, Aapo Hyvärinen, and Antti Kerminen. “A Linear Non-Gaussian Acyclic Model for Causal Discovery”. In: *J. Mach. Learn. Res.* 7 (Dec. 2006), pp. 2003–2030. ISSN: 1532-4435.
- [134] Ali Shojaie and George Michailidis. “Discovering graphical Granger causality using the truncating lasso penalty”. In: *Bioinformatics* 26 (2010), pp. i517–i523. URL: <https://api.semanticscholar.org/CorpusID:388284>.
- [135] Xiao Shou, Tian Gao, Dharmashankar Subramanian, Debarun Bhattacharjya, and Kristin P. Bennett. “Concurrent Multi-Label Prediction in Event Streams”. In: *Proceedings of the AAAI Conference on Artificial Intelligence* 37.8 (June 2023), pp. 9820–9828. DOI: 10.1609/aaai.v37i8.26172. URL: <https://ojs.aaai.org/index.php/AAAI/article/view/26172>.
- [136] Xiao Shou, D. Subramanian, Debarun Bhattacharjya, Tian Gao, and Kristin P. Bennet. “Self-Supervised Contrastive Pre-Training for Multivariate Point Processes”. In: *ArXiv abs/2402.00987* (2024). URL: <https://api.semanticscholar.org/CorpusID:267406624>.
- [137] Avanti Shrikumar, Peyton Greenside, and Anshul Kundaje. “Learning Important Features Through Propagating Activation Differences”. In: *Proceedings of the 34th International Conference on Machine Learning*. Ed. by Doina Precup and Yee Whye Teh. Vol. 70. Proceedings of Machine Learning Research. PMLR, 2017, pp. 3145–3153. URL: <https://proceedings.mlr.press/v70/shrikumar17a.html>.
- [138] Ruben Sipos, Dmitriy Fradkin, Fabian Moerchen, and Zhuang Wang. “Log-based predictive maintenance”. In: *Proceedings of the 20th ACM SIGKDD International Conference on Knowledge Discovery and Data Mining*. KDD ’14. New York, NY, USA: Association for Computing Machinery, 2014, pp. 1867–1876. ISBN: 9781450329569. DOI: 10.1145/2623330.2623340. URL: <https://doi.org/10.1145/2623330.2623340>.
- [139] Peter Spirtes and Clark Glymour. “An Algorithm for Fast Recovery of Sparse Causal Graphs”. In: *Social Science Computer Review* 9.1 (1991), pp. 62–72. DOI: 10.1177/089443939100900106. eprint: <https://doi.org/10.1177/089443939100900106>. URL: <https://doi.org/10.1177/089443939100900106>.

- [140] Peter Spirtes, Clark Glymour, and Richard Scheines. “Causation, Prediction, and Search, 2nd Edition”. In: *Causation, Prediction, and Search (Second Edition)*. 2001. URL: <https://api.semanticscholar.org/CorpusID:124969922>.
- [141] Emma Steele and Allan Tucker. “Consensus and Meta-analysis regulatory networks for combining multiple microarray gene expression datasets”. In: *Journal of Biomedical Informatics* 41.6 (Dec. 2008), pp. 914–926. ISSN: 1532-0464. DOI: 10.1016/j.jbi.2008.01.011. URL: <https://doi.org/10.1016/j.jbi.2008.01.011>.
- [142] Jianlin Su, Murtadha Ahmed, Yu Lu, Shengfeng Pan, Wen Bo, and Yunfeng Liu. “RoFormer: Enhanced transformer with Rotary Position Embedding”. In: *Neurocomput.* 568.C (Mar. 2024). ISSN: 0925-2312. DOI: 10.1016/j.neucom.2023.127063. URL: <https://doi.org/10.1016/j.neucom.2023.127063>.
- [143] Ilya Sutskever, Oriol Vinyals, and Quoc V. Le. “Sequence to sequence learning with neural networks”. In: *Proceedings of the 28th International Conference on Neural Information Processing Systems - Volume 2*. NIPS’14. Montreal, Canada: MIT Press, 2014, pp. 3104–3112.
- [144] Hao Hao Tan and Mohit Bansal. “LXMERT: Learning Cross-Modality Encoder Representations from Transformers”. In: *Conference on Empirical Methods in Natural Language Processing*. 2019. URL: <https://api.semanticscholar.org/CorpusID:201103729>.
- [145] Pablo Torrijos, José M. Puerta, José A. Gámez, and Juan A. Aledo. *Informed Greedy Algorithm for Scalable Bayesian Network Fusion via Minimum Cut Analysis*. 2025. arXiv: 2504.00467 [cs.LG]. URL: <https://arxiv.org/abs/2504.00467>.
- [146] Hugo Touvron, Thibaut Lavril, Gautier Izacard, Xavier Martinet, Marie-Anne Lachaux, Timothée Lacroix, Baptiste Rozière, Naman Goyal, Eric Hambro, Faisal Azhar, Aurelien Rodriguez, Armand Joulin, Edouard Grave, and Guillaume Lample. *LLaMA: Open and Efficient Foundation Language Models*. 2023. arXiv: 2302.13971 [cs.CL]. URL: <https://arxiv.org/abs/2302.13971>.
- [147] Ioannis Tsamardinos, Constantin Aliferis, and Alexander Statnikov. “Algorithms for Large Scale Markov Blanket Discovery”. In: Jan. 2003, pp. 376–381.
- [148] Ioannis Tsamardinos and Constantin F. Aliferis. “Towards Principled Feature Selection: Relevancy, Filters and Wrappers”. In: *Proceedings of the Ninth International Workshop on Artificial Intelligence and Statistics*. Ed. by Christopher M. Bishop and Brendan J. Frey. Vol. R4. Proceedings of Machine Learning Research. Reissued by PMLR on 01 April 2021. PMLR, Jan. 2003, pp. 300–307. URL: <https://proceedings.mlr.press/r4/tsamardinos03a.html>.
- [149] Caroline Uhler, Garvesh Raskutti, Peter Bühlmann, Bin Yu, et al. “Geometry of the faithfulness assumption in causal inference”. In: *The Annals of Statistics* 41.2 (2013), pp. 436–463.

## Bibliography

- [150] Ashish Vaswani, Noam Shazeer, Niki Parmar, Jakob Uszkoreit, Llion Jones, Aidan N Gomez, Lukasz Kaiser, and Illia Polosukhin. “Attention is All you Need”. In: *Advances in Neural Information Processing Systems*. Ed. by I. Guyon, U. Von Luxburg, S. Bengio, H. Wallach, R. Fergus, S. Vishwanathan, and R. Garnett. Vol. 30. Curran Associates, Inc., 2017. URL: [https://proceedings.neurips.cc/paper\\_files/paper/2017/file/3f5ee243547dee91fbd053c1c4a845aa-Paper.pdf](https://proceedings.neurips.cc/paper_files/paper/2017/file/3f5ee243547dee91fbd053c1c4a845aa-Paper.pdf).
- [151] Changzhang Wang, You Zhou, Qiang Zhao, and Zhi Geng. “Discovering and orienting the edges connected to a target variable in a DAG via a sequential local learning approach”. In: *Computational Statistics and Data Analysis* 77 (2014), pp. 252–266. ISSN: 0167-9473. DOI: <https://doi.org/10.1016/j.csda.2014.03.003>. URL: <https://www.sciencedirect.com/science/article/pii/S0167947314000802>.
- [152] Sinong Wang, Belinda Li, Madian Khabsa, Han Fang, and Hao Ma. *Linformer: Self-Attention with Linear Complexity*. cite arxiv:2006.04768. 2020. URL: <http://arxiv.org/abs/2006.04768>.
- [153] Zhaoyu Wang, Pingchuan Ma, and Shuai Wang. “Towards Practical Federated Causal Structure Learning”. In: *Machine Learning and Knowledge Discovery in Databases: Research Track: European Conference, ECML PKDD 2023, Turin, Italy, September 18–22, 2023, Proceedings, Part II*. Berlin, Heidelberg: Springer-Verlag, 2023, pp. 351–367. ISBN: 978-3-031-43414-3. DOI: 10.1007/978-3-031-43415-0\_21. URL: [https://doi.org/10.1007/978-3-031-43415-0\\_21](https://doi.org/10.1007/978-3-031-43415-0_21).
- [154] Jason Wei, Xuezhi Wang, Dale Schuurmans, Maarten Bosma, Brian Ichter, Fei Xia, Ed H. Chi, Quoc V. Le, and Denny Zhou. “Chain-of-thought prompting elicits reasoning in large language models”. In: *Proceedings of the 36th International Conference on Neural Information Processing Systems*. NIPS ’22. Red Hook, NY, USA: Curran Associates Inc., 2022. ISBN: 9781713871088.
- [155] Sarah Wiegreffe and Yuval Pinter. “Attention is not not Explanation”. In: *Proceedings of the 2019 Conference on Empirical Methods in Natural Language Processing and the 9th International Joint Conference on Natural Language Processing (EMNLP-IJCNLP)*. Ed. by Kentaro Inui, Jing Jiang, Vincent Ng, and Xiaojun Wan. Hong Kong, China: Association for Computational Linguistics, Nov. 2019, pp. 11–20. DOI: 10.18653/v1/D19-1002. URL: <https://aclanthology.org/D19-1002/>.
- [156] Andreas Winter. “Tight Uniform Continuity Bounds for Quantum Entropies: Conditional Entropy, Relative Entropy Distance and Energy Constraints”. In: *Communications in Mathematical Physics* 347.1 (Mar. 2016), pp. 291–313. ISSN: 1432-0916. DOI: 10.1007/s00220-016-2609-8. URL: <http://dx.doi.org/10.1007/s00220-016-2609-8>.

- [157] Thomas Wolf, Lysandre Debut, Victor Sanh, Julien Chaumond, Clement Delangue, Anthony Moi, Pierric Cistac, Tim Rault, Rémi Louf, Morgan Funtowicz, Joe Davison, Sam Shleifer, Patrick von Platen, Clara Ma, Yacine Jernite, Julien Plu, Canwen Xu, Teven Le Scao, Sylvain Gugger, Mariama Drame, Quentin Lhoest, and Alexander M. Rush. *HuggingFace’s Transformers: State-of-the-art Natural Language Processing*. 2020. arXiv: 1910.03771 [cs.CL]. URL: <https://arxiv.org/abs/1910.03771>.
- [158] Xingyu Wu, Bingbing Jiang, Yan Zhong, and Huanhuan Chen. “Multi-label Causal Variable Discovery: Learning Common Causal Variables and Label-specific Causal Variables”. In: *CoRR* abs/2011.04176 (2020). arXiv: 2011.04176. URL: <https://arxiv.org/abs/2011.04176>.
- [159] Enze Xie, Wenhai Wang, Zhiding Yu, Anima Anandkumar, Jose M. Alvarez, and Ping Luo. “SegFormer: simple and efficient design for semantic segmentation with transformers”. In: *Proceedings of the 35th International Conference on Neural Information Processing Systems*. NIPS ’21. Red Hook, NY, USA: Curran Associates Inc., 2021. ISBN: 9781713845393.
- [160] Feng Xie, Zheng Li, Peng Wu, Yan Zeng, Chunchen Liu, and Zhi Geng. “Local causal structure learning in the presence of latent variables”. In: *Proceedings of the 41st International Conference on Machine Learning*. ICML’24. Vienna, Austria: JMLR.org, 2024.
- [161] Hongteng Xu, Mehrdad Farajtabar, and Hongyuan Zha. “Learning Granger Causality for Hawkes Processes”. In: *Proceedings of The 33rd International Conference on Machine Learning*. Ed. by Maria Florina Balcan and Kilian Q. Weinberger. Vol. 48. Proceedings of Machine Learning Research. New York, New York, USA: PMLR, June 2016, pp. 1717–1726. URL: <https://proceedings.mlr.press/v48/xuc16.html>.
- [162] Peng Xu, Xiatian Zhu, and David A. Clifton. “Multimodal Learning With Transformers: A Survey”. In: *IEEE Trans. Pattern Anal. Mach. Intell.* 45.10 (Oct. 2023), pp. 12113–12132. ISSN: 0162-8828. DOI: 10.1109/TPAMI.2023.3275156. URL: <https://doi.org/10.1109/TPAMI.2023.3275156>.
- [163] Shunyu Yao, Jeffrey Zhao, Dian Yu, Nan Du, Izhak Shafran, Karthik Narasimhan, and Yuan Cao. “ReAct: Synergizing Reasoning and Acting in Language Models”. In: *ArXiv* abs/2210.03629 (2022). URL: <https://api.semanticscholar.org/CorpusID:252762395>.
- [164] Jianxin Yin, You Zhou, Changzhang Wang, Ping He, Cheng Zheng, and Zhi Geng. “Partial orientation and local structural learning of causal networks for prediction”. In: *Proceedings of the Workshop on the Causation and Prediction Challenge at WCCI 2008*. Ed. by Isabelle Guyon, Constantin Aliferis, Greg Cooper, André Elisseeff, Jean-Philippe Pellet, Peter Spirtes, and Alexander Statnikov. Vol. 3. Proceedings of Machine Learning Research. Hong Kong: PMLR, June 2008, pp. 93–105. URL: <http://proceedings.mlr.press/v3/yin08a.html>.

## Bibliography

- [165] Kui Yu, Xianjie Guo, Lin Liu, Jiuyong Li, Hao Wang, Zhaolong Ling, and Xindong Wu. “Causality-based Feature Selection: Methods and Evaluations”. In: *ACM Comput. Surv.* 53.5 (Sept. 2020). ISSN: 0360-0300. DOI: 10.1145/3409382. URL: <https://doi.org/10.1145/3409382>.
- [166] Yue Yu, Jie Chen, Tian Gao, and Mo Yu. “DAG-GNN: DAG Structure Learning with Graph Neural Networks”. In: *Proceedings of the 36th International Conference on Machine Learning*. Ed. by Kamalika Chaudhuri and Ruslan Salakhutdinov. Vol. 97. Proceedings of Machine Learning Research. PMLR, 2019, pp. 7154–7163. URL: <https://proceedings.mlr.press/v97/yy19a.html>.
- [167] Manzil Zaheer, Guru Guruganesh, Kumar Avinava Dubey, Joshua Ainslie, Chris Alberti, Santiago Ontanon, Philip Pham, Anirudh Ravula, Qifan Wang, Li Yang, and Amr Ahmed. “Big Bird: Transformers for Longer Sequences”. In: *Advances in Neural Information Processing Systems*. Ed. by H. Larochelle, M. Ranzato, R. Hadsell, M.F. Balcan, and H. Lin. Vol. 33. Curran Associates, Inc., 2020, pp. 17283–17297.
- [168] Biao Zhang and Rico Sennrich. “Root Mean Square Layer Normalization”. In: *Advances in Neural Information Processing Systems*. Ed. by H. Wallach, H. Larochelle, A. Beygelzimer, F. d' Alché-Buc, E. Fox, and R. Garnett. Vol. 32. Curran Associates, Inc., 2019. URL: [https://proceedings.neurips.cc/paper\\_files/paper/2019/file/1e8a19426224ca89e83cef47f1e7f53b-Paper.pdf](https://proceedings.neurips.cc/paper_files/paper/2019/file/1e8a19426224ca89e83cef47f1e7f53b-Paper.pdf).
- [169] Chongsheng Zhang, George Almpantidis, Gaojuan Fan, Binqian Deng, Yanbo Zhang, Ji Liu, Aouaidjia Kamel, Paolo Soda, and João Gama. “A Systematic Review on Long-Tailed Learning”. In: *IEEE Transactions on Neural Networks and Learning Systems* PP (Feb. 2025), pp. 1–21. DOI: 10.1109/TNNLS.2025.3539314.
- [170] Libo Zhang and Yue Ning. *Large Language Models as Interpolated and Extrapolated Event Predictors*. 2024. arXiv: 2406.10492 [cs.CL]. URL: <https://arxiv.org/abs/2406.10492>.
- [171] Min-Ling Zhang and Zhi-Hua Zhou. “A Review On Multi-Label Learning Algorithms”. In: *Knowledge and Data Engineering, IEEE Transactions on* 26 (Aug. 2014), pp. 1819–1837. DOI: 10.1109/TKDE.2013.39.
- [172] Qiang Zhang, Aldo Lipani, Omer Kirnap, and Emine Yilmaz. “Self-Attentive Hawkes Process”. In: *Proceedings of the 37th International Conference on Machine Learning*. Ed. by Hal Daumé III and Aarti Singh. Vol. 119. Proceedings of Machine Learning Research. PMLR, July 2020, pp. 11183–11193. URL: <https://proceedings.mlr.press/v119/zhang20q.html>.
- [173] Wei Zhang, Thomas Kobber Panum, Somesh Jha, Prasad Chalasani, and David Page. “CAUSE: learning granger causality from event sequences using attribution methods”. In: *Proceedings of the 37th International Conference on Machine Learning*. ICML’20. JMLR.org, 2020.

- [174] Wenyu Zhang, Devesh K. Jha, Emil Laftchiev, and Daniel Nikovski. “Multi-label Prediction in Time Series Data using Deep Neural Networks”. In: *CoRR* abs/2001.10098 (2020). arXiv: 2001.10098. URL: <https://arxiv.org/abs/2001.10098>.
- [175] Pushe Zhao, Masaru Kurihara, Junichi Tanaka, Tojiro Noda, Shigeyoshi Chikuma, and Tadashi Suzuki. “Advanced correlation-based anomaly detection method for predictive maintenance”. In: *2017 IEEE International Conference on Prognostics and Health Management (ICPHM)*. 2017, pp. 78–83. DOI: 10.1109/ICPHM.2017.7998309.
- [176] Weike Zhao, Chaoyi Wu, Yanjie Fan, Xiaoman Zhang, Pengcheng Qiu, Yuze Sun, Xiao Zhou, Yanfeng Wang, Ya Zhang, Yongguo Yu, Kun Sun, and Weidi Xie. *An Agentic System for Rare Disease Diagnosis with Traceable Reasoning*. 2025. arXiv: 2506.20430 [cs.CL]. URL: <https://arxiv.org/abs/2506.20430>.
- [177] Xun Zheng, Bryon Aragam, Pradeep Ravikumar, and Eric P. Xing. “DAGs with NO TEARS: continuous optimization for structure learning”. In: *Proceedings of the 32nd International Conference on Neural Information Processing Systems. NIPS’18*. Red Hook, NY, USA: Curran Associates Inc., 2018, pp. 9492–9503.
- [178] Yun Zhou, Yawei Wang, Huan Song, Tesfagabir Meharizghi, Mohamad Al Jazayeri, Panpan Xu, Denisse Colin-Magana, and Aruna Abeyakoon. “Deep sequence modeling for event log-based predictive maintenance”. In: *KDD 2023 International Workshop on Mining and Learning from Time Series (MileTS)*. 2023. URL: <https://www.amazon.science/publications/deep-sequence-modeling-for-event-log-based-predictive-maintenance>.
- [179] Simiao Zuo, Haoming Jiang, Zichong Li, Tuo Zhao, and Hongyuan Zha. “Transformer Hawkes Process”. In: *Proceedings of the 37th International Conference on Machine Learning*. Ed. by Hal Daumé III and Aarti Singh. Vol. 119. Proceedings of Machine Learning Research. PMLR, July 2020, pp. 11692–11702. URL: <https://proceedings.mlr.press/v119/zuo20a.html>.



# A Appendix of Part I

## A.1 Error Pattern Prediction

This section contains the appendix material for Chapter 3.

### A.1.1 Multivariate Hawkes Process Log-likelihood Derivation

The likelihood for any point process parametrized by  $\theta$  with observations  $\{t_1, \dots, t_L\}$  within a time horizon  $0 \leq t \leq T$  can be computed as the sum of the log-likelihood for each process [73]:

$$\ln \mathcal{L}(\theta|t_1, \dots, t_L, T) = \sum_{k=1}^{|\mathcal{X}|} \ln \mathcal{L}_k(\theta|t_1, \dots, t_L)$$

where each term is defined by:

$$\ln \mathcal{L}_k(t_1, \dots, t_L) = \ln \left( \left[ \prod_{i=1}^L \lambda_k^*(t_i) \right] \exp \left( - \int_0^T \lambda_k^*(t) dt \right) \right) \quad (\text{A.1})$$

This expression reduces to:

$$\begin{aligned} &= \sum_{i=1}^L \ln \lambda_k^*(t_i) + \ln \left( \exp \left( - \int_0^T \lambda_k^*(t) dt \right) \right) \\ &= \sum_{i=1}^L \ln \lambda_k^*(t_i) - \int_0^T \lambda_k^*(t) dt \end{aligned} \quad (\text{A.2})$$

Finally, we have for the total log-likelihood:

$$\ln \mathcal{L}(\theta|t_1, \dots, t_L, T) = \sum_{k=1}^{|\mathcal{X}|} \sum_{i=1}^L \ln \lambda_k^*(t_i) - \sum_{k=1}^{|\mathcal{X}|} \int_0^T \lambda_k^*(t) dt \quad (\text{A.3})$$

### A.1.2 CarFormer Pretraining Details

We trained the CarFormer model for 70,000 steps with a learning rate of  $5 \times 10^{-4}$ , scheduled using a cosine warm restart with 10,000 warm-up steps, and a weight decay of 0.1. The loss coefficients were set to  $\alpha = 1$  and  $\beta = 1$ . The model architecture comprised

12 attention heads, 6 layers, and a feature size of 600, using the GELU activation function in all feedforward layers. We employed the AdamW optimizer with a batch size of 192 and a sequence length of 258, resulting in approximately 34 million parameters. In all experiments, we fixed the same number of parameters when introducing new embeddings for all evaluated models to provide a fair comparison, same for EPredictor. The training data was split into 85% training and 15% testing without up-sampling, and random events were injected with a probability of  $p = 0.05$  per sample. On average, each training session lasted about 20 hours on an Nvidia A10G GPU.

### A.1.3 Models Definition

A GPT [121] model is added to improve comparison over baseline models. We kept the original implementation of the feed-forward layers [150] but initialize the intermediate layers with:  $W_l \sim \mathcal{N}(0, \frac{2}{L\sqrt{d_l}})$ . We used root-mean-square normalization (RMS Norm) from [168] instead of traditional layer normalization. We initialized all other linear layers using the SMALLINIT schema [102]  $W_l \sim \mathcal{N}(0, \sqrt{\frac{2}{d_l+4d_l}})$ . The names printed in the Tab 3.2 are model variations based on the embeddings given to CarFormer:

**time** : Along with the event type **E** an absolute time embedding is added such as input  $\mathbf{U} = \mathbf{E} + \mathbf{T}$

**mileage** : Same as time except we add a mileage embedding **M** such as  $\mathbf{U} = \mathbf{E} + \mathbf{M}$

**rot** : A RoPE [142] is applied to **Q, K** such as  $\mathbf{Q} = \mathbf{R}_{\Theta}^d \mathbf{W}^Q \mathbf{E}$ ,  $\mathbf{K} = \mathbf{R}_{\Theta}^d \mathbf{W}^K \mathbf{E}$

**ce** : We add a context embedding  $\mathbf{CE} = \mathbf{T} + \mathbf{M}$  to **Q, K** such as  $\mathbf{Q} = \mathbf{U}\mathbf{W}^Q + \mathbf{CE}$  to every attention layers.

**m2c, c2m** : Inspired by the Disentangled Attention mechanism from DeBerta [55]. Attention score  $\mathbf{A}_{i,j}$  between tokens  $i$  and  $j$  is computed from hidden states vector  $\{\mathbf{H}_i\}$  at event step  $i$  and a mileage vector  $\{\mathbf{M}_i\}$  at event step  $i$  such as:  $\mathbf{A}_{i,j} = \{\mathbf{H}_i, \mathbf{M}_i\} \times \{\mathbf{H}_j, \mathbf{M}_j\}^T = \mathbf{H}_i \mathbf{H}_j^T + \mathbf{H}_i \mathbf{M}_j^T + \mathbf{M}_i \mathbf{H}_j^T + \mathbf{M}_i \mathbf{M}_j^T = \text{"content-to-content"} + \text{"content-to-mileage"} + \text{"mileage-to-content"} + \text{"mileage-to-mileage"} = \text{"c2c"} + \text{"c2m"} + \text{"m2c"} + \text{"m2m"}$ .

### A.1.4 Random Event Injection

Let  $A_i$  be the random variable representing the number of random events injected at step  $i$ . We can say that:

$$P(A_i = r) = (1 - p)p^r \quad \text{for } r = 0, 1, 2, \dots$$

Where  $A_i$  is the number of random events injected at step  $i$ ,  $r$  is the number of trials (injected events) until the first failure,  $p$  is the probability of injecting a random event. Therefore, it is trivial to derive the expected number of random events injected per

## A.2 Multimodal Error Pattern Offline Prediction

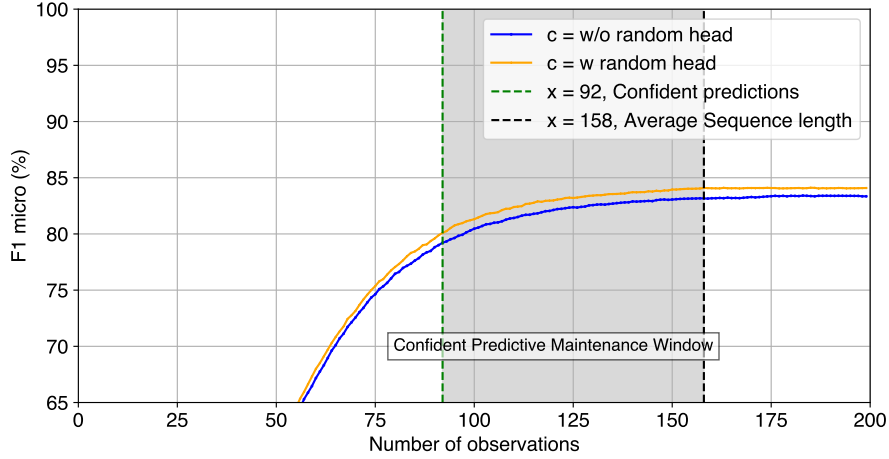


**Figure A.1: Confident Predictive Maintenance Window Evolution** with and w/o the random head.

sequence  $S$  of length  $L$ : Therefore, the expected total number of injected fake events over the entire sequence of length  $L$  is:

$$\mathbb{E} \left[ \sum_{i=1}^L A_i \right] = Lp$$

Which in our case would translate  $\sim 150 \times 0.05 = 7.5$  random events per sequence.

## A.2 Multimodal Error Pattern Offline Prediction

This section contains the appendix material for Chapter 4.

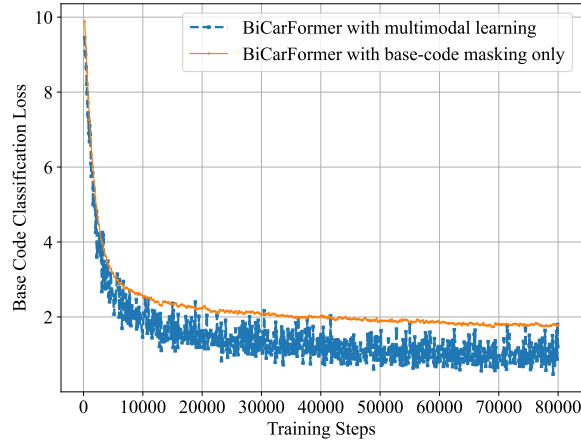


**Figure A.2: Pretraining Loss Comparison.** Base-DTC classification loss comparison with and without multimodal learning.



# B Appendix of Part II

## B.1 Sample-Level Multi-Label Causal Discovery

This section contains the appendix material for the one-shot causal discovery Chapter 6.

### B.1.1 PyCausalFS

Local structure learning algorithms were all used with  $\alpha = 0.1$  in the associated code: <https://github.com/wt-hu/pyCausalFS/tree/master/pyCausalFS/LSL>.

### B.1.2 MI-MCF

MI-MCF [84] was used for comparison following the official implementation at <https://github.com/malinjlu/MI-MCF> we used  $\alpha = 0.05, L = 268, k_1 = 0.7, k_2 = 0.1$ .

### B.1.3 NADEs Quality.

We did several ablations on the quality of the NADEs and their impact on the one-shot causal discovery phase. In particular, Table B.1 presents multiple  $Tf_x, Tf_y$  with respectively 90 and 15 million parameters or 34 and 4 million parameters. We also varied the context window (conditioning set  $\mathbf{Z}$ ), trained on different amounts of data (Tokens), and reported the classification results on the test set of  $Tf_y$  alone. We did not output the running time since it was always the same for all NADEs: 1.27 minutes for 50,000 samples and 0.14 for 5000.

### B.1.4 Sampling Procedure for CMI

We performed an ablation (Tab B.2) on the effect of sampling methods to estimate the expected value over all possible context  $\mathbf{Z}$ . We used one A10 GPU on a sample of the test dataset (4000 random samples) composed of 205 labels with a batch size of 4 during inference. We tested top-k sampling with  $k = \{20, 35\}$  [34] with and w/o a temperature scaler of  $T$  to log-probabilities  $\hat{\mathbf{x}}$  such that

$$\hat{\mathbf{x}}' = \text{softmax}(\log \hat{\mathbf{x}}/T)$$

and a combination of top-k and a top-nucleus sampling [60] with different probability mass  $p = \{0.8, 1.2\}$  and finally a permutation of token position within the context  $c$ . We fixed a dynamic threshold with z score  $k = 3$  and performed 10 runs. We then reported the mean and standard deviation for each classification metric and elapsed time (sec).

## B Appendix of Part II

Tokens	Param.	Context	Prec. ( $\uparrow$ )	Rec. ( $\uparrow$ )	F1 ( $\uparrow$ )	Tfy F1 ( $\uparrow$ )
<i>For <math>n = 50,000</math> samples</i>						
1.5B	105m	$c = 4$	$47.95 \pm 1.05$	$30.65 \pm 0.51$	$37.39 \pm 0.67$	88.6
1.5B	105m	$c = 12$	$54.62 \pm 1.03$	$29.88 \pm 0.73$	$38.63 \pm 0.85$	90.43
1.5B	105m	$c = 15$	<b><math>55.26 \pm 1.42</math></b>	<b><math>31.37 \pm 0.82</math></b>	<b><math>40.02 \pm 1.03</math></b>	90.57
1.5B	105m	$c = 20$	$49.52 \pm 1.59$	<b><math>31.76 \pm 0.85</math></b>	$36.54 \pm 1.10$	91.19
1.5B	105m	$c = 30$	$36.65 \pm 1.18$	$22.75 \pm 0.78$	$26.57 \pm 0.91$	<b>92.64</b>
300m	47m	$c = 20$	$39.49 \pm 1.77$	$26.30 \pm 0.89$	$29.01 \pm 1.10$	83.6
<i>For <math>n = 500</math> samples</i>						
1.5B	105m	$c = 12$	$54.84 \pm 4.55$	<b><math>31.45 \pm 2.23</math></b>	<b><math>39.95 \pm 2.83</math></b>	90.43
1.5B	105m	$c = 15$	$55.04 \pm 3.36$	$29.90 \pm 1.78$	$38.74 \pm 2.24$	90.57
1.5B	105m	$c = 20$	$48.84 \pm 4.01$	<b><math>31.65 \pm 2.37</math></b>	$36.19 \pm 2.65$	<b>91.19</b>
300m	47m	$c = 20$	$38.23 \pm 2.91$	$25.31 \pm 2.39$	$27.92 \pm 2.25$	83.6

**Table B.1:** Ablations of the performance of Phase 1 (One-shot **MB** retrieval) as a function of different NADEs with  $n = 50,000$  and  $n = 500$  samples, averaged over 5-folds. Classification metrics use weighted averaging. Metrics are given in %.

Sampling increases the predictive performance of OSCAR by a large margin. More interestingly, different sampling types have different effects on specific averaging. This has a ‘smoothing’ effect on the CMI curve when multiple labels are present in the sequence. Without upsampling, the CMI’s sensitivity across labels increases, making it more challenging to determine a threshold and a potential cause. We observe that, broadly, top-k sampling yields better results, particularly when followed by top-p=0.8. Sampling with the same tokens (*Permutation*) is not a good choice; sampling from the next-event prediction  $Tf_x$  yielded better results. We will choose **Top-k+p=0.8** for the increased F1 Micro and high F1 Macro, and Weighted.

Proposal	F1 Micro (%)	F1 Macro (%)	F1 Wtd. (%)	Time (s)
w/o Sampling	14.07	12.29	16.67	<b><math>49.30 \pm 0.30</math></b>
Permutation	$18.22 \pm 0.36$	$13.75 \pm 0.09$	$19.21 \pm 0.03$	$557.82 \pm 0.13$
Top-k=20	$26.77 \pm 0.71$	$23.83 \pm 0.19$	$29.25 \pm 0.07$	$557.40 \pm 0.13$
Top-k=35	$26.57 \pm 0.96$	$24.08 \pm 0.23$	$29.30 \pm 0.07$	$557.35 \pm 0.10$
Top-k=35+T=0.8	$27.36 \pm 0.65$	$23.77 \pm 0.21$	$28.98 \pm 0.07$	$557.45 \pm 0.11$
Top-k=35+T=1.2	$26.59 \pm 1.49$	<b><math>24.62 \pm 0.29</math></b>	<b><math>29.52 \pm 0.06</math></b>	$557.45 \pm 0.12$
Top-k=25+p=0.8	$27.98 \pm 0.67$	$23.82 \pm 0.28$	$29.18 \pm 0.07$	$558.07 \pm 0.07$
<b>Top-k=35+p=0.8</b>	<b><math>28.82 \pm 0.75</math></b>	$24.06 \pm 0.25$	$29.17 \pm 0.07$	$558.16 \pm 0.14$
Top-k=35+p=0.9	$26.39 \pm 0.99$	$24.12 \pm 0.31$	$29.26 \pm 0.11$	$558.11 \pm 0.12$
Top-k=35+p=0.9+T=0.9	$27.63 \pm 0.75$	$23.90 \pm 0.24$	$29.04 \pm 0.09$	$558.07 \pm 0.12$
Top-k=35+p=0.9+T=1.1	$26.75 \pm 1.30$	<b><math>24.47 \pm 0.24</math></b>	$29.45 \pm 0.09$	$558.06 \pm 0.11$

**Table B.2:** One-shot classification performance and elapsed time (sec) across different sampling methods. Best results are in **bold**, and equal performance are in underline.

### B.1.5 Sampling Number

We experimented with different numbers of  $N$  for the sampling method across different averaging methods (micro, macro, weighted), Fig .B.1. We performed eight different runs and reported the average, standard deviation, and elapsed time. In general, sampling with a larger  $N$  tends to decrease the standard deviation and yield more reliable Markov Boundary estimation. As we process more samples, the model gradually improves with logarithmic growth until it converges to a final score. We also verify that our time complexity is linear with the number of samples  $N$ . Based on these results, we generally choose  $N = 68$ .

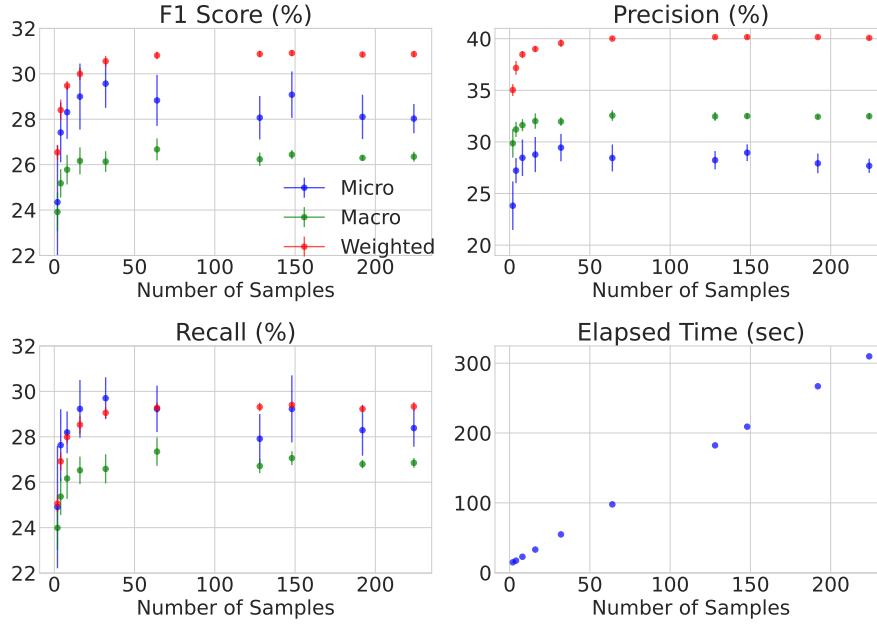
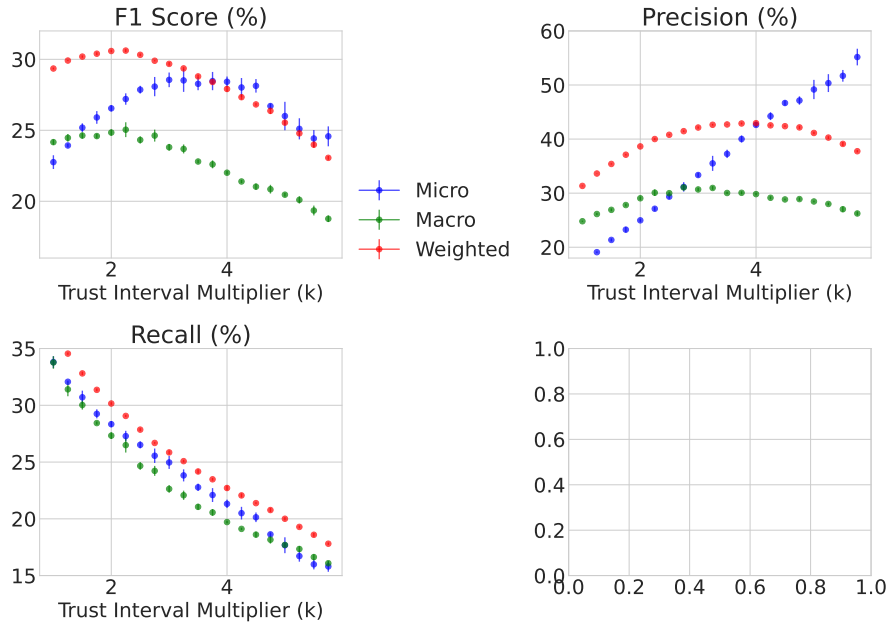


Figure B.1: Ablation of the Number of Particles  $N$ . Results are reported using 1-sigma error bar.

### B.1.6 Dynamic Thresholding

We performed ablations on the effect of  $k$  during the dynamic thresholding of the CMI in Eq. 6.11 to assess conditional independence in Fig. B.2. To balance the classification metrics across the different averaging, we set  $k = 2.75$ .



**Figure B.2: Sensitivity Analysis.** Evolution of the one-shot F1 Score, Precision, and Recall as a function of coefficient  $k$ . Results are reported using 1-sigma error bar.

## B.1.7 Figures

### B.1.7.1 Explanation Examples

To enhance interpretability and illustrate the learned relationships, we present graphical explanations of EP occurrences based on sequences of DTCs. For each case, we selected representative samples that reflect diverse yet intuitive failure scenarios. Fig. B.3 depicts a clear-cut example involving a single failure label related to the emergency antenna system. In contrast, Fig. B.4 captures a more intricate case where airbag and tire pressure (RDC) malfunctions co-occur. These graphs highlight the influence of preceding events, with causal contributions shown in orange and red, and inhibitory effects illustrated in pink. Such visualizations serve to provide both human-understandable insights and support for the model’s reasoning process.

## B.1 Sample-Level Multi-Label Causal Discovery

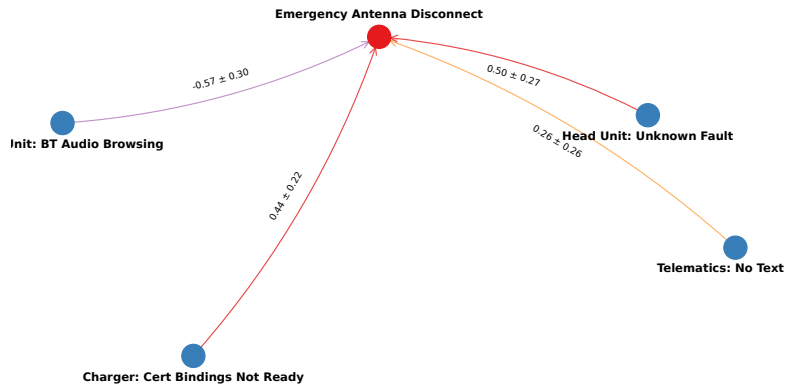


**Figure B.3:** Example of a sequence of events (DTCs) that lead to an emergency antenna dysfunction as outcome labels. The inhibitory strengths are shown in pink and causal strengths in orange and red

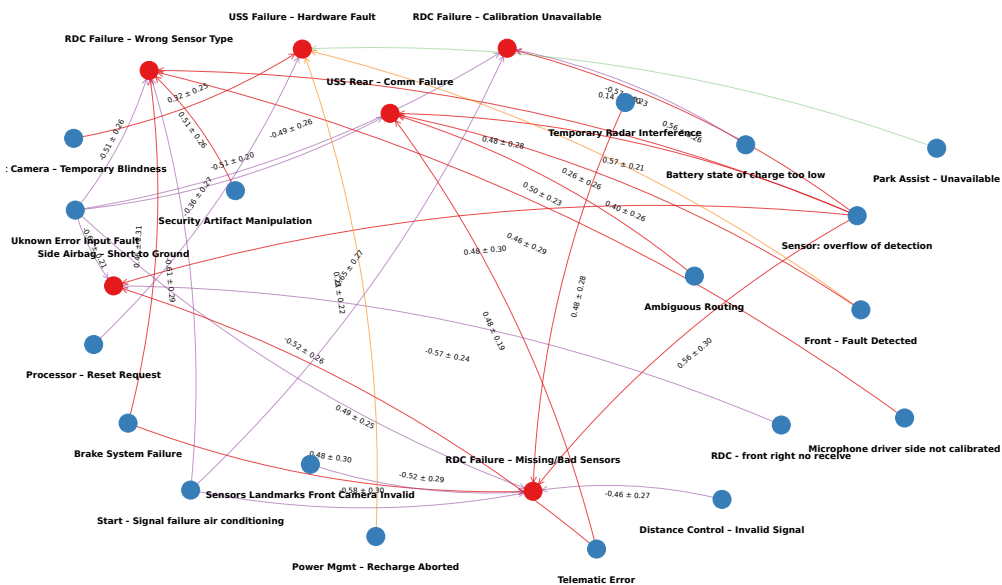


**Figure B.4:** Example of a sequence of events (DTCs) that lead to an airbag and tire pressure malfunctions as outcome labels. The inhibitory strengths are shown in pink and causal strengths in orange and red

### B.1.8 Implementation of OSCAR

The following is the implementation of OSCAR in PyTorch [110].

```

1 def topk_p_sampling(z, prob_x, c: int, n: int = 64, p: float = 0.8, k:
  int = 35,
2                       cls_token_id: int = 1, temp: float = None):
3     # Sample just the context
4     input_ = prob_x[:, :c]
```

## B Appendix of Part II

```
5
6 # Top-k first
7 topk_values, topk_indices = torch.topk(input_, k=k, dim=-1)
8
9 # Top-p over top-k values
10 sorted_probs, sorted_idx = torch.sort(topk_values, descending=True,
11 dim=-1)
12 cum_probs = torch.cumsum(sorted_probs, dim=-1)
13 mask = cum_probs > p
14
15 # Ensure at least one token is kept
16 mask[..., 0] = 0
17
18 # Mask and normalize
19 filtered_probs = sorted_probs.masked_fill(mask, 0.0)
20 filtered_probs += 1e-8 # for numerical stability
21 filtered_probs /= filtered_probs.sum(dim=-1, keepdim=True)
22
23 # Unscramble to match the original top-k indices
24 # Need to reorder the sorted indices back to the original top-k
25 reorder_idx = torch.argsort(sorted_idx, dim=-1)
26 filtered_probs = torch.gather(filtered_probs, -1, reorder_idx)
27
28 batched_probs = filtered_probs.unsqueeze(1).repeat(1, n, 1, 1)
29 # (bs, n, seq_len, k)
30 batched_indices = topk_indices.unsqueeze(1).repeat(1, n, 1, 1)
31 # (bs, n, seq_len, k)
32
33 sampled_idx = torch.multinomial(batched_probs.view(-1, k), 1)
34 # (bs*n*seq_len, 1)
35 sampled_idx = sampled_idx.view(-1, n, c).unsqueeze(-1)
36
37 sampled_tokens = torch.gather(batched_indices, -1, sampled_idx).
38 squeeze(-1)
39 sampled_tokens[..., 0] = cls_token_id
40
41 # Reconstruct full sequence
42 z_expanded = z.unsqueeze(1).repeat(1, n, 1)[..., c:]
43 return torch.cat((sampled_tokens, z_expanded), dim=-1)
44
45 from torch import nn
46 def OSCAR(tfe: nn.Module, tfy: nn.Module, batch: dict[str, torch.Tensor
47 ], c: int, n: int, eps: float=1e-6, topk: int=20, k: int=2.75, p
48 =0.8) -> torch.Tensor:
49     #tfe, tfy: are the two autoregressive Transformers (event type and
50     label)
51     # batch: dictionary containing a batch of input_ids and
52     attention_mask of shape (bs, L) to explain.
53     # c: scalar number defining the minimum context to start
54     inferring, also the sampling interval.
55     # n: scalar number representing the number of samples for the
56     sampling method.
57     # eps: float for numerical stability
```

## B.1 Sample-Level Multi-Label Causal Discovery

```

47 # topk: The number of top-k most probable tokens to keep for
    sampling
48 # k: Number of standard deviations to add to the mean for dynamic
    threshold calculation
49 # p: Probability mass for top-p nucleus
50
51 o = tfe(attention_mask=batch['attention_mask'], input_ids=batch['
input_ids'])['prediction_logits'] # Infer the next event type
52 x_hat = torch.nn.functional.softmax(o, dim=-1)
53
54 b_sampled = topk_p_sampling(batch['input_ids'], x_hat, c, k=topk, n=
n, p=p) # Sampling up to (bs, n, L)
55 n_att_mask = batch['attention_mask'].unsqueeze(1).repeat(1, n, 1)
56
57 with torch.inference_mode():
58     o = tfy(attention_mask=n_att_mask.reshape(-1, b_sampled.size(-1)
), input_ids=b_sampled.reshape(-1, b_sampled.size(-1))) # flatten
and infer
59     prob_y_sampled = o['ep_prediction'].reshape(b_sampled.size(0), n
, batch['input_ids'].size(-1)-c, -1) # reshape to (bs, n, L-c)
60
61     # Ensure probs are within (eps, 1-eps)
62     prob_y_sampled = torch.clamp(prob_y_sampled, eps, 1 - eps)
63
64     y_hat_i = prob_y_sampled[..., :-1, :] # P(Yj|z)
65     y_hat_iplus1 = prob_y_sampled[..., 1:, :] # P(Yj|z, x_i)
66
67     # Compute the CMI & CS and average across sampling dim
68     cmi = torch.mean(y_hat_iplus1*torch.log(y_hat_iplus1/y_hat_i)+
(1-y_hat_iplus1)*torch.log((1-y_hat_iplus1)/(1-y_hat_i)), dim=1)
69     # (BS, L, Y)
70     cs = y_hat_iplus1 - y_hat_i
71     cs_mean = torch.mean(cs, dim=1)
72     cs_std = torch.std(cs, dim=1)
73
74     # Confidence interval for threshold
75     mu = cmi.mean(dim=1)
76     std = cmi.std(dim=1)
77     dynamic_thresholds = mu + std * k
78
79     # Broadcast to select an individual dynamic threshold
80     cmi_mask = cmi >= dynamic_thresholds.unsqueeze(1)
81
82     cause_token_indices = cmi_mask.nonzero(as_tuple=False)
83     # (num_causes, 3) --> each row is [batch_idx, position_idx,
label_idx]
84     return cause_token_indices, cs_mean, cs_std, cmi_mask

```

**Remark 6.** Since *tfy* contains *tfe* as backbone, in practice we need only one forward pass from *tfy* and extract also  $\hat{x}$ , so *tfe* is not needed. We let it to improve understanding and clarity.

## B.2 Population-Level Multi-Label Causal Discovery

This section contains the appendix material for the chapter 7.

### B.2.1 Definition of Scoring Criteria

**Definition 26.** (*Decomposable Criterion*). We say that a scoring criterion  $S(\mathcal{G}, \mathcal{D})$  is decomposable if it can be written as a sum of measures, each of which is a function only of one node and its parents. In other words, a decomposable scoring criterion  $f_s$  applied to a DAG  $\mathcal{G}$  can always be expressed as:

$$S(\mathcal{G}, \mathcal{D}) = \sum_i^n f_s(X_i, Pa_{\mathcal{G}}(X_i)) \quad (\text{B.1})$$

**Definition 27** (Score equivalent). [21]. A score  $f_s$  is score equivalent if it assigns the same score to all the graphs in the same MEC.

**Definition 28** (Local Consistency). [21] Let  $\mathcal{D}$  contain  $m$  i.i.d samples from some distribution  $P(\cdot)$ . Let  $\mathcal{G}$  be any possible DAG and  $\mathcal{G}'$  a different DAG obtained by adding the edge  $i \rightarrow j$  to  $\mathcal{G}$ . A score  $f_s$  is locally consistent if both hold:

- If  $X_i \not\perp_p X_j | Pa_{\mathcal{G}}(X_j)$ , then  $f_s(\mathcal{G}', \mathcal{D}) > f_s(\mathcal{G}, \mathcal{D})$
- If  $X_i \perp_p X_j | Pa_{\mathcal{G}}(X_j)$ , then  $f_s(\mathcal{G}', \mathcal{D}) < f_s(\mathcal{G}, \mathcal{D})$

### B.2.2 Criteria

This section presents the different criteria used for comparison in the experimental evaluation of Chapter 7.

### B.2.3 Frequency

Frequency-based heuristics that apply fixed thresholds  $\tau$  to the empirical frequency of the occurrence of  $X_i$  in each of the Markov Boundary  $\mathbf{MB}(Y_j)$ . Formally, for each label  $Y_j$ , after merging all local edge sets into a global set  $E = \bigcup_{i=1}^m E_i$ , we evaluate each candidate variable  $X_i \in \mathbf{MB}_j$  based on its frequency of appearance across the local models. If this frequency exceeds the threshold  $\tau$ , the variable is retained in the final merged  $\mathbf{MB}_j$ ; otherwise, it is discarded.

### B.2.4 Expected FPR Adjustment

Same principle as in [36] except that we fit the two Beta distributions on the mutual information of  $I(Y_j, X_i)$  instead of the raw frequencies.

### B.2.5 Mutual Information

**BES** The Backward Equivalence Search (BES) is the second phase of GES [21], where edges are removed one after the other to maximize a criterion  $S$ . Heuristics approaches [117, 126] aim to solve this problem by optimizing:

$$E = \arg \max_{E_i \in \varepsilon} \sum_{e \in E_i} S(e) \quad (\text{B.2})$$

Where  $\varepsilon$  denotes the search space (all possible edges over  $\mathbf{U}$ ) and  $S(e)$  a criterion function for edge relevance (e.g. edge frequency, thresholds,  $\dots$ ). This formulation accounts for the characteristics of the underlying edges but not for the overall network structure, complexity, or missing data [112], leading to a *consensus fusion approach* [145].

**Estimating Mutual Information** We want to reuse the estimated conditional mutual information, Eq. 6.8, and profit from the parallelized inference of Phase 1 (Fig. 7.2). As argued out by [67], a causal strength measure (or criterion)  $C_{X_i \rightarrow Y_j}$  should possess multiple properties. Notably, if  $C_{X_i \rightarrow Y_j} = 0$ , then the joint distribution satisfies the Markov condition with respect to the DAG obtained by removing the arrow  $X_i \rightarrow Y_j$ . The true DAG reads  $X_i \rightarrow Y_j$  iff  $C_{X_i \rightarrow Y_j} = I(X_i, Y_j)$ .

It is a natural criterion for merging edges across multiple causal graphs. However, it remains tricky to estimate [70]. Using the chain rule of conditional mutual information [23], we can rewrite it as:

$$I(Y_j, X_i | \mathbf{Z}) = I(Y_j, X_i) - I(Y_j, X_i, \mathbf{Z}) \quad (\text{B.3})$$

Where  $I(Y_j, X_i, \mathbf{Z})$  is the interaction information [23], which tells us whether knowing  $\mathbf{Z}$  explains away the dependency between  $X_i$  and  $Y_j$  (negative interaction), or enhances it (positive interaction):

$$I(Y_j, X_i, \mathbf{Z}) \triangleq I(Y_j, \mathbf{Z}) - I(Y_j, \mathbf{Z} | X_i)$$

$I(Y_j, \mathbf{Z})$  can be estimated using the same Monte-Carlo sampling as for  $I(Y_j, X_i | \mathbf{Z})$  6.8. Since  $I(Y_j, \mathbf{Z}) = H(Y_j) - H(Y | \mathbf{Z}_j)$ , the marginal  $p(y)$  is needed. Fortunately, the dataset  $\mathcal{D}$  is large enough, hence the frequencies of  $y_j$  are recovered empirically and an estimate  $\hat{p}(y)$ , which we assume to be equal to the true marginal  $p(y)$ . We acknowledge that under a restricted dataset,  $\hat{p}(y)$  might differ from  $p(y)$ . This yields to:

$$I(Y_j, \mathbf{Z}) = \mathbb{E}_{p(z)} D_{KL}(P(Y_j | \mathbf{Z}) || \hat{P}(Y_j)) = \mathbb{E}_{p(z)} I_G(Y_j, \mathbf{Z}) \quad (\text{B.4})$$

Formally, we assume that for long sequences i.e.,  $i \rightarrow +\infty$ , our event sequences form a stationary ergodic stochastic process and  $I(Y_j, \mathbf{Z} | X_i)$  is negligible compare to  $I(Y_j, \mathbf{Z})$  since  $\mathbf{Z}$  is containing most of the information to predict  $Y_j$ . This reduces the mutual information to

$$I(Y_j, X_i) \approx I(Y_j, X_i | \mathbf{Z}) + I(Y_j | \mathbf{Z})$$

**Criterion.** We propose a **Class-Aware Information Gain (CAIG)** score for evaluating candidate edges during Phase 2 of CARGO. Given  $m$  i.i.d. samples from a dataset  $\mathcal{D}$ , CAIG balances three key factors: mutual information derived from information gain, class imbalance, and network complexity.

For each label node  $Y_j$ , with candidate parent set  $\mathbf{Pa}_j^{\mathcal{G}}$ , the CAIG score is:

$$f_s(\mathcal{G}, \mathcal{D}) = \sum_{j=1}^n f_I(Y_j, \mathbf{Pa}_j^{\mathcal{G}}) - \alpha \cdot |\mathbf{Pa}_j^{\mathcal{G}}| \cdot \log\left(\frac{m}{m_j} + 1\right) \quad (\text{B.5})$$

With  $f_I(Y_j, \mathbf{Pa}_j^{\mathcal{G}}) = \sum_{X_i \in \mathbf{Pa}_j^{\mathcal{G}}} I(Y_j, X_i)$ ,  $\alpha$  is a regularization hyperparameter,  $m_j$  is the number of positive instances for class  $Y_j$ .

This formulation encourages informative yet parsimonious graph structures and corrects for underrepresented labels via the regularization term. It is also efficient since CAIG is *decomposable* [21] like BIC with the local  $s_I$ . This criterion is denoted as *BES mi imbalance par* in our experiments in Fig. 7.4.

## B.2.6 Implementation of Phase 2

```

1 import random
2 def create_auto_adaptive_threshold_fn(all_m_j, tau_max=0.5, tau_min
   =0.05, k=None, m0='median'):
3     m_0 = np.median(all_m_j)
4
5     if k == None:
6         q25, q75 = np.percentile(all_m_j, [25, 75])
7         if q75 == q25:
8             k = 1.0
9         else:
10            log_iqr = np.log(q75) - np.log(q25)
11            k = (2 * np.log(3)) / log_iqr
12
13    def threshold_function(m_j):
14        log_m_j = np.log(m_j + 1e-9)
15        log_m_0 = np.log(m_0)
16        logistic_decay = 1 / (1 + np.exp(k * (log_m_j - log_m_0)))
17        return (tau_max - tau_min) * logistic_decay + tau_min
18
19    return threshold_function
20
21 def adaptive_thresholding_frequency(graphs: list,
22     present_labels: dict,
23     frequency_threshold: float = 0.5,
24     k: float=None,
25     tau_min: float=0.05,
26     tau_max: float=0.5,
27     m0: str='median',
28     verbose=False,
29     **kwargs):

```

## B.2 Population-Level Multi-Label Causal Discovery

```
30
31 #Frequency voting: keep edges appearing with frequency > threshold
    across samples.
32
33 #:param graphs: list of local graphs (e.g., from Phase 1). Each
    graph is a dict[label][token] = list of #stats.
34 #:param present_labels: labels present in evaluation
35 #:param frequency_threshold: e.g. 0.5 for majority, 0.8 for
    conservative
36 #:return: filtered_labels, sample_per_label, elapsed_time
37
38 start_time = datetime.now()
39 # Step 1: Aggregate graphs
40 labels, sample_per_label = union(graphs) # user-defined union
    function
41 old_labels = labels.copy()
42 nodes = count_nodes(labels)
43 samples = len(graphs)
44
45 # Create threshold function
46 auto_threshold_fn = create_auto_adaptive_threshold_fn(list(
    sample_per_label.values()), k=k, tau_max=tau_max, tau_min=tau_min,
    m0=m0)
47
48 # Step 2: Frequency voting with dynamic thresholds
49 edge_counts = defaultdict(lambda: defaultdict(int)) # edge_counts[
    label][token] = count
50
51 for g in graphs:
52     for label, token_dict in g.items():
53         if label not in labels:
54             continue
55         for token in token_dict:
56             edge_counts[label][token] += 1
57
58 # Step 3: Keep edges above frequency threshold
59 filtered_labels = defaultdict(dict)
60 for label in labels:
61     total = sample_per_label.get(label, samples) # fallback to
    total graphs if missing
62     for token, count in edge_counts[label].items():
63         freq = count / total
64         if freq >= auto_threshold_fn(sample_per_label.get(label, 1))
    :
65             filtered_labels[label][token] = {'frequency': freq}
66             if verbose:
67                 print(f'[{label}] token {token} kept (freq={freq:.2f
    })')
68
69 nb_of_edges = sum(len(v) for v in filtered_labels.values())
70 print(f'Time: {(datetime.now() - start_time).total_seconds():.2f}s')
71 return filtered_labels, sample_per_label, (datetime.now() -
    start_time).total_seconds()
```

## B.3 Sample-Level Event-to-Event Causal Discovery

### B.3.1 Flexible Assumptions

**Assumption 9** (Bounded Lagged Effects). *There exists an integer  $m \geq 1$ , referred to as the lag bound, such that for any sequence  $s$  and any target event  $X_j$  with index  $t > m$ , all past events prior to  $t - m$  are conditionally independent of  $X_t$  given its  $m$  most recent predecessor events. Formally,*

$$X_t \perp X_{0:t-m} \mid X_{t-m:t-1}$$

### B.3.2 Evaluation

We used an *ml.g5.4xlarge* instance from AWS Sagemaker, which contains 8 vCPUs and 1 NVIDIA A10G as GPU with 24GiB for training and inference.

**Justification for Evaluating on SCMs.** As we saw, standard causal discovery algorithms for multivariate time series (e.g., PCMCI, Neural Hawkes Processes, CASCADE) are not applicable in our setting. Moreover, evaluating causal discovery in large scale event sequences is notoriously difficult due to the lack of ground-truth annotations in real-world traces (e.g., server logs, medical records). Furthermore, generic high-order MC are computationally intractable to materialize due to the state space  $|\mathcal{X}|^m$  of  $\{X_t\}$  and unlearnable in high dimensions without structural assumptions.

**Synthetic Data** We introduce a synthetic benchmark based on a linear Structural Causal Model (SCM). This DGP models the transition distribution  $P(X_t | X_{t-m:t-1})$  via an additive mechanism where past events exert independent *excitatory* or *inhibitory* influences on future outcomes such as:

$$P(X_t | X_{t-m:t-1}) = \text{softmax} \left( \mathbf{b} + \sum_{k=1}^m \mathbf{W}_{x_{t-k}}^{(k)} \cdot \lambda(k) \right)$$

where  $\mathbf{W}^{(k)} \in \mathbb{R}^{|\mathcal{X}| \times |\mathcal{X}|}$  is a sparse weight matrix representing the causal influence of an event at lag  $k$ , and  $\lambda(k)$  is a temporal decay function. Importantly, weights  $\mathbf{W}_{i,j}$  can be *positive (excitation)* or *negative (inhibition)*, allowing for real-world causal mechanisms present in sequences. We tune the sparsity of the weight matrix  $\mathbf{W}$  to obtain a predictability score  $\text{Pred} = \frac{H(P)}{H_{max}} = \frac{H(P)}{\log(|\mathcal{X}|)}$  superior or equal to 58% across the benchmarked SCMs.

**Practical Monitoring: The Oracle Score.** Since the true entropy  $H(P)$  and thus the true KL divergence are unknown, we must approximate  $\epsilon$  empirically. We observe that the cross-entropy loss decomposes as  $\mathcal{L}_{AR}(\theta) = H(P) + D_{KL}(P || P_\theta)$ . We propose the *Oracle Score*  $\hat{\epsilon}$  as a normalized estimator of the excess entropy:

$$\hat{\epsilon}(P_\theta) = \frac{\mathcal{L}_{AR}(\theta) - H(P)}{H_{max} - H(P)} \quad (\text{B.6})$$

where  $H_{max} = \log |\mathcal{X}|$  is the maximum entropy (uniform noise) and  $H$  is the irreducible entropy of the DGP (approximated by the minimum validation loss observed).

This metric provides a vocabulary-agnostic measure of fit:  $\hat{\epsilon} \rightarrow 0$  implies convergence to the theoretical limit ( $P_\theta \rightarrow P$ ).

### B.3.3 Additional Ablations

#### B.3.3.1 Number of Particles $N$

We observe in Fig. B.5 that the number of particles  $N$  reduce the amount of missing causal relationships (Recall) and SHD. After  $N > 256$ , however, we did not observe significant changes.

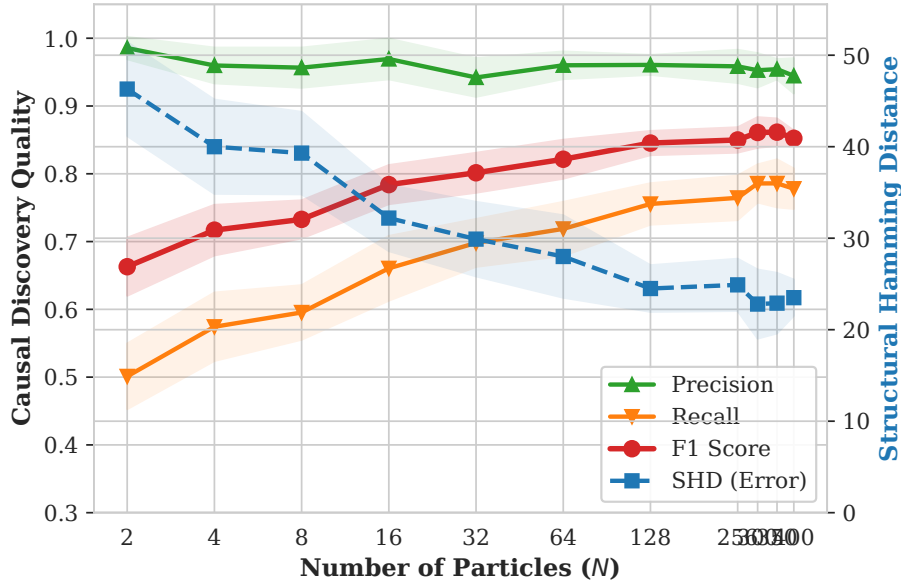


**Figure B.5: Ablation of the Number of Particles  $N$ .** Evolution of causal discovery performance as a function of the number of particles  $N$  at  $|\mathcal{X}| = 1000, m = 6$

#### B.3.3.2 Empirical Validation of $\epsilon$ -Strong Faithfulness.

Fig. B.6 demonstrates that the standard faithfulness assumption ( $\tau = 0$ ) is untenable in practice, as it fails to distinguish causal signals from finite-sample approximation noise (resulting in low precision). Conversely, the distinct performance peak at  $\tau_{opt} \approx 1.4 \times 10^{-5}$  empirically validates the  $\epsilon$ -**Strong Faithfulness** hypothesis (Def. 23), confirming that causal discovery requires a minimum signal-to-noise ratio. Especially,  $\tau_{opt}$  is orders of magnitude lower than the worst-case theoretical bound derived in Theorem 2, suggesting that the *average-case* estimation error is significantly tighter than the Alicki-Fannes-Winter inequality implies.

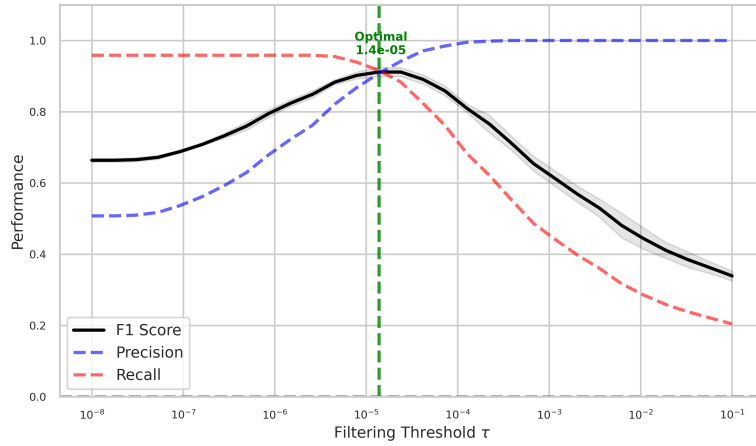


**Figure B.6: Sensitivity Analysis.** Classification metrics relative to the filtering threshold  $\tau$  with  $|\mathcal{X}| = 1000, \epsilon = 0.04, c = 6, m = 6, L = 64, N = 128$ ).

### B.3.3.3 Scaling Law for Causal Identifiability

In the right  $\epsilon$ -regime  $\epsilon \in [0, 0.1]$ , we observe an inverse scaling law  $\tau_{opt} \propto |\mathcal{X}|^{-1}$  for the optimal threshold  $\tau$  in Fig. B.7:

$$\tau(\mathcal{X}) = \frac{C}{|\mathcal{X}|}, C = 1.72 \cdot 10^{-2}$$

This indicates that while the density estimation task becomes harder in high dimensions (higher entropy), the structural identifiability actually improves. The sparsity of the event space dilutes spurious correlations, effectively lowering the noise floor and allowing for the discovery of weaker causal signals.

### B.3.4 Additional Summary Causal Graph

## B.4 CAREP: Multi-Agent System for Automatic Rule Generation

This section contains the appendix material for the chapter 9.

### B.4.1 Input Format

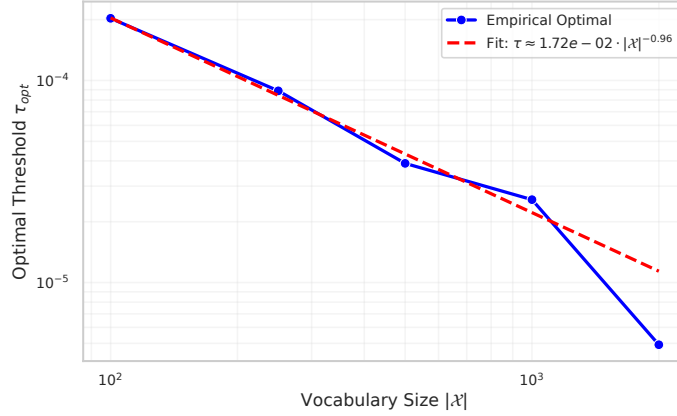


**Figure B.7: The Scaling Law of Causal Identifiability.** We perform a sensitivity analysis across vocabulary sizes  $|\mathcal{X}| \in \{100, \dots, 2000\}$  to find the optimal filtering threshold  $\tau_{opt}$  (maximizing F1-score) with  $\epsilon = 0.04$ . The result reveals a power-law relationship  $\tau_{opt} \propto |\mathcal{X}|^{-0.96}$ .

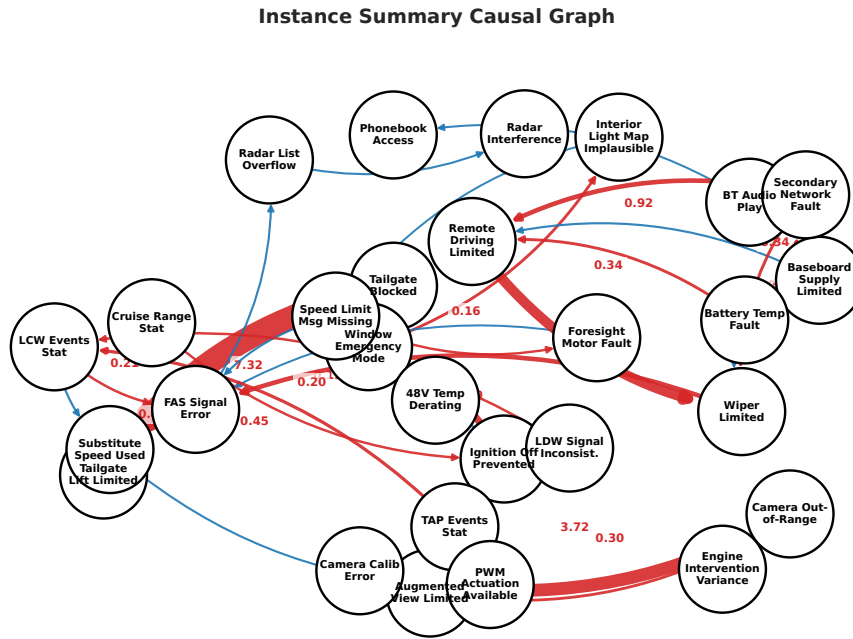


**Figure B.8: Instance Summary Causal Graph.** The global causal structure  $\mathcal{G}_s$  aggregated from TRACE inferences over the validation set. While the instance graph (Fig. 8.6) details *when* events occur, this summary graph captures the invariant mechanism types. The density of the graph highlights the complexity of modern vehicle architectures, where high-degree nodes often represent central control units (e.g., ECU, Battery Management) that propagate cascading faults. The conditional mutual information is reported as causal strength.

```

1  "unknown EP": {
2    "potential_causes": {
3      "DTC3": {
4        "frequency": 0.78,
5        "ACE_mean": 0.70,
6        "ACE_std": 0.13,
7        "pmi": {
8          "DTC345": -1.89
9        }
10     },
11    "DTC345": {
12      "frequency": 0.49,
13      "ACE_mean": 0.59,
14      "ACE_std": 0.12,
15      "pmi": {
16        "DTC3": -1.89
17      }
18    },
19    "dtcs_samples": {
20      "0X001 0X008 0X0120 0X8900 .. META .. CCM 111",
21      "0x6052 0X0204 0X0129 0X3410 .. META .. CCM 111",
22      ...
23    }
24  }
25 }

```

**Figure B.9: Input Examples Given to the Agentic System.** The *potential causes* are output by the causal discovery algorithm. For instance, *DTC3* is a cause of *unknown EP* and has an Average Causal Effect (*ACE*) of 0.7, i.e., it increases the likelihood of observing the EP on average by 70% (Eq. (9.1)). Examples of defective vehicles exhibiting this error pattern are provided in the *DTC samples*.